CANADIAN THESES ON MICROFICHE

I.S.B.N.

THESES CANADIENNES SUR MICROFICHE

National Library of Canada
Collections Development Branch

Canadian Theses on
Microfiche Service

Ottawa, Canada
K1A 0N4

Bibliothèque nationale du Canada
Direction du développement des collections

Service des thèses canadiennes
sur microfiche

NOTICE

The quality of this microfiche is heavily dependent upon the quality of the original thesis submitted for microfilming. Every effort has been made to ensure the highest quality of reproduction possible.

If pages are missing, contact the university which granted the degree.

Some pages may have indistinct print especially if the original pages were typed with a poor typewriter ribbon or if the university sent us a poor photocopy.

Previously copyrighted materials (journal articles, published tests, etc.) are not filmed.

Reproduction in full or in part of this film is governed by the Canadian Copyright Act, R.S.C. 1970, c. C-30. Please read the authorization forms which accompany this thesis.

THIS DISSERTATION
HAS BEEN MICROFILMED
EXACTLY AS RECEIVED

AVIS

La qualité de cette microfiche dépend grandement de la qualité de la thèse soumise au microfilmage. Nous avons tout fait pour assurer une qualité supérieure de reproduction.

S'il manque des pages, veuillez communiquer avec l'université qui a conféré le grade.

La qualité d'impression de certaines pages peut laisser à désirer, surtout si les pages originales ont été dactylographiées à l'aide d'un ruban usé ou si l'université nous a fait parvenir une photocopie de mauvaise qualité.

Les documents qui font déjà l'objet d'un droit d'auteur (articles de revue, examens publiés, etc.) ne sont pas microfilmés.

La reproduction, même partielle, de ce microfilm est soumise à la Loi canadienne sur le droit d'auteur, SRC 1970, c. C-30. Veuillez prendre connaissance des formules d'autorisation qui accompagnent cette thèse.

LA THÈSE A ÉTÉ
MICROFILMÉE TELLE QUE
NOUS L'AVONS REÇUE

NL-339 (r. 82/08)

Canada

STABILIZATION OF ARAGONITE TO LOW-Mg CALCITE: TRACE ELEMENTS AND STABLE ISOTOPES IN RUDISTS

A
Thesis
submitted to the
School of Graduate Studies
in partial fulfillment of the requirements
for the
Degree of Doctor of Philosophy in Geology

by
IHSAN SHAKIR AL-AASM
September 1984

Dr. J. Veizer — Thesis Supervisor

© Ihsan Shakir Al-Aasm, Ottawa, Canada, 1985.

UNIVERSITÉ D'OTTAWA
UNIVERSITY OF OTTAWA

TO MY WIFE LOOLA

ABSTRACT

Diagenetic stabilization of marine carbonate minerals, such as aragonite (A), high-Mg calcite (HMC), and low-Mg calcite (LMC) into their successor diagenetic low-Mg calcite (dLMC) has occurred under a wide spectrum of phreatic and vadose meteoric realms. Such transformation is accompanied by textural, trace elemental and stable isotopic modifications. The theoretically advocated diagenetic repartitioning leads to an increase in some elemental and isotopic concentrations in the stable successor phases (Fe, Cu, Mn, Zn, Ba, Mg, ^{16}O and ^{12}C), and decrease in others (Sr, Na, U, ^{18}O and ^{13}C), with increasing degree of diagenetic stabilization.

Cretaceous rudists, having thick multilayered bimineralic (aragonite and low-Mg calcite) shells, have been studied for the effects of phreatic/vadose meteoric diagenesis on their textural, ultrastructural, and chemical attributes.

The original fine compact prismatic or cellular-prismatic ultrastructures of low-Mg calcitic layers have frequently been preserved, despite the vagaries of their subsequent diagenetic histories. The low-Mg calcitic layers usually suffered only partial recrystallization, which caused fusion of crystal units, rounding of prism corners, and partial cementation confined to intercrystalline and

intraparticle pore spaces. In contrast, the originally aragonitic parts of the shell suffered either complete dissolution or, at best, retained some vestiges of their crossed-lamellar, complex crossed-lamellar, or composite prismatic ultrastructures. Where total dissolution of the originally aragonitic layers occurred, the cavity has been filled by ferroan calcite. In such instances, the original mineralogy may only be inferred by the shape of micritic envelopes mimicking the original architecture.

Synsedimentary submarine diagenetic events, such as borings by endolithic fauna, internal micritic and/or peloidal sedimentation in primary voids, submarine radiaxial and micritic aragonite and high-Mg calcite cements within the primary inter- and intraparticle pore spaces, were coeval with rudist accretion. The subsequent meteoric cementation has been characterized by the formation of bladed and equant ferroan calcites which occluded the available primary and secondary porosities.

Diagenetic stabilization of A $\longrightarrow$ dLMC and LMC $\longrightarrow$ dLMC is believed to have been a two-stage process. Initially, Sr and Na have been partially depleted during an early meteoric diagenetic phase (calcitization of metastable phases). The expulsion of Sr is thought to have occurred at a much slower rate than that of Na. This stage is followed by incorporation of more Mn, Fe and Mg due to precipitation of late ferroan calcite. It must be noted that trace element

diagenetic shifts caused by LMC → dLMC transition are of lesser magnitude than those of A → dLMC type. This may argue that diagenetic stability of LMC, is only a relative phenomenon. Alternatively, the observed diagenetic trends in originally LMC phases may also reflect stabilization of cements in primary and secondary pore voids, which have been formed during early marine as well as subsequent meteoric diagenesis. The magnitudes of the observed diagenetic trends depend not only on mineralogy, but also on the structural buildup of a given shell layer. This suggests that factors such as water/rock ratio (surface kinetics) are of considerable significance for the process of diagenetic stabilization.

Rudist skeletal components with preserved original mineralogy of aragonite and low-Mg calcite, and with preserved texture, have chemical and isotopic signatures analogous to Recent marine bivalves. This similarity argues for comparable chemical and isotopic composition of the Cretaceous and Recent seawater, as well as for similar mode of incorporation of trace elements and stable isotopes into their shells.

In analogy to trace elements, stable isotopes also reflect the two-stage diagenetic stabilization. This is particualrly evident for A → dLMC, but to some extent also for LMC → dLMC transformation. The A → dLMC and (HMC → dLMC) transformation affects mostly the oxygen value, resulting in ~≤2‰ depletion in ^{18}O. The subsequent

diagenetic precipitation of ferroan calcite spar causes further depletion in ^{18}O and also in ^{13}C, due to the introduction of organically derived CO_2 into the diagenetic aquifer. In contrast, originally LMC skeletal components show both, $\delta^{18}O$ and $\delta^{13}C$, isotopic depletion to be related mostly to this late diagenetic precipitation of ferroan sparry calcite cements. The early calcitization diagenetic stage, typical of aragonitic skeletal components, has been only of subordinate importance for LMC skeletal parts.

Partial preservation of aragonitic ultrastructures as ghost relics, of textural features, and of trace element and stable isotope signatures in rudist shells, suggests that diagenetic A (HMC) $\longrightarrow$ dLMC transformation has been accomplished in micron-scale semi-closed environments.

The discrete shell layers have specific chemical (Sr, Mn, Fe, Na, Mg) and isotopic ($\delta^{18}O$, $\delta^{13}C$) composition, which depends on mineralogy, physiological factors, and perhaps on texture.

The results show that each of the four cement types, occluding primary and secondary pore spaces within rudist shells, has specific chemical and isotopic signatures. Their overall chemistry is a reflection of both, original and diagenetic attributes. Both marine and meteoric waters were contributing to the formation of these cements.

AKNOWLEDGEMENTS

I thank my thesis supervisor, Dr. J. Veizer, for his continuous assistance, constructive discussions, and encouragement; Dr. N.F. Sohl (United States Geological Survey) for donation of rudist samples from the Caribbean and the U.S.A. and for helpful discussion; Dr. J. Philip (Université de Provence) for valuable information during field work in southeastern France; Drs. O.A. Dixon (University of Ottawa), Lynn M. Walter (Washington University), Paul Enos (University of Kansas), and W. Schlager (University of Miami) for constructive criticism of a part of Chapter I; Dr. P. Fritz (University of Waterloo) for access to mass-spectrometer; Parks Canada for access to SEM facility.

Thanks are also due to D. Garrette, R. Hartree, B. Taylor, E. Hearn, J. Loop, R. Drimmie, and C. Coustine for technical assistance; to R. Nasser for advice in computer work, and to Nancy Makila for typing the thesis.

This study was supported by a scholarship from the Directorate General of the Geological Survey and Mineral Investigations of Iraq and by the Natural Sciences and Engineering Research Council of Canada grant to J. Veizer.

I would like to express my deepest gratitude to my wife, Loola, and my son, Ali, for their continuous encouragement and support, and to my mother, brothers, sisters, and in-laws for their confidence and support.

TABLE OF CONTENTS

FIGURES

TABLES

PLATES

GENERAL INTRODUCTION

Transformation of aragonite (A) into diagenetic low-Mg calcite (dLMC) in marine sediments is a wet dissolution-reprecipitation phenomenon which involves chemical, isotopic and textural modifications. This transformation could be best understood and quantified through studies of internal constituents of carbonate rocks and of their associated chemical and isotopic trends. Each internal component is characterized by its own trace elemental and isotopic shifts. Fossils, because of the relative ease of manual separation and because of the reasonable control on their original mineralogical and chemical composition, can be sampled from facies of variable diagenetic alteration. The resulting geochemical grid may be utilized for quantification of diagenesis. Rudist bivalves of the Cretaceous age were selected for this study because they have thick, multi-layered, bimineralic shells and because they have been abundant in the shallow warm Tethyan seas.

The main objectives of the study are:

1. To delineate mineralogical and textural modification related to advancing diagenetic alteration of original skeletal components.
2. To quantify chemical and isotopic shifts for mineralogic stabilizations of A → dLMC and LMC → dLMC types.
3. To evaluate the degree to which original mineralogy,

texture, and ultrastructure of discrete shell layers control trace elements and stable isotopic composition in the process of progressive diagenetic stabilization in meteoric waters, and

4. To estimate, based on well preserved skeletal components, the trace element and stable isotopic composition of Cretaceous seawater.

This thesis is composed of three chapters. Chapter One deals with an introductory outline of rudist buildups in the Cretaceous seas, classification of shell ultrastructures for different families, preservation and alteration of these ultrastructures, and with general sequential diagenesis in rudist buildups. Chapter Two will evaluate trace element repartioning during diagenetic mineralogical stabilization of the originally aragonitic and low-Mg calcitic skeletal components. The last chapter is devoted to the behaviour of stable isotopes, and their relationships to trace elements, as indicators of diagenetic processes.

CHAPTER I

ULTRASTRUCTURES AND DIAGENETIC DEVELOPMENT OF RUDIST SHELLS

1.1 INTRODUCTION

Rudists were a group of bivalves with calcitic and aragonitic shells that lived in a variety of shallow water environments and were capable of constructing true reef structures and other types of carbonate buildups. They thrived during Cretaceous times characterized by widespread development of carbonate platforms in tropical to temperate latitudes (Kauffman, 1973; Wilson, 1975).

Rudist shells, because of their moderately high original porosity and particularly because of their pronounced secondary porosity (produced by successive meteoric vadose and phreatic leaching of aragonitic layers during periods of regression or sea level changes), were suitable for hydrocarbon accumulation and were prime targets for oil exploration in the Middle East, Texas and Mexico, where giant oil reservoirs exist in rocks of Cretaceous age (Arthur and Schlanger, 1979).

The main objectives of this chapter are the following: (1) to study the mineralogy and petrography of rudist shells of different families and of varied geologic ages and locations; (2) to document and classify shell ultrastructures for different rudist families; (3) to delineate mineralogical and textural changes with advancing diagenetic alteration of original shell components; and (4) to elucidate the general

sequence of diagenesis in rudist carbonate buildups, including both syndepositional and post-depositional diagenetic events.

1.2. EVOLUTION OF RUDISTS IN CRETACEOUS TETHYS

Rudist bivalves of superfamily Hippuritacea comprise a group of massive-shelled, solitary and gregarious, inequivalve, suspension-feeding, sessile, epifaunal molluscs (Dechaseaux, 1969; Heckel, 1974; Wilson, 1975; Coogan, 1977; Dodd and Stanton, 1981). Their first recorded history is marked by the appearance of Diceras during the late Jurassic (Dechaseaux, 1969). They flourished in the Tethyan seas during the Cretaceous, contributing much to varied and abundant reefs and other carbonate buildups, and replacing hermatypic corals as the main framework-building organisms. They became extinct at the end of the Cretaceous and left no close relatives in recent times (Dodd and Stanton, 1981).

The presence of rudists in the Tethyan tropical realm was particularly pronounced within a belt confined by the latitudes of southern Sweden in the north and Madagascar in the south (40°N to 20°S, Fig. I-1). These geographic limits encompassed the Caribbean, the west coast of America, south Asian margin, and the east and west African coasts (Chubb, 1971; Kauffman, 1973). The

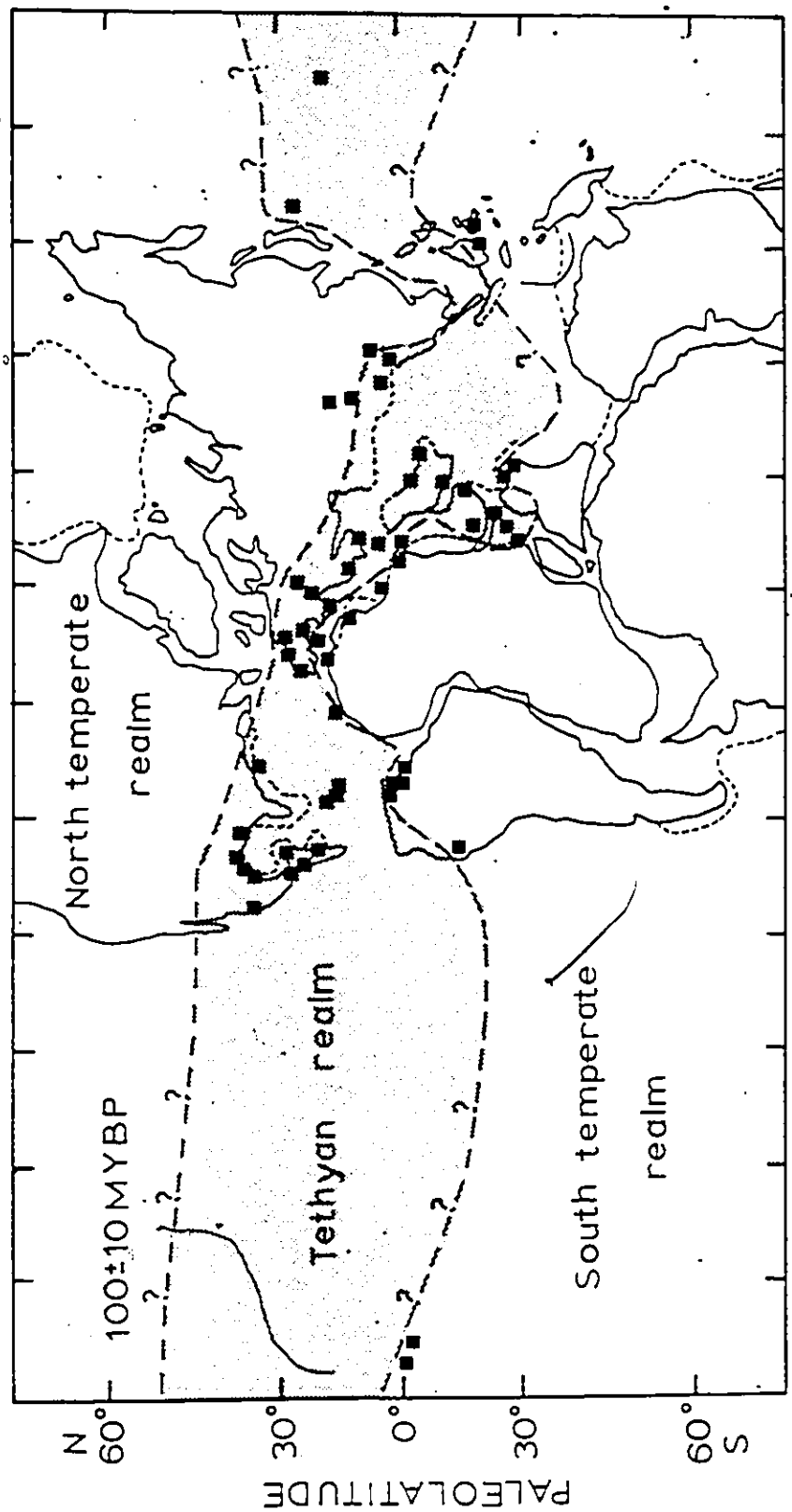

Fig. 1-1. Distribution of Cretaceous rudist buildups plotted on Cretaceous continental reconstruction (Kauffman, 1973; Coats, 1973; Coogan, 1977; Arthur and Schlanger, 1979). The shaded area represents the Tethyan realm.

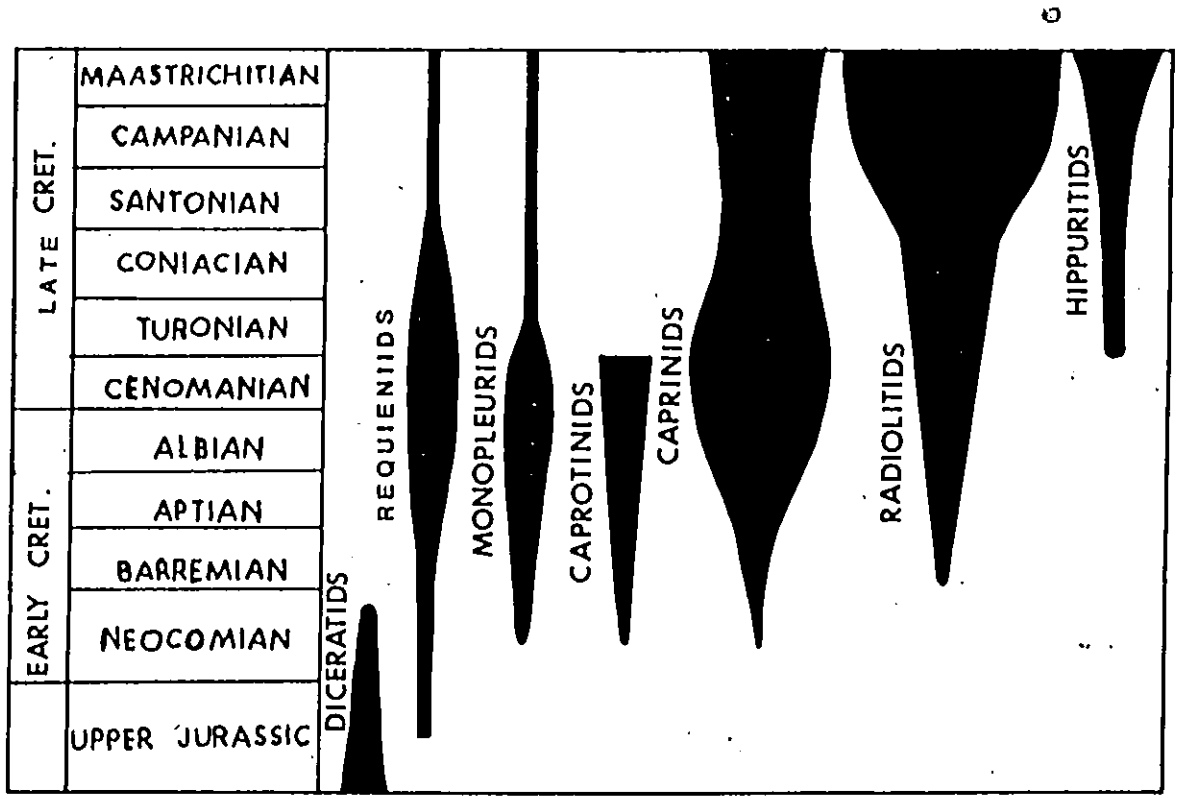

Fig. I-2. Rudist families and their distribution in time (modified from Wilson, 1975).

Tethys is regarded as the most mature Mesozoic biogeographic unit, with a long history of environmental stability. Bivalves in this unit reached high diversity and strong provincialism. These features may reflect events such as continental separation (e.g. opening of the Atlantic ocean, or closing of the Mediterranean accompanied by a breakup of the Mediterranean platform into microcontinents), which subsequently may have caused genetic isolation (Kauffman, 1973; Coats, 1973).

Rudists evolved into crowded, bizarre forms on shallow-photic shelves, platforms and along shelf margins (Kauffman, 1973; Wilson, 1975). Their classification into different families and their distribution through time are summarized in Fig. I-2.

1.3 GENERAL GEOLOGY AND SAMPLE LOCATIONS

Because of the wide geographic and stratigraphic distribution of the sampled material only a brief geologic and geographic background will be presented in this section.

1.3.1 Southeastern France

Rudist carbonate buildups are known from different localities of southeastern France. Their distribution and generic development were of limited extent during the Early Cretaceous, but they expanded and diversified

greatly in the Late Cretaceous (Dechaseaux and Sornay, 1960; Philip, 1981). These carbonate buildups have been extensive in warm intertidal-subtidal environments characterized by stable climate and tectonics (Masse and Philip, 1981).

The Southeastern Basin spread from the Jura mountains to the Provence. During the Early Cretaceous times, this basin was characterized by a belt of shallow water carbonate sediments, the Urgonian Facies, which was developed on the western and southern fringes of the Alpine geosyncline. Subsequently, during the Albian-Lower Cenomanian tectonic movements, the Austrian phase, gave rise to an emergent area covering the main part of the Provence-Languedoc region. This land, separating the Alpine Basin from the Provence Basin, remained as a barrier also during the Late Cretaceous. During the latter period, clastic deposition hindered the formation of rudist buildups which grew therefore only on offshore banks and platforms. Towards the end of the Cretaceous, the whole Southeastern Basin emerged from the sea due to Laramide orogeny (Masse and Philip, 1981).

Rudist formations in southeastern France are represented mainly by platform and bank deposits (Philip, 1972, 1974, 1981), although formation of true reefs has not been completely discounted. Other organisms, such as corals, algae and foraminifera played

only a minor role (Freyetet, 1973; Philip, 1980). Rudist banks, a few feet thick, were formed in quiet shallow subtidal or intertidal environments and were particularly abundant during Early and Late Cretaceous times. In contrast, rudist platforms were ubiquituous during the whole Cretaceous. In general, rudists and miliolids were believed to have been abundant in the inner parts of the platforms, while corals dominated the outer parts of the platforms (Masse and Philip, 1981; Philip, 1981).

Rudist samples collected from southeastern France originated from a variety of carbonate formations of various ages (Fig. I-3). Requieniids were collected mostly from the Urgonian Limestone, radiolitids mostly from the Cenomanian facies east of Martiques, and a few hippuritids were recovered from the Turonian facies of the Bassin d'Eusuis la Radonne and Cossis. The majority of hippuritids and radiolitids from the Santonian and Coniacian platformal facies originate from the Chainon de la Fare, St. Chamas, Martiques, and from St. Baumes Massif. For details of sedimentology, palaeontology and sample locations, see Philip (1972, 1974, 1978, 1980, 1981), Skelton (1974, 1976), and Appendices I and II.

1.3.2 Texas and Gulf Coast Areas

Rudists were the major reef building organisms in

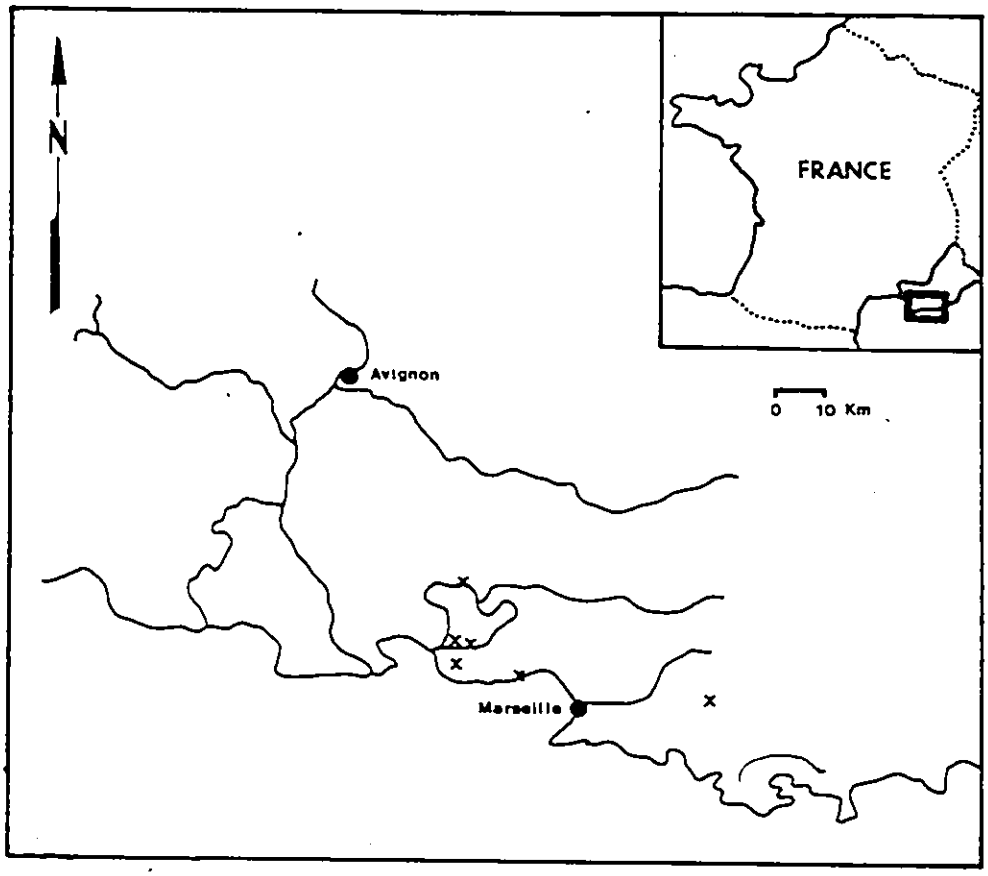

Fig. 1-3. Geographic setting and locations of the studied sample areas (x) in southeastern France.

Texas and Gulf regions during the Cretaceous. Some reefs were built exclusively by rudists, while others were built by corals and stromatoporoids in addition to rudists (Perkins, 1969).

Lower Cretaceous rocks in Texas were deposited on a vast, generally submerged plain called the Comanche shelf (Fig. I-4). These rocks were divided into three divisions. They are, in ascending stratigraphic order, the Trinity, the Fredericksburg, and the Washita groups (Perkins, 1961; Rose, 1972). The Edwards Formation, mainly limestones and dolostones, was the dominant rock unit deposited over the central Texas Platform (Fig. I-4). This platform was protected on the southeast by the Stuart City reef, which is a ridge-like belt of rudist, coral and algal debris (Rose, 1970). In the southwest, the platform was protected by the Devils River bank, on the northeast by low sand banks and mounds, and in the northwest by a broad area of shallow marine waters in the interior of the Comanche shelf. The Edward Formation encompasses patch reefs and small scale bioherms and biostromes which were deposited in a shallow subtropical sea along shelf edges and in the inner shelf areas (Fisher and Rodda, 1969; Perkins, 1969, 1970; Kerr, 1977; Longman and Mench, 1978). Five rudist families (Requieniidae, Monopleuridae, Caprotinidae, Radiolitidae, and Caprinidae) flourished

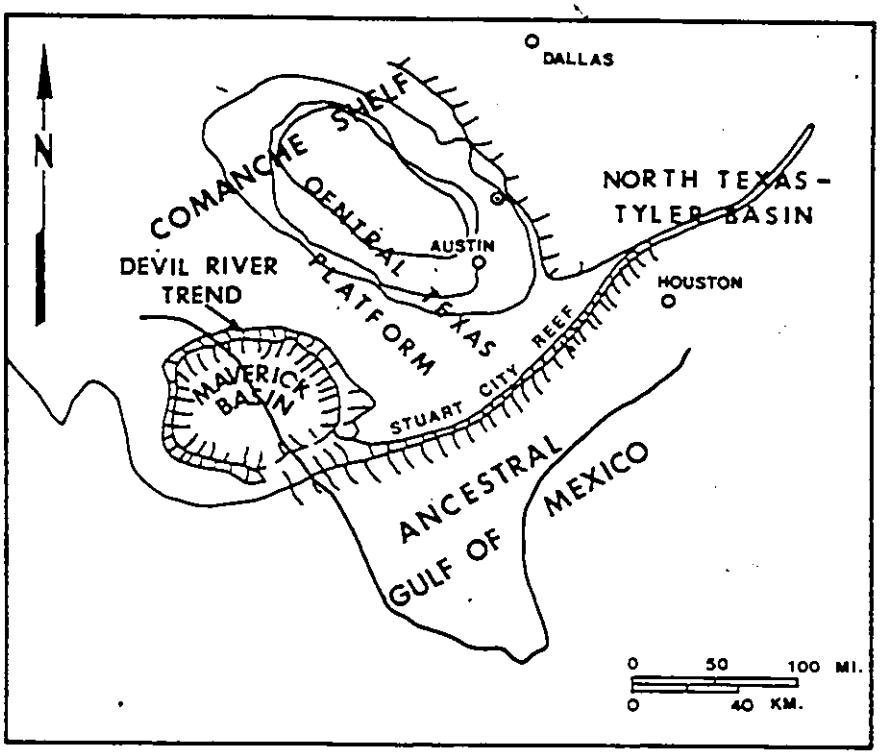

A

WASHITA GROUP	Buda Limestone
	Del Rio Clay
	Georgetown Formation
	Kiamichi Formation
FREDERICKSBURG GROUP	Edwards Formation
	Comanche Peak Formation
	Walnut Clay
TRINITY GROUP	Paluxy Sand
	Glen Rose Formation

B

Fig. I-4. Paleogeographic map of Edwards Formation (A), and stratigraphic succession of the Washita - Fredericksburg sequence (B) in northern Texas (reproduced from Rose, 1972, and Kerr, 1977).

in these regions (Coogan, 1977). The reef core facies of the above mentioned carbonate buildups were subjected to repeated subaerial exposure during their subsequent geologic history (Nelson, 1973).

In contrast, during Early and Late Cretaceous, coastal regions of the Gulf were dominated by clastic sediments, although locally, chalk was deposited (Sohl, 1960b). At the same time, the Caribbean region and Mexico were characterized by dominantly rudist carbonate sediments.

Rudist specimens, collected from the Lower Cretaceous Edwards Formation, originated from the central Texas region of Lake Whitney Dam. Additional Upper Cretaceous rudist samples, collected from the Coon Creek tongue of the Ripley Formation, Tennessee, which is composed from dark to bluish grey, micaceous, glauconitic, calcareous and fossiliferous silty sand beds with remarkably preserved fossil contents (Sohl, 1960a). Some samples were also collected from the Upper Cretaceous Prairie Bluff Chalk and San Vicente Formations. For details of stratigraphy, paleontology, and sample locations, see Lozo and Smith (1964), Sohl (1960a), Fisher and Rodda (1969), Rose (1972), Nelson (1973), Coogan (1977), and Appendices I and II.

1.3.3 Caribbean Islands (Greater Antilles)

The Cretaceous shelf sediments of the Caribbean Islands reflect a history of long periods of instability characterized by submarine volcanic activity and by tectonism (Kauffman, 1973; Kauffman and Sohl, 1974; Butterlin, 1983). The Caribbean region is considered to have been a part of a Late Jurassic orthogeosyncline, consisting of a miogeosyncline in the north and eugeosyncline in the south (cf. Khudoley and Meyerhoff, 1971). During periods of relative tectonic stability, rudist buildups dominated strongly over corals and formed patchy frameworks in warm, clear shelf platform environments.

The Albian and Cenomanian time span of Greater Antillean geological history represents the initial time of widespread and extensive development of carbonate platform deposits dominated by thin rudist-bearing limestones interbedded with thick shallow water volcaniclastic rocks (Kauffman and Sohl, 1976).

1.3.3.1 Jamaica

The major Cretaceous organic buildups in Jamaica, at least in certain inliers (Fig. I-5), are dominated by rudists. The Cretaceous sequence consists mainly of volcaniclastics, tuffaceous shales, and limestones (Chubb, 1971; Coat, 1977 a & b). These limestones are

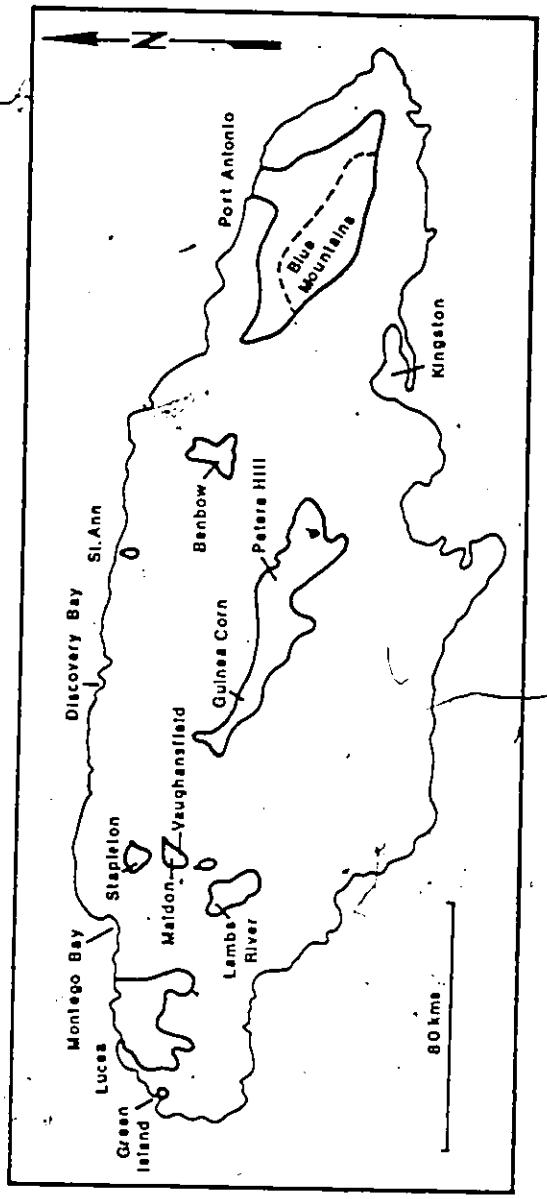

Fig. 1-5. Geographic setting and locations of Cretaceous inliers of Jamaica (reproduced from Coats, 1977)

usually thin, tabular or lenticular in shape, rich in rudists, corals, and other faunas. The classification and evolution of Jamaican rudist frameworks are discussed in Kauffman and Sohl (1974).

The studied specimens came mostly from the Upper Cretaceous carbonate formations of different inliers, such as the Central, Benbow, Maldon, Marchmont, Sunderland, and Greenland. For details of paleontology, sedimentology, and sample locations, see Chubb (1955, 1956, 1971); Kauffman and Sohl (1974, 1976), Sohl (1976), Coats (1973, 1977a, 1977b), Butterlin (1983), and Appendices I and II.

1.3.3.2 Puerto Rico

Puerto Rico is the easternmost and smallest of the Greater Antilles. The general geology of the Cretaceous of Puerto Rico is similar to that of the Greater Antilles and is dominated by submarine lavas, lava breccias, volcaniclastic rocks and shallow marine, rudist-rich limestones (Pease, 1968, Mattson, 1967). Figure I-6 is a geologic map of the Cretaceous outcrops in Puerto Rico. All rudist specimens utilized in this study originated from various localities of the Upper Cretaceous carbonate formations and they are represented by caprinids, radiolitids, and monopleurids. For detailed geology, paleontology, and sample locations,

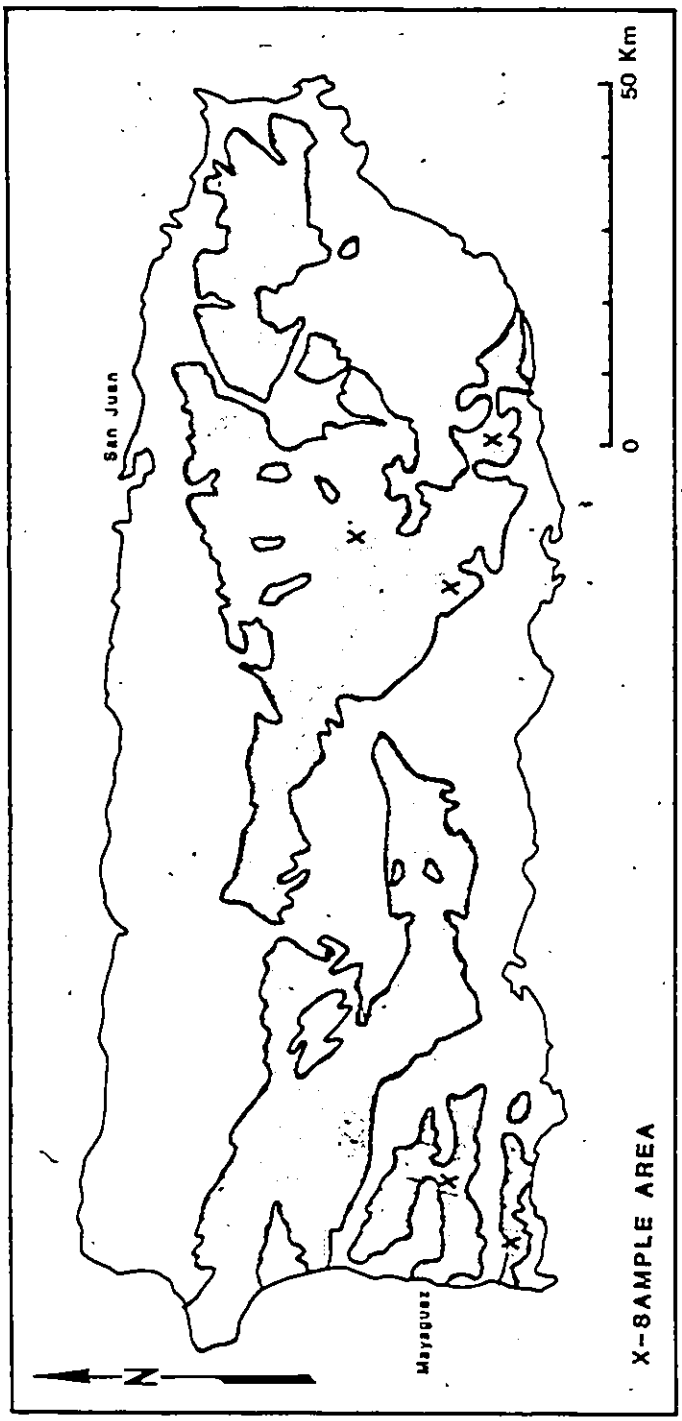

Fig. I-6. Location map of Puerto Rico with Cretaceous exposures (reproduced from Weaver and Mitchell, 1959).

see Mattson (1967), Pease (1968), Khudoley and Meyerhoff (1971), Sohl (1976), Butterlin (1983), and Appendices I and II.

1.3.3.3 Cuba

Numerous rudist faunas were described and studied from the Cretaceous carbonate rocks of Cuba (for review, see Chubb, 1956, 1961; Sohl, 1976). Figure I-7 shows the area of Cretaceous outcrops in Cuba. The studied rudists originated from different Lowere and Upper Cretaceous formations from the provinces of Havana, Santa Rosa, Santa Clara, Matazas, Canaguey, and Pinar del Rio. Appendix I gives sample locations.

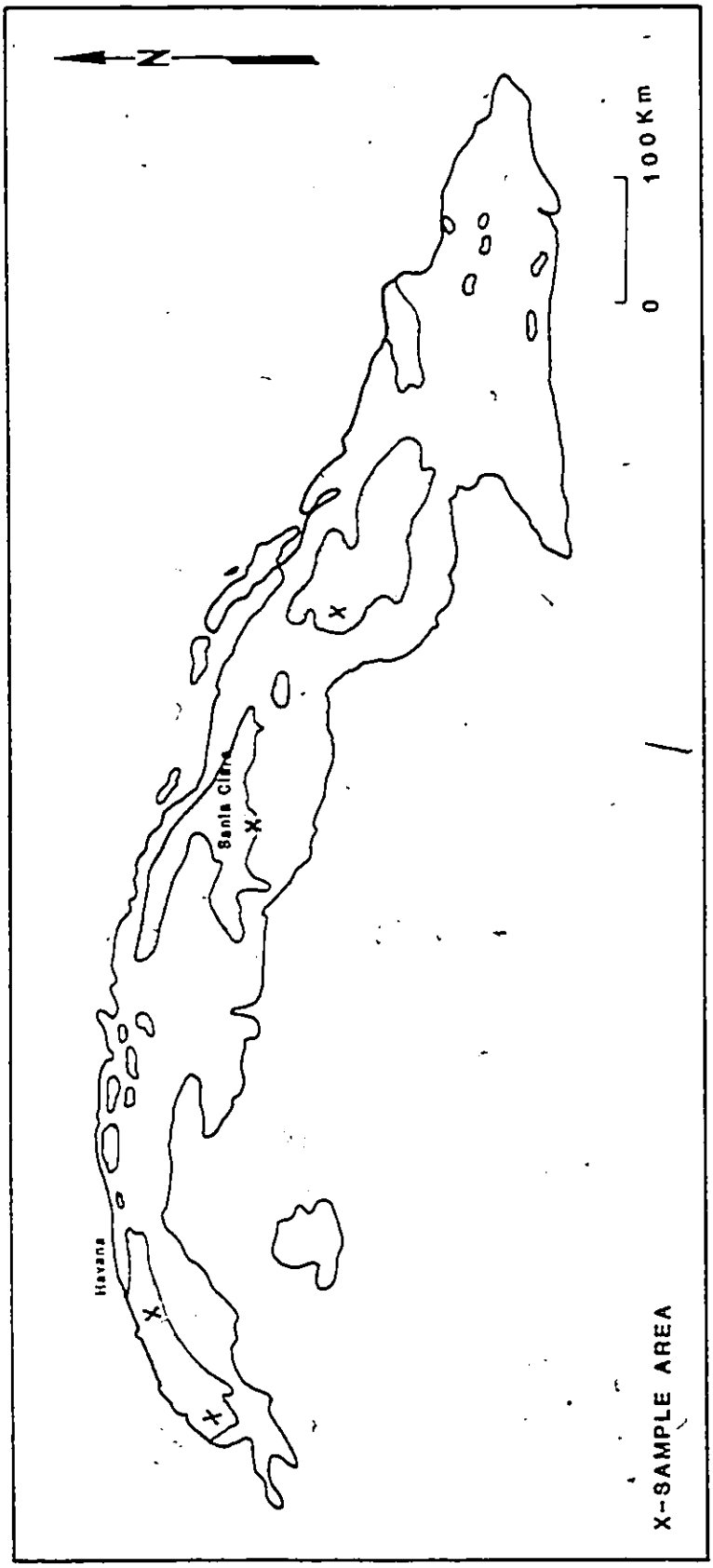

Fig. I-7. Geographic setting of Cuba with areas of Cretaceous outcrops (reproduced from Bermúdez, 1959).

1.4 PETROGRAPHY AND SEM STUDY OF RUDIST SHELLS AND ASSOCIATED ROCKS

The preceding four decades of studies of mollusc shells resulted in the following advances:

(a) classification of ultrastructures and a progress in understanding of the processes of calcification (Bøggild, 1930; Lowenstam, 1954b, 1963; Hall and Kennedy, 1967; Kennedy et al., 1969; Carter and Tavesz, 1978);

(b) delineation of diagenetic evolution of ultrastructures (Bathurst, 1964, 1975; Weyl, 1964; Dodd, 1966; Sandberg et al., 1973; Scherer, 1977; Wardlow et al., 1978; De Renz and Marquez-Aliaya, 1980; Weiner and Lowenstam, 1980), including the relationship of this evolution to mineralogical transformation of aragonite (A) into diagenetic low-Mg calcite (dLMC) in the phreatic/vadose meteoric realms (Pingitore, 1976; Longman, 1980); and

(c) evolution of chemical and isotopic signals due to the above phenomena (Curtis and Krinsley, 1965; Veizer, 1974, 1983a; Ragland et al., 1979; Brand, 1981a, b; Buchardt and Weiner, 1981; Crik and Ottensman, 1983; Sandberg and Hudson, 1983). This subject will be discussed in detail in Chapters II and III.

1.4.1 Samples and Techniques

A total of 176 rudist specimens, representing five different families, were utilized for this study. The studied families are: Hippuritidae, Radiolitidae, Requieniidae, Monopleuridae, and Caprinidae. Plates 1 and 2 show different natural and polished sections of some examples representing these families. In addition, a total of 47 enclosing rocks were studied petrographically for their textural components.

Thin sections were prepared and stained for Fe-calcite following the method described by Lindholm and Finkelman (1972). Forty rudist shells, in varying degrees of preservation, were examined by NANOLAB 7 SEM for ultrastructures, shell components, and their diagenetic texture. Polished slabs and fresh fractured surfaces were thoroughly washed with ultrasonic cleaner, etched with 50% acetic acid for 3-5 minutes, gold plated and examined. Mineralogy of fossil components was determined by X-ray diffraction (XRD) with Cu-α radiation and Ni-filter. The percentages of aragonite and calcite in the shells were calculated following the method described in Milliman (1974, p. 23-24).

1.4.2 Ultrastructure and Mineralogy of Rudist Shells

Petrographic and SEM studies of rudists revealed

PLATE 1
MORPHOLOGY OF RUDIST SHELLS

Fig. 1. Transverse section of hippuritid Vaccinites giganteus (sample no. 61, St. Baume, France). (a) is the outer prismatic layer. (b) is a pillar. Bar scale: 2 cm.

Fig. 2. Transverse section of a hippuritid Barrettia (sample no. 208), showing the morphologic features of the outer beaded layer. (a) is the internal body cavity infilled by internal sediments. Bar scale: 5 cm.

Fig. 3. Hippuritid Parastroma (sample no. 161, Santa Clara Province, Cuba). Notice the folded structure of the outer layer. Bar scale: 2 cm.

Fig. 4. Transverse section of a radiolitid shell (sample no. 35, Martique, Southeastern France). (a) is the thick cellular-prismatic layer. (b) is a cement fill in the body cavity. Bar scale: 1 cm.

Fig. 5. Transverse section of radiolitid Bournonia (sample no. 205, Santa Clara Province, Cuba). (a) is the outer thick cellular-prismatic layer. (b) is the inner thin layer of originally aragonitic composition. (c) is the major body cavity infilled by micritic-silty internal sediments. Bar scale: 5 cm.

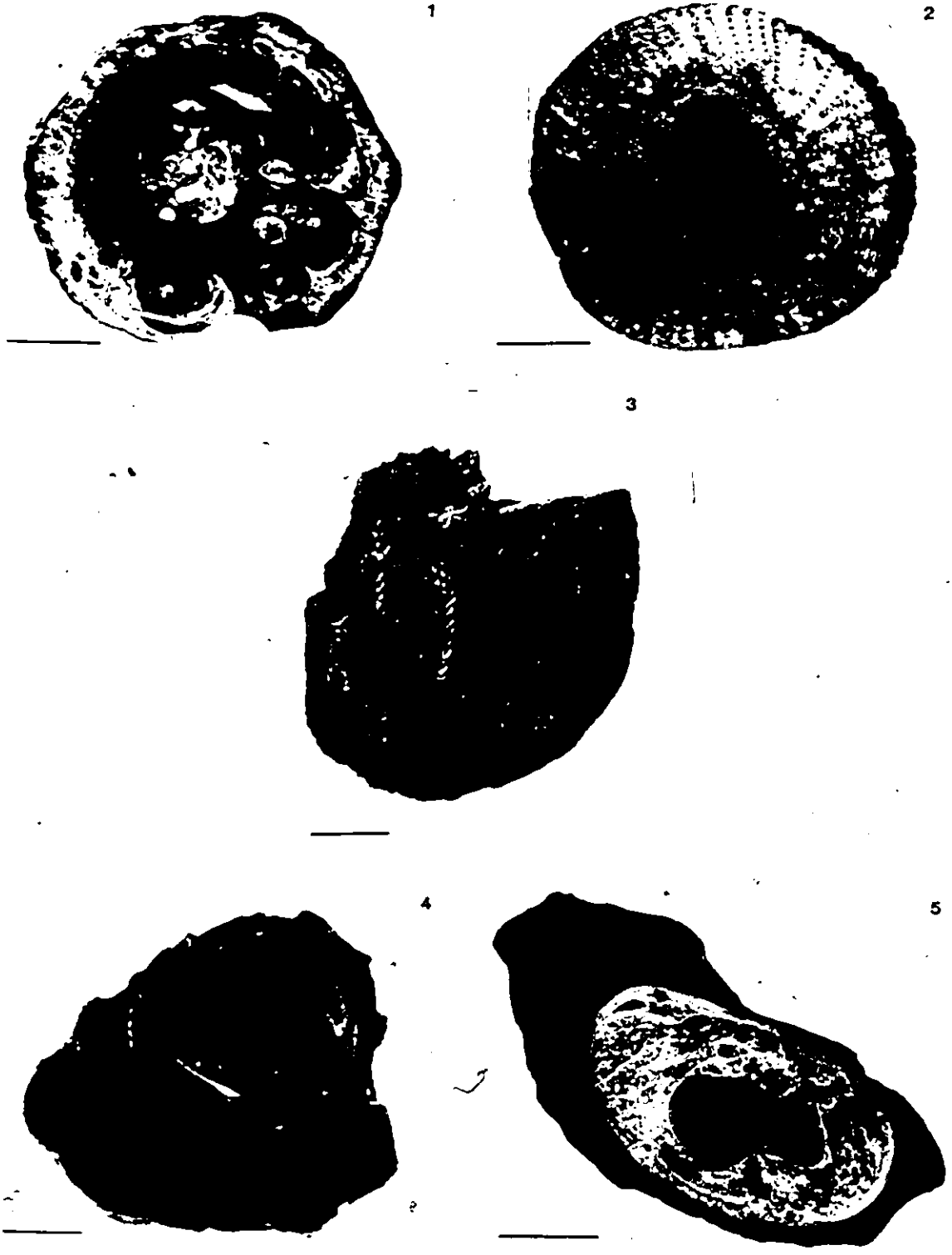

PLATE 2
MORPHOLOGY OF RUDIST SHELLS

Fig. 1. Transverse section of a caprinid (sample no. 197, Lake Whitney Dam, Texas). (a) is the outer pullial canal layer. (b) is a cavity occupied by two generations of cement fill. Bar scale: 1 cm.

Fig. 2. Caprinid Antillocaprina (sample no. 133, Jamaica). The outer layer is composed of small canals at the outer periphery and bigger canals underneath. Bar scale: 3 cm.

Fig. 3. Transverse section of Monopleura (sample no. 127, Sunderland Inlier, Jamaica). Bar scale: 2 cm.

Fig. 4. Requieniid shell (sample no. 82, Urgonian facies, southeastern France). Bar scale: 2 cm.

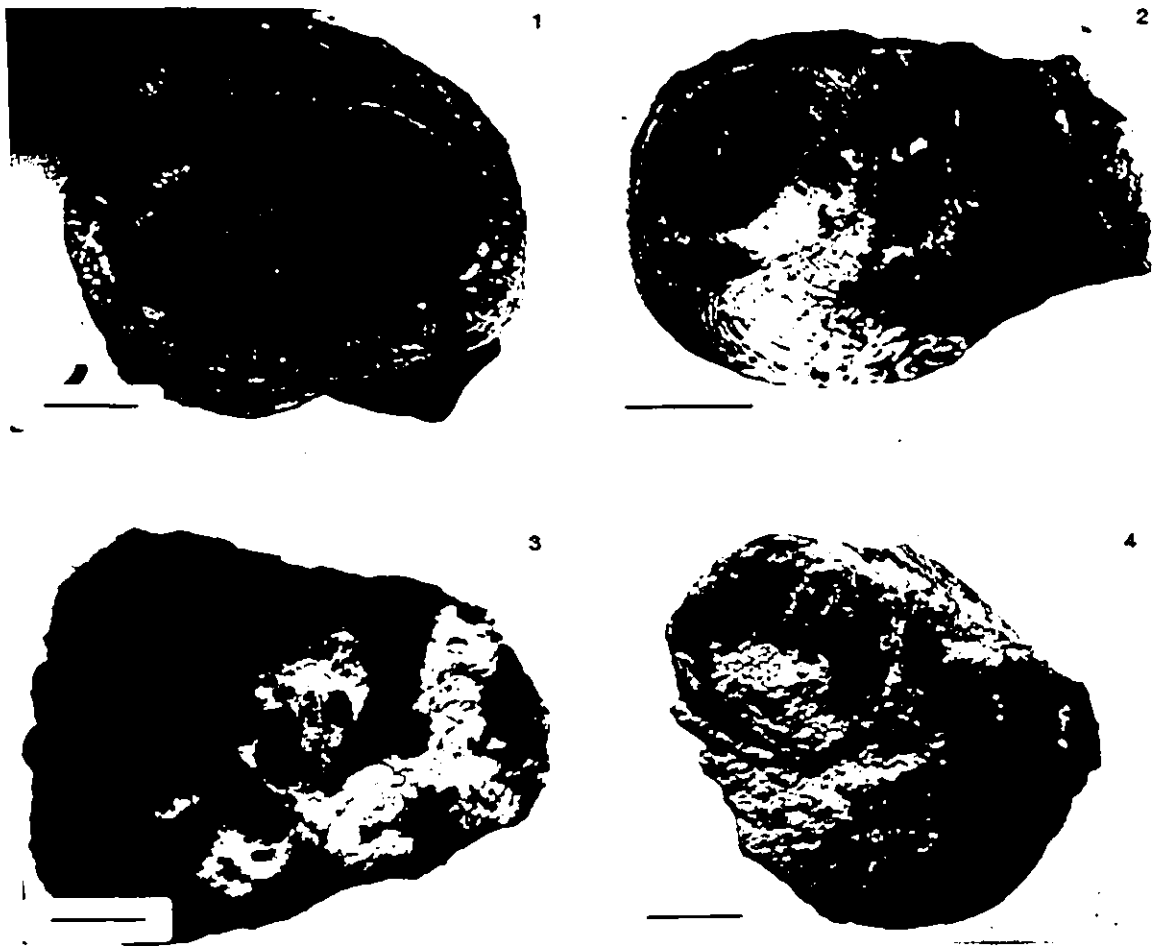
1
2
3
4

the existence of more than one type of ultrastructure, regardless of whether the original shell was composed solely of aragonite or of a mixture of aragonite and calcite. The classification of ultrastructures outlined below follows the basic terminology proposed by Bøggild (1930) and modified by Kennedy et al. (1969), and Rhoads and Lutz (1980).

1.4.2.1 Family Hippuritidae

The hippuritid shell is of conical, elongate to cylindrical shape with the right attached valve larger than the left free one. The latter is operculiform or flat. The shell is composed, at least in well preserved forms, of three crystalline layers (Plate 1, Figs. 1 and 2), each separate layer consisting of aragonite or low-Mg calcite (see also Bøggild), 1930; Kennedy and Taylor, 1968; Skelton, 1976).

(a) Outer Layers

The outer layer in many hippuritid right valves is relatively thick and composed from a fine compact and simple prismatic ultrastructure with distinct growth lines; the latter particularly visible in well preserved ultrastructures (Plate 3, Fig. 1). The prisms in the outer layer lie at right or oblique angles to the depositional surface of the shell. They are composed of

low-Mg calcite, as shown by XRD and confirmed by their good original preservation, if compared to the often replaced inner, originally aragonitic layers. The ultrastructure of the hippuritid pillar, which is an extension of the outer layer and may serve for current passage (Coogan, 1969), is similar. However, the outer layer of some genera, such as Barrettia, is relatively thick and composed of a simple and possibly non-denticular composite prismatic beaded structure (Plate 3, Figs. 3 and 4). The beads, which are thought to be an extension of the pillars towards the center of the shell and serve the same function as the pillars (Perkins, 1969), consist of very fine (approximately 5 μ) prisms of low-Mg calcite.

In only one specimen, Parastroma, the outer layer was found to be composed of simple and composite prisms of aragonite (Plate 3, Figs. 5 and 6). Mineralogically, the ultrastructure is 83% aragonite, the remainder being calcite, possibly as a result of polymorphic transformation from aragonite. Frequently, the outer layer in many hippuritids is bored by varied borers, such as sponges, algae, and bivalves.

(b) Middle and Inner Layers

These layers are usually thin (approximately 700 μ) and today often composed almost entirely of low-Mg

PLATE 3
ULTRASTRUCTURES OF HIPPURITID SHELLS

Fig. 1. Transverse section of a hippuritid shell (sample no. 15, Santonian Facies, Chainon de la Fare, southeastern France), showing the fine prismatic compact outer layer. Bar scale: 0.5 mm.

Fig. 2. SEM micrograph of the hippuritid outer layer (sample no. 41, Santonian Facies, Martiques, southeastern France), showing the prismatic ultrastructure partly affected by recrystallization.

Fig. 3. Transverse section of the hippuritid Barrettia (sample No. 165, Santa Clara Province, Cuba), showing part of the thick prismatic outer layer with beaded rays. Bar scale: 1.0 mm.

Fig. 4. SEM micrograph of the same specimen as in Fig. 3, showing recrystallized parts of the prismatic outer layer with fused crystal corners and microporosity.

Fig. 5. Transverse section of the hippuritid Parastroma (sample no. 161, Middle ? Cretaceous, Santa Clara Province, Cuba), with the outer layer composed from simple and composite aragonite prisms. The inner part shows a lamellar ultrastructure. Bar scale: 1.0 mm.

Fig. 6. SEM micrograph of the same specimen as in Fig. 5, showing lamellar ultrastructure.

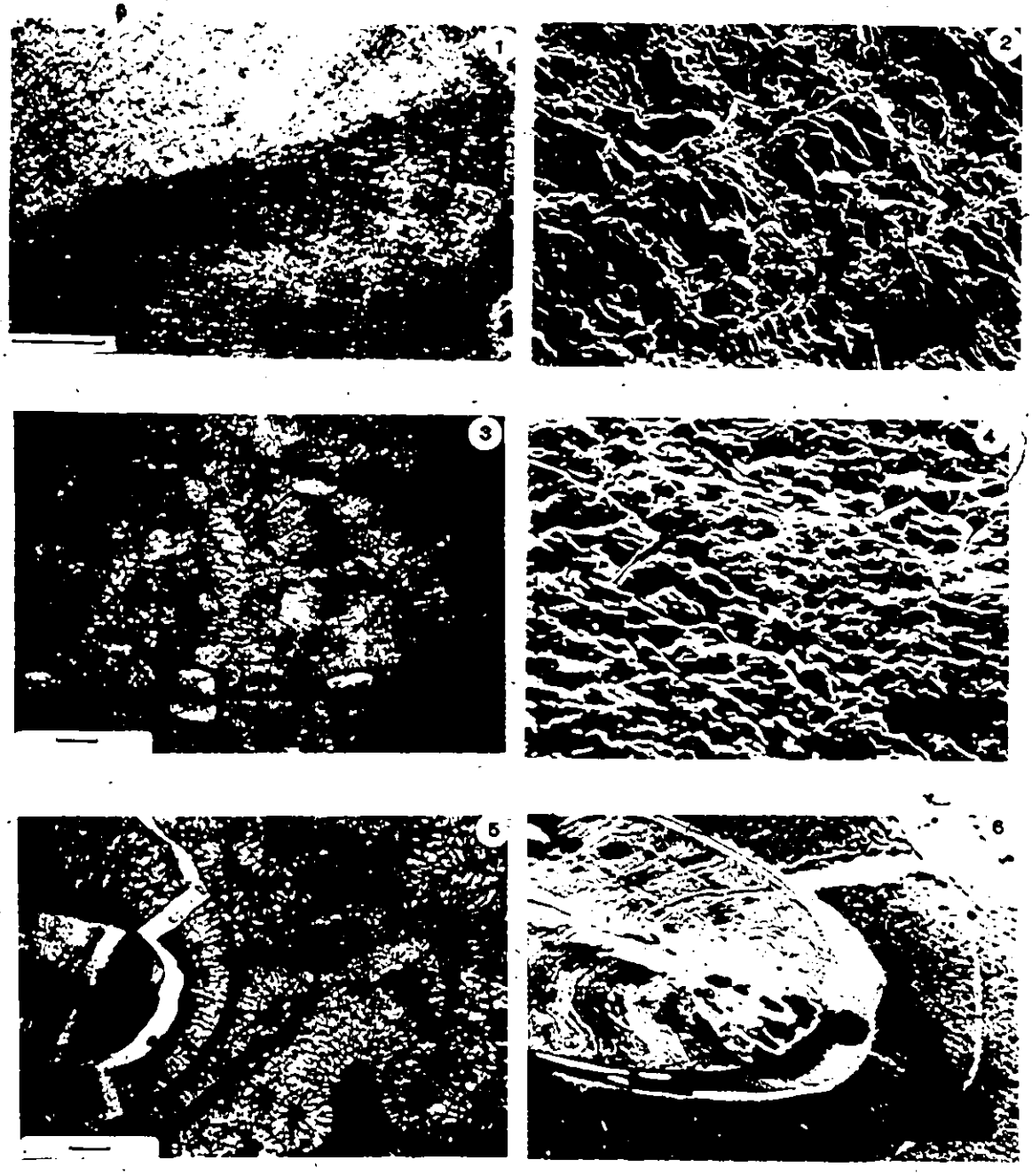
1
2
3
4
5
6

calcite. The preservation of clear relic crossed-lamellar ultrastructure with pseudopleochroism (cf. also Hudson, 1962) suggests that their original mineralogy was aragonite (Plate 3, Figs. 5 and 6; Plate 7, Figs. 1, 3 and 4). This deduction was confirmed by microsampling of the inner layer of sample 43 (Plate 7, Fig. 3). XRD camera determinations showed that aragonite was the main constituent of the well preserved relics, while the less preserved adjacent areas were composed of a mixture of aragonite and calcite. Similar ultrastructures were described previously by Skelton (1976), who observed that some hippuritids had crossed-lamellar middle layers and thin complex crossed-lamellar inner layers.

1.4.2.2 Family Radiolitidae

The radiolitid shell has a conical shape with an attached right valve. This valve is partly bored by borers such as encrusting algae, clionid sponges, and bivalves and is infilled with internal sediment. The left valve is operculiform (Plate 1, Figs. 4 and 5.)

(a) Outer Layer

In the majority of the studied specimens from southeastern France, Jamaica, Puerto Rico and Cuba, the outer layer of the right valve (i.e. attached valve) is characterized by a thick, cellular-prismatic

ultrastructure. The cells are of rectangular, polygonal, or oval shape in transverse section, with distinctive, brown-grey, thin (approximately 70 μ), ghost-like, organic?, growth lines of fine micritic diffused crystallites (Plate 4, Figs. 1, 2, 3, and 4). The cell wall (approximately 50 μ) formed by radial and transverse funnel-shaped plates is composed of finely crystalline fibres and prisms (width approximately 20 μ) of non-ferrous low-Mg calcite. In some species, the fine prisms of the wall grew in preferred directions (at normal and oblique angles to the depositional surface), thus forming large masses of prisms (Plate 6, Fig. 1). The interiors of the cells are occupied partly by finely pelleted micritic sediments and partly by fine equant spar.

(b) Middle and Inner Layers

Considering the preservation of brown, pseudopleochroic, crossed-lamellar ultrastructure in these two layers, they probably were composed originally of aragonite. This deduction has been confirmed for at least one well-preserved specimen of Bournonia (samples 131b, 131c, Upper Cretaceous, Central Inlier, Jamaica), where the XRD analysis showed the presence of 94% aragonite in the middle and inner layers.

The middle layer is generally thin (less than 1000

PLATE 4
ULTRASTRUCTURES OF RADIOLITID AND HIPPURITID SHELLS

Fig. 1. Transverse section of the outer layer of a thick radiolitid shell wall (sample no. 170, Upper Cretaceous, Collin County, Texas) showing cellular ultrastructure. The walls are formed by finely crystalline fibres or prisms of calcite. Bar scale: 0.5 mm.

Fig. 2. SEM micrograph showing details of Fig. 1. Note the cellular ultrastructure of horizontal and vertical plates.

Fig. 3. Transverse section of the outer cellular layer of radiolitid Chiapasella (sample no. 164, Upper Cretaceous, Pinar del Rio Province, Cuba). Bar scale: 0.5 mm.

Fig. 4. SEM micrograph of the same shell as in Fig. 3. Notice that the crystal sizes of the cell wall appear as ghosts or shadows of inclusions.

Fig. 5. Transverse section of a hippuritid shell (sample no. 43, Santonian Facies, Martiques, southeastern France), showing the outer compact fine prismatic ultrastructure. The thin middle layer was replaced by mosaic spar bound by micritic envelopes. The inner part shows an infill by large equant cement. Bar scale: 0.5 mm.

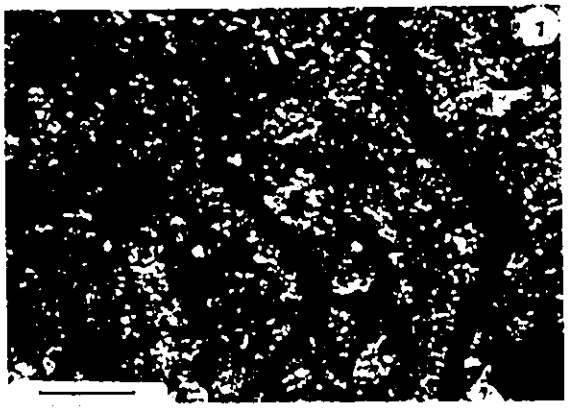
1

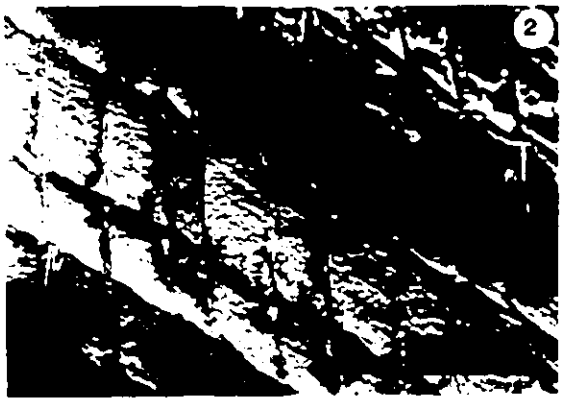
2


3

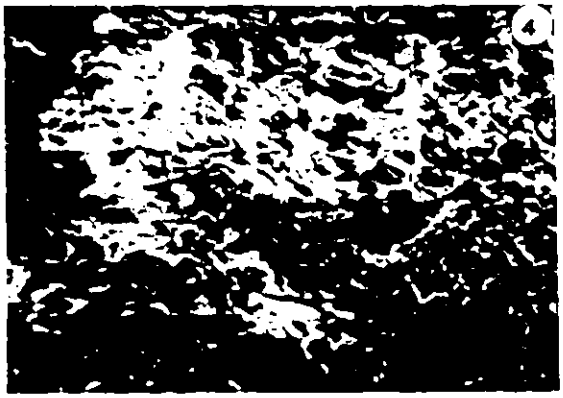
4


5

μ) and, in many cases, composed of neomorphosed microspar (Plate 8, Figs. 1 and 2). The inner layer is somewhat thicker than the middle one, brown in colour, and sometimes exhibits clear complex crossed-lamellar ultrastructures in accordance with the observations of Skelton (1974, 1979) for radiolitid species from Austria and southeastern France.

1.4.2.3 Family Caprinidae

The attached valve of the caprinid shell is larger than the free valve (Coogan, 1977). Well preserved caprinid shells consist of three layers (Plate 2, Figs. 1 and 2).

(a) Pallial Canal Layer

This layer is usually thick and contains abundant pallial canals. The latter may be absent in some specimens. Chubb (1971), in his study of Jamaican rudists, considered that the pallial canals existed in the middle and inner layers, whereas the outer layer was thin and lacked these canals. However, in this study, it has been observed that the pallial canals existed only in the outer thick layer, whereas the middle and inner layers were characterized by their typical lamellar ultrastructures.

The canal walls (approximately 200 μ thick) are

aragonitic, as supported by XRD analysis of three exceptionally well-preserved specimens with chalky-white luster, which contain over 90% aragonite (samples 96a = 99%A, 167a = 98%A and 104a = 90%A). This is in agreement with SEM observations showing no evidence of recrystallization or cementation. Pallial canals are more complicated in more advanced species (Coogan, 1969, Figure E241). In well-preserved specimens, they are soft, and polygonal or oval in shape (Plate 5, Figs. 1, 2, 3, and 4; Plate 7, Figs. 1 and 2), with a well-developed crossed-lamellar ultrastructure (Plate 5, Fig. 5).

The presence of pallial canals in the Caprinidae results in their sponge-like ultrastructure and high primary porosity. Such pores may be infilled subsequently by internal sediment, spar cement of variable generations, or both. This will be discussed in detail in the subsequent sections. Such pallial canals served for weight reduction, food entrapment, and respiration purposes (Perkins, 1969; Vogal, 1978).

In some specimens (e.g. Plagioptychus, Upper Cretaceous, Marchmont Inlier, Jamaica) a very thin calcite (99% LMC) outer layer has been observed. This layer is brown in colour, has no pallial canals, and is characterized by prismatic ultrastructure.

PLATE 5
ULTRASTRUCTURES OF CAPRINID SHELLS

Fig. 1. SEM micrograph of the well preserved aragonitic canals (Antillocaprina, sample no. 96, Upper Cretaceous, Ripley Formation, Tennessee). Notice the polygonal shape of the canals and the empty inner spaces bounded by cross plates, which may later be infilled by micritic internal sediment or cement.

Fig. 2. Transverse section of the aragonitic outer canal layer of Plagioptychus (sample no. 167, Upper Cretaceous, Ripley Formation, Tennessee). Crossed-polars. Bar scale: 0.5 mm.

Fig. 3. SEM micrograph of the same sample as in Fig. 2. Notice the excellent preservation of the canal walls (longitudinal section).

Fig. 4. Transverse section of the originally aragonitic outer layer of Antillocaprina (sample no. 97, Maastrichtian, Prairie Shale Formation, Gulf Coast). Note the fine preservation of the oval canal walls, with subsequent infilling by secondary calcite. Crossed-polars. Bar scale: 0.5 mm.

Fig. 5. SEM micrograph of a canal wall of the same sample as in Fig. 4. Note the well preserved lamellar ultrastructure of the wall (left) and the fine cement crystals within the canal (right).

Fig. 6. Cross section of the same specimen as in Fig. 4 showing the crossed-lamellar nature of the aragonitic inner layer. Crossed-polars. Bar scale: 0.5 mm.

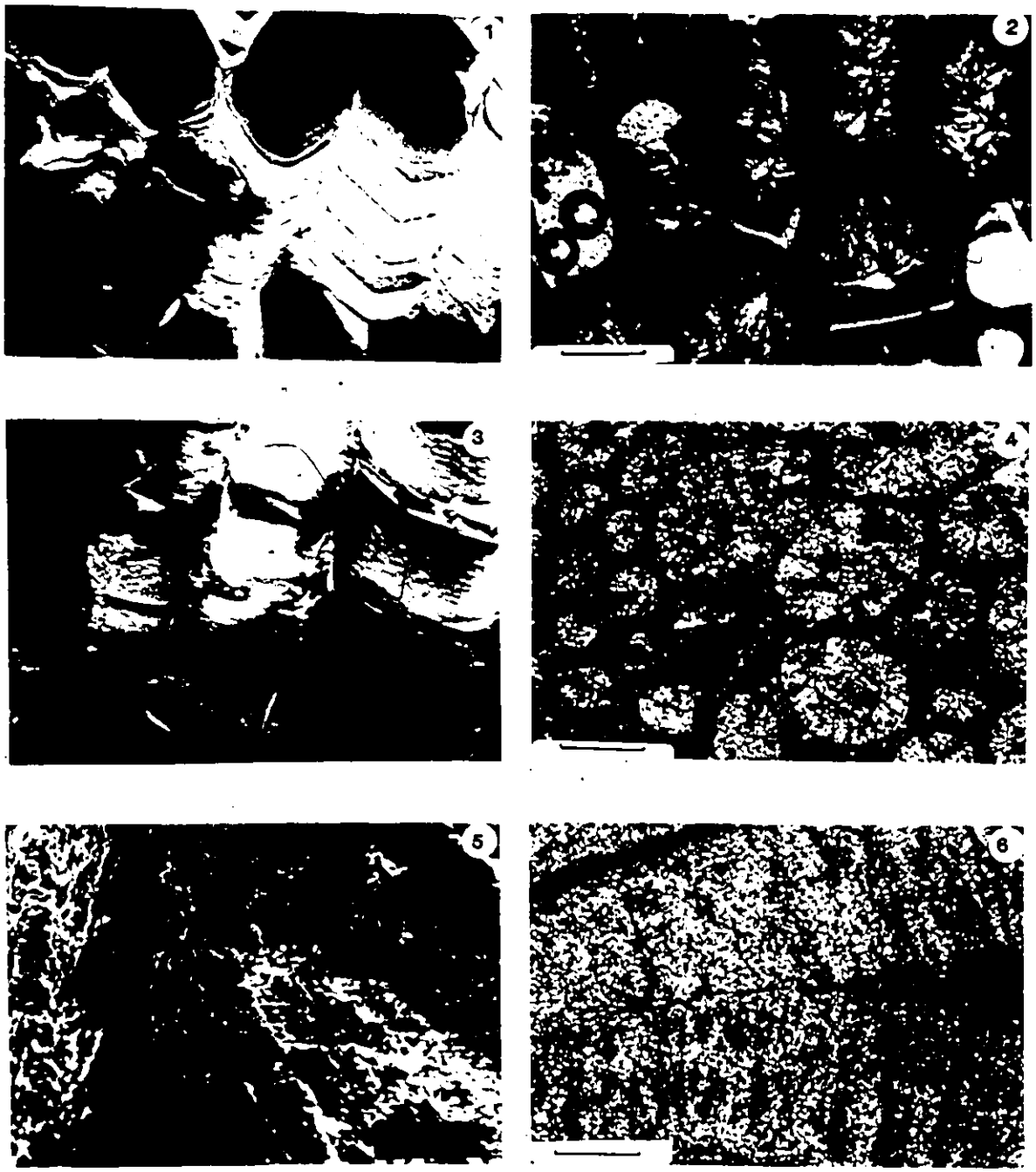
1
2
3
4
5
6

(b) Middle and Inner Layers

These two layers, which were presumably originally composed of aragonite, are usually poorly preserved. Traces of aragonite with crossed-lamellar ultrastructures are retained only in some well preserved specimens, such as Antillocaprina (Plate 5, Fig. 6; Plate 8, Fig. 4) and Plagioptychus (Plate 9, Figs. 1 and 2). SEM study reveals the presence of small pockets of cement and formation of fine granular crystals with irregular intercrystalline boundaries (Plate 9, Fig. 2), the latter due to recrystallization of crystallites (= calcitization of Bathurst, 1975, Chapter 12).

In addition to the above-discussed ultrastructural elements of caprinid shells, accessory cavities may also be present. These are usually infilled by micritic, partly fossiliferous, internal sediment or by spar cement.

1.4.2.4 Family Monopleuridae

Only the genus Monopleura from Jamaica and Puerto Rico was available for this study and the shell ultrastructure described below is based solely on this single genus. The shell has a thin, brown outer layer with moderately preserved simple prismatic compact (LMC) ultrastructure (Plate 2, Fig. 3; Plate 6, Fig. 3). The inner layer is also thin, with partly preserved brown,

pseudopleochroic, inclusion-rich relics. This layer contains possible remnants of lamellar ultrastructure, presumably of original aragonitic mineralogy (Plate 7, Figs. 5 and 6).

1.4.2.5 Family Requieniidae

Only eight specimens representing this family were recovered from the Urgonian Limestone of southeastern France. The requieniid shell has a large coiled, attached left valve and an operculiform-flat right free valve (Plate 2, Fig. 4). The outer layer is relatively thin (< 1 mm) and composed from simple compact prismatic (LMC) ultrastructure, with longitudinal non-ferroan prisms arranged at a right angle to the depositional surface (Plate 6, Fig. 4). This layer, however, is frequently, partially recrystallized.

The middle and inner layers have not been clearly documented. A thin (100 μ) layer underlying the outer layer has been observed in one requieniid shell and it contained remnants of pseudospar. The rest of the shell, including the body cavity, was infilled by micritic pelletal internal sediments containing some fossil fragments, such as rudists, foraminifera, and crinoid plates.

Summaries of the rudist ultrastructures and of their states of preservation are given in Table I-1.

PLATE 6
ULTRASTRUCTURES OF RADIOLITID, REQUIENIID, AND MONOPLEURID SHELLS

Fig. 1. Transverse section of a radiolitid prismatic outer layer (sample no. 173, Upper Cretaceous, Gulf Coast). Notice the enhanced growth of prisms. Crossed-polars. Bar scale: 0.5 mm.

Fig. 2. Inner originally aragonitic layer of Bournonia (sample no. 131, Upper Cretaceous, Jamaica). Notice the well preserved relics of crossed-lamellar ultrastructure. Crossed-polars. Bar scale: 0.5 mm.

Fig. 3. Transverse section of the outer shell layer of Monopleura (sample no. 127, Upper Cretaceous, Sunderland Inlier, Jamaica). Note the prismatic habit of the shell. Bar scale: 1.0 mm.

Fig. 4. Transverse section of the outer shell layer of a requieniid shell (sample no. 86, Urgonian Facies, southeastern France). Notice the simple, partly recrystallized, prisms. Crossed-polars. Bar scale: 0.5 mm.

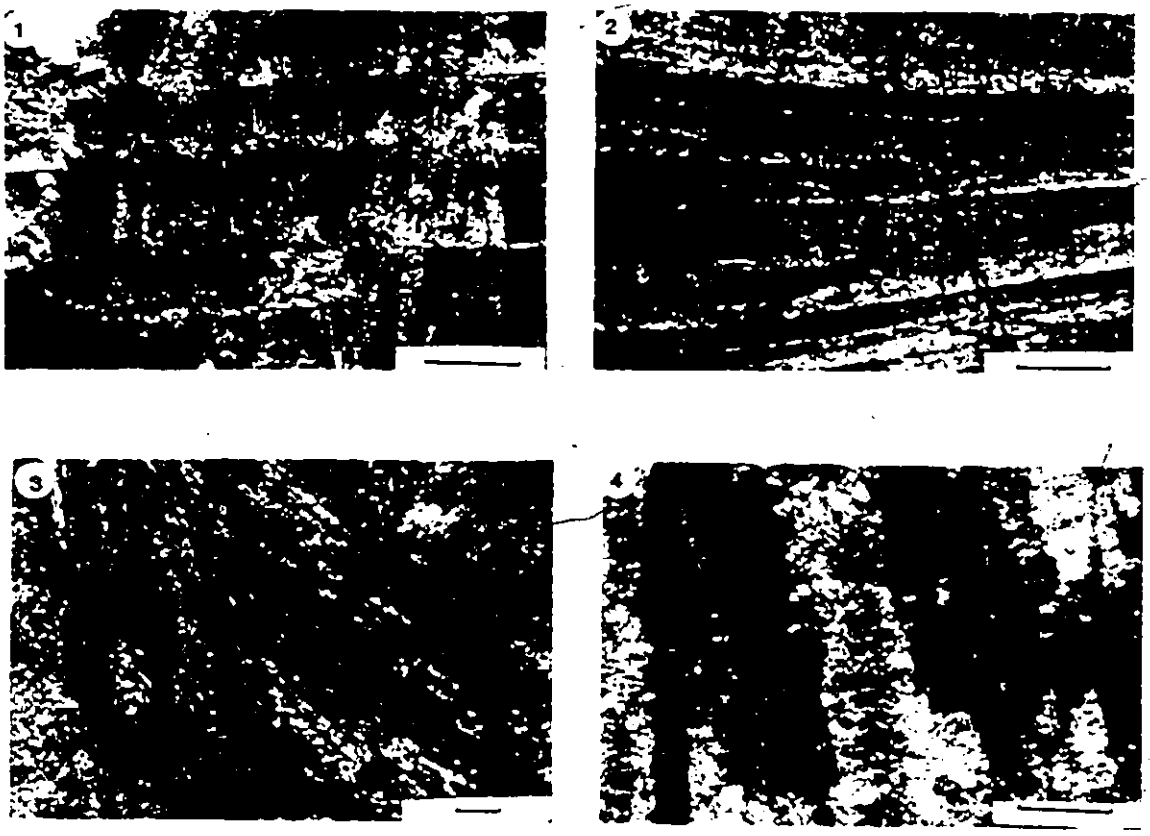
1
2
3
4

TABLE I-1

SUMMARY OF RUDIST ULTRASTRUCTURES, THEIR MINERALOGY, AND THE STATE OF PRESERVATION
(A: ARAGONITE, LMC: LOW-MG CALCITE)

FAMILY	SHELL ULTRASTRUCTURE			ORIGINAL MINERALOGY			STATE OF PRESERVATION		
	OUTER	MIDDLE	INNER	OUTER	MIDDLE	INNER	OUTER	MIDDLE	INNER
Hippuritidae	1. Compact-fine prismatic 2. Beaded prismatic 3. Composite-prismatic	Crossed-lamellar	Crossed-lamellar and complex crossed-lamellar	LMC LMC LMC & A	A	A	good fair good	fair to poor	fair to poor
Radiolitidae	1. Cellular-prismatic	Crossed-lamellar	Crossed-lamellar and/or complex crossed-lamellar	LMC	A	A	good to fair	seldom good fair to good	fair to poor
Caprinidae	1. Pallial canals "crossed-lamellar" 2. Rarely, thin prismatic (eg. Plagioptychus)	Crossed-lamellar	Crossed-lamellar	A LMC	A	A	Seldom good Mostly fair to good	fair to poor	fair to poor
Monopleuridae	1. Compact, fine prismatic	Lamellar		LMC	A		good to fair	fair	
Requieniidae	1. Compact, fine prismatic	Thin neomorphosed calcite	?	LMC	?	?	good to fair	poor	

1.4.3 Differential Preservation of Original Ultrastructures and Diagenetic Implications

The previous discussion of ultrastructures and mineralogy of rudist shells showed that, regardless of the family, they can be assigned to three types of preservation: (1) shells with preserved original mineralogy and ultrastructures; (2) shells with aragonite neomorphically transformed into LMC, but with well preserved relic ultrastructures; and (3) shells with no visible relic ultrastructures, usually containing only drusy calcite mosaic.

1.4.3.1 Shells with Original Mineralogy and Ultrastructures

Low-Mg calcite (= LMC) ultrastructures are present in most cases only in the outer layers, pillars and beads of Hippuritidae, the outer layers of Radiolitidae, the outer layers of Monopleuridae and the outer layers of Requieniidae. These components are, in general, well preserved with fine prismatic and cellular-prismatic ultrastructures. LMC, despite its relative stability, sometimes suffers differential recrystallization, which causes fusion of ultrastructural units and rounding of prism corners. This structural modification has been accompanied by chemical and isotopic signals (see Chapters II and III). A similar partial diagenetic

modification of LMC shells has been advocated previously on chemical and structural grounds for LMC belmnites (Veizer, 1974) and brachiopods (Al-Aasm and Veizer, 1982). This partial alteration of the shell matrix can be accompanied by incipient cementation between the planes of the prisms, and, in the case of the compact prismatic structure, by cementation in the primary intercrystalline pore spaces (Plate 3, Figs. 1, 2, 3, and 4). In addition, radiolitids, because of their cellular ultrastructure (intraparticle porosity; Choquette and Pray, 1970) frequently contain early micritic and/or peloidal internal sediment in their cells. This sediment may be recrystallized later to microspar. Alternatively, the cells may be infilled by one or more generations of cement (Plate 4, Figs. 1, 2, 3, and 4). However, the cell wall preserves its original identity and structure. Outer layers of some hippuritid and radiolitid shells were bored by organisms such as sponges, algae and perhaps bivalves causing obliteration of their prismatic ultrastructures. These early borings are of various sizes and shapes and later they may have been infilled by micritic peloidal internal sediments.

The differences in preservation of LMC layers of hippuritids and radiolitids may result in different chemical and isotopic signals. Such variations,

however, may reflect, principally, the types of primary porosity in the outer layers of both families as well as the structural architecture of their shells. This matter will be discussed in Chapters II and III of this thesis.

The preservation of the metastable aragonitic ultrastructures in some rudists (e.g. the outer layer of Parastroma (Plate 3, Figs. 5 and 6), the outer pallial canal layers of Antillocaprina (Plate 5, Fig. 1), Plagioptychus (Plate 5, Figs. 2 and 3), and the middle and inner layers of Bournonia) could be attributed to this embedding in organic-rich sediments of low permability (cf. Sohl, 1960a; Hudson, 1962; Kennedy and Hall, 1967).

1.4.3.2 Shells with Partially Preserved Ultrastructures

The ultrastructures of this group are usually preserved as brown, pseudopleochroic, inclusion-rich neomorphic spar with discernible crossed-lamellar features mimicing the original aragonite shapes (gross fabric retention of Wilkinson, 1983). This preservation is restricted to the middle and inner layers of hippuritids, radiolitids, caprinids, possibly requieniids and to some outer layers of pallial canal walls of caprinids.

The retention of relic structures in mollusc shells can be achieved only if the transformation of aragonite to low-Mg calcite occurs essentially in situ, without a cavity stage (Bathurst, 1964, 1975; Sandberg et al., 1973; Pingitore, 1976). Such polymorphic transformation (Bathurst, 1964) or neomorphism (Folk, 1965) is believed to have been a result of a wet dissolution-reprecipitation process on a micron scale. The absence, on petrographic and SEM scales, of large gaps and void spaces in the neomorphosed calcite mosaic and the irregular contacts of these calcites (Plate 7, Figs. 3, 4, 5, and 6; Plate 8, Figs. 1, 2, 3, and 4; Plate 9, Figs. 3 and 4) argue against the proposed porous chalkification stage during mineralogical transformation (e.g. Pingitore, 1976). These observations can, however, be reconciled with the transformation models based on a thin solution film principle (e.g. Pingitore, 1976; Brand and Veizer, 1980; Veizer 1983). The likelihood of solid state conversion of aragonite to calcite is very low because of the slow rates of the process (Fyfe and Bischoff, 1965; Carlson, 1983). XRD analysis of microsamples from a preserved relic crossed-lamellar ultrastructure in the inner layer of the hippuritid shell (Plate 7, Fig. 3) suggests, however, that the preservation of structural details may be at least partially due to the retention of some aragonite. The brown, well preserved, parts of the

PLATE 7
DIAGENETIC ALTERATION OF RUDIST SHELL ULTRASTRUCTURES

Fig. 1. Transverse section of outer canal layer of Antillocaprina (sample no. 157, Upper Cretaceous, Matanzas Province, Cuba), showing differential preservation of the rounded canal walls which appear as brown ghost relics. The interior areas of the shell are occupied by equant spar. Crossed-polars and stained. Bar scale: 0.5 mm.

Fig. 2. Transverse section of another type of canal in Antillocaprina (sample no. 133, Upper Cretaceous, Marchmont Inlier, Jamaica), where the polygonal canals have been occupied by early micritic pelletal internal sediment resulting in some preservation of relic canal walls. Plane-polarized light. Bar scale: 0.5 mm.

Fig. 3. Transverse section of the inner layer of a hippuritid (sample no. 43, Santonian Facies, southeastern France). Note the preserved relic crossed-lamellar ultrastructure of the inner layer, with large equant neomorphosed spar. A and B are microsampled areas for XRD. Bar scale: 0.5 mm.

Fig. 4. SEM micrograph of the same shell as in Fig. 3 showing the relic lamellar ultrastructure of the middle layer.

Fig. 5. Transverse section of Monopleura (sample no. 127, Upper Cretaceous, Sunderland Inlier, Jamaica) showing a relic, presumably originally aragonitic, ultrastructure appearing as dark inclusions within the inner layer. Plane polarized light. Bar scale: 0.5 mm.

Fig. 6. SEM micrograph of the inner layer of the same specimen as in Fig. 5, showing a relic of recrystallized lamellar ultrastructure.

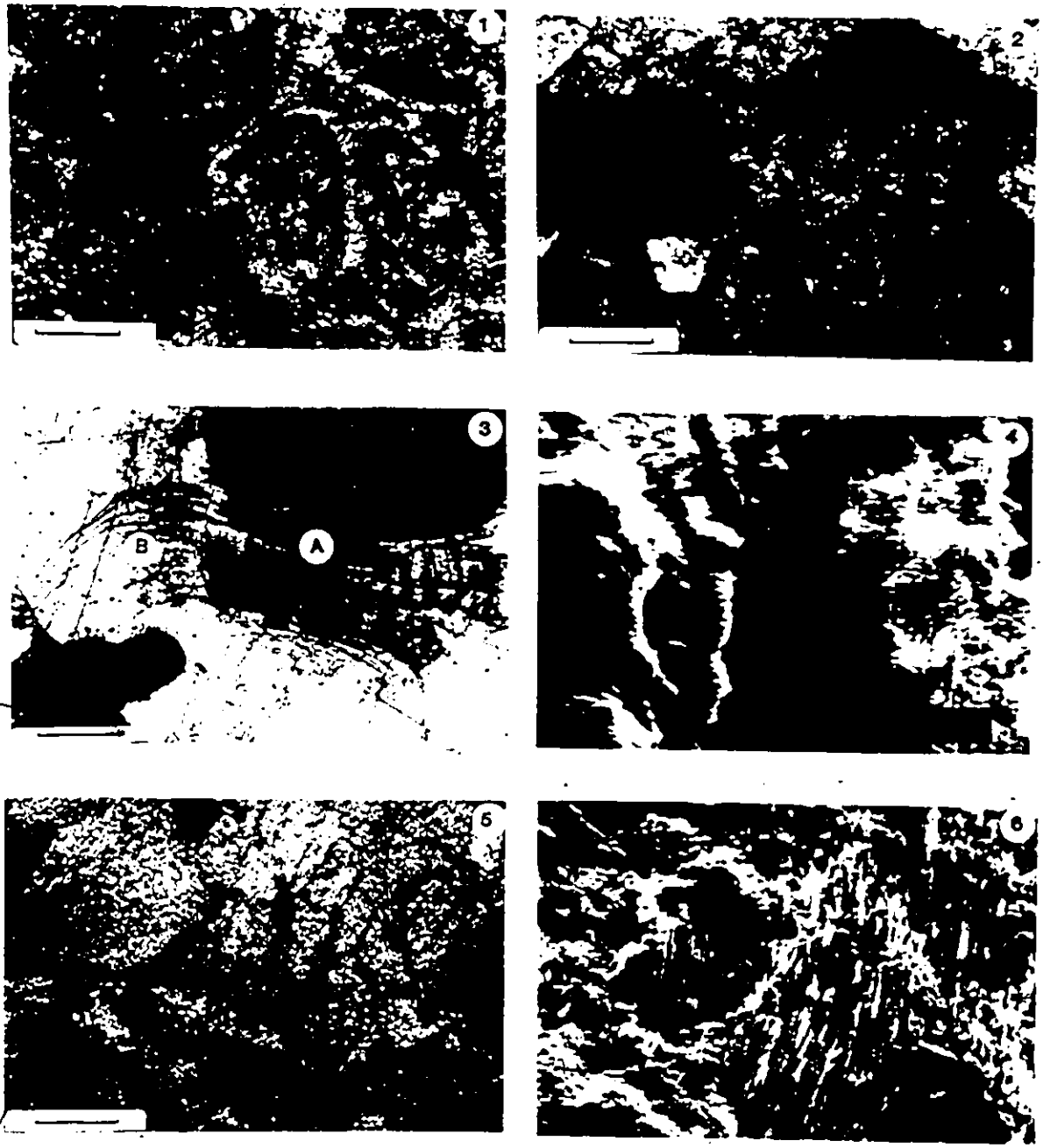
1
2
3
A
B
4
5
6

PLATE 8
DIAGENETIC ALTERATION OF RUDIST SHELL ULTRASTRUCTURES

Fig. 1. Transverse section of a radiolitid Chiapasella (sample no. 164, Upper Cretaceous, Pinar del Rio Proince, Cuba), showing parts of the middle and inner layers. The middle layer contains inclusion-rich relic ultrastructure whereas the inner layer consists of bladed, crystalline, inclusion-rich cement. Crossed-polars. Bar scale: 0.5 mm.

Fig. 2. SEM micrograph of the same sample as in Fig. 1 showing the middle layer with a relic lamellar ultrastructure which has undergone severe recrystallization.

Fig. 3. Transverse section through a part of the pillar of hippuritid Vaccinites giganteus (sample no. 58, Upper Cretaceous, southeastern France). It shows fine prismatic compact ultrastructure (rarely bored) of the outer part (A), and a part of the middle layer of a pseudo-pleochroic neomorphosed calcite (B). Note also some micritic envelopes beneath this layer (C). Crossed-polars. Bar scale: 0.5 mm.

Fig. 4. SEM micrograph of Antillocaprina (sample no. 176, Upper Cretaceous, San German Formation, Puerto Rico), showing crossed-lamellar ultrastructure.

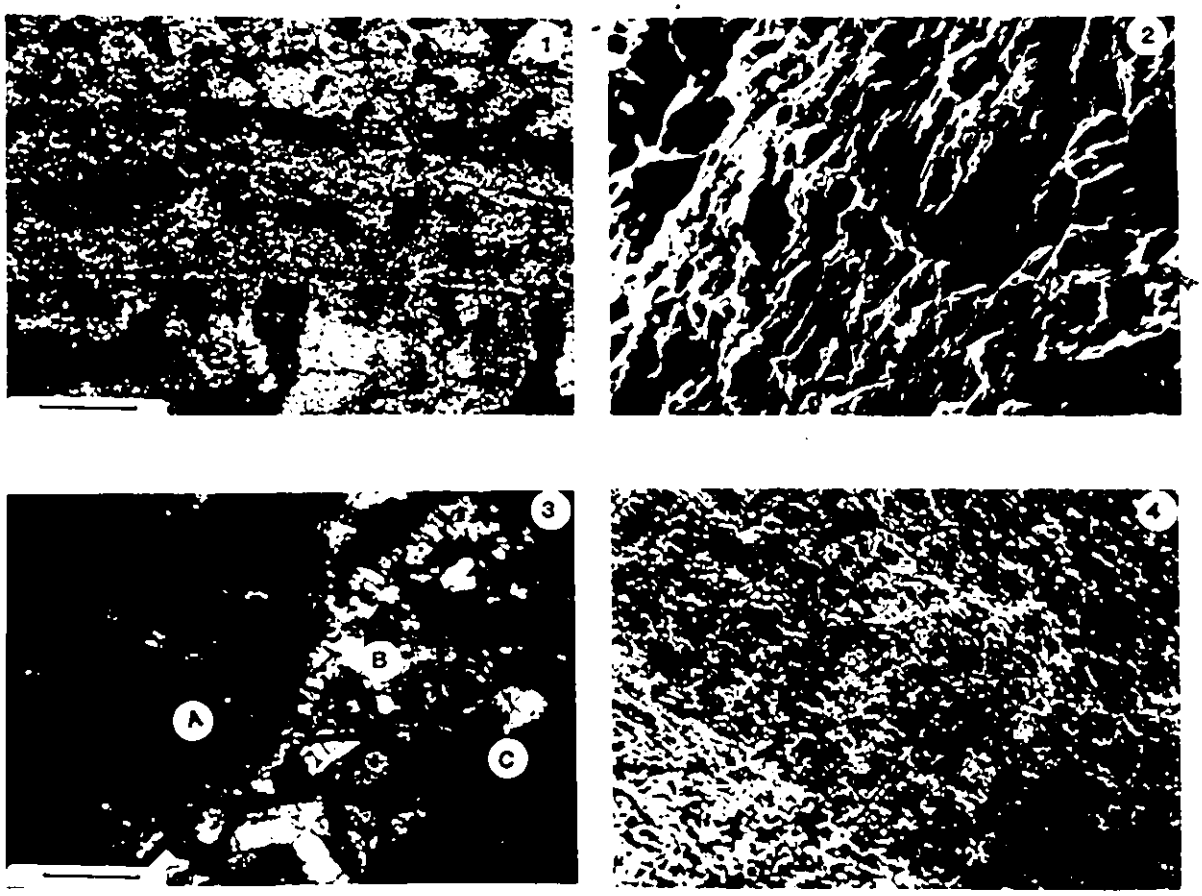
1
2
3
A
B
C
4

PLATE 9
DIAGENETIC ALTERATION OF RUDIST SHELL ULTRASTRUCTURES

Fig. 1. Transverse section of the multilayered Plagioptychus (AV) (sample no. 153, Upper Cretaceous, Marchmont Inlier, Jamaica). Notice the thin prismatic, partly preserved, outer layer and the middle and inner layers with preserved crossed-lamellar relic ultrastructure. Crossed-polars. Bar scale: 0.5 mm.

Fig. 2. SEM micrograph of the outer layer of the same specimen as in Fig. 1. Recrystallization of the preserved original prismatic layer into granular crystallites and partial cementation.

Fig. 3. Transverse section of another part of the inner layer as in Fig. 1 and 2, showing well preserved crossed-lamellar ultrastructure (A) and the micritic body cavity fill (B). Crossed-polars. Bar scale: 0.5 mm.

Fig. 4. SEM micrograph of Antillocaprina (sample no. 137, Upper Cretaceous, Marchmont Inlier, Jamaica), showing the crystalline nature of the middle layer.

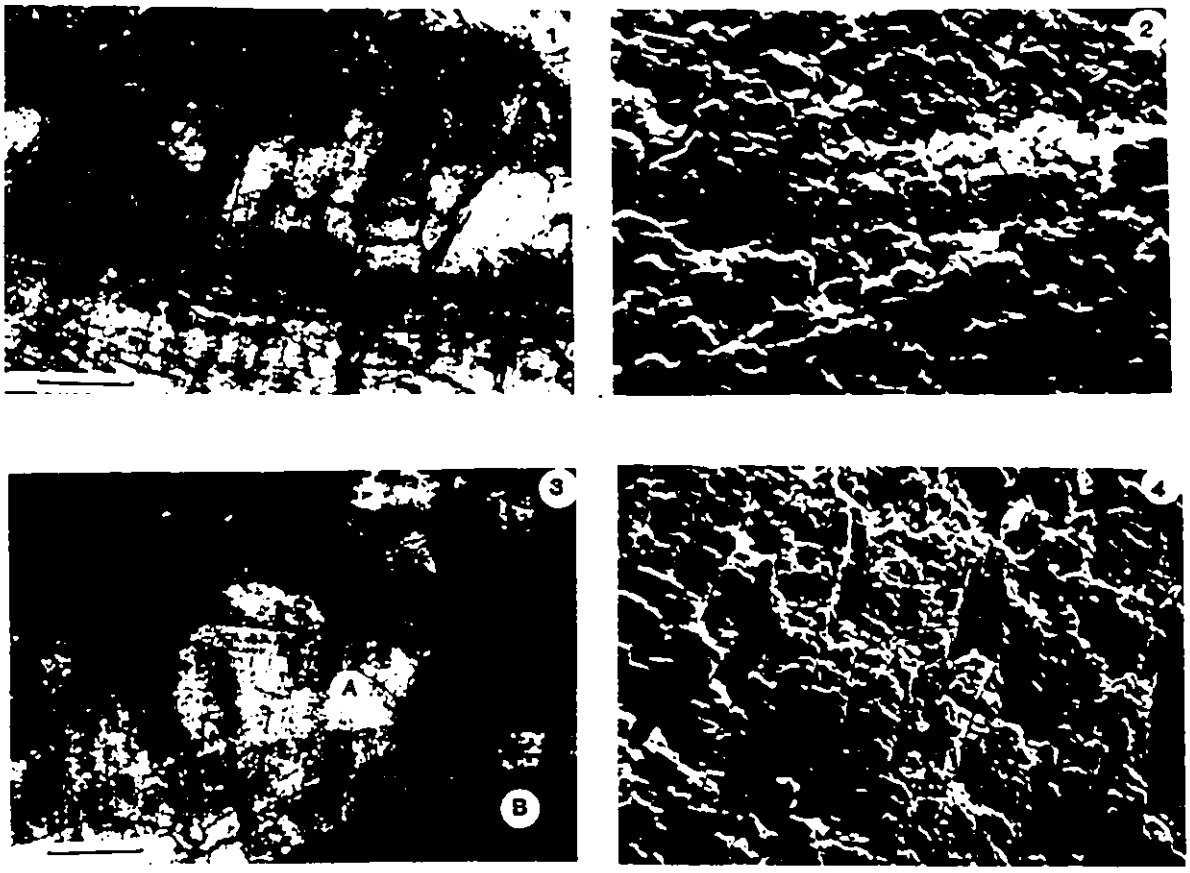
1
2
3
A
B
4

of the structure (A) are composed primarily of aragonite, whereas the adjacent, more abundant and more altered parts with frequent clear irregular neomorphic mosaic (B) are principally calcite. In addition, it has been observed, that ultrastructures with relic aragonitic traces have retained some original chemical and isotopic signals, if compared to those shell components which lack visible relic structures (see Chapters II and III for details).

1.4.3.3 Shells with No Visible Relic Ultrastructures

These shells underwent almost total leaching and subsequent replacement by calcite cement (wholesale fabric obliteration of Wilkinson, 1983). Such transformation is typical of many outer layers of caprinids, which were originally composed of aragonite. In addition, the high original porosity of this outer pallial canal layer resulted in internal peloidal and/or micritic sedimentation during early diagenetic history. Furthermore, this porosity enabled active flushing of the system by meteoric waters, leading to complete leaching of the walls and to preservation of only micritic envelopes which were formed during an earlier stage. A combination of all these phenomena resulted in a complete loss of the original ultrastructures. Plate

7 (Figs. 1 and 2) shows the progressive stages in diagenesis of pallial canals.

The middle and inner layers of hippuritids, radiolitids, caprinids, monopleurids and possibly requieniids also suffered complete dissolution and subsequent infilling by clear equant ferroan spar calcite (Plate 4, Fig. 5).

In analogy to caprinids, the highly open network of the outer cellular radiolitid ultrastructures also resulted in the infill of the cells either by marine micritic sediment or by early to late equant spar cement (see subsequent sections for details).

1.4.4 General Sequential Diagenesis in Rudist Buildups

Since most rudists thrived in warm, shallow, well circulated, clear waters, associated primarily with carbonate platform and shelf facies, they eventually were subjected to a variety of diagenetic processes. The emphasis in the subsequent text will be on the general diagenetic evolution of rudist carbonate buildups in Cretaceous deposits. This approach, because of the wide geographic distribution of the studied rudist communities, does not explain all local vagaries of their varied diagenetic histories, but it will enable the erection of a suitable sequence of events for later geochemical interpretations.

1.4.4.1 Diagenetic Environments in Carbonate Rocks

Diagenesis, as defined here, is the sum of all processes (physical, chemical and biological) that bring about changes in a sediment or sedimentary rock deposited in water (Berner, 1980). Two major diagenetic environments, with their subdivisions, can be held responsible for lithification and alteration of carbonate components (Flügel, 1982). These are: (1) submarine phreatic environments; and (2) meteoric environments. Bricker (1972), Folk (1974), Bathurst (1975), Moore (1979), Longman (1980, 1981), Flügel (1982), Heckel (1983), and Lohmann (1983) summarized the characteristics of each diagenetic realm and this summary is presented below.

1. Submarine phreatic environment

This environment is related to shallow depth, with the pore system filled by marine waters (e.g. seaward side of platform margins, reef cavities, etc.). It has been subdivided into two zones (Longman 1980):

(a) Active Zone. In this zone tides, waves and currents, in combination with other processes such as photosynthesis, respiration of organisms and CO_2 degassing, are responsible for moving the water into sediments. The result is cementation by aragonite and high-Mg calcite (Shinn, 1969; Alexanderson, 1972; James

et al., 1976). Turbulence is required, since tens to hundreds of thousands of pore volumes of sea water are needed to fill the pore spaces with cement (Bathurst, 1980). Some of the characteristic products of this zone are the formation of isopachous fibrous and micritic aragonitic cements, botryoidal aragonite (Ginsburg and James, 1976), micritic high-Mg calcite rims, borings in cement, and interbedded cements and sediments (see Longman, 1980 for a summary).

(b) Stagnant marine zone. In this zone, water movement through the sediment is relatively slow, with some micritization (Kobluk and Risk, 1977) and no cementation. Lohmann (1983) proposed a third zone, namely the burial marine phreatic zone, which is characterized by burial of marine sediments with their entrapped water under the conditions of elevated temperature and compactional load.

2. Meteoric environment

This environment is subdivided into:

(a) Meteoric vadose zone. This zone lies below the land surface and above the water table, where both air and fluids may occupy the pores. The pore waters, mainly rain waters, are highly undersaturated with respect to calcite or aragonite, causing extensive leaching of these minerals. Longman (1980) divided

this zone into two parts; the soil zone, typified by dissolution of metastable carbonate components, and the zone of precipitation, typified by minor cementation (e.g. meniscus cements of Dunham, 1971; gravitative or pendant cements of Muller, 1971; and Jacka and Brand, 1977).

(b) Meteoric phreatic zone. This zone is considered to be the most important diagenetic realm for shallow marine sediments (Longman, 1981). All pores are filled entirely with meteoric waters undersaturated with respect to aragonite and high-Mg calcite. The zone lies between the vadose and the mixed marine-meteoric water zones. Cementation in this realm is generally in the form of a fine to coarse granular equant calcite spar in intergranular or moldic pore spaces. This zone has been subdivided further (Longman, 1980) into :

i) undersaturated subzone, where the phreatic water is undersaturated with respect to $CaCO_3$ (such as in caves or fractures), causing dissolution of sediments and forming moldic and/or vuggy porosity;

ii) active saturated subzone, with a possibility of extensive cementation. This is due to active water circulation through the sediments. The common diagenetic features of this stage are equant calcite spars which coarsen towards the center of the pore; syntaxial overgrowths on echinoderms, isopachous bladed

calcites, and complete leaching of metastable carbonate components (for additional details, see Bricker (1971)); and

iii) stagnant phreatic subzone, characterized by minor or no cementation. Metastable carbonate components may be neomorphically altered to low-Mg calcite with preservation of some relic ultrastructures. These products are due to slow movement of phreatic waters.

(c) Mixing zone. This zone is present where the meteoric phreatic lens is mixed with the underlying marine phreatic waters. The zone is characterized by undersaturation with respect to $CaCO_3$, and oversaturation with respect to dolomite (Badiozamani, 1973).

(d) Burial subsurface phreatic zone (Lohmann, 1983). This zone represents a system isolated from the shallow phreatic environment and where both, lithostatic pressure and compaction are active. Cementation products here are fine to coarse granular sparry calcites.

1.4.4.2 Diagenetic Stages of Rudist Carbonate Buildups

Previous studies of rudist buildups (reefal and nonreefal facies), for both eastern and western

hemispheres, produced evidence for early, as well as late, diagenetic phenomena (Rose, 1970; Bein, 1976; Achouer, 1977; Jacka and Brand, 1977; Kerr, 1977; Petta, 1977; Longman and Mench, 1978; Bay and Bebout, 1983). These phenomena encompass both marine and meteoric diagenetic realms.

Several diagenetic events or stages (with one or more events absent in some samples), have been recognized in the studied rudists and their enclosing rocks. Table I-2 shows a summary of these diagenetic stages (for discussion of geochemical and isotopic data, see Chapters II and III).

1.4.4.2.1 Stage I: Deposition and Calcification of Rudist Communities

The warm, shallow, clear, well circulated, oxygenated shelf and platform waters were ideal for the creation and biological explosion of the benthic rudist communities. As mentioned earlier (Section 1.2), the rudists were dominantly cemented or attached to the muddy or sandy substrate by one of their valves and they grew in a crowded bizarre form (Kauffman, 1974).

The primary porosity of rudists was variable, depending primarily on shell architecture. It was moderately high in caprinids and radiolitids and relatively low in hippuritids, monopleurids and

TABLE I-2
SUMMARY OF DIAGENETIC EVENTS IN RUDIST CARBONATE BUILDUPS
(*: Well Preserved Specimens)

STAGE	ORIGINAL AND DIAGENETIC PHENOMENA	DIAGENETIC REALM					GEOCHEMICAL SIGNATURE		
		Shallow Marine	Shallow Meteoric				Trace Elements (in ppm)	$\delta^{18}O$‰	$\delta^{13}C$‰
			Burial	Phreatic	Mixed	Vadose			
I	Deposition and calcification of rudists communities (A+LHC)	←					A components*: Sr=1790, Mg=70, Mn=5, Na=2730, Fe=85	-2.2	+3.5
							LHC components*: Sr=985, MG=3810, Mn=65, Na=353, Fe=375	-3.8	+2.0
II	Syndepositional Diagenetic events:						Sr=1500, Mg=4995, Mn=134, Na=110, Fe=760	-4.0	+3.1
	1. Rudists framework borings and formation of micrite envelopes	←							
	2. Internal peloidal sedimentation	←							
	3. Submarine cementation (A+HMC)	←							
	4. No leaching of metastable components (complete fabric preservation)	←							
III	Early subaerial and shallow burial:						Sr=1240, Mg=3710, Mn=370, Na=645, Fe=835	-3.6	+0.5
	1. Neomorphic replacement of aragonitic shell parts in under-saturated micro-environments (partial preservation of original ultrastructures)			- - -		- - -			
	2. Partial collapse of shell components with slight compactional features.		- - -						
IV	Meteoric water diagenesis:						Sr=595, Mg=5625, Mn=2755, Na=155, Fe=3530	-9.2	-4.5
	1. Cementation of pore spaces in rudist shell ultrastructure (intraskeletal porosity) by equant and bladed spars (LHC).			←	- - -				
	2. Wholesale fabric leaching of the remaining aragonitic shell parts with consequent cementation by clear equant ferroan LHC cements (moldic porosity)			←			Shells: Sr= 605, Mg=4145, Mn=185, Na=105, Fe=925	-5.1	+1.0
							Cements: Sr=650, Mg=3015, Mn=505, Na=90, Fe=980	-6.3	+1.1
V	Final recrystallization of the originally preserved LHC components and of the stabilized micrites			←	←	←	LHC phase: Sr=600, Mg=3265, Mn=195, Na=390, Fe=385	-4.5	+1.2
							Internal sediments: Sr=680, Mg=3890, Mn=435, Na=140, Fe=970	-5.2	+0.4

requieniids. This was due (cf. Section 1.4.2) to the presence of open network ultrastructures in the former group while the latter group was characterized by compact ultrastructures. This high primary porosity was a result (Choquette and Pray, 1970) of intraparticle porosity in the cellular open ultrastructures and of intercrystalline porosity in the prismatic layers (Plate 4, Figs. 1, 2, and 3; Plate 3, Figs. 1, 2, and 4). In addition, living body chambers or cavities could be considered as being primary void spaces. At this stage, original mineralogy of carbonate components is still preserved.

1.4.4.2.2 Stage II: Syndepositional Diagenetic Events: Constructive and Destructive Processes

These events include rudist framework borings, formation of micritic envelopes, internal sedimentation, and early submarine cementation.

Rudist Framework Borings

Activities of organisms play an important role in carbonate buildup, especially reef dynamics. Organisms which penetrate hard carbonate substrates by chemical or mechanical means, are called borers and the resulting excavations are termed borings (Milliman, 1974; Golubic et al., 1975; Warme, 1975). Boring organisms, their

types and morphologies, have been studied previously in the Comanche Cretaceous of Texas (Perkins, 1971; Petta, 1977), in the Greater Antilles rudist-bearing rocks (Kauffman and Sohl, 1974), and in southeastern France (Philip, 1980; Maurin et al., 1981). These borers were abundant in shallow Cretaceous seas and contributed variably as important bioeroders and sediment producers. Some of these borers are bacteria, fungi, algae, sponges, bivalves, barnacles, and worms (Perkins, 1971).

Rudist shells in the studied localities have experienced various degrees of boring activities, having bores of various shapes and sizes. Most of the observed borings were restricted to the outer layers of the shells. However, in some specimens, middle and inner layers have also suffered some boring activities. The borings are oval, elliptical, longitudinal, tube-like, or irregular in outlines (Plate 10). Their sizes range from <50 μ to few mm in diameter. The present borings are remnants of borings produced by algae (blue-green and red), sponges (probably clionid sponges), bivalves, and some other unidentified organisms. The borings, in most cases, are primary features formed during accretion of carbonate buildups. In some examples, they post-date neomorphic inversion of aragonitic parts, as evidenced by cross cutting or superposition of borings on the already transformed

PLATE 10. Photomicrograph of a portion of a bored radiolitid shell "Biradiolites" (sample no. 99, Middle Cretaceous, Santa Clara Province, Jamaica) showing part of the outer cellular layer (A), middle layer (B) and inner layer with brown relic ultrastructure (C). Note that the borings are superimposed on the already neomorphosed, originally aragonitic, middle and inner layers. Plane polarized light and stained. Bar scale: 1.0mm.

PLATE 11. Collapsed micritic envelope (A) in the inner part of a radiolitid shell (sample no. 47, Santonian facies, southeastern France). Original aragonitic shell layer was totally dissolved and replaced by late diagenetic equant sparite (B). Crossed-polars and stained. Bar scale: 0.5mm.

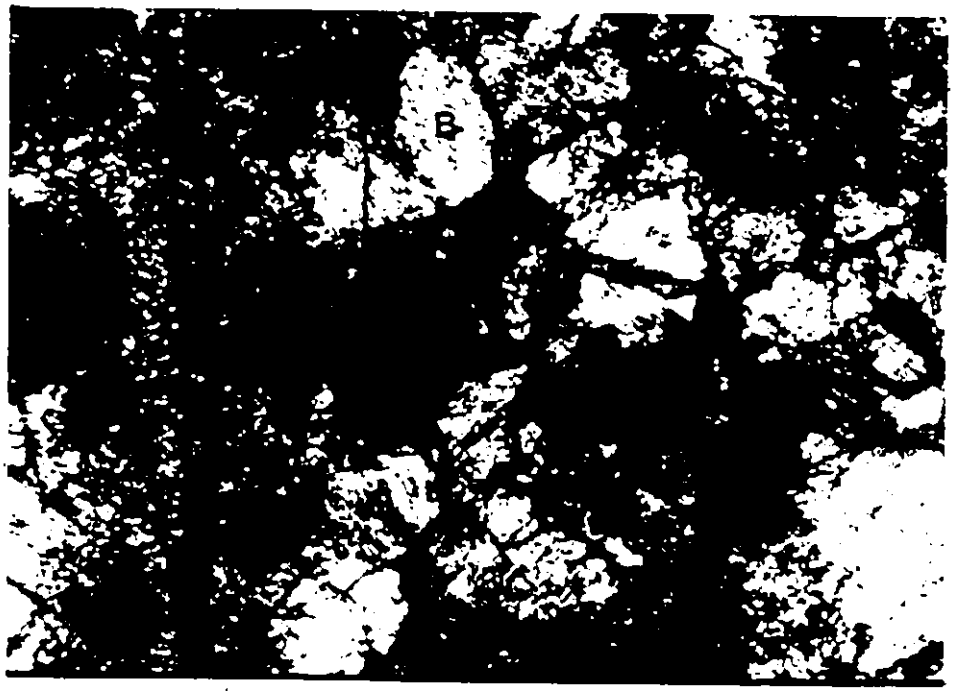
B

aragonitic components of the shells (Plate 10). Mineralogical inversion could have been achieved during short time periods during which rudists were subaerially exposed to vadose environment. Subsequently, they have been again submerged and bored. Borings in rudists are often infilled by marine internal sediments. These sediments are sometimes comparable, compositionally and texturally, to internal sediments in major body cavities or to enclosing rock. They are usually micritic, silty and peloidal, with some fossil fragments. In the later stages, they could have been partially cemented by equant spar.

Bathurst (1966) and Kobluk and Risk (1977) attribute the presence of micritic envelopes, or micritic rims in mollusc shells, to vague processes of organic boring and skeletal degradation by endolithic algae and fungi. Such micritic rims are common in modern carbonate sediments (Winland, 1969). Micritic envelopes may have been composed originally of aragonite and high-Mg calcite and later transformed into low-Mg calcite, but their textural identity remains intact (Friedman, 1975). They have been observed as the internal components of rudists (see Section 1.4.3), particularly in the middle and inner skeletal layers as well as in body cavities (Plate 11). In addition, micritic rims have been observed surrounding and

lining some caprinid canals (Plate 12). Such envelopes may have originated in submarine environments through the activity of algal boring which have been infilled by lime mud (Bathurst, 1975, Chapter 9).

Internal Sedimentation

Internal marine sediment, which sometimes may be mistaken for vadose silt of Dunham (1969), is defined in this thesis as all micritic to silty, peloidal - with or without fossil fragments - sediment (wackestone) that fills primary pore spaces within rudist shells. It usually fills: (a) some caprinid canals and radiolitid cell chambers, sometimes forming geopetal fabrics (Plate 12); (b) many borings; and (c) major and accessory vacated body cavities. The allochems in the internal sediments are micrites of $<4\ \mu$ in crystal sizes (Plates 12; 13; Plate 22, Figs. 1 and 2) rounded to oval peloids of structureless micrite with diameters $<200\ \mu$, and fossil fragments mostly of rudist shells, foraminifera (e.g. miliolid), crinoidal plates, bryozoans and corals. The latter were in some instances leached away, leaving behind an empty mold which was later filled with equant spar. Rarely, detrital quartz also contributes as an allochem. Internal sediments in many rudist shells resemble, compositionally and texturally, their enclosing rocks.

Internal marine sediments have been described from

PLATE 12. Geopetal fabric in caprinid canals (sample no.199, Edwards Limestones, Texas) infilled by micritic pelletal internal sediments. Notice the partial preservation of canal walls as inclusion-rich areas (A). Crossed-polars and stained. Bar scale: 1.0mm.

PLATE 13. Internal marine sediments infilling major body cavity of a requieniid shell (sample no. 80, Urgonian facies, southeastern France). The sediments are micritic, pelletal with some miliolids. Miliolid chambers are occupied by equant spar. Plane polarized light. Bar scale: 0.5mm.

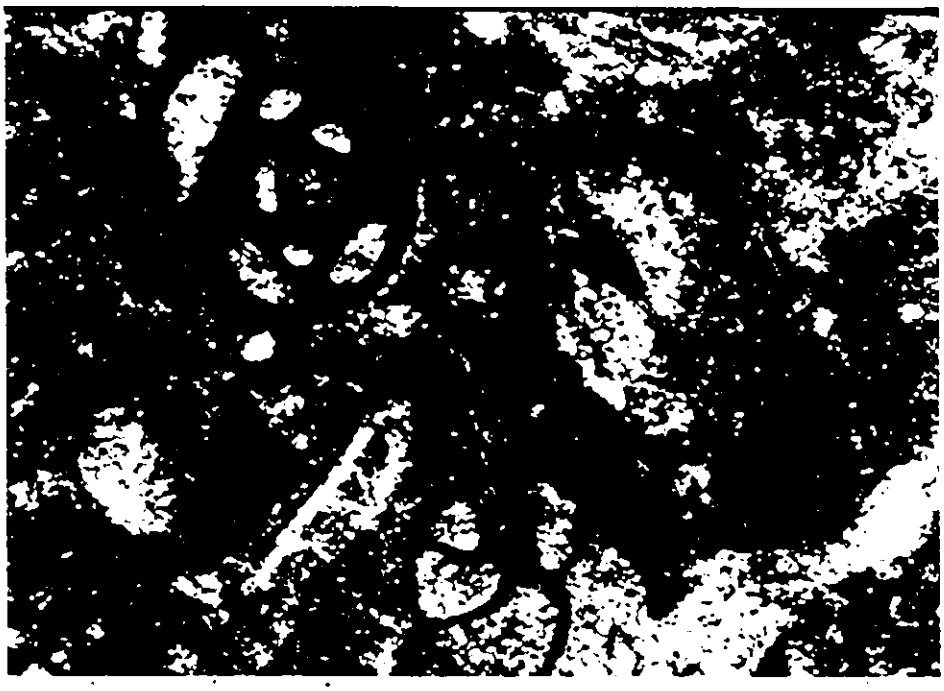

modern reefs (fine to coarse-grained, peloidal to fossilfierous algae cup reefs of Bermuda (Ginsburg et al., 1971); Jamaican coral reefs (Land and Goreau, 1970)), as well as from ancient deposits (Kendall, 1975; Petta, 1977; Frost et al., 1983). Mineralogically, the recent internal sediments are a mixture of aragonite and high-Mg calcite (Shinn, 1971; James et al., 1976; Marshall, 1983). The mud size sediment is believed to have originated by the breakdown of worm tubes, foraminiferal tests, and coralline algae. In contrast, the silt size particles are thought to have been formed by boring organisms, especially in the reef environment (Flügel, 1982, Chapter 4; James, 1983). In the present context, because of the mud and silt sizes of bioclastic constituents, the internal sediments in rudists are believed to have originated by mechanical movement and breakdown of organisms, as well as by boring activities.

Submarine Cementation

Submarine cementation is mostly achieved in environments where both water turbulence and stabilized sediments play a major role. Such environments are, for example, reefs, particularly in the vicinity of platform margins (James and Choquette, 1984). Both high Mg-calcite and aragonite were reported as submarine cements filling primary voids in modern carbonate reefs.

Examples are the Belize reefs (Ginsburg and James, 1976; James et al., 1976), the Galeta point reef of Panama (MacIntyre, 1977), the Jamaican reefs (Land and Goreau, 1970), the Red Sea reefs (Friedman and Schneiderman, 1974), and the Arabian Gulf reefs (Shinn, 1969). Submarine cement precursors were reported also from ancient examples as old as the Early Paleozoic (Rose, 1970; Achauer, 1977; Davies, 1977; Petta, 1977; Bathurst, 1982).

Some primary pore spaces, such as the cell chambers in radiolitids, originally vacant canals in caprinids, and other body cavities in rudists have been occluded partly by precipitation of non-ferroan radiaxial fabric and isopachous rim cements. Radiaxial fabric cement is characterized by cloudy, inclusion-rich, long fibrous crystals, with divergent subcrystals and convergent optical axes, and wavy extinction under cross polarization (Plate 14). This type of early cement has been described in detail by Bathurst (1975). The isopachous rim cement consists of thin (<200 μ) rinds of fine equant to bladed, inclusion-rich crystals lining some primary pores (Plate 15).

The evidence utilized to interpret the submarine origin for these cements is: (1) they are always the first generation of cements; (2) their inclusion-rich character suggests a marine phreatic water; (3) their crystal morphology is mostly isopachous or radiaxial; (4)

PLATE 14. Early radiaxial, inclusion-rich, fibrous cement of submarine origin filling a void in the caprinid "Titanosarcolites" (sample no. 150, Upper Cretaceous, Marchmont inlier, Jamaica). Notice the cloudy nature of this cement with curved twin crystals. Crossed-polars and stained. Bar scale: 1.0mm.

PLATE 15. Early inclusion-rich micrite rim (A) cementation, lining a primary void in radiolitid shell (sample no. 77, Coniacian facies, southeastern France). This cement is followed by precipitation of meteoric ferroan equant spar (B). Plane polarized light and stained. Bar scale: 0.5mm.

they are interbedded with internal marine sediments containing marine faunas (cf. James and Klappa, 1983); (5) they have borings that transect or are superimposed over the cements. These borings may represent periods of slow or absent cementation (Plate 10); and (6) they have specific chemical and isotopic signals. (This topic will be discussed in detail in Chapters II and III, respectively.)

1.4.4.2.3 Stage III: Early Subaerial and/or Shallow Burial Diagenesis

During this stage, aragonitic shell parts of rudists have been inverted neomorphically into low-Mg calcite, with preservation of their ultrastructures as clear relics in micro-sized domains. This was likely achieved during short periods of exposure to undersaturated meteoric vadose waters or to a stagnant zone of meteoric phreatic waters. These physical environments permitted inversion of original metastable carbonate phases without destruction of the bulk of their primary porosity (cf. Longman, 1980; and Heckel, 1983, for further details). Such diagenetic stabilizaton of carbonate minerals has been discussed in detail in Section 1.4.3.

Partial compaction and fracturing within rudist shells resulted in breakage of outer and inner layers,

collapse of micritic envelopes, and formation of small veins. This partial compaction is believed to have been caused either by an early local compaction caused by the stress imposed by the weight of crowded living rudists or by pressure during shallow burial. Both of these processes appear to have been confined to the early diagenetic history of rudists, because the breakage of shell components and the collapse of micritic envelopes pre-date late equant ferroan cement but post-date early marine cementation (Plate 11).

Microstylolites, noticed in few samples (Plate 16), represent zones of discontinuity generated from pressure solution around points of contacts (cf. Wanless, 1983, for details).

1.4.4.2.4 Stage IV: Diagenesis in Meteoric Waters

Exposure to meteoric phreatic waters has affected rudist shells and their enclosing rocks in a variety of ways. Primary interparticle and intraparticle porosities were reduced further by precipitation of one or more generations of bladed and equant calcite cements. Secondary moldic and vuggy porosities have been created by the wholesale dissolution (cf. Wilkinson, 1983) of the mineralogically metastable shell components. In addition, silicification and dolomitization played a minor role at this stage. The

PLATE 16. Microstylolite in a hippuritid shell (sample no. 56, southeastern France). It represents a solution zone in the inner part of the shell and is caused by partial compaction. Plane polarized light and stained. Bar scale: 0.5mm.

PLATE 17. Two episodes of meteoric water cementation; bladed (A) and large equant spar (B) infilling a vacant body cavity of the radiolitid shell "Bournonia" (sample no. 121, Upper Cretaceous, Marchmont inlier, Jamaica). Crossed-polars and stained. Bar scale: 1.0mm.

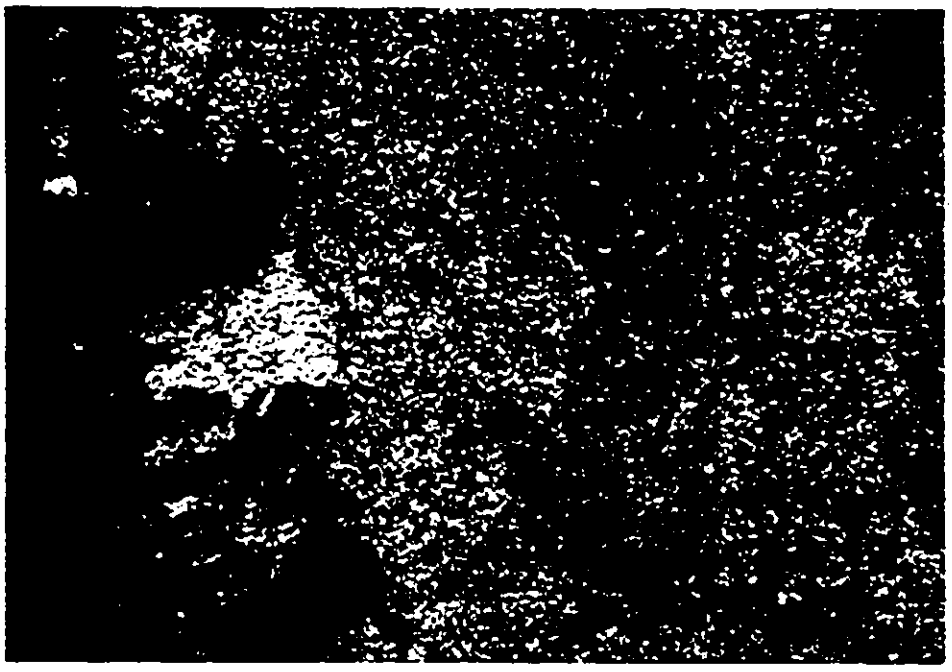

primary and secondary pore systems have been occluded, to various degrees, during single or multiple episodes by nonferroan to slightly ferroan equant and bladed low-Mg calcite cement, followed by the late large equant ferroan cement with straight crystal boundaries and abundant enfacial junctions (cf. Bathurst, 1975, Chapter 10). Congruent and incongruent dissolutions of aragonitic (both shell layers and submarine cements) and high-Mg calcitic (early submarine fibrous cement) parts have been accomplished during shallow and burial meteoric stages of diagenesis. Continuous dissolution of these metastable carbonate phases eventually resulted in the supersaturation of the pore water with respect to the least soluble phase (low-Mg calcite), which then precipitated as sparry calcite (cf. Gavish and Friedman, 1969; Bathurst, 1980, 1983). The morphology, composition and mineralogy of the precipitated calcium carbonate are believed to have been governed by such factors as kinetics of surface nucleation and the amount of reactants (Given and Wilkinson, 1984). The response of rudist shells to meteoric phreatic diagensis has been discussed earlier (Section 1.4.3.3).

Bladed low-Mg calcite cements are elongated crystals of nonferroan to slightly ferroan calcite, projecting inward normal to the pore walls (Plate 17; Plate 22, Figure 3). The early equant calcite cement

PLATE 18. Two stages of cementation occluding a radiolitid cell chamber (Sauvagesia; sample no. 162, Havana Province, Cuba). The relatively early nonferroan equant cement (A) is followed by late ferroan equant calcite (B). Notice the cell wall which exists as brown preserved boundary (C). Plane polarized light and stained. Bar scale: 0.5mm.

PLATE 19. Late large equant spar filling a major body cavity of the hippuritid shell (sample no. 16, Santonian facies, southeastern France). Crossed-polars and stained. Bar scale: 1.0mm.

is composed of fine (≥20 μ) nonferroan to slightly ferroan crystals, which sometimes occlude primary pore spaces, such as radiolitid cells and caprinid canals. They usually form a thin rim with some inclusions (Plate 18). Both of these types of cements post-date early submarine cements and internal sediments and pre-date late coarse, clear, equant, ferroan, inclusion-free cement. The latter is characterized also by an increase in crystal size towards the center of the pore (Plates 17; 18; 19; Plate 22, Figs. 3, 4, 5, and 6).

Other diagenetic features, such as authigenic silicification and dolomitization, have been noticed in few samples and they were confined to primary intraskeletal pore spaces (Plates 20 and 21).

1.4.4.2.5 Stage V: Final Recrystallization of Rudist Components

The culmination of diagenesis of rudists was the recrystallization of the stable low-Mg shell parts and of the already stabilized, originally metastable, micritic and other components. Recrystallization, however, may have started earlier, but it reached its peak during this stage.

Recrystallization has affected different parts of the shell, such as the outer layers and pillars of hippuritids and the outer layers of radiolitids,

PLATE 20. Authigenic silicification infilling cell chamber of the radiolitid outer shell layer (sample no. 173, Gulf Coast area). Crossed-polars. Bar scale: 1.0mm.

PLATE 21. Diagenetic dolomitization (A) of the internal sediment infilling a radiolitid cell chamber in the outer layer (Durania; sample no. 190, Upper Cretaceous, Puerto Rico). Notice the well preserved cell wall (B) and the early equant cementation (C) lining the cell chamber. Crossed-polars and stained. Bar scale: 0.5mm.

PLATE 22
INTERNAL SEDIMENTATION AND METEORIC CEMENTATION IN RUDIST SHELLS

Fig. 1. SEM micrograph of a canal wall (a) of a caprinid shell (sample no. 199, Edwards Limestone, Texas). Internal micritic sediment infilled the primary pore space of the canal (left).

Fig. 2. SEM micrograph of internal micritic sediment occupying body cavity of a radiolitid shell (sample no. 68, Coniacian facies, southeastern France).

Fig. 3. SEM micrograph of bladed cement infilling of moldic pore of Antillocaprina (sample no. 176, San German Formation, Puerto Rico).

Fig. 4. SEM micrograph of late equant spar cement occupying a body cavity of the radiolitid shell (sample no. 41, Santonian facies, southeastern France). Notice that the crystals increase in size towards the center of the pore (to the right).

Fig. 5. SEM micrograph of late equant spar infilling the inner cavity of radiolitid Chiapasella (sample no. 111, Upper Cretaceous, Jamaica).

Fig. 6. SEM micrograph of a large equant spar cement infilling a void in hippuritid Barrettia (sample no. 168, Jamaica).

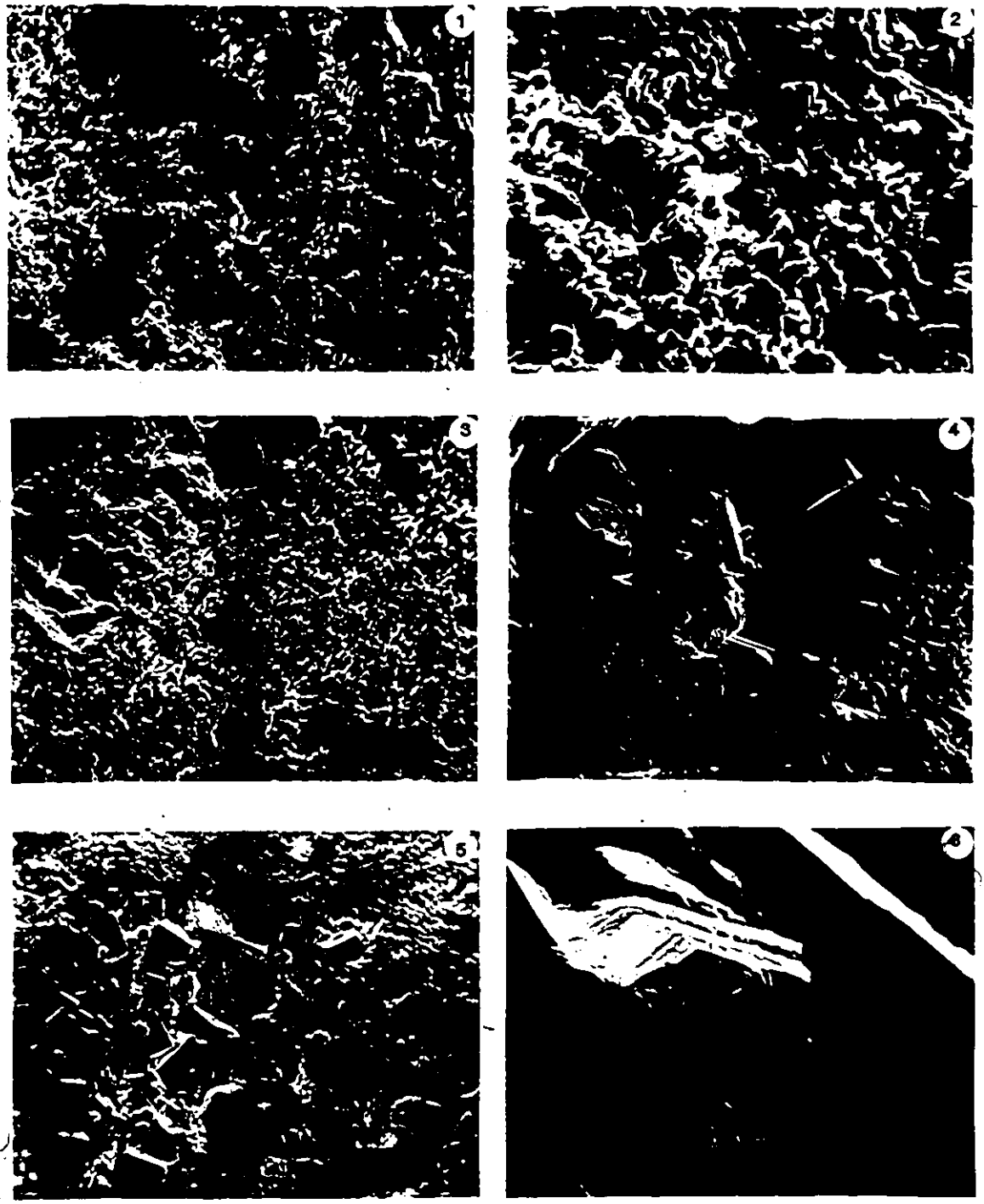
1
2
3
4
5
6

PLATE 23
RECRYSTALLIZATION OF LMC SKELETAL COMPONENTS

Fig. 1. SEM micrograph of a portion of the outer beaded prismatic ultrastructure of the hippuritid Barrettia (sample no. 165, Middle Cretaceous ?, Santa Clara Province, Cuba) showing the effect of recrystallization of this part of the shell. The prisms have rounded crystal corners and fused boundaries.

Fig. 2. SEM micrograph of an enlarged portion of the hippuritid outer prismatic shell layer (sample no. 95, Santonian facies, southeastern France). Notice the granular texture produced by recrystallization.

Fig. 3. Micritic internal sediments recrystallized into microspar (sample no. 127, Upper Cretaceous, Sunderland Inlier, Jamaica).

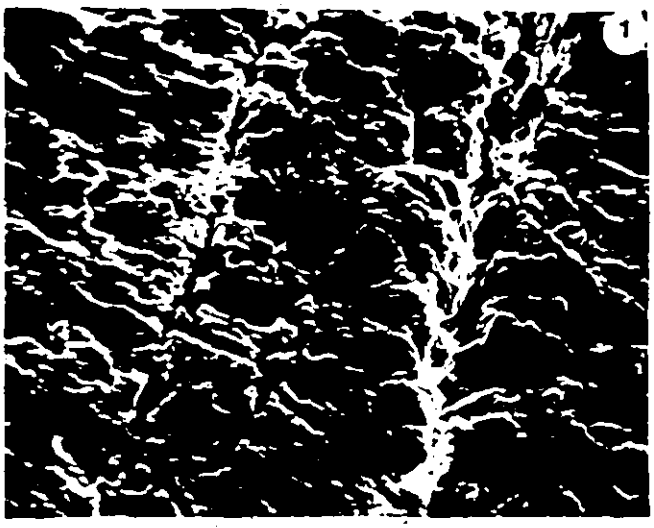
1

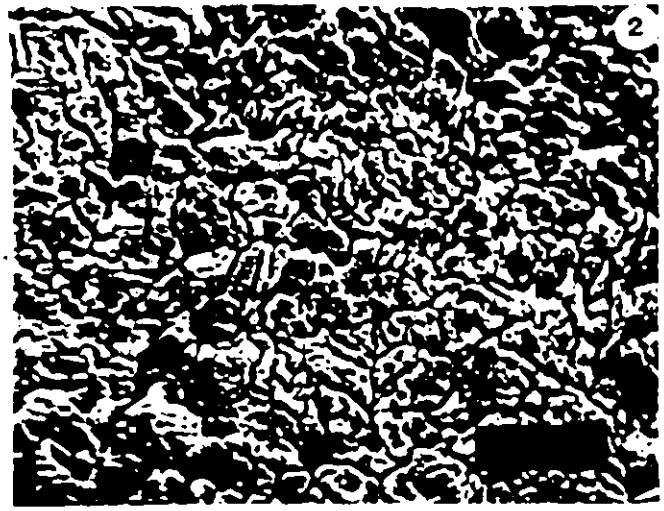
2

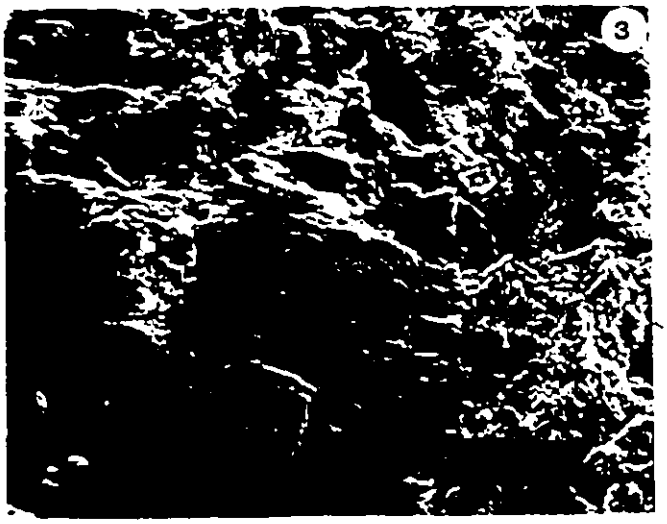
3

PLATE 24. Bioclastic wackestone (sample no. 17, Santonian facies, southeastern France). Note the micritic pelletal matrix with miliolids (A), and rudist shell fragments (B). Plane polarized light. Bar scale: 1.0mm.

monopleurids, and requieniids, to variable degrees. It was more pronounced in requieniid outer layers, causing the obliteration of the existing prisms by pseudospars (Plate 23, Fig. 1). In general, recrystallization is responsible for the rounding of prism corners for destruction of radiolitid fibres or prisms (Plate 23, Fig. 2). The already stabilized aragonitic components were also modified by this late recrystallization (see Section 1.4.3). Lithification and stabilization of carbonate mud into micrite (subrounded crystals of ~3 μ size) could have been achieved earlier, but the late recrystallization probably caused size enlargement to microspar (Plate 23, Fig. 3).

1.4.4.3 Petrography of the Enclosing Rock

The lithotypes of the available enclosing rocks are variable due to the multitude of sampled localities. In terms of their lithofacies, they fall generally within the open platform (shelf lagoon), sea shelf with open water circulation (cf. Flügel, 1982, p. 406, SMF9), or the flank facies (SMF5); the latter characterized by bioclastic debris derived from reef builders. However, these facies, being mostly bioclastic wackestones, bioclastic floatstones, and sometimes bioclastic grainstones (Dunham, 1962) have some common characteristics. They contain abundant micritic,

clotted, sometimes pelletal matrix (up to 60% of the total components), and many large (>2 mm) and small (<2 mm) broken rudist fragments. Other biota and its fragments, such as sponges (calcisphere), red algae, crinoidal plates, few corals, various foraminifera (mostly miliolids, nummulitids, and rotalids (Plate 24)) are also present. The rocks also contain evidence of bioturbation.

Mineralogically, the enclosing rocks were composed originally of a mixture of low-Mg calcite (fragments of hippuritids, radiolitid outer layers, some foraminifera), high-Mg calcite (crinoids, algae, sponge, some foraminifera (Milliman, 1974)), and aragonite (rudists and corals).

1.5 SUMMARY AND CONCLUSIONS

Petrographic, SEM, and mineralogical investigation of rudist shells and of their enclosing carbonate rocks leads to the following conclusions:

1. The shell architecture of rudists is multi-layered and these layers were originally composed of either aragonite (e.g. caprinids, hippuritids (Parastoma)), or from aragonite plus low-Mg calcite (e.g. hippuritids, radiolitids, requieniids and monopleurids).

2. The low-Mg calcitic ultrastructures (prismatic and cellular-prismatic) in the shells suffered differential recrystallization, and sometimes partial cementation, despite the relative diagenetic stability of low-Mg calcite. The localized partial cementation is usually confined to intercrystalline pore spaces.

3. The originally aragonitic ultrastructures are usually preserved as brown, crossed-lamellar, pseudopleochroic relics; particularly within the middle and inner layers of the shells. The neomorphic mineralogical transformation of the original ultrastructures suggests that the inversion of aragonite to calcite has been achieved via a micron scale solution film in undersaturated vadose or stagnant phreatic realms. Alternatively, the aragonitic parts may have suffered total dissolution, with subsequent

precipitation of ferroan phreatic cement in the form of clear equant spar. In this case, the identity of the original material is discernible only through micritic envelopes. In contrast, the stable low-Mg calcite portions of the same shells still retain their original ultrastructures and mineralogy.

4. Synsedimentary marine diagenetic events (e.g. borings by endolithic fauna, internal micritic and/or peloidal marine sedimentation in primary voids, submarine high-Mg calcite and aragonite cementation (radiaxial fabric and micrite) within the primary inter- and intraparticle pore spaces) were coeval with rudist accretion.

5. Meteoric cementation is characterized by the presence of bladed, and inclusion-rich, equant spar in the primary and secondary pore spaces.

6. Late, coarse equant ferroan, phreatic cementation post-dates the bladed-equant cements and occludes the remainder of the available porosity.

CHAPTER II

TRACE ELEMENTS IN RUDIST SHELLS

2.1 INTRODUCTION AND THEORETICAL CONCEPTS

Marine carbonate sediments, of organic and inorganic origin, undergo various diagenetic modifications with time. The bulk composition of these sediments is principally a mixture of aragonite (A), low-Mg calcite with <4 mole %, $MgCO_3$ (LMC), dolomite (D), and high-Mg calcite with 4-30 mole % $MgCO_3$ (HMC). The latter is divided (Milliman, 1974, p. 267) into intermediate-Mg calcite (4-12 mole % $MgCO_3$), and high-Mg calcite (12-28 mole % $MgCO_3$). Aragonite and high-Mg calcite are dominant in Recent, shallow marine sediments, while low-Mg calcite predominates in deep marine environments (Kinsman, 1969, MacKenzie et al., 1983). However, ancient carbonate sediments are composed almost exclusively from the stable low-Mg calcite. The post-depositional stabilization of carbonate phases involves textural, mineralogical and chemical changes (Bathurst, 1975; Brand and Veizer, 1980; Veizer, 1983a). This stabilization proceeds within a short time space (Gavish and Friedman, 1969), through dissolution-reprecipitation mechanisms, in waters of marine and/or meteoric derivation (Bathurst, 1975, Chapters 6, 8, 9; Pingitore, 1976; Veizer, 1983 a, b).

A carbonate phase may incorporate certain minor (Mg, Sr) and trace elements (Na, Mn, Fe, Zn) into its

structure by a variety of ways (McIntire, 1963; Zemann, 1969; Ishikawa and Ichikuni, 1984), such as substitution for Ca in calcium carbonate, occupation of lattice positions which are free due to defects in the structure, adsorption directly onto the surface of the crystals, or be present interstitially between lattice planes. The distribution and repartitioning of these elements is governed by a cumulative effect of both depositional and diagenetic factors.

The incorporation of trace elements into $CaCO_3$ lattice is best understood through the partitioning theory (McIntire, 1963; Kinsman, 1969; Pingitore, 1978), which enables quantitative modelling of trace element distribution between a solid (in this case $CaCO_3$) and a liquid (water) by the following equation:

$$\left(\frac{m_{Me}}{m_{Ca}}\right)_s = D \left(\frac{m_{Me}}{m_{Ca}}\right)_w \qquad \text{- - - - - - - - (1),}$$

where "m" represents molar concentration, "Me" stands for trace element, "s" for solid phase, and "w" for the liquid phase. The magnitude of the positive or negative deviation of a partition coefficient (D) from unity determines the degree of enrichment or depletion of a particular trace element in the solid with respect to its parent liquid phase. Veizer (1983a, Table 3-1) summarized the approximate values of D's for carbonate

minerals. Although some uncertainties in these values exist (Lorens, 1981), their existing crude estimates help to pinpoint chemical trends and the relative magnitudes of chemical displacements (Veizer, 1983a). Upon exposure to meteoric waters, which are undersaturated with respect to metastable carbonate minerals (A, HMC) but saturated with respect to low-Mg calcite, redistribution or repartitioning of trace elements commences. This diagenetic repartitioning of trace elements between marine A and HMC and their successor dLMC is controlled by a complex interplay of the following factors (Kinsman, 1969; Veizer, 1977, 1983a, b; Pingitore, 1978, 1982; Veizer et al., 1978; Brand and Veizer, 1980):

(1) precursor mineralogy (A, HMC, LMC), which determines the original trace element concentrations and subsequently contributes to diagenetic solutions;

(2) the deviation of the partition coefficient (D) from unity;

(3) molar difference in trace element concentration of the diagenetic solution relative to the water of the sedimentary environment;

(4) openness of the system, also commonly known as the water/rock ratio. Veizer (1983a, b) proposed the term solute index (SI) for trace elements and carbon isotopes. As SI approaches 100, it means that a specific cation or isotope was derived completely from

the intervening water (= open system), whereas SI of zero signifies that the cation or isotope was derived entirely from the dissolving solid phase (= closed system); and

(5) biologic fractionation, which may lead to enhancement or supression of some elements in the $CaCO_3$ phase. This factor has been documented to be of importance, particularly for Na, Sr, Mg (Lowenstam, 1963; Dodd, 1965; Brand and Veizer, 1980; Al-Aasm and Veizer, 1983; Crick and Ottensman, 1983). Figure (II-1) shows the principal trends of diagenetic repartitioning for trace elements and isotopes in carbonate minerals, with some elements and isotopes (Fe, Cu, Mn, Zn, Ba and MG(?)) increasing and others (Sr, Na, U, O, C) decreasing in concentration with increasing degree of diagenetic stabilization.

The wet diagenetic stabilization of aragonite (A), high-Mg calcite (HMC), and low-Mg calcite (LMC), whether in a closed, partly closed, or open system, is thought to proceed through an interplay of two processes. Firstly, there is a sequential stabilization, with the chemistry of the bulk aquifer water being controlled by sequential dissolution-reprecipitation of the progressively less soluble mineral phase. This is what determines the overall chemistry and gradients in an aquifer. Secondly, at any given point in the aquifer

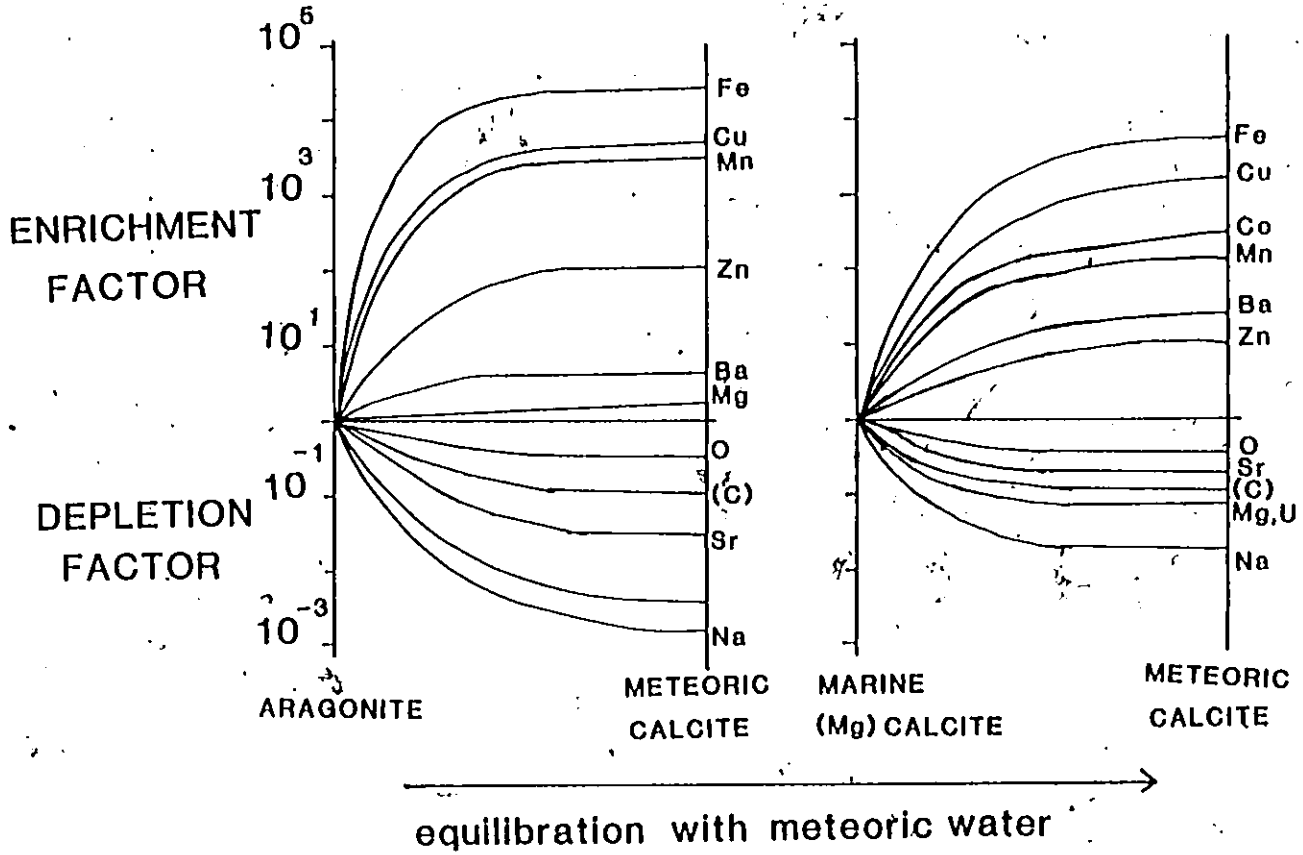

Fig. II-1. Theoretical diagenetic repartitioning of trace elements and of oxygen and carbon isotopes between aragonite and high-Mg calcite and their successor dLMC (reproduced from Veizer, 1983b).

the dissolution-reprecipitation proceeds via micron scale reaction zones (Pingitore, 1978, 1982; Veizer, 1978b, 1983a; Brand and Veizer, 1980), with the chemistry of waters in these reaction zones not necessarily in equilibrium with the bulk pore water (= bulk water disequilibrium system of Veizer, 1978b). The latter process may explain the partial preservation of textural and chemical signatures in carbonate components. Carlson (1983) and Morse (1983) presented a comprehensive review of the kinetics of dissolution-reprecipitation process in aqueous solutions and the reader is refered to these two references for further details.

The transformations of A $\longrightarrow$ dLMC, HMC $\longrightarrow$ dLMC, and LMC $\longrightarrow$ dLMC types could best be studied chemically through consideration of the chemistry of the internal constituents of carbonate rocks. This enables quantification of chemical trends with advancing stages of diagenetic stabilization. As shown, for example, by Brand and Veizer (1980), Al-Aasm and Veizer (1982), and Veizer (1983a), each internal component will be characterized by its own tracer shifts. The original mineralogy and chemistry of these components can be assumed with some certainty and this reduces the difficulties caused by the uncertainties concerning the original composition of the heterogenous and

multicomponent systems. In order to quantify diagenetic phenomena, it is therefore necessary to trace their chemical shifts for as many types of internal components, and across as many variable diagenetic environments, as possible. As an absolute minimum, at least the major internal components representing aragonite (A), high-Mg calcite (HMC),and low-Mg calcite (LMC), and their transformation to diagenetic low-Mg calcite (dLMC) have to be deciphered. This can be achieved by the study of fossils, because of their relative ease of manual separation, reasonable control of their original mineralogical and chemical composition, and their presence in facies of variable diagenetic alteration. Such studies were previously reported, for example by Dodd (1967), Pingitore (1976), Veizer (1974, 1977), Wardlaw et al., (1978), Brand and Veizer (1980), Brand (1981, 1983), Buchardt and Weiner (1981), Ragland et al., (1979), Weiner and Lowenstam (1980) and others. The development of a diagenetic (chemical and isotopic) grid that will emerge from such studies will eventually lead to quantitative treatment of diagenesis, somewhat akin in methodology to that of the oxygen isotope thermometry - the latter based on the $\delta^{18}O$ of mineral pairs (compare Hoefs, 1980, Chapter 2). However, in the case of diagenesis, the "mineral pairs" may be represented by internal constituents (e.g.

fossils, cements, internal sediments, etc.) and the Δ's can be those of trace elements and of O and C isotopes (see Fig. II-2). As the degree of post-depositional modification (= stabilization) increases, the elemental and isotopic Δ's among internal constituents decrease. Because, particularly in case of the fossils, the original composition can be assumed with some certainty, the intercomponent Δ's will thus give a quantitative measure of the absolute shifts in concentration as well as of the relative decrease in the intercomponent differences in chemistry (Fig. II-2) (see also Veizer, 1983a for a detailed explanation of this approach).

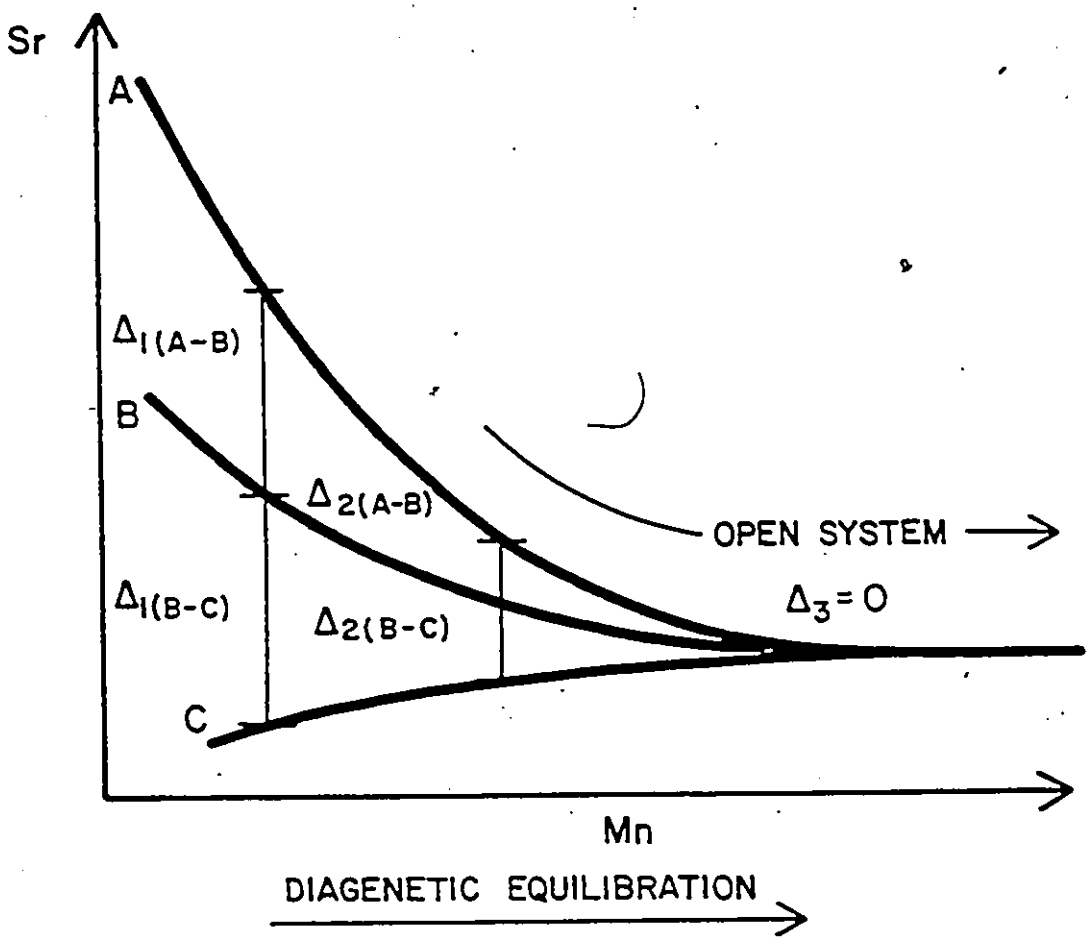

Fig.II-2. Theoertical decrease in Sr and increase in Mn contents in dLMC due to increasing degree of diagenetic stabilization with meteoric waters. Note that the total concentrations vary and the Δ's decrease as the open system of diagenesis is approached. The three components can be for example, A) corals (originally high Sr A), B) molluscs (originally low Sr A), and C) crinoids (originally HMC). Other fossils, cements, and matrix constituents can serve as alternative components. Furthermore, other elements and isotopes can be considered in a similar grid. A,B,C represent envelopes rather than lines, (reproduced from Al-Aasm and Veizer, 1982).

2.2 PURPOSE OF THE STUDY

The emphasis in this thesis is on the study of the thick, multilayered rudist shells, because each single layer and component can be mechanically separated and studied chemically. This can be achieved by taking into consideration mineralogical complexities and generic classification of rudists. The main objectives of this chapter are the following; (1) quantification of diagenetic chemical shifts during mineralogic stabilization of A $\longrightarrow$ dLMC; (2) evaluation of the degree to which the original mineralogy, texture and ultrastructure of discrete shell layers controlled trace element chemistry as the sediment underwent diagenetic stabilization with meteoric waters; (3) testing of the relative post-depositional stability of LMC phases within the rudist shells; and (4) testing physiological and biochemical factors as a control of elemental distribution within discrete shell layers of various families.

2.3 SAMPLING AND ANALYTICAL METHODS

A total of 414 rudist shells and their enclosing rocks were selected and separated for chemical analysis (Appendices III 1, 2, 3).

The shell layers (and other components, such as internal sediments and cements) of each individual rudist were separated manually under binocular and petrographic microscopes. They were cut by dental drill and by a small diamond saw. The separated components, as shall chips, were then washed with deionized water and 5% (V/V) HCl for few seconds, followed by cleaning in ultrasonic cleaner, and finally rinsed in deionized water to remove any outer contamination.

The powdered components of rudist shells were digested in 40 ml of 7% (V/V) HCl for four hours. This timing followed the leaching experiments of Brand and Veizer (1980), which showed that leaching of the insoluble residue was extensive at longer time intervals.

Calcium, magnesium, strontium, manganese, iron, sodium, zinc and aluminum were determined on a Varian Techtron AA-175. Ca, Mg, Mn, Fe, NA and Zn were analyzed in air-acetylene flame, while Sr and Al were analyzed in acetylene-nitrous oxide flame. $Sr(NO_3)_2$ was added to Ca and Mg samples, calibration, and standard rock solutions. KCl (2000 ppm K) was added to Al and Sr

samples, calibration, and standard rock solutions.

The average accuracies, as compared to recommended values (Thompson et al., 1970; Flanagan, 1973; Gladney and Burns, 1983) for the U.S.G.S. (G-1, GSP-1, 88a, 1b) and the Z.G.I. (KH and TB) standard rocks, and instrumental as well as analytical precisions were as follows: Ca (9.9, 8.5, 4.8); Mg (5.8, 5.3, 4.5); Sr (6.4, 7.6, 1.0); Mn (4.7, 10.3, 3.2); Fe (3.9, 6.3, 4.6); Na (10.0, 6.0, 3.7); Zn (25.7, 24.6, 6.2); and Al (4.0, 6.1, 7.2) relative percent, respectively. Insoluble residue was determined gravimetrically with average reproducibility of 5.6 relative percent.

The evaluation of chemical data and the forthcoming discussions are based entirely on data recalculated on the insoluble residue free basis (100% soluble carbonate).

For data handling and processing, the SPSS package version 6 (Nie et al., 1975) was utilized. Factor analysis was employed using the PA2 procedure with varimax rotation. All these analyses were done on an IBM 360 computer.

2.4 EVALUATION AND DISCUSSION OF RESULTS

2.4.1 Whole Rudist Fossils and Their Enclosing Rocks

Varimax rotated factor analysis of all studied samples, including all layers of rudist shells, cements, and internal sediments, shows that three almost equable factors controlled the overall chemical variation (Table II-1). About 40% of the total variation in chemistry is due to late, or second stage, meteoric precipitation of ferroan calcite into residual pore spaces. This controls the distribution of Mn, Fe and Mg(?) (additional discussion concerning cementation is presented in the subsequent sections). The second factor is interpreted as an early diagenetic phenomenon, with the loss of Na and Sr reflecting mostly calcitization of the originally metastable aragonite. The overall depletion in Sr and Na, and enrichment in Mn, Fe and Mg, during A $\longrightarrow$ dLMC transition is primarily dependent on their D values and the $^{m}Me/^{m}Ca$ ratios of meteoric waters. The former group of elements has $D < 1$ and low ($^{m}Me/^{m}Ca$) of meteoric waters, whereas the latter group is characterized by opposite attributes (cf. Veizer 1983 a, b for details). Laboratory leaching of Al from the insoluble aluminosilicate fraction of studied samples accounts for the last factor.

The above described pattern is in full agreement

with theoretical models of diagenetic repartitioning of trace elements in meteoric waters (Fig. II-1). However, in contrast to models and previous studies (e.g. Brand and Veizer, 1980; Veizer, 1974) the data do not show any clear negative correlation between Sr and Mn. This is likely a consequence of the fact that the late ferroan calcite was by far the dominant contributor to Mn concentrations, completely overwhelming the early diagenetic signal of Mn gain. At this late stage, most Sr has already been lost from dLMC and they and ferroan calcites did not differ much in their Sr contents. Thus, addition of late ferroan calcites causes an increase in Mn but not in Sr contents.

Factor analysis of the enclosing rocks, composed originally of a mixture of LMC, A and HMC (fossils and matrix, see Chapter I), shows that only two factors account for the total variations of their chemistry (Table II-2). Factor 1, explaining 82% of the total variation, is probably a combined factor of laboratory leaching from the insoluble residues (positive loadings by I.R., Fe, Mn, Mg, Al and possibly Zn) and of early diagenetic calcitization (loadings by Sr and Na). Factor 2 appears to be solely a consequence of diagenetic mineralogical stabilization in meteoric waters, as exemplified by the negative correlation of Sr with Mn and Zn.

TABLE II-1

Varimax rotated factor analysis of all studied samples (components of shell layers, cements, internal sediments). Enclosing rocks were excluded from consideration (N = 354)

	Factor 1	Factor 2	Factor 3
log IR	0.037	-0.046	**0.700**
log Ca	0.337	0.041	-0.004
log Mg	**0.523**	0.196	0.009
log Sr	0.358	**0.926**	-0.067
log Mn	**0.847**	-0.329	-0.056
log Fe	**0.439**	-0.269	0.314
log Na	-0.131	**0.467**	0.060
log Zn	-0.131	0.031	0.355
log Al	0.201	0.053	**0.719**
Percent of Variation Explained	39.7	32.7	27.7
Eigen value	1.607	1.325	1.121
Interpretation	Diagenetic Stabilization II (late ferroan calcite)	Diagenetic Stabilization I (calcitization)	Laboratory Leaching

TABLE II-2

Varimax rotated factor analysis of enclosing rocks (N = 47)

	Factor 1	Factor 2
log IR	0.801	0.230
log Ca	0.006	-0.295
log Mg	0.895	-0.186
log Sr	0.722	-0.537
log Mn	0.662	0.322
log Fe	0.916	0.303
log Na	0.622	-0.001
log Zn	0.347	0.650
log Al	0.930	0.233
Percent of Variation Explained	81.8	18.2
Eigen value	4.708	1.049
Interpretation	Laboratory Leaching and Diagenetic Stabilization	Diagenetic Stabilization

2.4.2 Cements

The types, morphology, and inferred original mineralogy of cements have been discussed earlier (cf. Section 1.4.4).

Factor analysis of all cement samples (Table II-3) shows that their precipitation and diagenetic stabilization may be responsible for the substantial portion of the observed chemical variations. Early marine cementation by aragonite and possibly high-Mg calcite and their transformation into dLMC explains the positive association of Mg, Sr, and Na (Factor 2; Figs. II-3, 4, 5). The concentrations of Mg, Sr, and Na are low, if compared to aragonite and/or high Mg-calcites precipitated as cements in present day seas (cf. Milliman, 1974), and these elements have been lost during neomorphism of the precursor cement to fibrous and micritic calcites.

Cements have been subdivided petrographically (Section 1.4.4, Chapter I) into four categories: fibrous or micritic inclusion-rich nonferroan calcite; equant inclusion-rich ferroan and nonferroan calcite; equant-bladed ferroan calcite; and clear large equant ferroan spar (Table II-4). The average elemental and isotopic values of these types of cements reflect to a considerable degree the values in their original and later diagenetic mineralogical precursors. Early

TABLE II-3

Varimax rotated factor analysis of all cements (N = 53)

	Factor 1	Factor 2	Factor 3
log IR	-0.303	-0.187	0.522
log Ca	0.353	0.147	-0.046
log Mg	0.195	0.755	0.200
log Sr	-0.138	0.671	0.027
log Mn	0.996	0.023	-0.065
log Fe	0.529	-0.125	-0.002
log Na	0.068	0.593	-0.144
log Zn	-0.023	0.184	0.295
log Al	0.077	-0.034	0.788
Percent of Variation Explained	41.6	34.0	24.4
Eigen value	1.703	1.389	0.997
Interpretation	Late Cementation by Ferroan LMC calcite	Diagenetic Calcitization of early (HMC + A) Cements	Laboratory Leaching

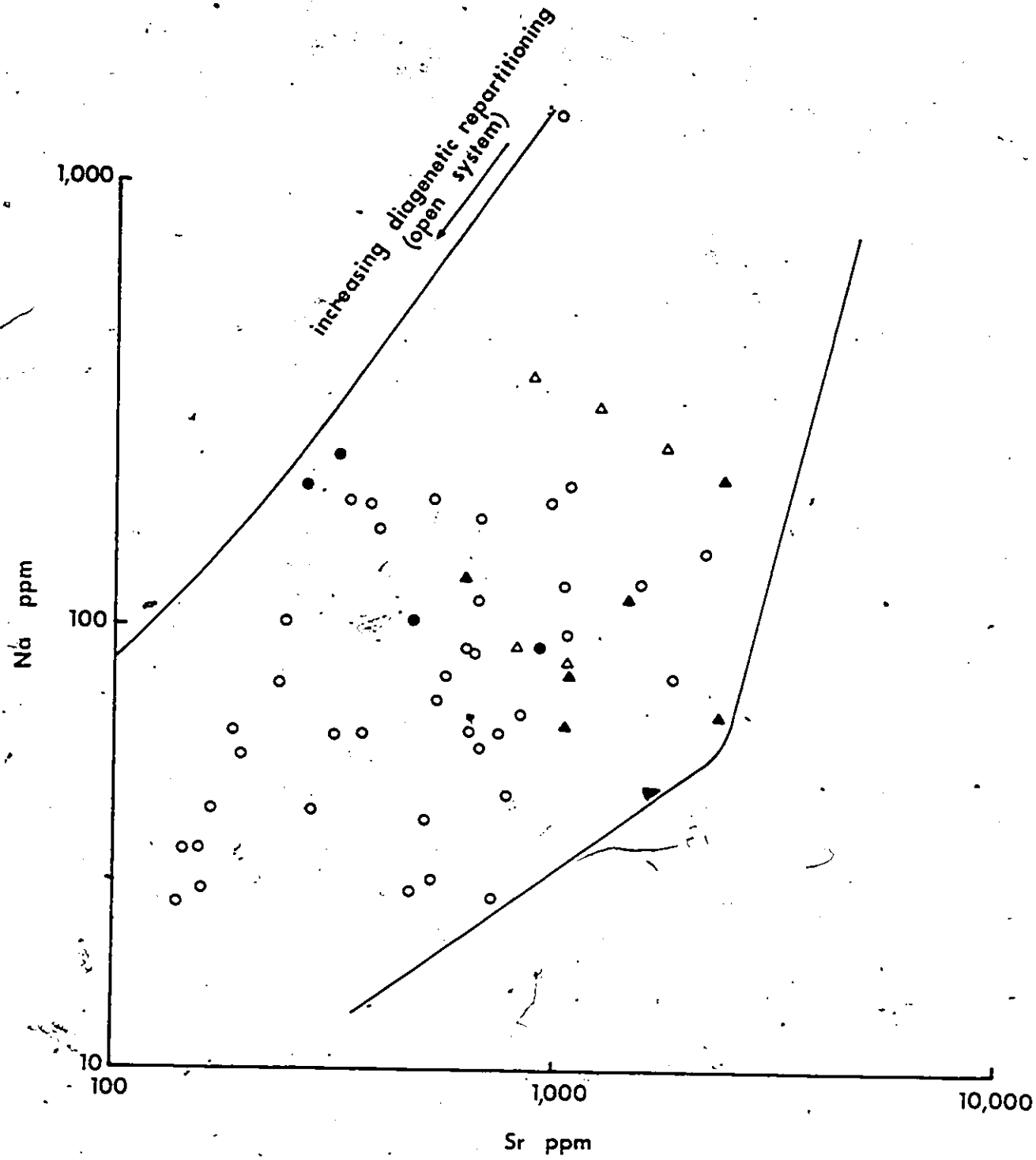

Fig. II-3. Scatter diagram of Na vs. Sr for all cement samples.

▲ early radiaxial fibrous and micritic cements.
△ inclusion-rich equant spar.
● late bladed ferroan cements.
o late clear equant ferroan cements.

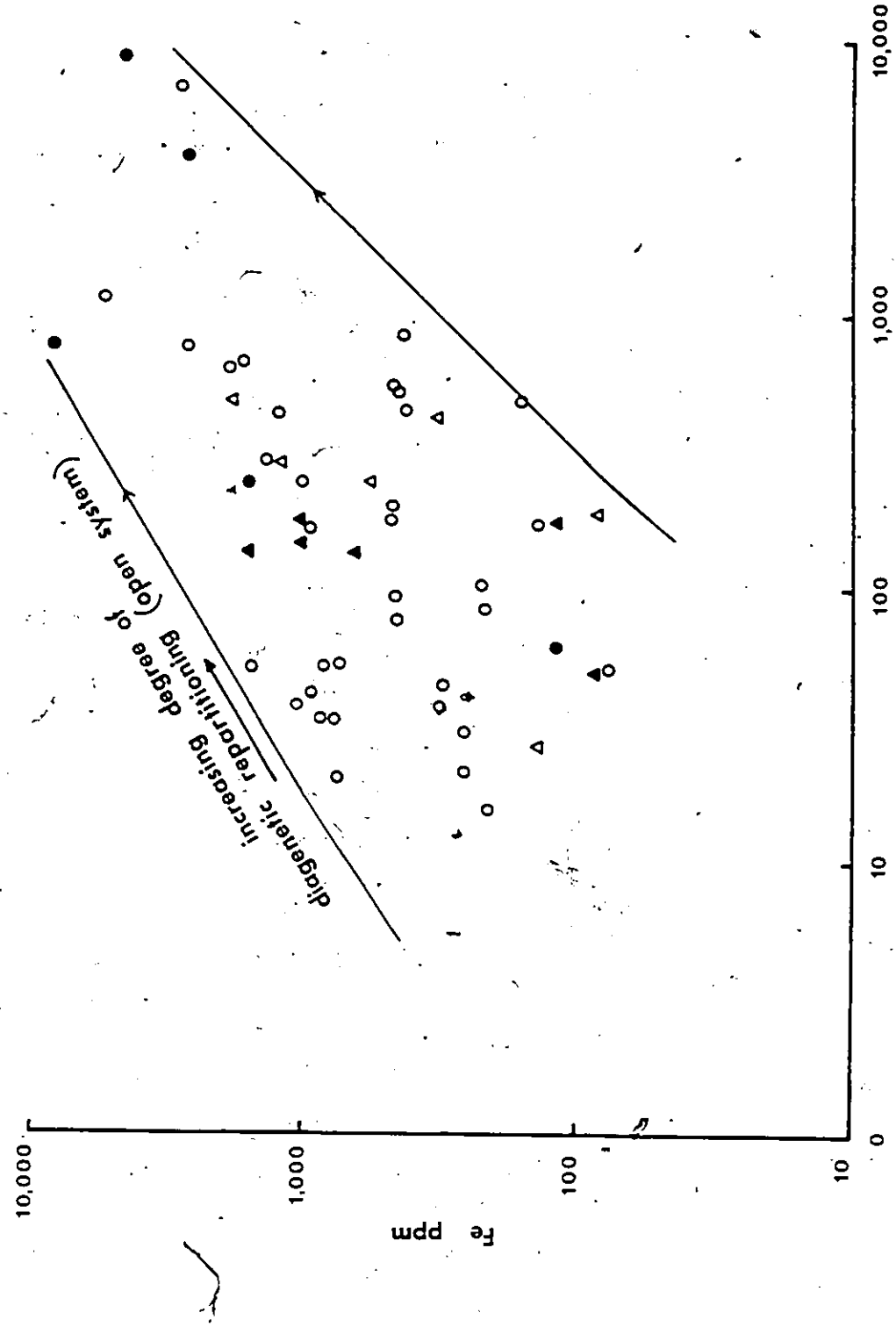

Fig. II-4. Scatter diagram of Fe vs. Mn for all cement samples. Explanations as in Fig. II-3.

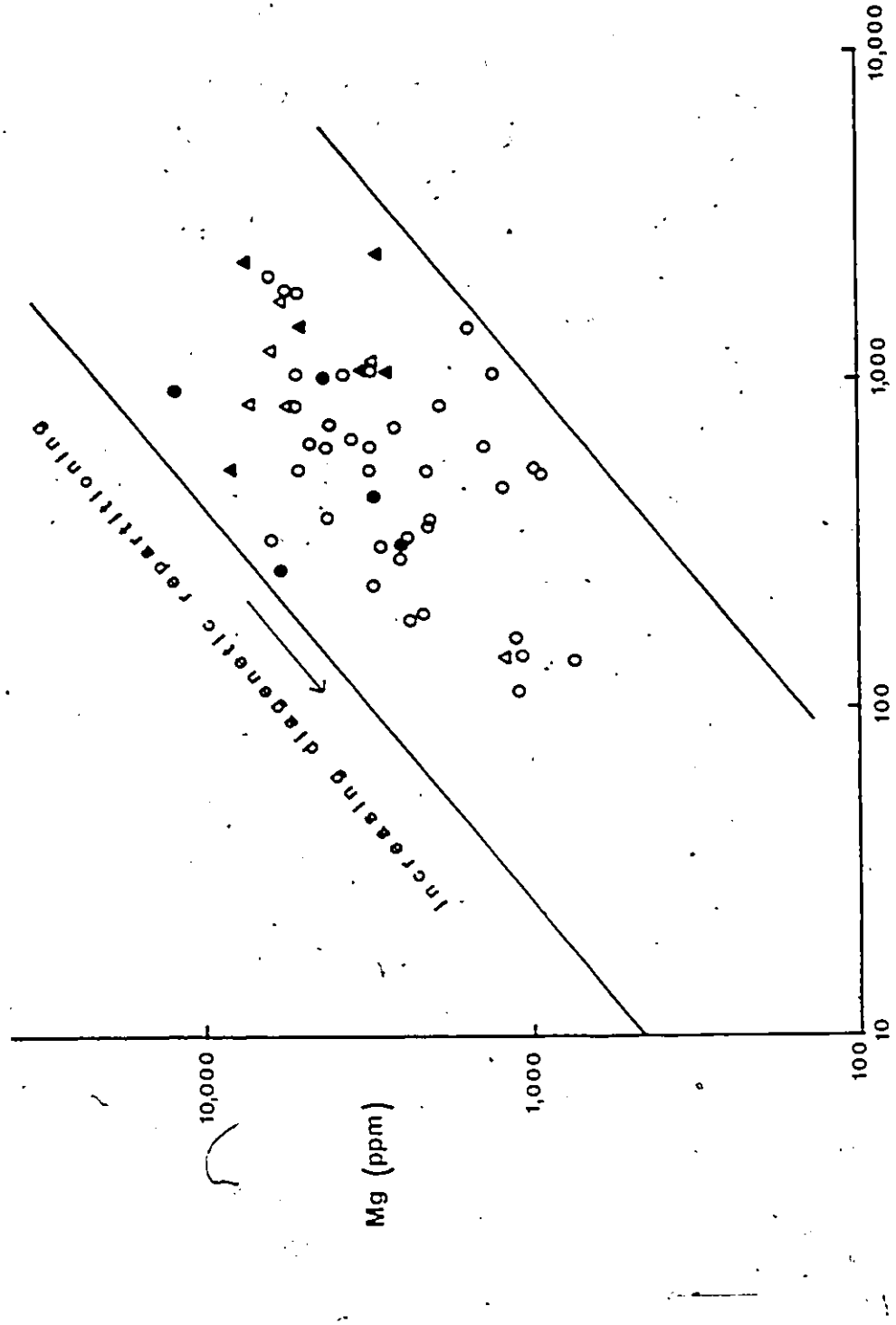

Fig.II-5. Scatter diagram of Mg vs. Sr for all cement samples. Explanations as in Fig.II-3.

(originally HMC) cements have relatively high Sr and Na and low Mn and Fe (Figs. II-3, 4) as well as heavier $\delta^{18}O$ and $\delta^{13}C$ (see Chapter III). In contrast, the late equant and bladed ferroan cements (originally LMC deposited exclusively in meteoric realm) have low Sr and Na, high Mn and Fe and lighter $\delta^{18}O$ and $\delta^{13}C$. The modes of early and late cements are ~1500 and ~350 ppm Sr, respectively. For Mn, they are ~140 and ~1200 ppm. With these data, rough estimates of composition of diagenetic waters can be provided. Table (II-4) shows the calculated ratios of $(^{m}Me/^{m}Ca)w$ for the possible diagenetic waters, as well as the same ratios for seawater and for shallow subsurface water, the latter thought to represent the most frequent diagenetic solution (Majid, 1983; Veizer, 1983a). Figures (II-6, 7) give the possible compositions of theoretical waters responsible for cement formation and compare them to seawater and shallow subsurface water, respectively. The composition of the theoretical diagenetic solutions seems to reflect a mixture of these two types of comparative waters. Compared to seawater, the theoretical waters were enriched in Fe and Mn and depleted in Na and Mg. The opposite relationships are observed, if compared to shallow subsurface waters (Fig. II-7), except that Mg/Ca ratios appear to be comparable. Sr/Ca ratios for late cement (ferroan equant spar)

TABLE II-4
Geometric mean of selected elements (in ppm), stable isotopes (in ‰ PDB), and (^{m}He/^{m}Ca)w for different types of cements and for open seawater (Drever, 1982) and shallow subsurface ground water (Hajid, 1983)

	Open Sea	Shallow Subsurface	Early Fibrous Inclusion-rich	Inclusion-rich Equant	Late Bladed Ferroan	Late large Equant Ferroan	D
Sr	8	0.34	1345	790	515	450	
(^{m}Sr/^{m}Ca)w	8.9 x 10-3	5.5 x 10-3	1.4 x 10-2 6.4 x 10-2	9.1 x 10-3 3.9 x 10-2	5.3 x 10-3 2.2 x 10-2	4.0 x 10-3 2.1 x 10-2	0.13 0.03
Mn	0.0002	0.059	125	200	825	155	
(^{m}Mn/^{m}Ca)w	3.5 x 10-7	1.6 x 10-3	1.9 x 10-5	3.2 x 10-5	1.1 x 10-4	2.3 x 10-5	15
Fe	0.002	1.45	475	420	1870	650	
(^{m}Fe/^{m}Ca)w	3.5 x 10-6	4.3 x 10-2	5.1 x 10-5	4.9 x 10-5	1.9 x 10-4	7.2 x 10-5	20
Na	10760	23	98	130	140	80	
(^{m}Na/^{m}Ca)w	455.0 x 10-1	14.3 x 10-1	268.7 x 10-1 179.1 x 10-1	376.0 x 10-1 250.7 x 10-1	358.6 x 10-1 239.1 x 10-1	218.2 x 10-1 163.6 x 10-1	0.0002 0.0003
Mg	1290	10.5	4540	4330	4760	2585	
(^{m}Mg/^{m}Ca)w	51.6 x 10-1	6.17 x 10-1	3.9 x 10-1 18.0 x 10-1	3.9 x 10-1 18.0 x 10-1	3.8 x 10-1 17.6 x 10-1	2.2 x 10-1 10.2 x 10-1	0.06 0.013
Ca	411	28	318500	301850	340090	316592	
δO^{18}			-4.0	-5.1	-9.2	-6.3	
δC^{13}			+3.1	+0.4	-4.5	+1.1	

waters appear to have been comparable to shallow subsurface waters. In contrast, the early (fibrous and inclusion-rich micritc) cement waters have had Sr/Ca ratios in excess of that for seawater. This may indicate that dissolution-reprecipitation of A ⟶ dLMC type in a relatively closed system resulted in high level Sr/Ca ratios, in the thin film (cf. Veizer, 1983a). In short, both marine (through dissolution of the precursor marine minerals) and meteoric waters contributed to solutions which precipitated the cements within the rudist framework in their final form. However, the rate of contribution from meteoric waters is more pronounced in the late cement types.

2.4.3 Internal Sediments

Micritic internal sediments were composed originally of a mixture of aragonite, high-Mg calcite (?) and low-Mg calcite (see Section 1.4.4.2.2 for details).

Factor analysis of all these sediments (Table II-5) shows that the major controlling factor of their chemistry (Factor 1) may be interpreted as a composite of two processes; diagenetic stabilization of metastable components (Mg, Sr, and Na) and an unknown variable controlling Ca, Al and possibly Mg distributions.

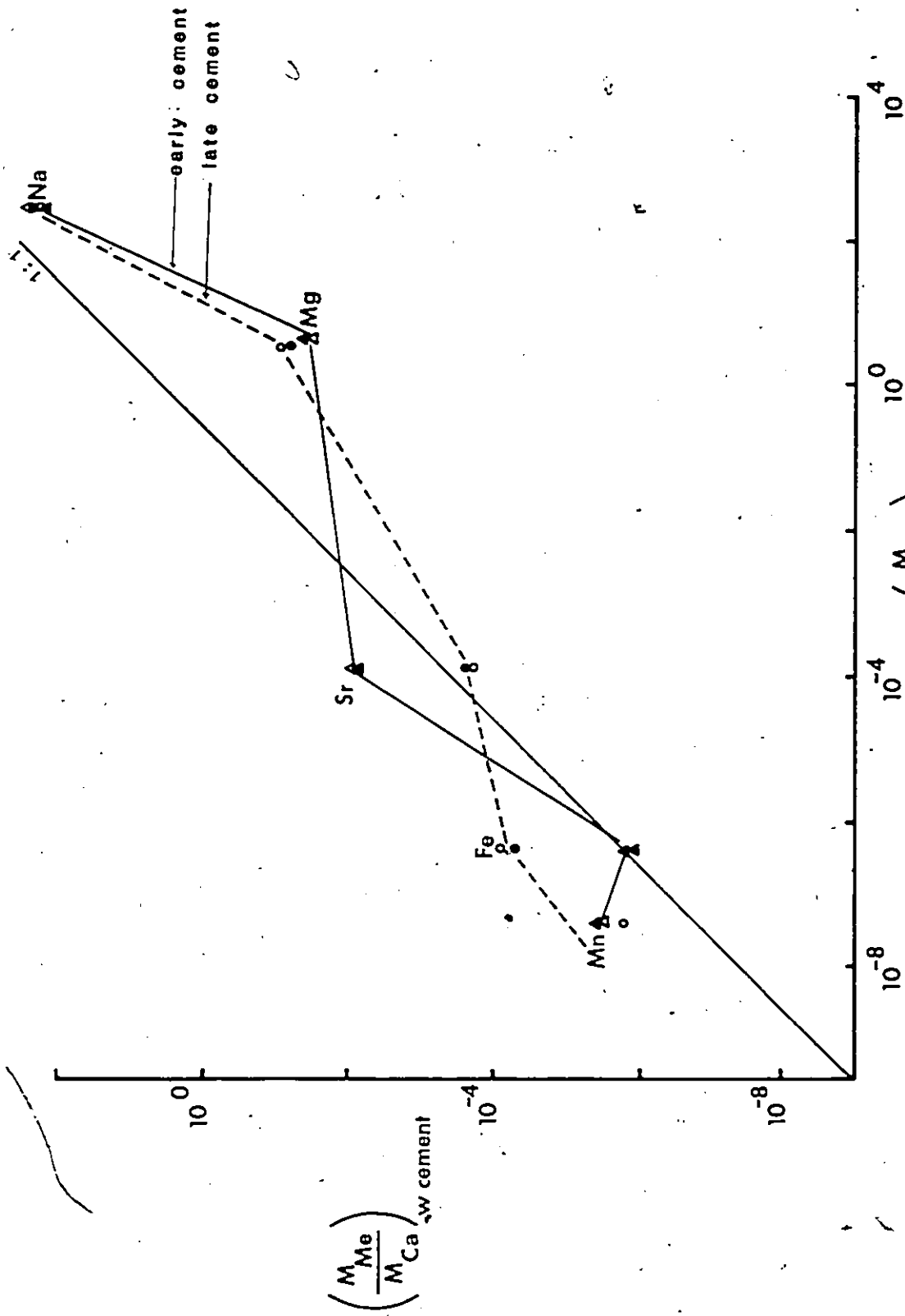

Fig. II-6 . Plot of $(M_{Me}/M_{Ca})_w$ ratios of seawater vs. the theoretical $(M_{Me}/M_{Ca})_w$ for different types of cement (see Fig. II-3, Table II-4 and the text for further details).

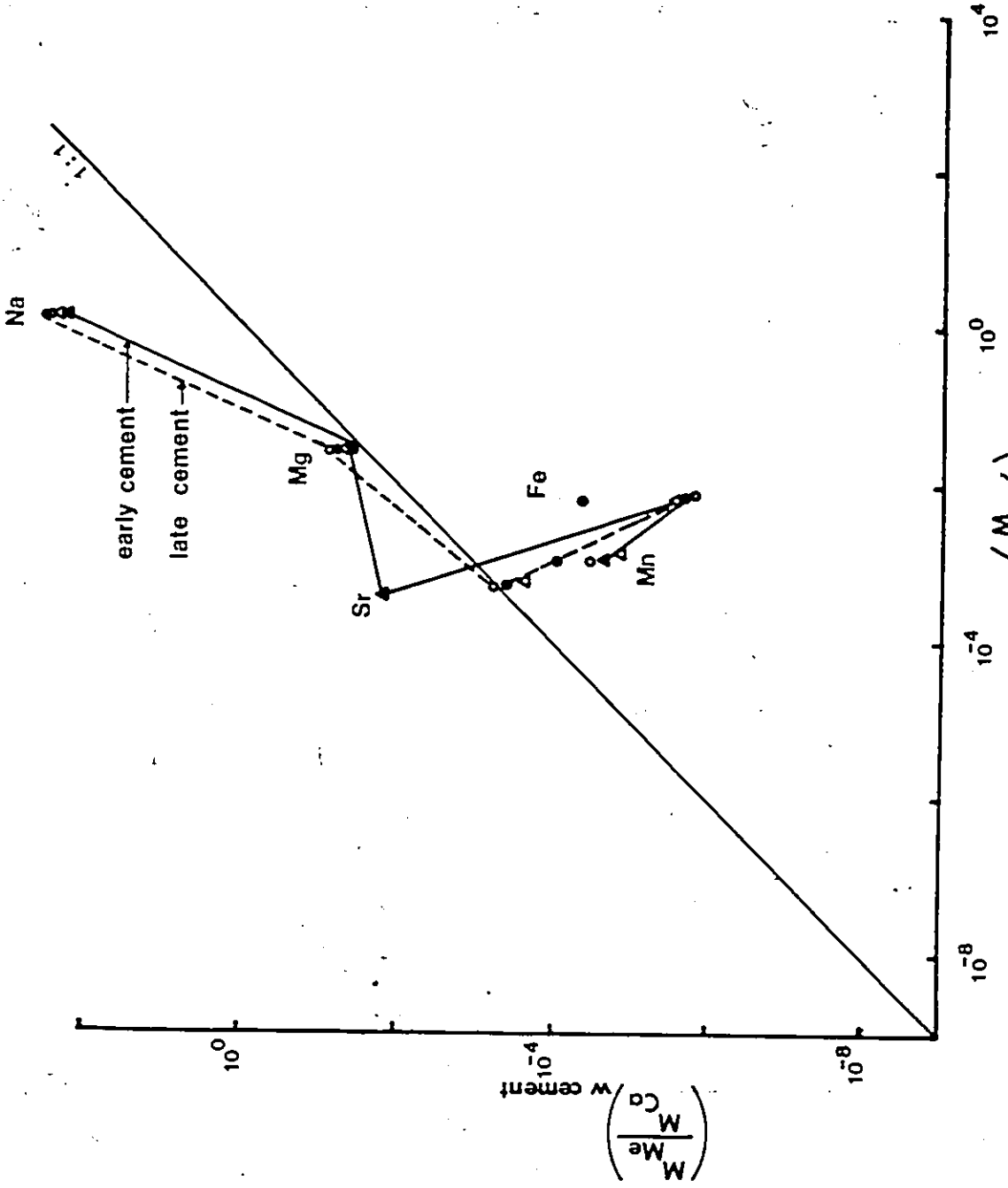

Fig. II 7. - Plot of $\left(M_{Me}/M_{Ca}\right)_{w}$ ratios for shallow subsurface water vs. the theoretical $\left(M_{Me}/M_{Ca}\right)_{w}$ for different types of cements. See Fig. II-3 and TableII-4 and the text for further details.

TABLE II-5

Varimax rotated factor analysis of all internal sediments (N = 64)

	Factor 1	Factor 2	Factor 3
log IR	0.415	-0.786	0.061
log Ca	0.497	0.000	0.267
log Mg	0.845	0.107	0.320
log Sr	0.847	0.131	0.046
log Mn	0.190	0.003	0.911
log Fe	0.234	0.499	0.626
log Na	0.442	0.402	0.046
log Zn	-0.180	0.578	0.033
log Al	0.534	0.668	0.201
Percent of Variation Explained	65.6	18.7	15.7
Eigen value	3.768	1.076	0.899
Interpretation	Diagenetic Stabilization I	Laboratory Leaching	Diagenetic Stabilization II

Factor 2 is laboratory leaching from insoluble residues, and the last factor can be attributed to late cementation of the available interparticle and moldic pore spaces by equant ferroan meteoric cement.

2.4.4 Aragonite Skeletal Components

Skeletal components utilized for statistical analysis in this section include all those which have been composed originally of aragonite and which may or may not have preserved some aragonitic ultrastructural identity. These are the pallial canal layers of the outer shells of caprinids and all middle and inner layers of caprinids, radiolitids, hippuritids and monopleurids (see Appendices 2, 3 for details). Factor analysis of these components (Table II-6) reveals the existence of three factors controlling their overall chemical variations. These factors are identical to those in Tables (II-1 and II-2). Factor 1 represents acid leaching of the insoluble residues, composed mainly of clay minerals, quartz and rare iron compounds, with leaching of I.R., Al, and possibly Fe. The distribution of other elements seems to have been controlled by two-stage diagenetic stabilization. Stage I (Factor 3), the A $\longrightarrow$ dLMC inversion, controls Sr and Na repartitioning, while the Factor 2 represents the final stage of meteoric phreatic diagenesis, probably precipitation of

TABLE II-6

Varimax rotated factor analysis of all presumably aragonitic components (N = 117)

	Factor 1	Factor 2	Factor 3
log IR	0.630	0.015	-0.183
log Ca	0.088	0.170	-0.009
log Mg	-0.102	0.636	0.092
log Sr	-0.203	0.132	0.660
log Mn	0.111	0.719	-0.167
log Fe	0.491	0.262	-0.097
log Na	0.224	-0.305	0.735
log Zn	0.366	-0.251	0.129
log Al	0.770	0.117	0.126
Percent of Variation Explained	40.3	36.1	23.6
Eigen value	1.527	1.366	0.893
Interpretation	Laboratory Leaching	Diagenetic Stabilization II (late ferroan calcite)	Diagenetic Stabilization I (calcitization)

ferroan cement in moldic pores (see Section 2.4.2). The first stage of diagenesis is characterized by some preservation of ultrastructural identities of shell components. The second, ferroan calcite, stage postdated a wholesale leaching of aragonitic components. This is reflected in chemical parameters, with those formerly aragonitic components which show a relic lamellar ultrastructure (see Section 1.4.3) having lesser trace element repartitioning than those preserved only as spar fillings of moldic pores (Table II-7). Sr, Na, $\delta^{18}O$ and possibly Mn and Fe show the best examples of partial preservation of chemical signals inherited from their original aragonitic precursors. Histograms of Na, Sr (Figs. II-8, 9) distributions show the existence of two populations for skeletal components with partially preserved relic aragonitic ultrastructures, and unimodal ones for those without any relic ultrastructures. The more pronounced modes of the "preserved" group approximate those of the completely recrystallized group. This again suggests a two stage diagenetic process.

The utilization of Sr as a diagenetic tracer has been well documented previously (e.g. Kinsman, 1969; Veizer, 1983a). For Na, it is not clear whether Na is present as true solid solution in the carbonate lattice (Land and Hoops, 1973; White, 1977), in entrapped

TABLE II-7

Geometric mean for selected elements and isotopes of rudist samples with and without clear relic aragonitic ultrastructures.
Sr, Mn, Fe, Mg, and Na in ppm;
$\delta^{18}O$ and $\delta^{13}P$ in ‰ relative to PDB

Element and Isotope	Samples with Relic Ultrastructures	Samples without Relic Ultrastructures
Sr	1395	430
Mn	95	130
Fe	330	480
Mg	3820	3685
Na	245	85
$\delta 18_O$	-3.7	-5.4
$\delta 13_O$	+1.5	+0.9

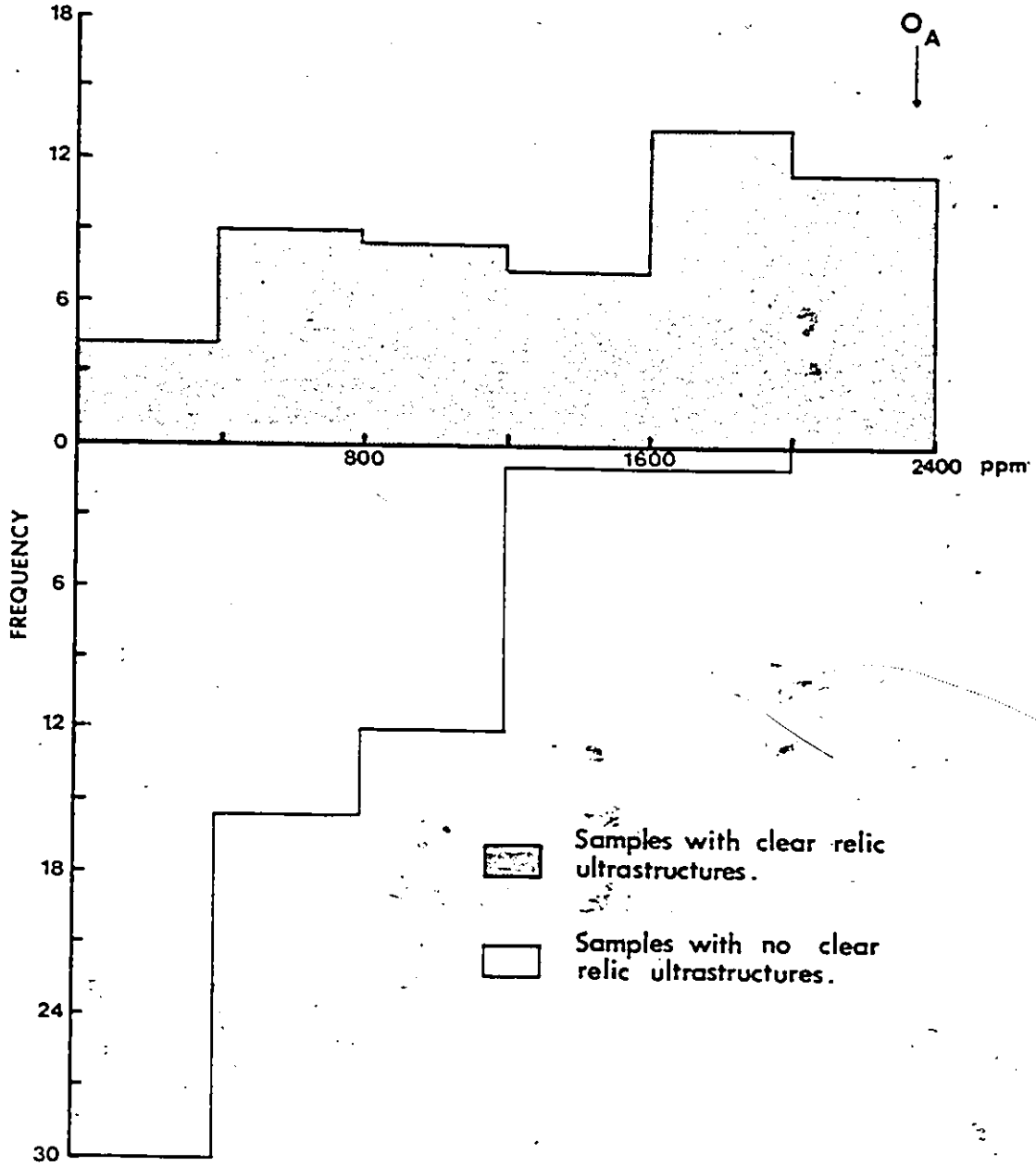

Fig. II-8. Histogram plots of Sr distribution in originally aragonitic components with and without partial preservation of relic ultrastructures. O_A represents the average value for organic aragonite for present day bivalves.

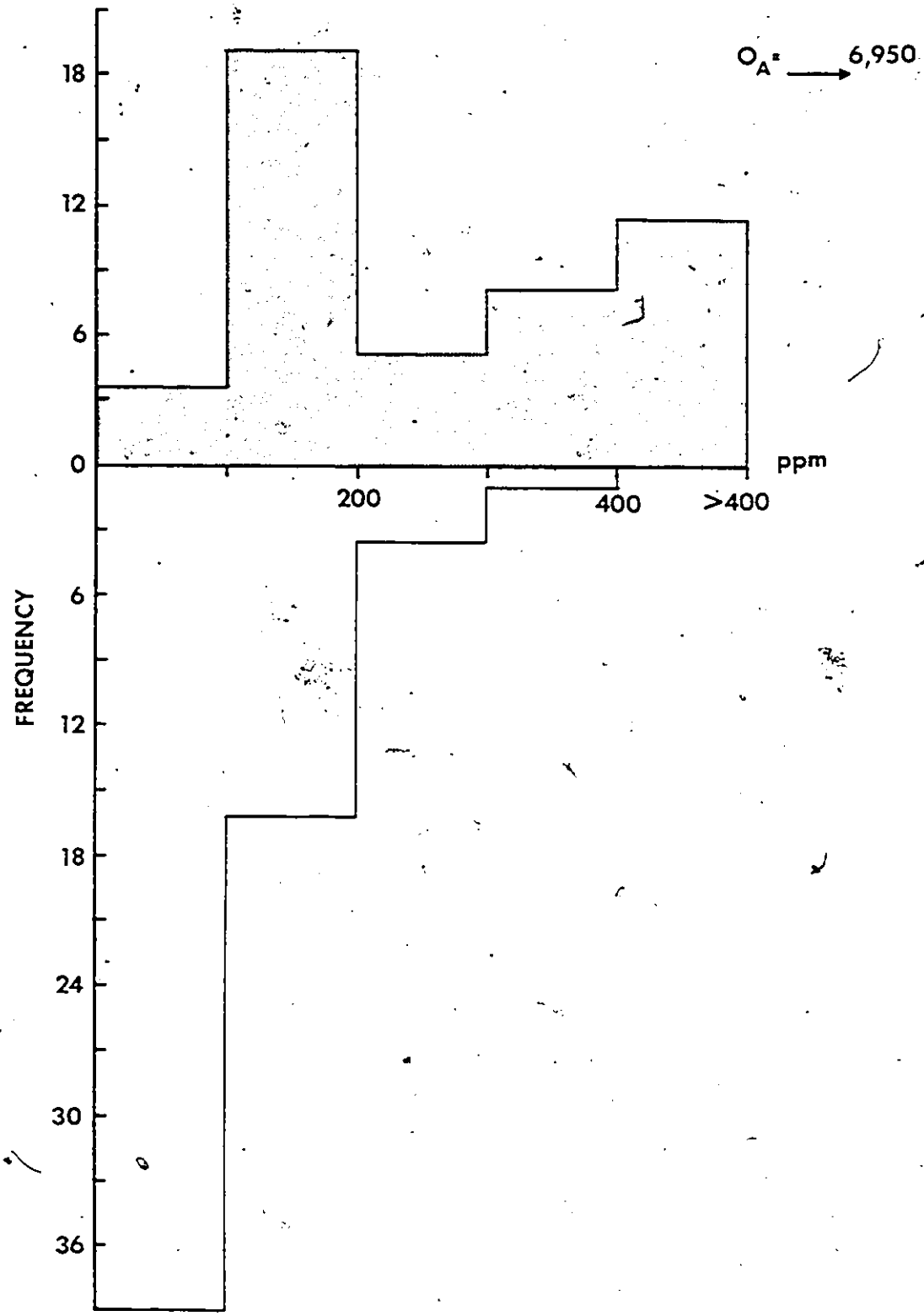

Fig. II-9. Histogram plots of Na distribution in originally aragonitic components with and without partial preservation of relic ultrastructures.

aluminosilicate particles, or - more likely - located in interstitial positions and in fluid inclusions (Veizer et al., 1978; Ishikawa and Ichikuni, 1984). For these reasons, its utilization as a paleosalinity indicator or as a diagenetic tracer is not as well understood, although the general repartitioning theory is still applicable (Land and Hoops, 1973; Brand and Veizer, 1980; Randazzo et al., 1983). Diagenetic loss of Sr and Na is well illustrated in Fig. II-10. Sr and Na concentrations in samples with aragonite still preserved approach those typical of present day marine pelecypods. This agreement indicates that neither the Na, Sr composition of Cretaceous seawater nor the biogenic partitioning by molluscs were markedly different from today. This is also true for other elements, such as Mn and Mg (Figs. II-11, 12). Furthermore, this figure also illustrates that the loss of Sr during early stages of diagenetic A → dLMC stabilization is much slower than that of Na. This is likely a consequence of three phenomena. In the first instance, it may reflect the fact that Na is more loosely bound in aragonite than the lattice bound Sr (see above). Secondly, the strong early repartitioning reflects the fact that $DC_{Na} < DC_{Sr}$. Thirdly, compared to original aragonite, the Na/Ca depletion in meteoric waters is considerably larger than Sr/Ca depletion. The scatter diagram quite evidently

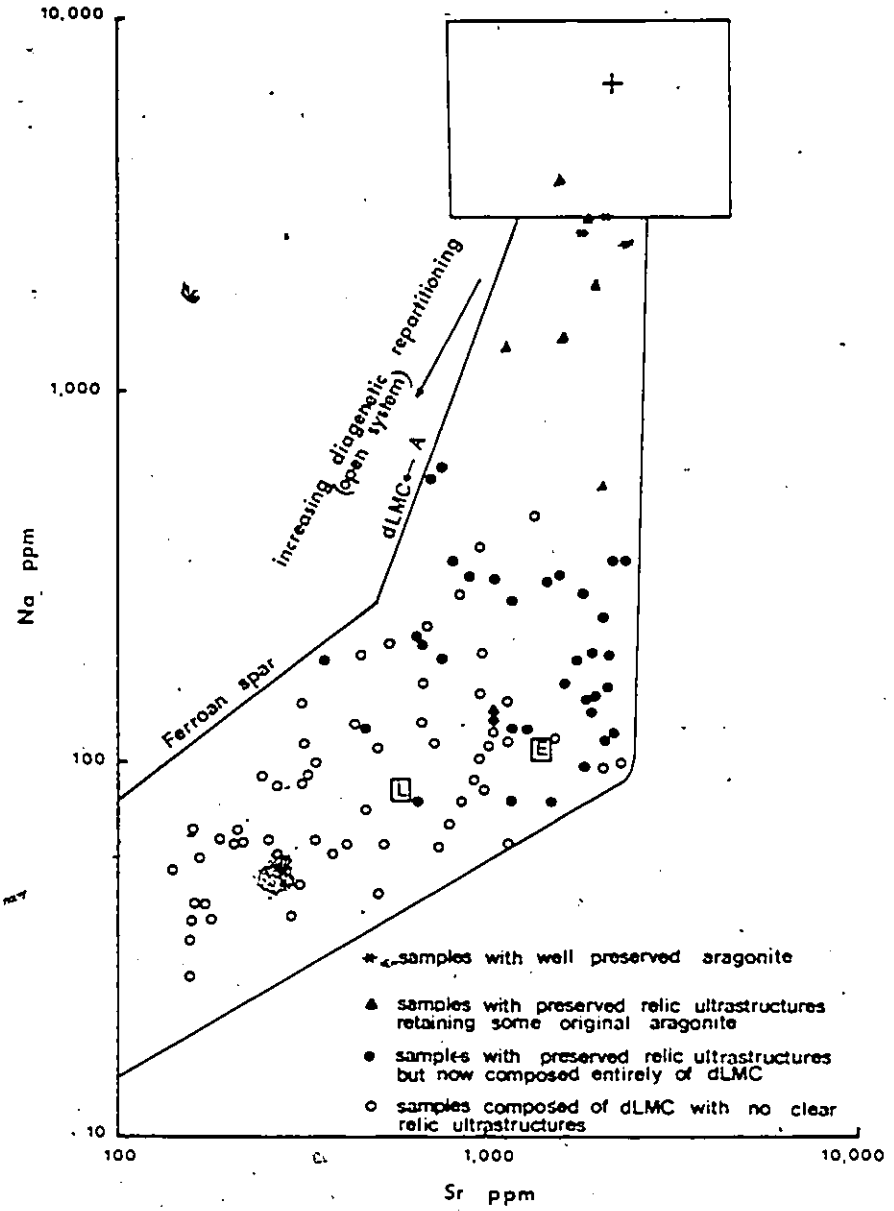

Fig.II -10. Scatter diagram of Na vs. Sr for all originally aragonitic components of rudist shell. The box and cross (+) represent the range and mean for present day marine bivalves (Chave, 1954; Lowenstam, 1963; Dodd, 1967; Polifka et al., 1972; Land and Hoops, 1973; Milliman, 1974; Zolotarev, 1976; Walker et al., 1977; Ragland et al., 1979). E and L are the mean values of early and late cement, respectively.

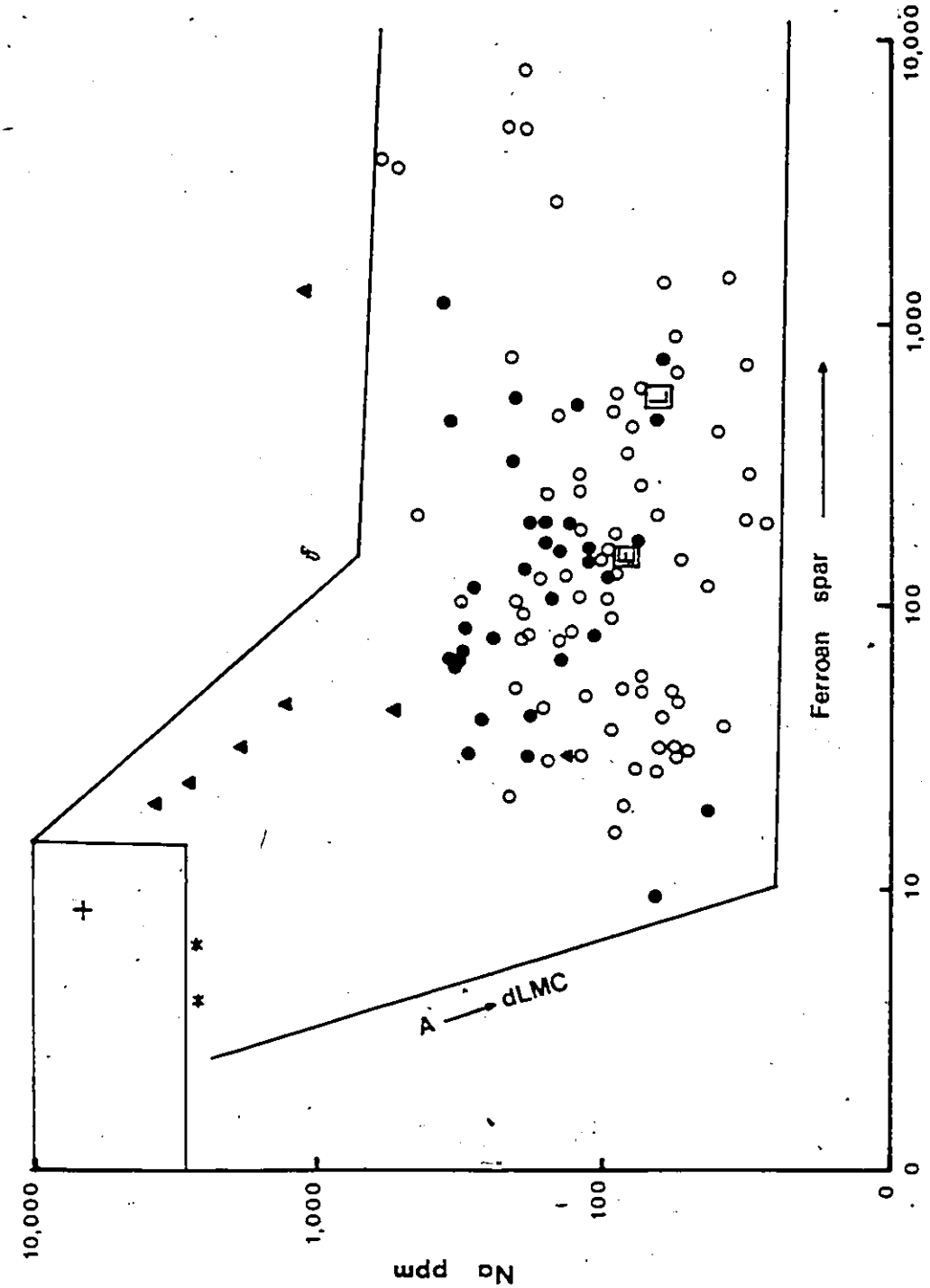

Fig. II-11. Scatter diagram of Na vs. Mn for all presumably originally aragonitic samples. Explanations as in Fig. II-10.

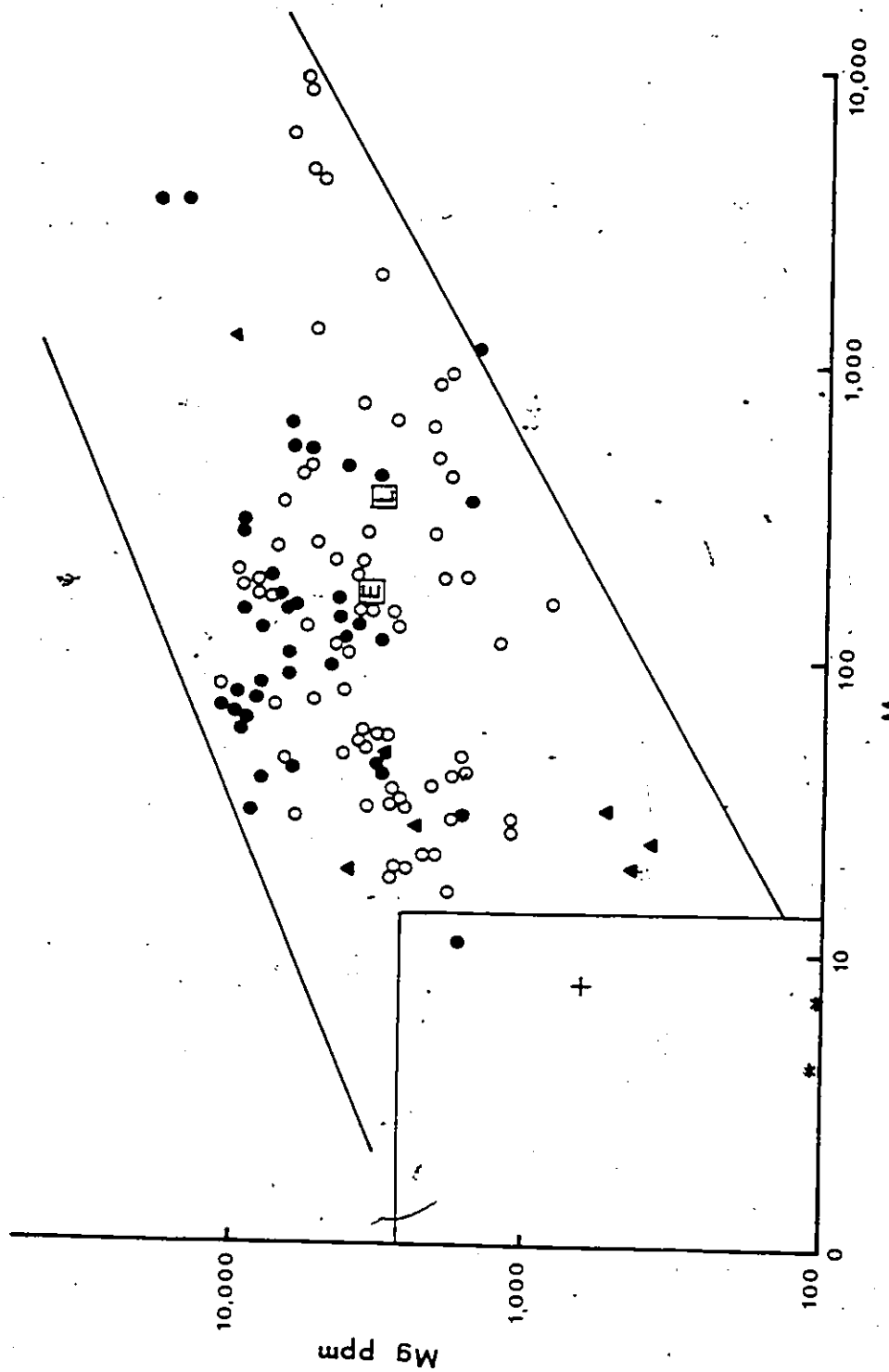

Fig. II-12. Scatter diagram of Mg vs. Mn for all presumably originally aragonitic samples. Explanations as in Fig. II-10.

represents more and more an open diagenetic system as the concentrations of Na and Sr decrease. A → dLMC recrystallization stage represented by the central part of the diagram, not only led to stronger retention of trace elements, but also to partial preservation of ultrastructures. This can be achieved only in partially closed diagenetic systems based on "thin film" or boundary layer principle (cf. Veizer, 1983a). In contrast, the samples with large loss of Na and Sr, and no relic ultrastructures, underwent A → dLMC transition through bulk removal of original A constituents and precipitation of dLMC from diagenetic meteoric waters. Hence, an open system of diagenesis. This dLMC (see late cement zone) is in equilibrium with the bulk pore water and not, as in the previous case, with the boundary layer water only.

In agreement with theoretical predictions (Fig. II-1), the studied samples show a negative relationship between Na and Mn (Fig. II-11). Again, samples with preserved aragonite approximate chemically present day pelecypods. The subsequent diagenetic repartitioning is, as previously advocated, a two-step process. During the actual A → dLMC transition (diagenetic repartitioning I; Table II-6), mostly Na is lost, while the enrichment in Mn is relatively slight. Once complete transformation is achieved, the residual pore

spaces are occluded by late ferroan calcite with large increase in Mn concentrations. At this stage, however, the bulk of Na was already lost from the system and the dLMC sensu stricto has comparable Na concentrations to the late ferroan spar.

The sympathetic relationship between Mn and Mg (Fig. II-12, and Factor 2, Table II-6) is also a consequence of A → dLMC transformation, since calcite structure is more suitable for Mg substitution than is the aragonitic one (cf. Graf, 1960). The conclusions advocated previously for Sr, Na and Mn are fully applicable to these trace elements as well, but the two stage process is not as clearly visible, because the Mg and Mn concentrations between dLMC and ferroan spar are not widely different.

2.4.5 Low-Mg Calcitic Skeletal Components

These components include outer shell layers, beads and pillars of hippuritids, and outer shell layers of radiolitids, requieniids and monopleurids. They are generally well preserved texturally with their ultrastructures still typical of LMC (see Section 1.4.2).

Factor analysis of all LMC components (Table II-8) shows that four factors are controlling their chemical variations. Factors 1 and 2 may be attributed to

TABLE II-8

Varimax rotated factor analysis of all LMC components (N = 113)

	Factor 1	Factor 2	Factor 3	Factor 4
log IR	0.046	-0.057	0.495	0.038
log Ca	0.256	0.032	-0.096	0.251
log Mg	0.355	0.171	0.041	0.499
log Sr	0.056	0.903	-0.103	0.229
log Mn	0.985	-0.019	-0.165	-0.038
log Fe	0.575	-0.152	0.290	0.008
log Na	-0.370	0.599	-0.085	-0.401
log Zn	-0.061	-0.029	0.572	-0.170
log Al	-0.075	-0.012	-0.045	0.282
Percent of Variation Explained	43.0	30.4	14.9	11.6
Eigen value	1.822	1.287	0.630	0.492
Interpretation	Diagenetic Stabilization II	Diagenetic Stabilization I	Laboratory Leaching	Biological Fractionation

diagenetic stabilization of the LMC ⟶ dLMC type. Factor 2 may represent an early diagenetic stage, during which the internal sediments and submarine cements in intraskeletal pore spaces of rudist shells have been stabilized. Stage 2 (Factor 1) again signifies a late cementation of the remainder of the intraskeletal pore spaces by ferroan calcite, particularly in radiolitids with the cellular ultrastructure. The inverse loadings of Mg and Na can perhaps be explained as biological fractionation. Shell formation in molluscs is governed by the chemistry of the extracellular fluids (Crick and Ottensman, 1983; Chave, 1984) and the concentration of a trace element in a mollusc shell is a direct response to the degree of disequilibrium between these fluids and ambient seawater. Biological fractionation of trace elements by recent molluscs, particularly for Sr and Mg, has been well documented previously (Lowenstam, 1963; Milliman, 1974, Chapter 4; Dodd and Stanton, 1981, Chapter 3). Other authors (e.g. Lowenstam, 1964; Lorens and Bender, 1977; Brand and Veizer, 1980; Al-Aasm and Veizer, 1982; Crick and Ottensman, 1983) documented the existence of biogenic fractionation of Sr, Mg and Na in other recent and ancient LMC shells as well. Rudists, in analogy to other LMC fossils, likely discriminated against Mg and incorporated, preferentially, Na into their shells. However, Ishikawa and Ichikuni (1984)

show high D value on their study of natural organic and inorganic calcites, but I believe that such D value obtained by these authors was a result of both biological and environmental factors.

Despite the usual notion of the stability of LMC in marine and meteoric environments, this phase suffers partial diagenetic modifications as well. Previous studies on Mezozoic belemnites (Veizer, 1974) and Paleozoic brachipods (Al-Aasm and Veizer, 1982) showed that their LMC skeletons were altered by <10 and <20%, respectively. The scatter diagram of Sr vs. Na for originally LMC components of rudists (Fig. II-13) reveals the existence of a diagenetic trend more pronounced than those described for LMC phase previously. Sr and Na values for samples to the far right are within the range of present day bivalves. In analogy to A ⟶ dLMC transition described previously, the loss of Na is more pronounced in early stages than is the loss of Sr. As discussed in factor analysis, I interpret this as predominantly the consequence of diagenetic stabilization of metastable marine cements in intraskeletal pore spaces. If so, cements must have formed a considerable portion of the separated skeletons and the trend is due chiefly to the difficulty of mechanical separation of pure skeletons. Although Mn does not show a negative correlation with Sr, such a relationship with Na is distinct (Fig. (II-14). This

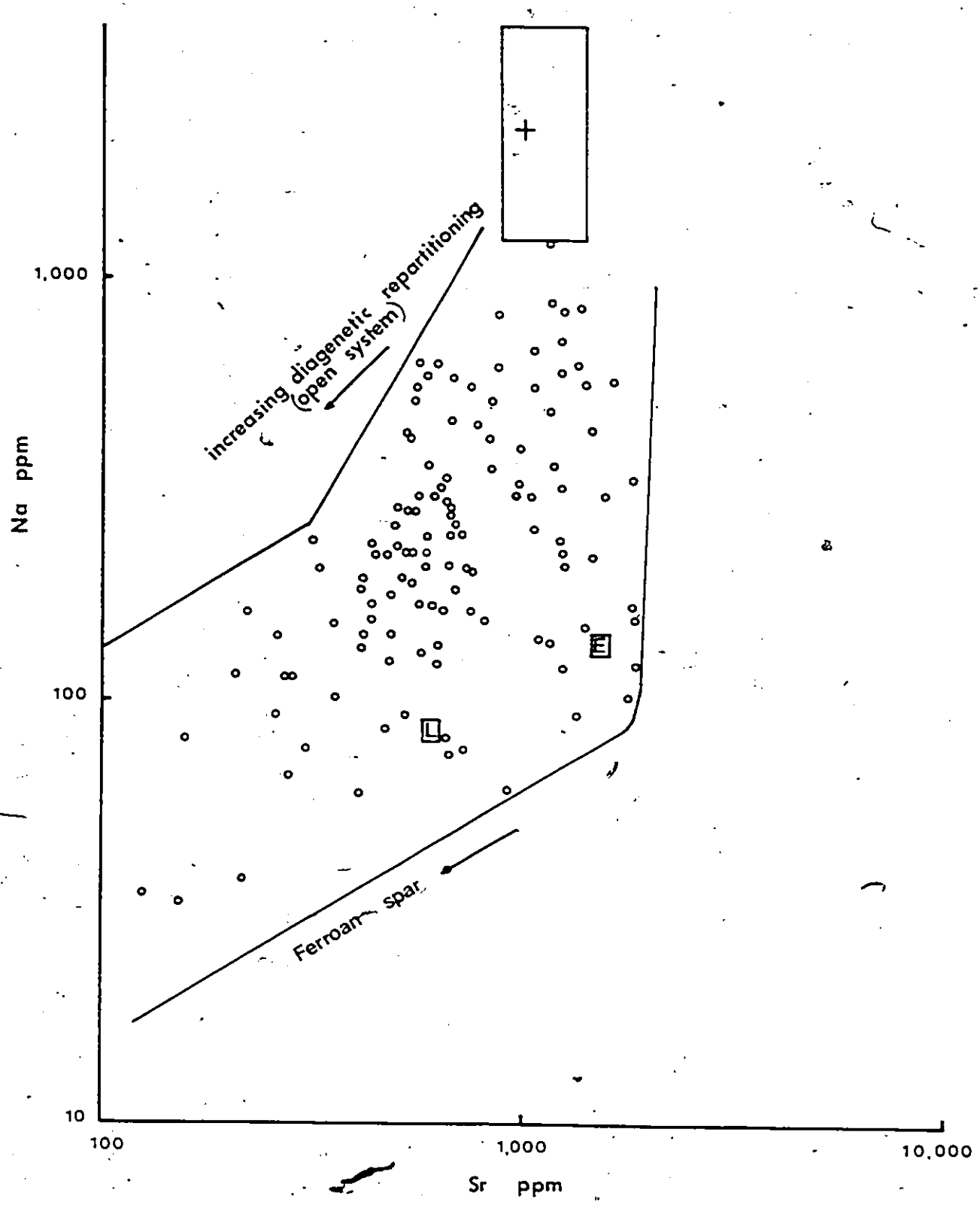

Fig. II-13 Scatter diagram of Na vs. Sr for all originally LMC skeletal components of rudist shells. The box and the cross (+) represent present day marine calcitic bivalves (Pilkey and Harris, 1966; Dodd, 1967; Milliman, 1974; Ragland et al, 1979).

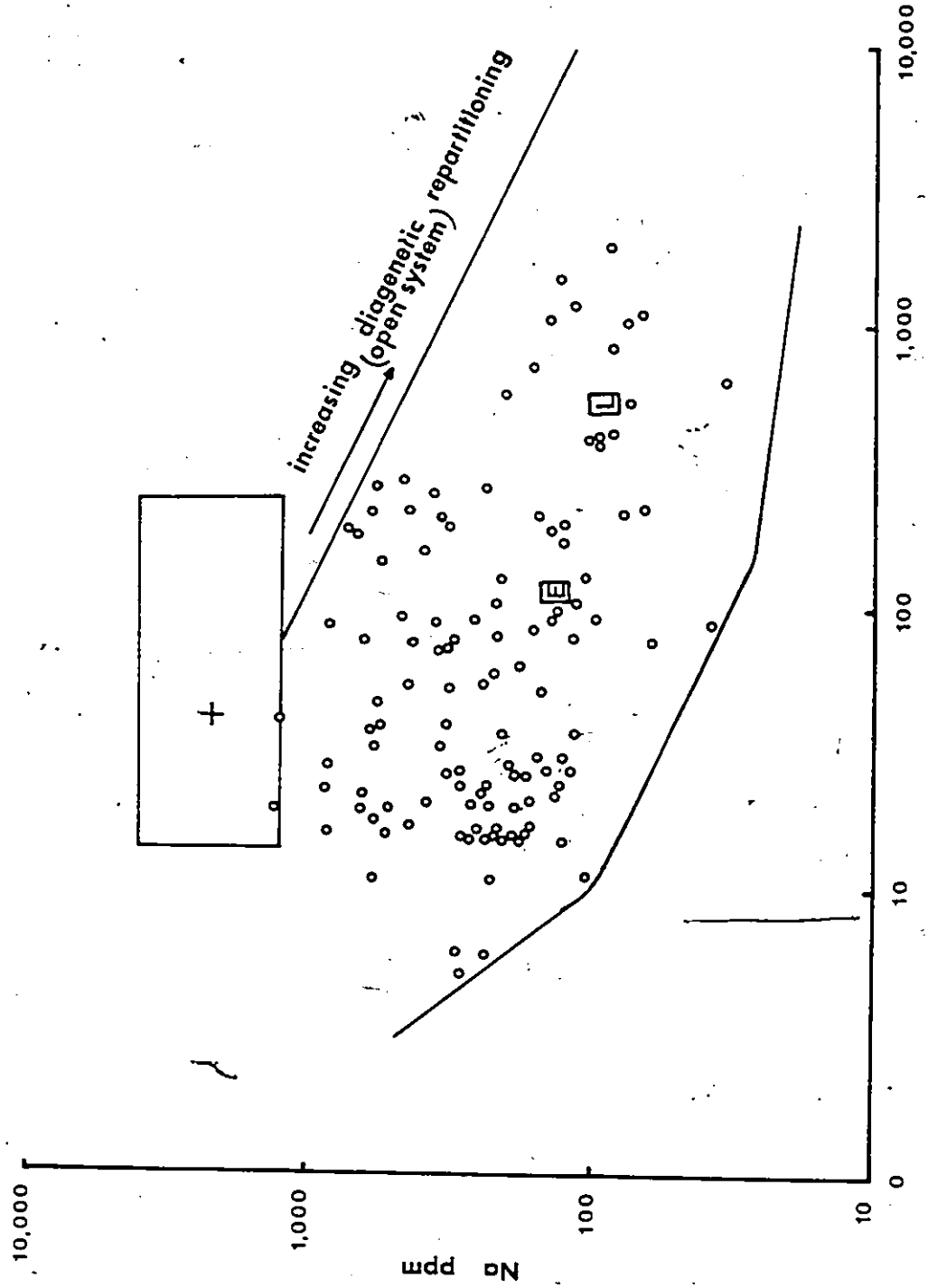

Fig. II-14. Scatter diagram of Na vs. Mn for all originally LMC skeletal components of rudist shells. Explanations as in Fig. II-13.

TABLE II-9

Comparison of chemical and isotopic parameters (geometric mean) for compact prismatic vs. cellular-prismatic ultrastructure (original mineralogy of both is LMC). Trace elements in ppm, $\delta^{18}O$ and $\delta^{13}C$ in ‰ vs. PDB

Element	Compact Prismatic	Cellular-Prismatic
Sr	710	760
Mn	35	95
Fe	280	420
Mg	2715	3805
Na	270	200
$\delta^{18}O$	-4.1	-4.3
$\delta^{13}C$	+1.2	+1.6

may be a consequence of the fact that the overall Sr decrease is considerably less distinct.

The role of ultrastructure of LMC phases on elemental concentrations is shown in Table II-9. Mn, Fe, and Mg are significantly higher, and Na lower, in layers with cellular-prismatic ultrastructure than with the prismatic one. This clearly supports the role of cements in development of the observed chemical signals.

2.4.6 Trace Element Distribution Within Rudist Families

In order to establish details of variations in the above diagenetic trends, the data for various families will be discussed separately in this section. Individual statistical analysis for Requieniidae and Monopleuridae have not been performed due to small number of samples. These two families, however, have been included in the pooled aragonitic and low-Mg calcitic populations.

2.4.6.1 Family Caprinidae

2.4.6.1.1 Outer Pallial Canal Layer

Factor analysis (Table II-10) of caprinid canal layers, which were presumably of original aragonitic mineralogy, shows that laboratory leaching of the insoluble residues is the dominant controlling factor

TABLE II-10

Varimax rotated factor analysis of all caprinids outer layers (N = 43)

	Factor 1	Factor 2	Factor 3	Factor 4
log IR	0.814	0.204	0.005	-0.091
log Ca	0.147	-0.060	-0.029	-0.237
log Mg	-0.008	0.175	0.891	-0.008
log Sr	0.197	0.229	0.091	0.788
log Mn	0.088	0.931	0.326	-0.088
log Fe	0.334	0.700	-0.018	-0.083
log Na	0.009	-0.130	-0.516	0.796
log Zn	0.511	0.116	-0.167	0.064
log Al	0.855	0.104	0.447	-0.009
Percent of Variation Explained	44.1	26.9	15.5	13.4
Eigen value	2.698	1.646	0.949	0.817
Interpretation	Laboratory Leaching	Diagenetic Stabilization II	Biological Fractionation or Diagenetic Stabilization	Diagenetic Stabilization I

of variations in I.R., Zn, and Al. Diagenetic stabilization is represented again (see Section 2.4.1) by a two-stage process (Factors 2 and 4, respectively), with late ferroan calcite controlling the Mn and Fe variations, whereas the early calcitization phase explains the positive relationship between Sr and Na (Fig. II-15). As shown earlier (Section 2.4.4), the degree of diagenetic repartitioning of Sr is much slower than that of Na. Theoretically, fresh water calcites should contain about 3200 ppm Mn^{+} and 1.7 - 3.5% Fe^{2+} (Brand and Veizer, 1983). The measured values are usually less than these values, but the trend towards higher Mn and Fe with increasing diagenetic stabilization is clear (Fig II-16). In agreement with theory (cf. Brand and Veizer, 1980; Veizer, 1983a), Sr in outer and inner layers of caprinids correlates weakly and negatively with Mn (Fig. II-17), despite the observation that this diagenetic trend has not been detected clearly by factor analysis.

Biological fractionation and/or diagenetic stabilization may explain the negative relationship between Mg and Na (Factor 3, Table II-10).

2.4.6.1.2 Inner Layers

The inner layers of caprinids, with lamellar and crossed-lamellar ultrastructures (cf. Section 1.4.2.3),

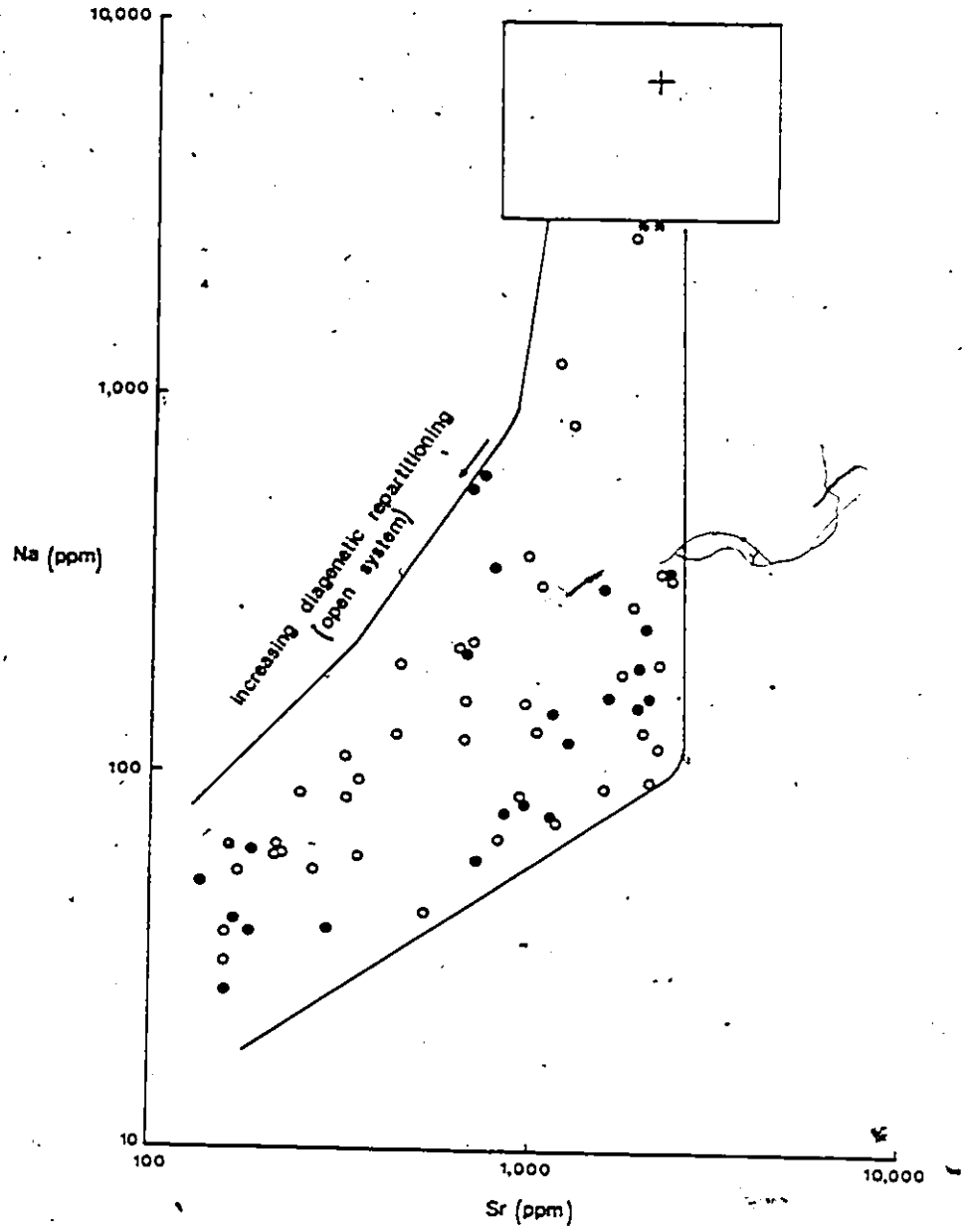

Fig.II-15. Scatter diagram of Na vs. Sr for all originally aragonitic skeletal components of caprinids. (*) and (+) as in Fig.II-10.The closed circles (●) represent inner layers and open circles (o) outer layers.

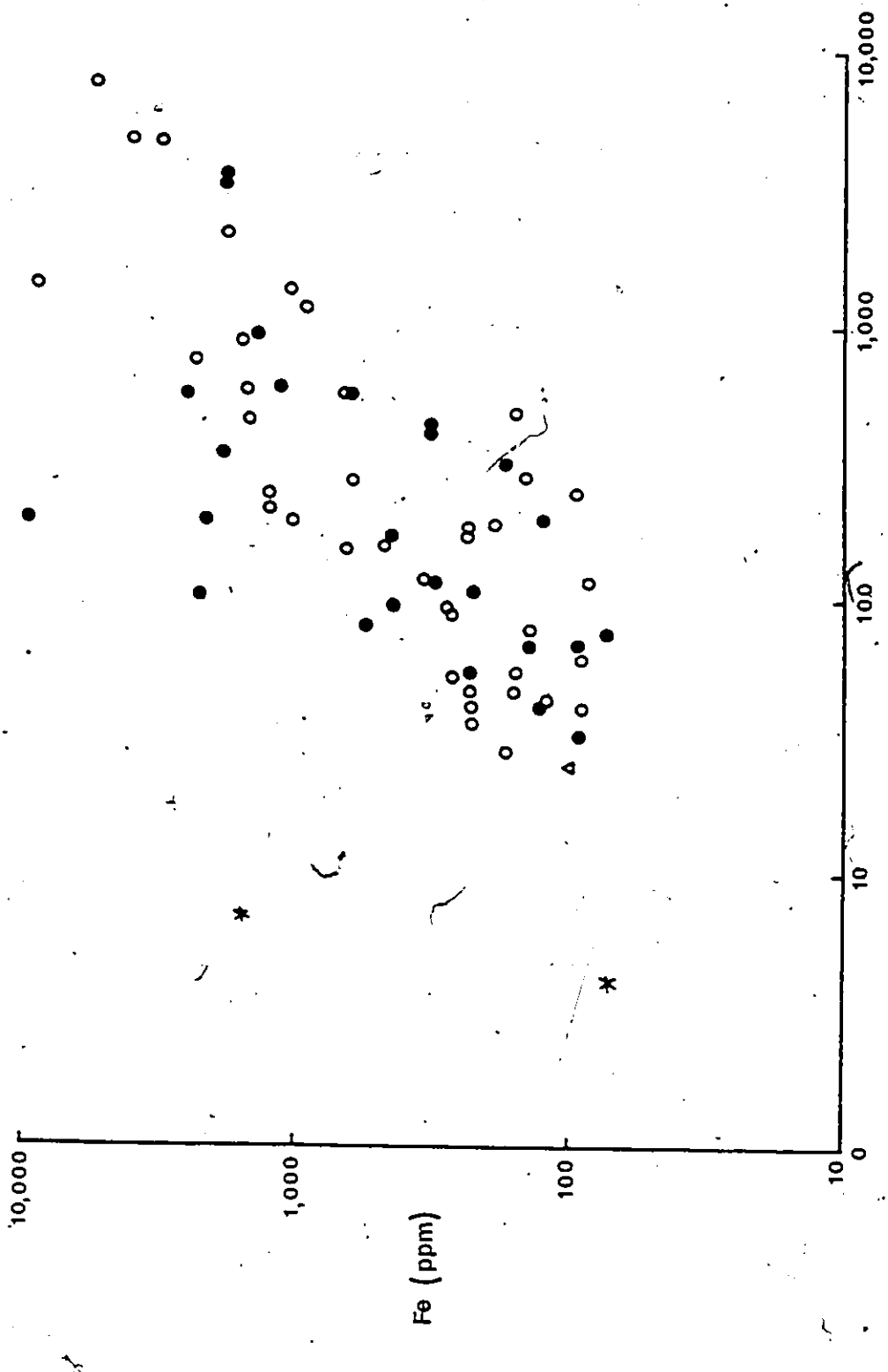

Fig.II-16. Scatter diagram of Fe vs. Mn of all originally aragonitic components of caprinids. Explanations as in Fig.II-15.

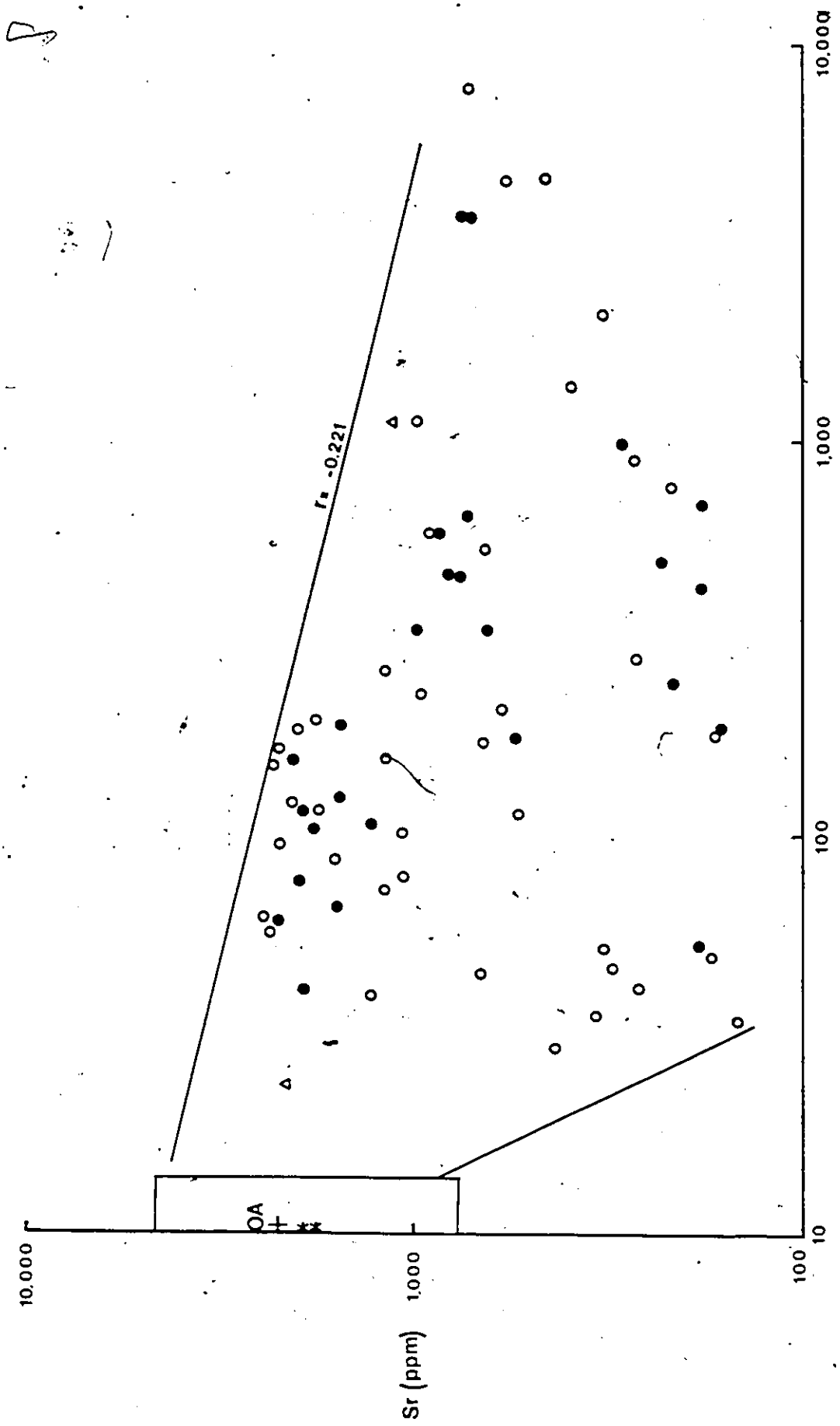

Fig. II-17. Scatter diagram of Sr vs. Mn for all originally aragonitic skeletal components of caprinids. (r) is correlation coefficient. Explanations as in Fig. II-10.

TABLE II-11

Varimax rotated factor analysis of all caprinids' inner layers (N = 27)

	Factor 1	Factor 2	Factor 3
log IR	-0.292	-0.020	0.545
log Ca	0.134	0.392	0.293
log Mg	0.744	0.172	-0.074
log Sr	0.802	-0.232	0.143
log Mn	0.019	0.964	-0.085
log Fe	0.075	0.594	0.036
log Na	0.871	0.026	-0.191
log Zn	-0.089	0.045	0.425
log Al	0.331	0.028	0.667
Percent of Variation Explained	45.6	31.9	22.5
Eigen value	2.186	1.526	1.078
Interpretation	Diagenetic Stabilization I	Diagenetic Stabilization II	Laboratory Leaching

are more compact than the more porous ultrastructure of the aragonitic outer layers. As a result, the dominant feature of their chemistry is the early diagenetic repartitioning of Na and Sr (Table II-11, and Fig. II-15). The covariance of Mg^{2+} is due to its earlier incorporation into dLMC rather than into a precursor aragonite. Late diagenetic ferroan calcite (Factor 2) is less important in this compact ultrastructure.

2.4.6.2 Family Hippuritidae

2.4.6.2.1 Outer Shell Layers, Pillars and Beads

Outer shell layers, pillars and beads of hippuritids were composed originally of the stable LMC of compact, prismatic ultrastructure (see Section 1.4.2).

Factor analysis of the outer layers (Table II-12) shows that Factor 1 is probably a composite of several effects. Firstly, the I.R. and Fe variations can be related to laboratory leaching from minerals present in the insoluble residues. Secondly, Mg variations can perhaps be explained by association of incipient dolomites with the I.R. Alternatively, biological fractionation may play a role in its distribution (see also Section 2.4.4). Diagenetic stabilization of the hippuritid LMC depicts again two-stage diagenetic trends (Factors 2 and 3, respectively), controlling Sr-Na (Fig.

TABLE II-12

Varimax rotated factor analysis of all Hippuritidae outer layers (N = 33)

	Factor 1	Factor 2	Factor 3	Factor 4
log IR	0.532	0.018	-0.081	-0.216
log Ca	0.090	-0.056	-0.018	0.458
log Mg	0.720	-0.200	0.064	0.101
log Sr	0.071	0.802	-0.159	-0.057
log Mn	0.177	-0.202	0.849	0.250
log Fe	0.676	0.070	0.671	0.265
log Na	-0.427	0.862	-0.197	-0.178
log Zn	0.197	0.055	-0.145	0.516
log Al	0.077	0.078	-0.199	0.045
Percent of Variation Explained	52.4	22.1	18.0	7.5
Eigen value	2.638	1.113	0.905	0.376
Interpretation	Laboratory Leaching and Biochemical Fractionation	Diagenetic Stabilization I	Diagenetic Stabilization II	?

TABLE II-13

'Varimax rotated factor analysis of all Hippuritidae pillars and beads (N = 21)

	Factor 1	Factor 2	Factor 3	Factor 4
log IR	0.359	0.106	-0.207	0.233
log Ca	0.224	-0.111	-0.511	0.203
log Mg	0.132	0.169	0.771	0.211
log Sr	0.380	0.633	0.411	0.048
log Mn	0.687	0.193	-0.284	-0.214
log Fe	0.879	-0.005	0.313	0.062
log Na	-0.079	0.893	0.144	-0.030
log Zn	-0.053	0.078	0.053	0.992
log Al	-0.258	-0.465	0.022	-0.292
Percent of Variation Explained	40.5	24.5	20.4	14.7
Eigen value	2.311	1.397	1.166	0.837
Interpretation	Diagenetic Stabilization II	Diagenetic Stabilization I	Dolomitization?	?

II-18) and Fe-Mn (Fig. II-19), respectively. The origin of these trends is the same as discussed previously.

If factor analysis for pillars and beads is performed (Table II-13), the late ferroan calcite precipitation appears as the dominant factor, but otherwise the factors are the same as for the outer layers. The only additional process may be an incipient dolomitization (Factor 3).

2.4.6.2.2 Inner Shell Layers

Factor analysis (Table II-14) of the presumably originally aragonitic inner layers, with variable degrees of textural preservation, shows that the two-stage diagenetic stabilization is also exemplified here (Factors 1 and 2, and Figs. II-18, 19, respectively). The negative loading of Zn on Factor 2 contradicts theoretical assumptions, since (due to its D > 1) Zn should be enriched in dLMC (Pingitore, 1978). I have no explanation for this observation. Similarly, the meaning of the last factor, which controls Ca, Mg and Fe, is not clear.

2.4.6.3 Family Radiolitidae

2.4.6.3.1 Outer Layer

The relatively thick outer cellular-prismatic low-Mg calcitic ultrastructure of radiolitids (see Section

TABLE II-14

Varimax rotated factor analysis of all Hippuritidae inner layers (N = 21)

	Factor 1	Factor 2	Factor 3
log IR	-0.661	-0.114	0.234
log Ca	0.146	0.159	0.529
log Mg	0.192	-0.069	0.598
log Sr	0.703	0.157	0.355
log Mn	0.478	0.704	0.248
log Fe	-0.196	0.609	0.538
log Na	0.913	-0.104	0.179
log Zn	0.254	-0.841	0.363
log Al	0.066	0.031	-0.455
Percent of Variation Explained	46.2	33.2	20.6
Eigen value	2.478	1.779	1.103
Interpretation	Diagenetic Stabilization I	Diagenetic Stabilization II	Total Carbonate?

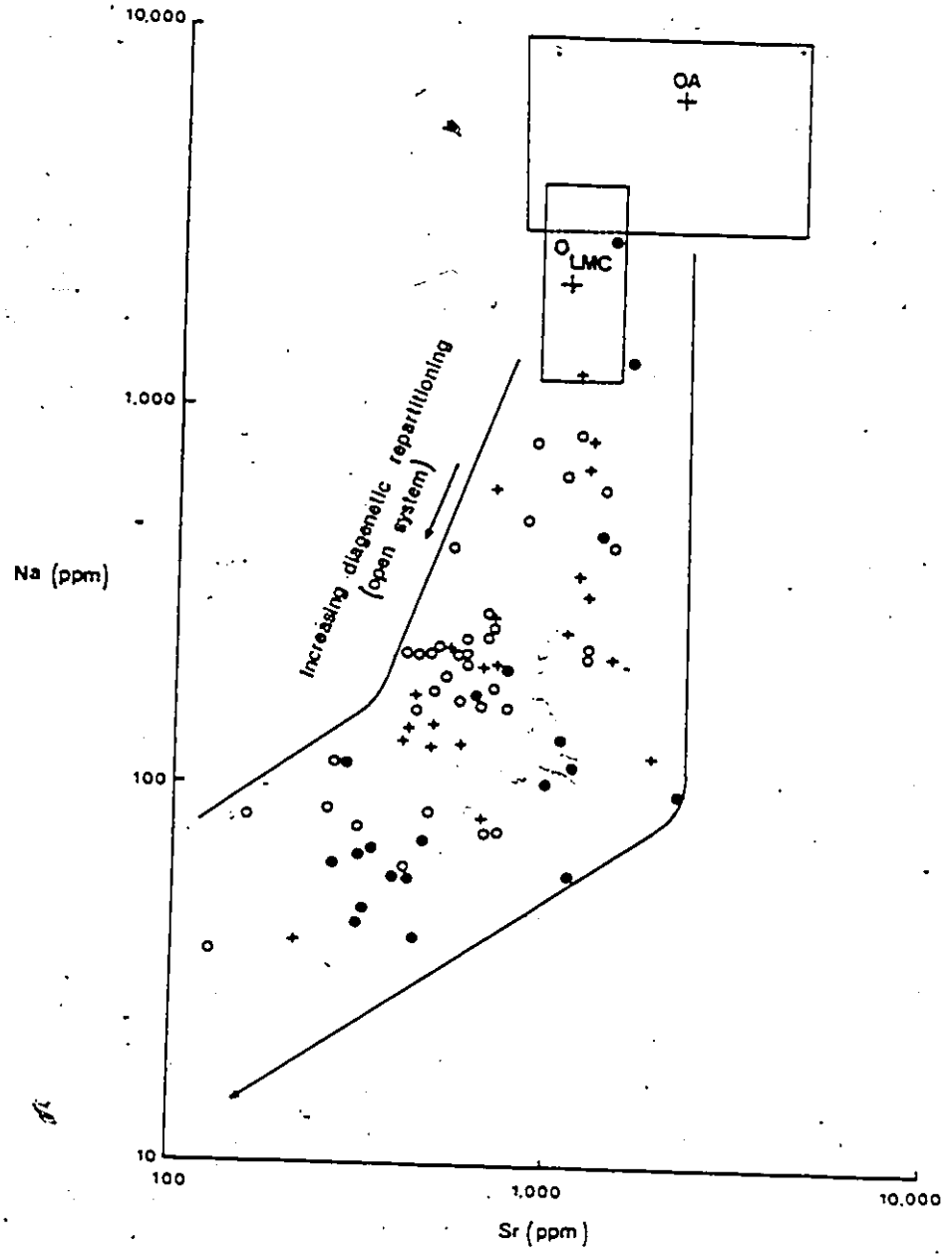

Fig.II-18. Scatter diagram of Na vs. Sr of hippuritid outer layers, pillars and beads (originally LMC) and inner layers (originally A). The (o) represents outer layer. The (+) represents pillar and bead, and the (•) represents inner layer. Other explanations as in Figs.II-10,13.

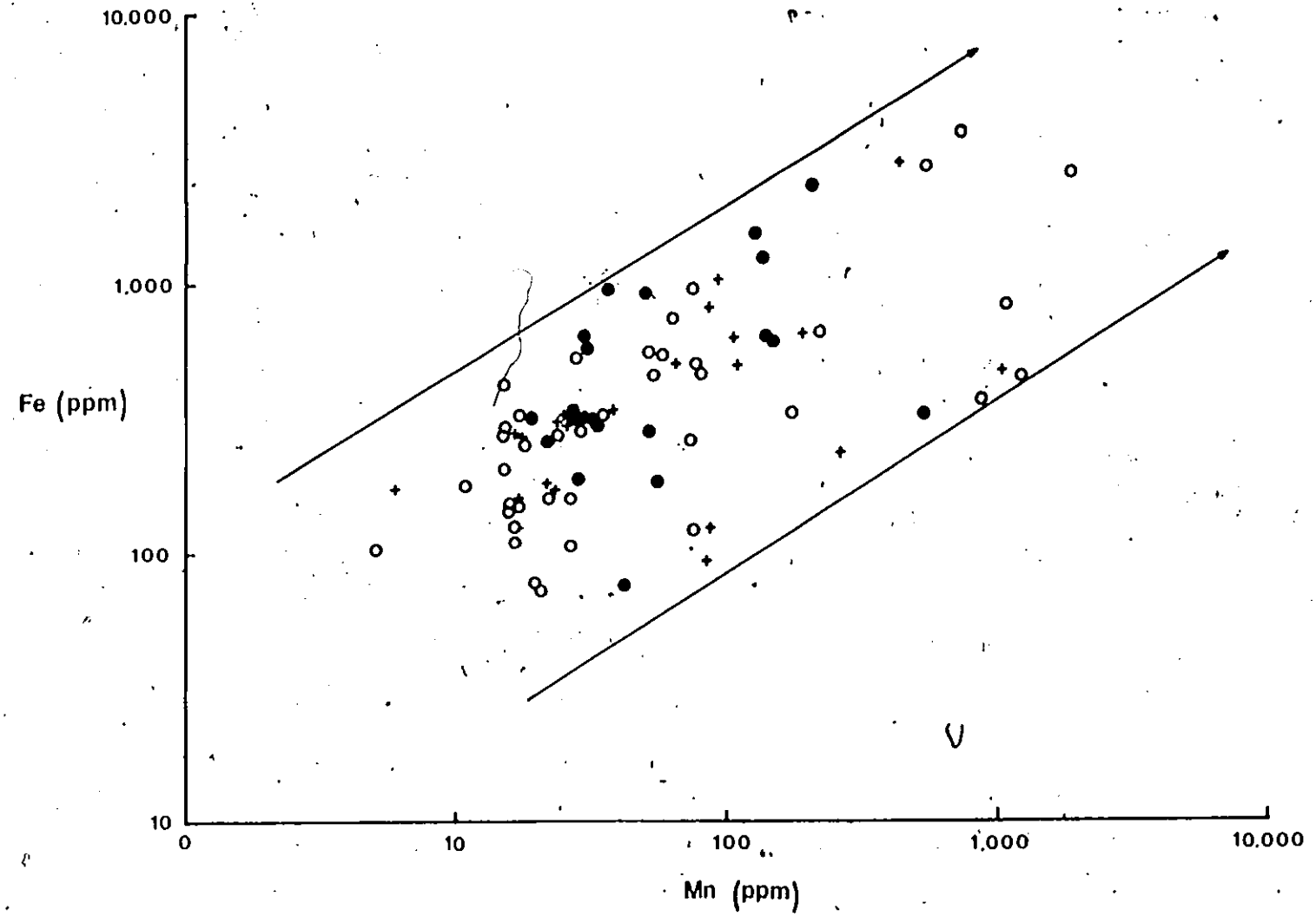

Fig.II-19. Scatter diagram of Fe vs. Mn of hippuritid outer layers, pillars and beads (originally LMC), and inner layers (originally A). Explanations as in Fig.II-18.

TABLE II-15

Varimax rotated factor analysis of all radiolitid outer layers (N = 53)

	Factor 1	Factor 2	Factor 3
log IR	-0.412	-0.347	0.297
log Ca	0.069	0.378	0.109
log Mg	0.507	0.404	0.101
log Sr	0.761	0.335	0.163
log Mn	-0.192	0.931	-0.076
log Fe	-0.629	0.223	-0.006
log Na	0.440	-0.227	0.035
log Zn	-0.426	-0.078	0.055
log Al	0.046	0.099	0.762
Percent of Variation Explained	48.4	34.0	17.6
Eigen value	1.973	1.387	0.718
Interpretation	Diagenetic Stabilization I	Diagenetic Stabilization II	Laboratory Leaching of Clay Minerals

1.4.2.2), with its moderate porosity, permits the incursion of internal sediments and of early and late cements during different periods of its diagenetic history. Factor analysis (Table II-15) of the outer layer shows that two diagenetic factors, already described in previous sections, control the chemical variation in Mg, Sr, Na, Fe, Mn and possibly Zn. Projection of Sr vs. Na values (Fig. II-20) shows that Sr of some samples is higher than in calcite in inorganic equilibrium with seawater (~1000 ppm Sr, Veizer, 1983a), and higher than its content in the present day LMC pelecypods. This may be a consequence of contamination by the early cement of a mineralogy with its original Sr content of about 9000 ppm.

2.4.6.3.2 Inner Layer

The observed chemical variations within radiolitid inner layers, originally of aragonitic composition, follow the same general diagenetic trends as the aragonitic components from other families. Factor 1 (Table II-16) shows that both laboratory leaching (positive correlation between I.R. and Al) and diagenetic stabilization (Sr negatively correlated with Fe) are the controlling parameters of their chemical variations. Factor 2, another diagenetic signal, shows a negative correlation between Mn and Na.

TABLE II-16

Varimax rotated factor analysis of all radiolitid inner layers (N = 26)

	Factor 1	Factor 2	Factor 3
log IR	0.657	0.086	0.743
log Ca	-0.068	-0.070	-0.004
log Mg	0.022	-0.370	-0.743
log Sr	-0.788	0.207	-0.144
log Mn	-0.071	-0.846	-0.176
log Fe	0.786	0.109	-0.004
log Na	0.286	0.878	0.315
log Zn	0.241	0.423	0.114
log Al	0.782	0.445	0.227
Percent of Variation Explained	68.1	20.7	11.3
Eigen value	3.969	1.203	0.657
Interpretation	Laboratory Leaching and Diagenetic Stabilization	Diagenetic Stabilization	?

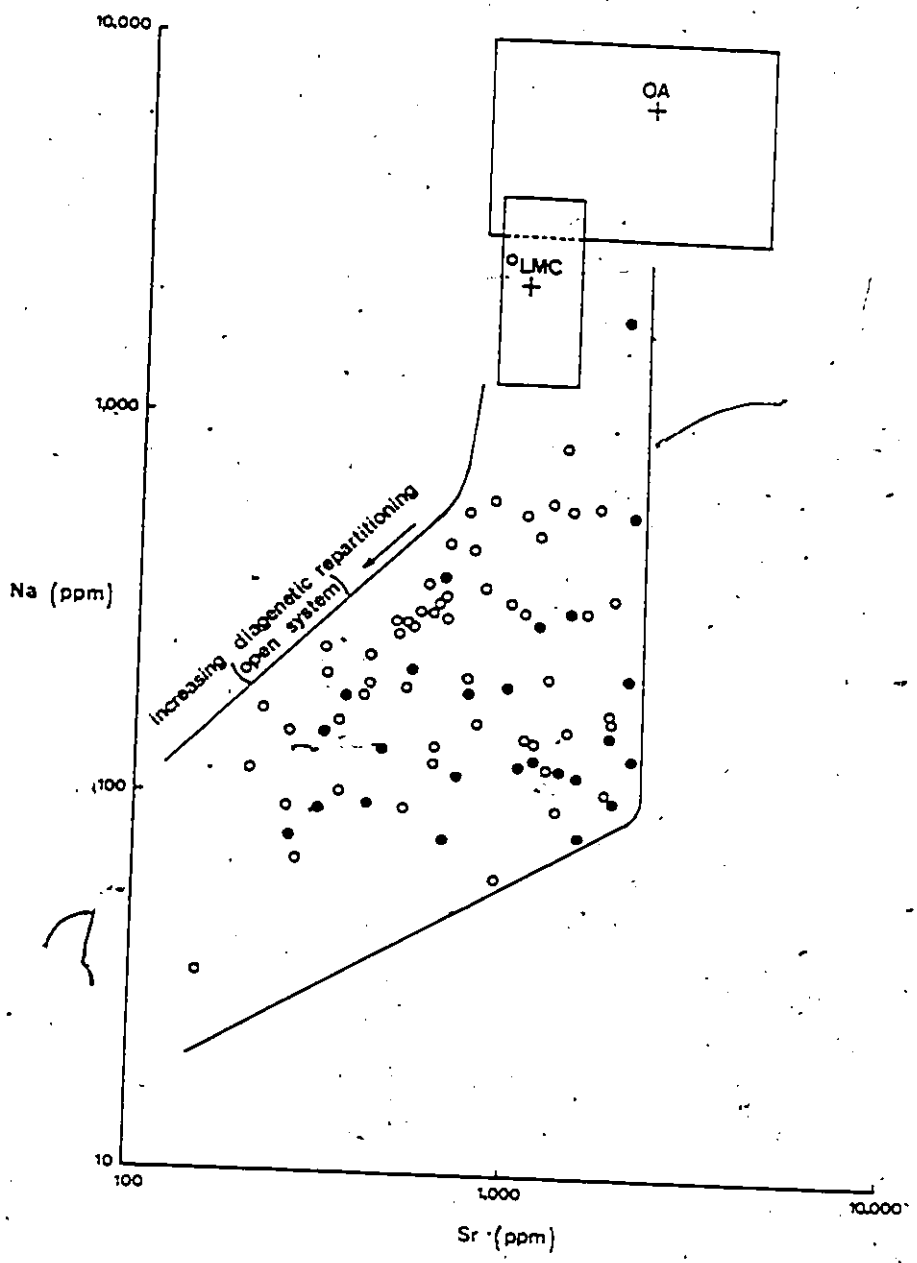

Fig.II-20. Scatter diagram of Na vs. Sr of radiolitid outer layers (originally LMC) and inner layers (originally A). Explanations as in Figs.II-10,13,18.

2.5 SUMMARY AND IMPLICATIONS OF DIAGENETIC TRENDS

The discussed diagenetic trends in all components of rudist shells and in their associated rock matrix have shown that some elements are sensitive indicators of diagenetic processes. In particular, Sr and Na, in conjunction with petrographic evidence, are good indicators of early diagenetic stabilization of aragonite (A) → dLMC type. The frequent partial preservation of ultrastructures and of trace element signal of the original aragonitic precursor, despite exposure to meteoric water, argue for A → dLMC transition being accomplished in small-scale, semi-closed microenvironments. Such microenvironments, or reaction zones, maintain a diffusion controlled gradient from given surface towards the bulk aquifer water (cf. Berner, 1980, p. 40; Pingitore, 1982; Veizer, 1983a). However, their diffusion gradients differ for each element. As a consequence, the diagenetic loss of Sr in partially stabilized aragonite is much slower than that of Na. However, the matter is complicated by the observation that Na may be present not only within the $CaCO_3$ lattices but also in fluid inclusions, whereas Sr is present mostly in lattice positions. It is therefore possible that Na from fluid inclusions could have been expelled preferentially during the early invasion by meteoric waters. At present, I cannot differentiate

between these two alternatives and they are not necessarily mutually exclusive.

In contrast, those aragonitic samples which underwent severe diagenetic alteration show only preservation of outlines but not ultrastructures. These outlines are filled mostly by coarse spar, mostly of ferroan calcite, with higher concentrations of Mn, Fe and Mg, and severe loss of Sr and Na. Such an intensive repartitioning is characteristic of high water/rock, or open, diagenetic systems.

Diagenetic trends in originally LMC components are almost the same as in the originally aragonitic components. However, the magnitudes of diagenetic shifts during LMC → dLMC transitions are smaller and the bulk of these trends may be due to the presence of cements in primary and secondary pore spaces. Biological fractionation appears to have affected, at least partly, the distribution of Na and Mg into rudist LMC. The former minor element was enriched, whereas the latter was depleted in comparison to other molluscs.

In summary, the magnitude of any trace element diagenetic shift could have been controlled by a variety of factors, such as original mineralogy and chemistry, ultrastructural build-up (= surface kinetics), physiochemistry, water/rock ratios, and molar differences between marine vs. diagenetic waters

(cf. Veizer, 1983a). Variable permutations of the above may result in variable degrees of diagenetic shifts, as illustrated by plots of averages for Sr vs. Mn and Sr vs. Na in each separate layer of caprinids, hippuritids, and radiolitids from American localities (Figs. II-21, 22, 23, 24, 25, 26). They all show the postulated sympathetic relationship between Na and Sr and their inverse behaviour to Mn, but the observed shifts differ among various shell components. For example, the inner layers of caprinids (Figs. II-21, 22), originally of aragonitic mineralogy, always have higher Sr and Na and lesser Mn than the remaining shell components. The more porous outer layers underwent more severe diagenetic alteration, but the most altered patterns are displayed by internal sediments and cements.

Analogous diagenetic shifts can be demonstrated for the other families (Figs. II-23, 24, 25, 26).

The chemistry of skeletal components still preserved in their original A and LMC mineralogy is comparable to that of Recent marine bivalves. This argues for similar chemistry for the Cretaceous and Recent marine waters and for analogous mechanisms of trace element incorporation into shells of all these molluscs. The advocated chemical signatures, associated with various depositional and diagenetic sequences, are summarized in Table (I-2).

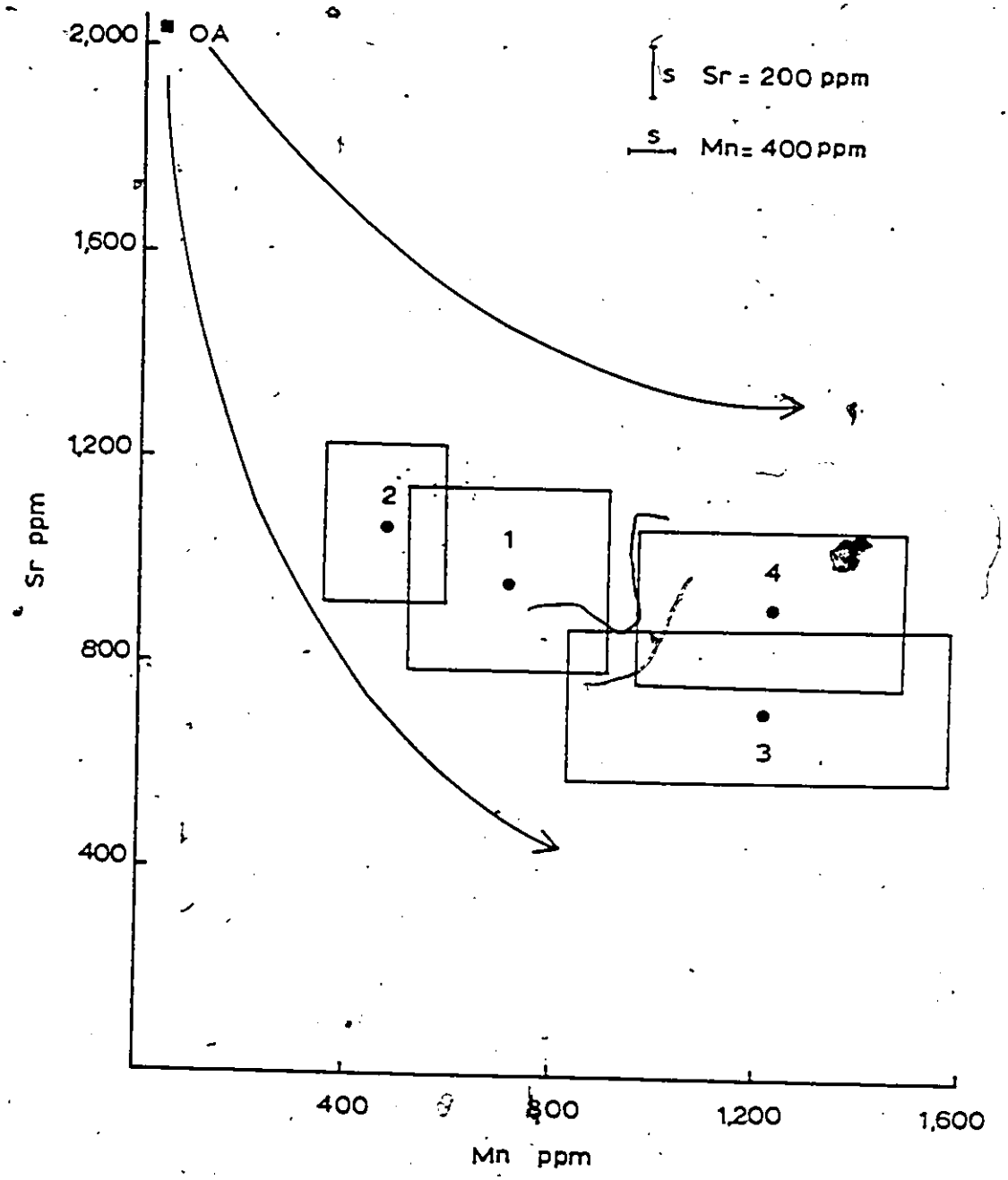

Fig.II-21. Plot of Sr vs. Mn for all samples of family Caprinidae (based on mean (•)±1 standard deviation (*s*)). Box (1) represents outer pallial canal layers. Box (2) represents inner layers. Box (3) represents enclosing cements. Box (4) represents enclosing internal sediments. O_A is the average value for presentday marine bivalves (see Fig.II-8).

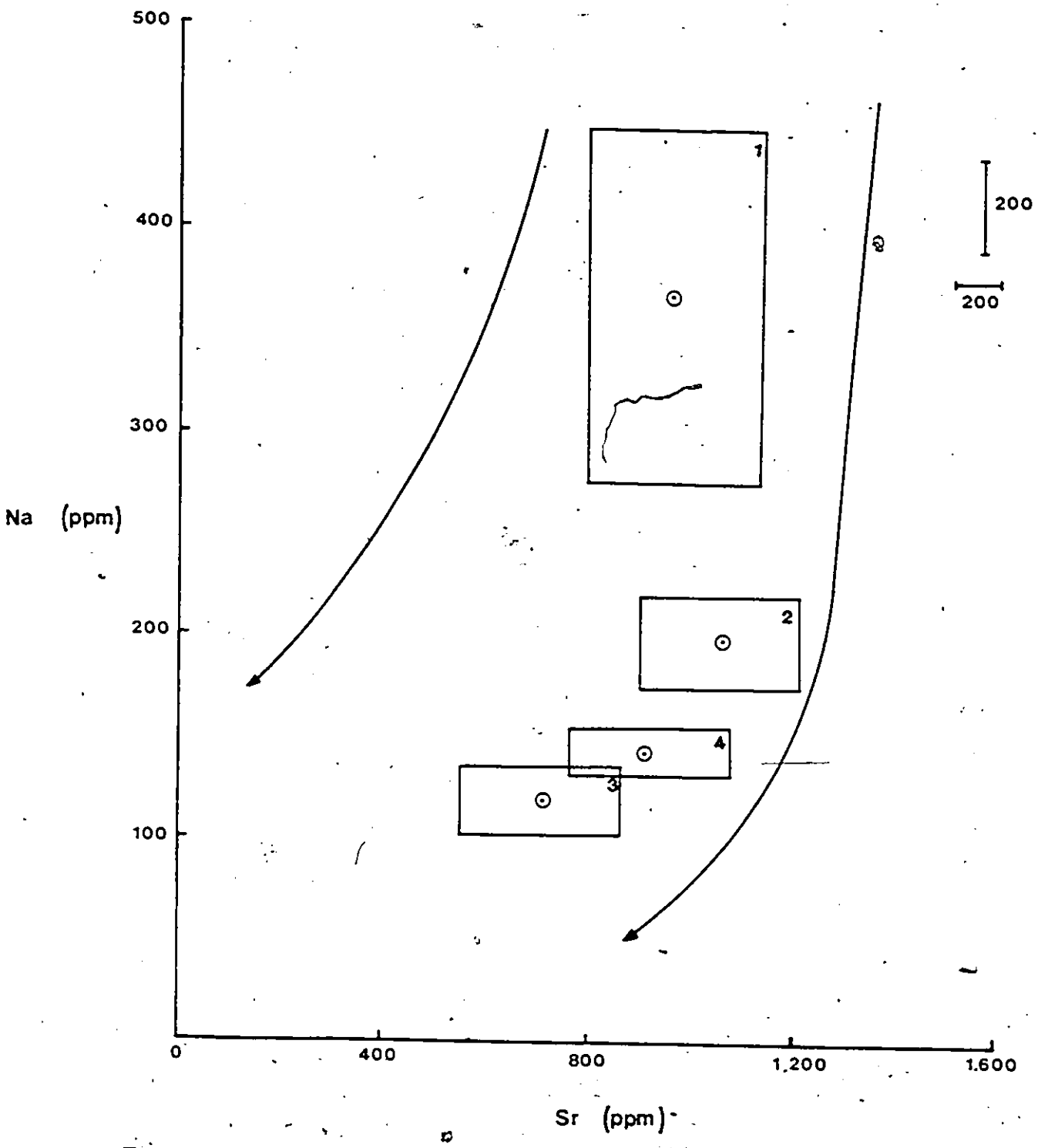

Fig.II-22. Plot of Na vs. Sr for all samples of family Caprinidae. Explanations as in Fig.II-21.

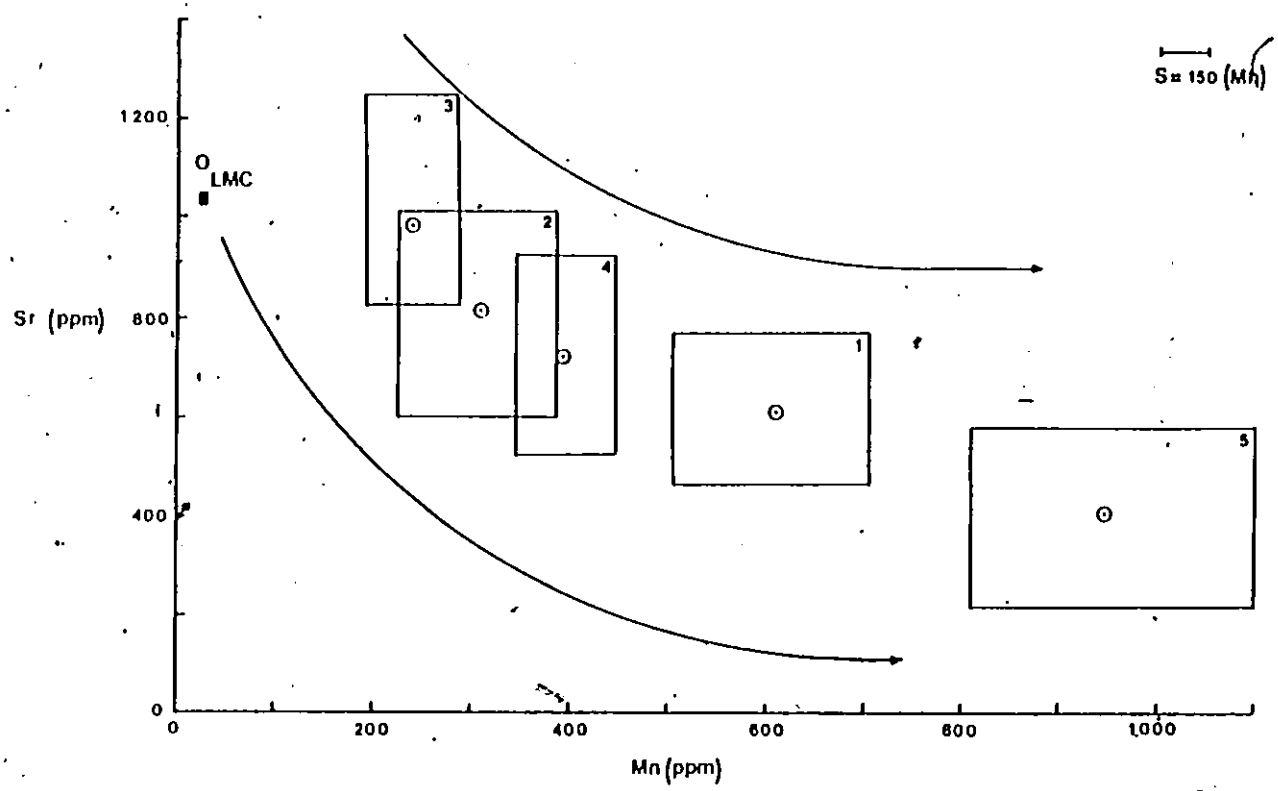

Fig.II-23. Plot of Sr vs. Mn for all samples of family Hippuritidae. Box (1) represents outer layer. Box (2) represents pillars and beads. Box (3) represents inner shell layers. Box (4) represents cements, and box (5) represents internal sediments. O_{LMC} is the average value for present day marine bivalves (see Fig.II-13). In this diagram only the samples from American localities were utilized. The samples from French localities were excluded due to their low Mn values (see the text for further details).

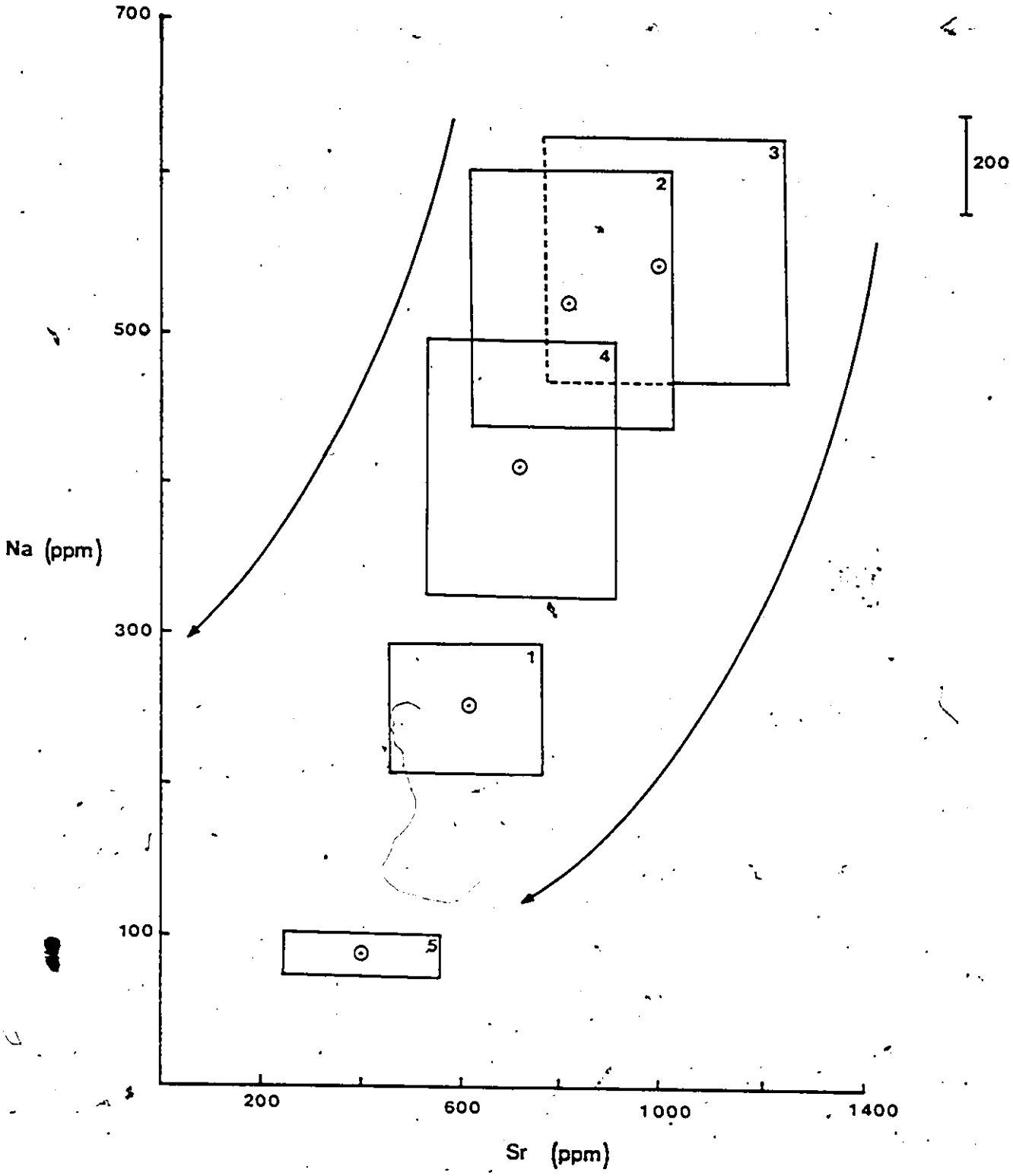

Fig.II-24. Plot of Na vs. Sr for all samples of family Hippuritidae. Explanations as in Fig.II-23.

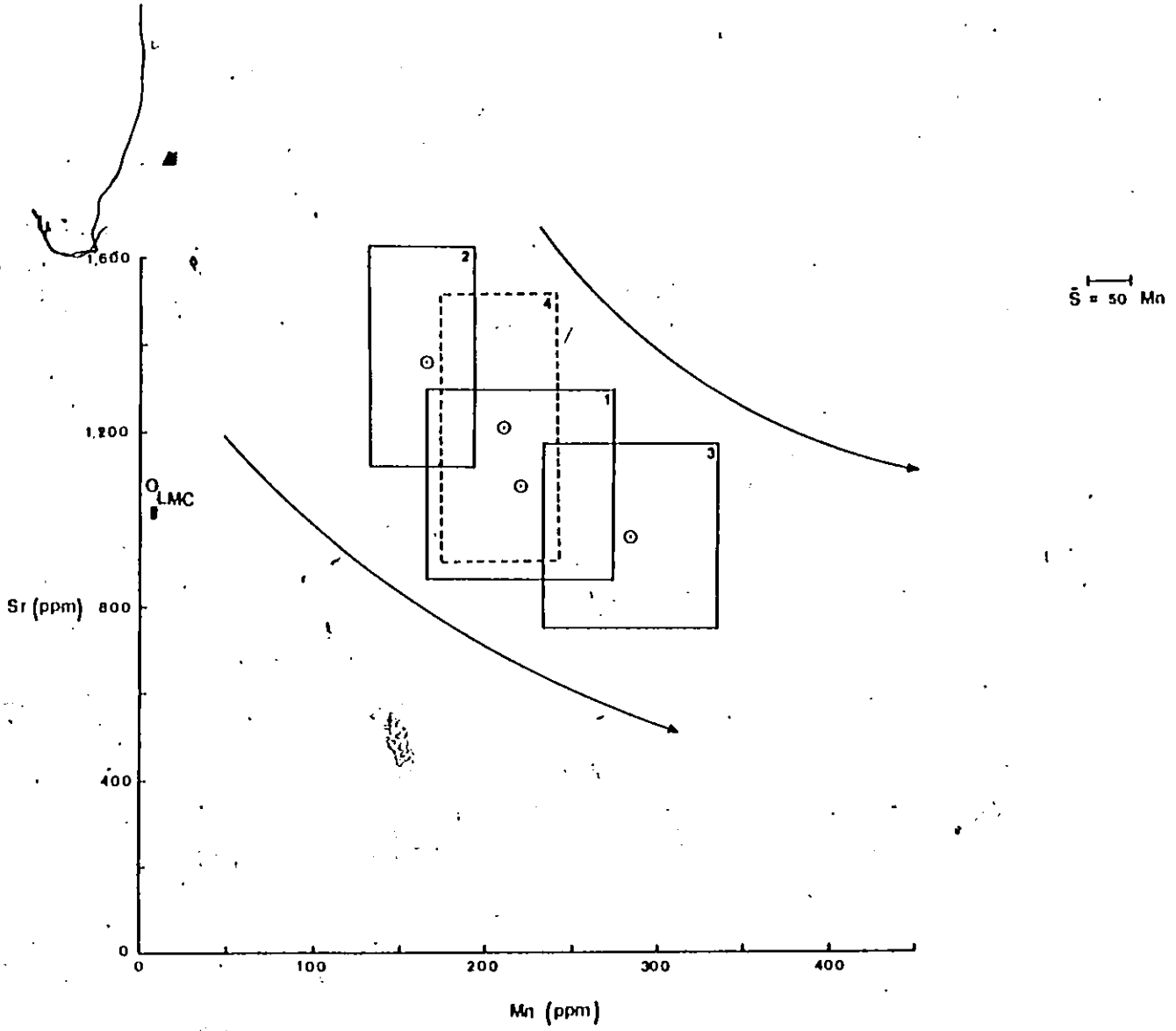

Fig.II-25. Plot of Sr vs. Mn for all samples of family Radiolitidae (american localities only). Box (1) represents outer layer, box (2) inner layers, box (3) cements, and box (4) internal sediments. O_{LMC} is the average value for present day marine bivalves (see Fig.II-13).

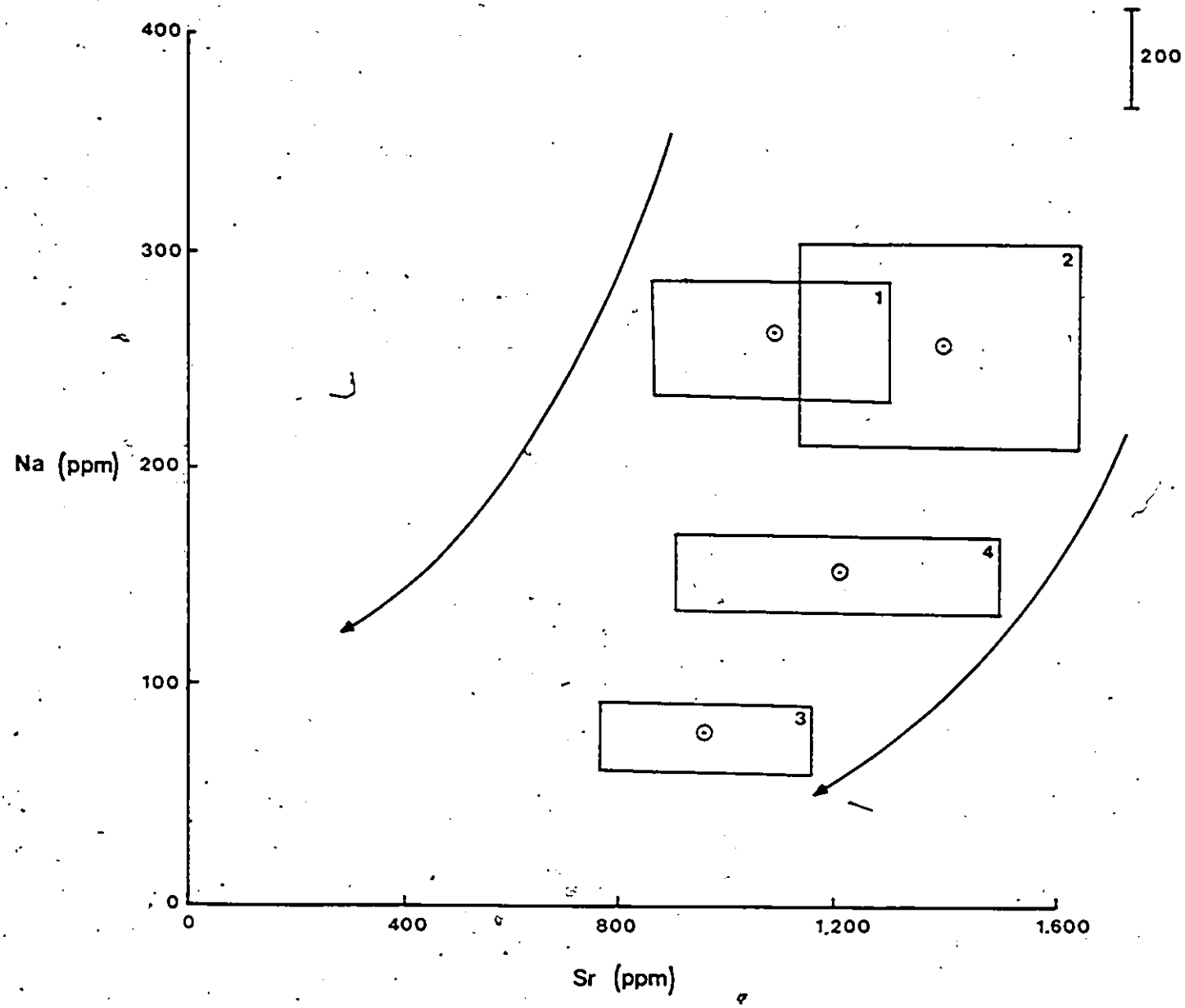

Fig.II-26: Plot of Na vs. Sr for all samples of family Radiolitidae (american localities only). For explanations see Fig.II-25.

2.6 CONCLUSIONS

The evaluation of chemical data for textural components of rudist shells and for their associated rocks leads to the following conclusions:

(1) Diagenetic stabilization of aragonitic and low-Mg calcitic components of Cretaceous rudist shells is a systematic process, which usually leaves behind distinctive signals in terms of their textural morphology and chemistry.

(2) Diagenetic stabilization of A → dLMC is a two-stage process. Initially, Sr and Na are partly depleted during an early meteoric diagenetic phase. The expulsion of Sr occurred in a much slower fashion than that of Na. This is followed by incorporation of Mn, Fe and Mg.

(3) Diagenetic repartitioning of trace elements during LMC → dLMC transformation follows the same pattern as in (2), but is of a lesser magnitude. This argues against diagenetic stability of LMC phases. The observed diagenetic trends may, however, also reflect stabilization of cements, which were precipitated into primary and secondary pore voids during early marine as well as subsequent meteoric diagenesis. At this stage, it is difficult to separate or quantify the role of these two factors. Nevertheless, and despite the observed chemical signals, textural identity of LMC

components is invariably preserved.

(4) The magnitude of the observed diagenetic trend in the successor dLMC depends not only on the original mineralogy, but also on the structural buildup of a given shell layer. This suggests that factors such as water/rock ratio (surface kinetics) are of considerable significance in the process of diagenetic mineralogical stabilization.

(5) Rudists appear to have exerted biological fractionation during secretion of their shells. They incorporated preferentially Na and discriminated against Mg.

(6) Partial preservation in rudist shells of (a) aragonitic ultrastructures as ghost relics, (b) trace element (Sr, Mn, Na and Fe) signatures inherited from precursors, and (c) textural features suggest that diagenetic transformation of aragonite into dLMC has been accomplished in a micron-scale environment.

(7) Each cementation phase, occluding the primary and secondary pore spaces, has its specific trace element chemistry. The theoretical composition of parent water for these cements was likely intermediate between that of sea and meteoric water. The marine component probably originated from dissolution marine precursors (A, HMC), which were therefore partially buffering the composition of the diagenetic solutions.

(8) The chemistry of the still preserved original A and LMC components in rudist shells is in general accord with that of Recent marine bivalves. This may argue for similar chemistries of Cretaceous and Recent seawater as well as for identical mechanism of trace element incorporation into mollusc shells.

3.1 INTRODUCTION AND THEORETICAL CONCEPTS

Carbonate minerals, in addition to minor and trace elements, also incorporate oxygen and carbon isotopes into their structures. The ratios of their isotopes in carbonate sediments may reflect isotopic composition and temperature of their ambient waters (Hudson, 1977; Anderson and Arthur, 1983).

Isotopic variations in carbonate rocks may be dealt with in terms of carbon and oxygen reservoirs. For carbon, the major reservoirs are the organic matter and the sedimentary carbonate which are isotopically quite different from each other (Hoefs, 1980, 1982). On the other hand, oxygen is contained within carbonate sediments ($CO_3^=$) and water (H_2O, HCO_3^-) (Lohmann, 1983). Diagenetic stabilization of marine carbonate sediments is a wet dissolution-reprecipitation process (Bathurst, 1975, Chapter 8). It involves equilibration of these components (including their original isotopic composition) with the intervening pore waters of different isotopic composition. Diagenetic repartitioning of stable isotopes will be accompanied also by trace element redistribution (Veizer and Fritz, 1976; Brand and Veizer, 1981; Lohmann, 1983; Veizer, 1983a, b). Such diagenetic repartitioning usually leads towards ^{12}C and ^{16}O enriched isotopic composition of the dLMC. This isotopic exchange can be expressed by the

following equation:

$$^{13}C^{18}O^{2-}_3 + H_2{}^{16}O + {}^{12}CO_2 \rightleftharpoons {}^{12}C^{16}O^{2-}_3 + H_2{}^{18}O + {}^{13}CO_2 \quad - - - (1)$$

The variation of $\delta^{18}O$ and $\delta^{13}C$ in the diagenetic carbonate phase is a consequence of interaction between isotopic reservoirs of the original carbonate mineral and the intervening diagenetic waters (Meyers and Lohmann, 1984). However, the isotopic distributions of O and C depend on the following factors (cf. Brand and Veizer, 1981; Brand, 1981b; and Anderson and Arthur, 1983 for more details):

(1) Isotopic composition of the seawater and the intervening meteoric water. This factor is of small relative importance for Recent seawater, due to the fact that its mass is much larger than that of the other reservoirs. Thus, the isotopic variations in seawater are small. In contrast, variations in the isotopic composition of meteoric waters are due mainly to evaporation and condensation processes. These waters are generally enriched in ^{16}O and their dissolved CO_2, if soil derived, is enriched in ^{12}C (Hudson, 1977).

(2) Temperature and salinity of seawater and meteoric waters. Isotopic fractionation of oxygen is highly dependent on the temperature of the ambient and precipitating fluids. The temperature dependence of isotopic fractionation results from the vibrational

frequencies of isotopic masses involved. With the increase in temperature, differences in their frequencies become less and thereby reduce isotopic fractionation (Friedman and O'Neil, 1977). The temperature dependence of isotopic fractionation is the basis for palaeotemperature determinations (Epstein et al., 1953) and the modified equation for calcite-water system (Craig, 1965) is:

$$t°(c) = 16.9 - 4.2\ (\delta c - \delta w) + 0.13\ (\delta c - \delta w)^2 \quad ...(2)$$

where $\delta c = \delta^{18}O$ of CO_2 generated from carbonate at 25° C (PDB)

$w = \delta^{18}O$ of CO_2 generated in equilibrium with water at 25°C (SMOW).

For aragonite-water system, Grossman and Ku (1981) gave this equation:

$$t°(c) = 19.0 - 3.52\ (\delta c - \delta w) + 0.03\ (\delta c - \delta w)^2 \quad ...(3)$$

Salinity, due largely to the evaporation process which preferentially extracts ^{16}O, influences the isotopic composition of seawater and meteoric waters. Similarly, continental glaciation affects isotopic composition of seawater, due to preferential extraction of ^{16}O during formation of ice caps and related increase in seawater salinity (Anderson and Arthur, 1983);

(3) Altitude, latitude and seasonal variations in $\delta^{18}O$ composition of the intervening pore waters.

(4) Secular variations in $\delta^{18}O$ and $\delta^{13}C$. The

advocated secular variations in $\delta^{18}O$ (increasing in ^{16}O with increasing geologic time) and $\delta^{13}C$ were explained in terms of three possible causes: (a) post-depositional diagenesis (Degens and Epstein, 1962); (b) decrease in seawater temperature (Knauth and Epstein, 1976); and (c) variations in $\delta^{18}O$ and $\delta^{13}C$ of seawater (Perry, 1967; Veizer et al., 1980). These alternatives were discussed in detail in Veizer (1983a, b) and Anderson and Arthur (1983) and the author refers to these references for more information. In all cases, the matter is still controversial and probably more than one mechanism may affect isotopic variations with time.

(5) Biochemical fractionation (vital effect) of isotopes in biogenic carbonates. Some organisms, such as molluscs (Lowenstam and Epstein, 1954; Lowenstam, 1963; Keith et al., 1964; Brand, 1982), foraminifera (Emiliani, 1955), and brachiopods (Lowenstam, 1961) seem to secrete their shell material at or near oxygen isotopic equilibrium with seawater. Others, such as corals (Weber and Woodhead, 1970; Brand and Veizer, 1981), algae (Keith and Weber, 1965), and crinoids (Weber and Raup, 1966a, 1968) clearly do not. The photosynthetic pathway is the dominant factor controlling the isotopic distribution of carbon in biogenic carbonates (Hudson, 1977).

(6) Diagenetic processes. The preservation of

of the original isotopic signal in fossil shells is essential for studies of past evolutionary and environmental changes. Isotopic fractionations, due to diagenetic reequilibration of carbonate sediments, have been abundantly documented (Lowenstam, 1961; Gross, 1964; Veizer and Fritz, 1976; Campos and Hallam, 1979; Dickson and Coleman, 1980; Brand and Veizer, 1981; Allan and Matthews, 1982; Meyers and Lohman, 1984). To minimize the effect of postdepositional diagenetic processes on original isotopic signatures, well preserved fossil shells are the preferred materials (e.g. Weiner and Lowenstam, 1980; Buchardt and Weiner, 1981; Brand, 1982).

(7) Other factors, such as original mineralogy of a carbonate phase or the effect of sedimentation rate. Tarutani et al. (1969), Rubinson and Clayton (1969), and Grossman and Ku (1981) indicated that, at 20-25°C, aragonite should be enriched with respect to calcite, by -0.5-0.6‰ in ^{18}O and by ~1.8‰ in ^{13}C. Furthermore, Turner (1982) has shown that the isotopic fractionation of oxygen and carbon is inversely proportional to precipitation rate.

3.2 OBJECTIVES OF THE STUDY

The main objectives of this chapter can be summarized as follows: (1) to quantify, in conjunction with trace element and petrographic criteria, isotopic shifts during diagenetic stabilization of A ⟶ dLMC and LMC ⟶ dLMC layers; (2) to trace, if possible, variations in isotopic composition of cements (and hence of diagenetic fluids) detected within rudist framework; (3) to estimate, utilizing well preserved shell components, the oxygen and carbon isotopic composition of Cretaceous seawater, and (4) to investigate the factors affecting the isotopic composition of each discrete structural component of rudist shells.

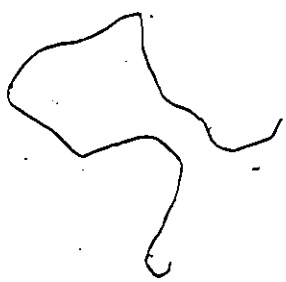

3.3 SAMPLING AND ANALYTICAL TECHNIQUES

The separation and preparation techniques for rudist samples as well as their enclosing rocks have been discussed in Chapter II of this thesis.

All powdered samples (N = 213) were initially heated to 50°C for more than two hours under vacuum and subsequently reacted with 100% phosphoric acid for no less than 30 minutes. The reaction vessels were connected to an on-line gas extraction system coupled directly to the inlet of a VG Micromass 903 mass spectrometer. All data were corrected for ^{17}O following the procedures of Craig (1957). Oxygen and carbon istopic ratios are expressed in the usual δ-notation and given in per mil relative to PDB standard.

Precision of the data was determined by daily analysis of NBS-19 and NS-3 (internal standard of the University of Waterloo isotope laboratory) and through the duplication of about 5% of all samples (1σ = 0.03‰ for $\delta^{18}O$, 0.02‰ for $\delta^{13}C$).

Average accuracies for NBS-19 standard rock, as compared to the values given by Coplen et al. (1983), were 0.10‰ for $\delta^{18}O$ and 0.18‰ for $\delta^{13}C$. For NS-3, they were 0.06‰ and 0.05‰, respectively.

3.4 RESULTS AND DISCUSSION

The statistical treatment employed in this chapter will be discussed only if the data have a direct bearing on distribution of O and C isotopes and their relationships to trace elements. All isotopic data are summarized in Appendix 3.

In order to discuss the role of diagenesis on the distribution of $\delta^{18}O$ and $\delta^{13}C$ in rudist shells, it is essential first to establish the range of starting conditions. This can be ascertained through studies of shell material with no, or only minor, diagenetic alteration effects. The well preserved canal layers of Antillocaprina (sample no. 96a) and Plagioptychus (sample no. 167a) satisfy such conditions, since they are composed of pure aragonite and their chemistry, petrography and SEM characteristics do not indicate any influence of recrystallization or cementation. These two samples were recovered from the Upper Cretaceous Coon Creek Tongue-Ripley Formation, which is well known for its exceptionally well preserved shells (Lowenstam and Epstein, 1954; Sohl, 1960a). The $\delta^{18}O$ values were -2.1‰ and -2.3‰, and the $\delta^{13}C$ values were +3.2‰ and +3.9‰ PDB, respectively. This is within the range of values considered typical for shell carbonates formed in equilibrium with present day (cf. Milliman, 1974) as well as Cretaceous seawater (Moldovanyi and Lohmann,

1984). Consequently, the present day isotopic composition of shallow low-latitude, open ocean water is a good first order approximation for its Cretaceous counterpart. However, because of the absence of Cretaceous glaciation, the $\delta^{18}O$ of the ancient seawater might have been ~1‰ lighter (Shackleton and Kennett, 1975; Barron, 1983).

Temperature variations of sea, as well as meteoric waters, are believed to have been of secondary importance, since the Cretaceous is considered to have been a warm and equable period with surfacial seawater temperatures of 25-30° C (Lowenstam and Epstein, 1959; Saltzman and Barron, 1982; Barron, 1983). It should be pointed out that Lowenstam and Epstein (1959) and Philip (1972) advocated that the robust and crowded nature of rudist colonies within the Tethyan belt may have been a consequence of higher temperatures.

Applying the palaeotemperature equation for aragonite-water system (equation 3, Section 3.1) to the best preserved aragonitic samples, the calculated isotopic temperatures range from 22.9 to 23.6°C. This is well within the range determined previously for the Cretaceous seawater for rudists (22.8-26.6°C, Lowenstam and Epstein, 1959), ammonites (12-31°C, Buchardt and Weiner, 1981), and planktonic foraminifera (25-27°C, Barron, 1983) and does not support the notion of higher

ambient temperatures. The calcite-water palaeotemperatures (equation 2, Section 3.1) applied to the best preserved components of rudist shells (average $\delta^{18}O$, -3.8‰ and $\delta^{13}C$, +2.0‰), gives a somewhat higher temperature of 29.6°C.

It is likely that salinity differences were not of great importance either, since rudists are considered to have flourished in normal salinity seawater. Furthermore, the influence of altitude, latitude and seasonal variations on isotopic composition of the intervening pore waters probably did not differ substantially from the present day temperate and tropical situation, since Cretaceous rudists inhabited a narrow zone of temperate to tropical waters (see Figure I-1).

Finally, molluscs are not known to exert biological control on isotopic equilibria during secretion of their shells (Lowenstam and Epstein, 1954; Milliman, 1974, p. 116; Brand, 1982; weter, in Veizer, 1983b) and it is therefore unlikely that this factor was of significance for Cretaceous rudists.

In summary, as a first approximation, one may assume that the two preserved aragonitic samples are shells precipitated in equilibrium with contemporaneous seawater. The trends from their values, usually towards $\delta^{18}O$ and $\delta^{13}C$ depleted members, are therefore a

consequence of diagenesis (cf. Hudson, 1977; Lohmann, 1983).

3.4.1 Undifferentiated Results For Rudist Shells and Their Enclosing Rocks

Varimax rotated factor analysis of all shell components and all rudist families shows that four factors control the overall chemical and isotopic variations (Table III-1). The isotopic composition is evidently controlled by the same two stage diagenetic sequence as was the case for trace elements (Chapter II). Diagenetic stabilization of metastable components (chiefly, A $\longrightarrow$ dLMC) (Factor 2) controls $\delta^{18}O$ and the resulting lighter values are a reflection of isotopic exchange with an ^{18}O depleted reservoir of meteoric waters. The $\delta^{13}C$, on the other hand, appears to have been controlled mostly by precipitation of late ferroan meteoric cements into primary and secondary void spaces (Factor 1). The trend toward ^{13}C depleted values reflects an interaction of original C from carbonate rocks with C derived from meteoric waters, some of it from soil sources.

In contrast, factor analysis of the enclosing rocks (Table III-2), composed originally of a heterogeneous mixture of different original components and mineralogies, shows less pronounced diagenetic trends than the rudists. In this case, both oxygen and carbon isotopic repartitioning are related to the early phase of diagenetic stabilization of the metastable components

(Factor 2), as attested by comparable positive loadings of Na and Sr. The overall $\delta^{18}O$ variation is -2.8 to -6.6‰ and for $\delta^{13}C$, it is from +3.3 to +0.6‰ PDB.

TABLE III-1

Varimax rotated factor analysis of all rudist shell components (N = 203)

	Factor 1	Factor 2	Factor 3	Factor 4
log IR	0.027	-0.034	**0.753**	-0.094
log Ca	0.287	0.079	**0.068**	-0.074
log Mg	**0.481**	**0.543**	-0.004	-0.248
log Sr	**-0.030**	**0.742**	-0.078	0.173
log Mn	**0.906**	**-0.109**	-0.002	-0.084
log Fe	**0.601**	-0.130	0.213	-0.063
log Na	**-0.148**	**0.424**	-0.007	**0.889**
log Zn	-0.025	**-0.066**	0.295	**0.195**
log Al	0.199	0.111	**0.637**	-0.029
$\delta^{18}O$	-0.210	**0.519**	**0.055**	0.150
$\delta^{13}C$	**-0.572**	**0.341**	0.119	-0.198
Percent of Variation Explained	40.7	26.0	19.5	13.8
Eigen value	2.259	1.442	1.079	0.764
Interpretation	Diagenetic Stabilization II	Diagenetic Stabilization Ib	Laboratory Leaching	Diagenetic Stabilization Ia

TABLE III-2

Varimax rotated factor analysis of all enclosing rocks (N = 10)

	Factor 1	Factor 2	Factor 3
log IR	0.322	0.380	0.805
log Ca	0.122	-0.334	0.651
log Mg	0.776	0.477	0.132
log Sr	0.450	0.694	0.294
log Mn	0.834	-0.039	0.044
log Fe	0.807	0.237	0.404
log Na	0.081	0.958	0.069
log Zn	-0.730	0.177	-0.256
log Al	0.689	0.215	0.634
$\delta^{18}O$	0.121	0.709	0.052
$\delta^{13}C$	-0.235	0.755	-0.285
Percent of Variation Explained	59.5	30.6	9.8
Eigen value	4.974	2.558	0.821
Interpretation	Diagenetic Stabilization II and Laboratory Leaching	Diagenetic Stabilization I	Total Carbonate (?)

3.4.2 Cements

The morphological, textural and chemical aspects of different types of cements present within rudist shells were discussed earlier (Chapters I and II). The isotopic signals for these cements may corroborate petrographic and chemical evidence, which shows a clear distinction of cement types. This distinction may be a function of the original mineralogy of cement precursors, of pore water chemistry, and of the degree of diagenetic interaction between the original carbonate precursor and the intervening fluids.

The distinguished four types of cements, occluding primary and secondary pore spaces of rudist shells (cf. Section 1.4.4), are: (1) the early fibrous or micritic, inclusion-rich, nonferroan calcite; (2) early or late equant, inclusion-rich, nonferroan or slightly ferroan calcite; (3) late ferroan bladed calcite; and (4) late large equant clear ferroan calcite. They all have specific $\delta^{18}O$ and $\delta^{13}C$ isotopic values (Appendix 3, and Table II-8). The fibrous and micritic, inclusion-rich calcites (No. 1) have the heaviest isotopic values, with average $\delta^{18}O$ of -4‰ and $\delta^{13}C$ of +3‰ PDB. The inclusion-rich equant calcites (No. 2) have the average $\delta^{18}O$ of -5.1‰ and $\delta^{13}C$ of +0.4‰, whereas the bladed (No. 3) and large clear equant calcites (No. 4) have average $\delta^{18}O$ of -9.2‰ and -6.3‰ and $\delta^{13}C$ of -4.5‰ and +1.1‰ PDB,

respectively.

Previous studies on carbonate cements (Wagner and Matthews, 1982; Lohmann, 1983; Czerniakowski et al., 1984; Meyers and Lohmann, 1984; Moldovanyi and Lohmann, 1984) show that, utilizing petrographic and isotopic signature, it is possible to distinguish types of cements as well as the timing of their formation and the nature of their parent solutions. The precipitation of submarine cements of A and HMC mineralogy in present day shallow warm seawater is marked by relatively heavy $\delta^{18}O$, up to +3‰, and heavy $\delta^{13}C$ (+2 to +5‰ PDB) (Gross, 1964; Milliman, 1974; Hudson, 1977; James and Choquette, 1984). Partial preservation of these isotopic signatures in ancient cements has also been documented (Davies, 1977; Prezbindowski, 1977; Hudson and Coleman, 1978; Walls et al., 1979; Marshall and Ashton, 1980; Moldovanyi and Lohmann, 1984).

Histogram plots for all cements separated from rudist shells show a bimodal behaviour for both $\delta^{18}O$ and $\delta^{13}C$ (Fig. III-1, A and B). For $\delta^{18}O$, the modes are -3‰ and -7‰, whereas for $\delta^{13}C$, the population with the mode of ~+3‰ is dominant and the light (mode -6‰) population is subordinate. These histograms suggest in terms of isotopes the existence of two dominant, early and late, cementation stages. The heavier oxygen and carbon modes are present mainly in samples with petrographic and

-A-

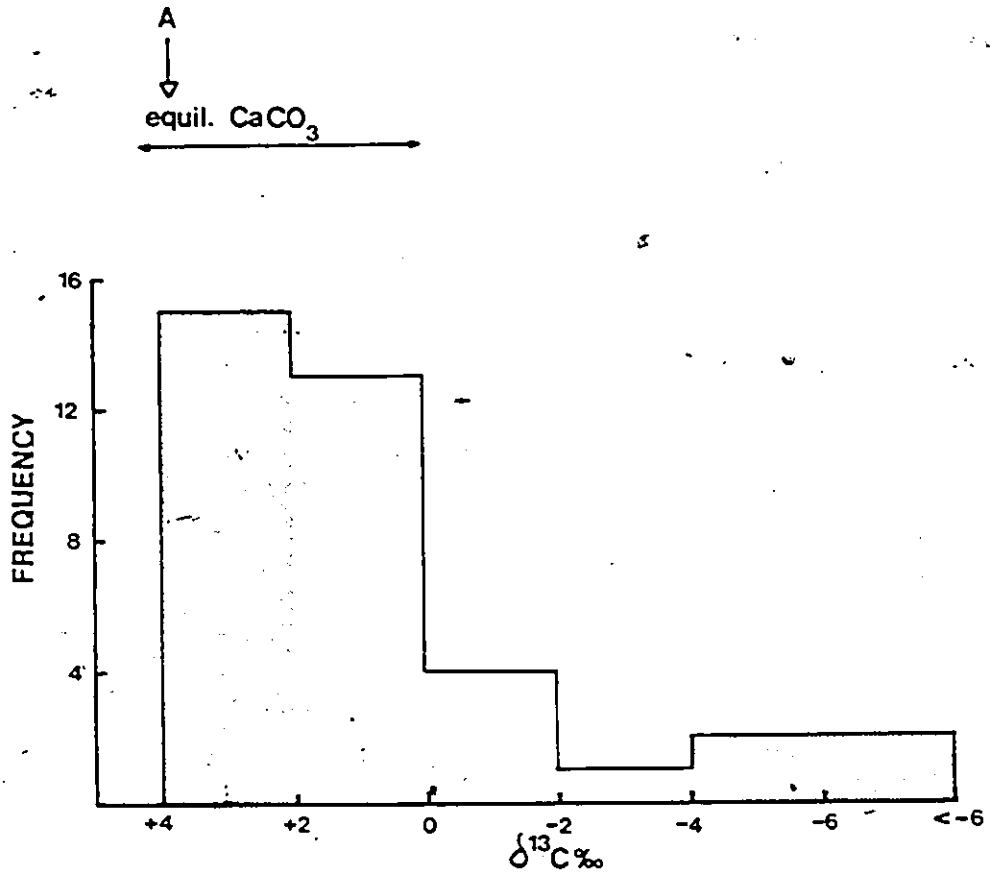

-B-

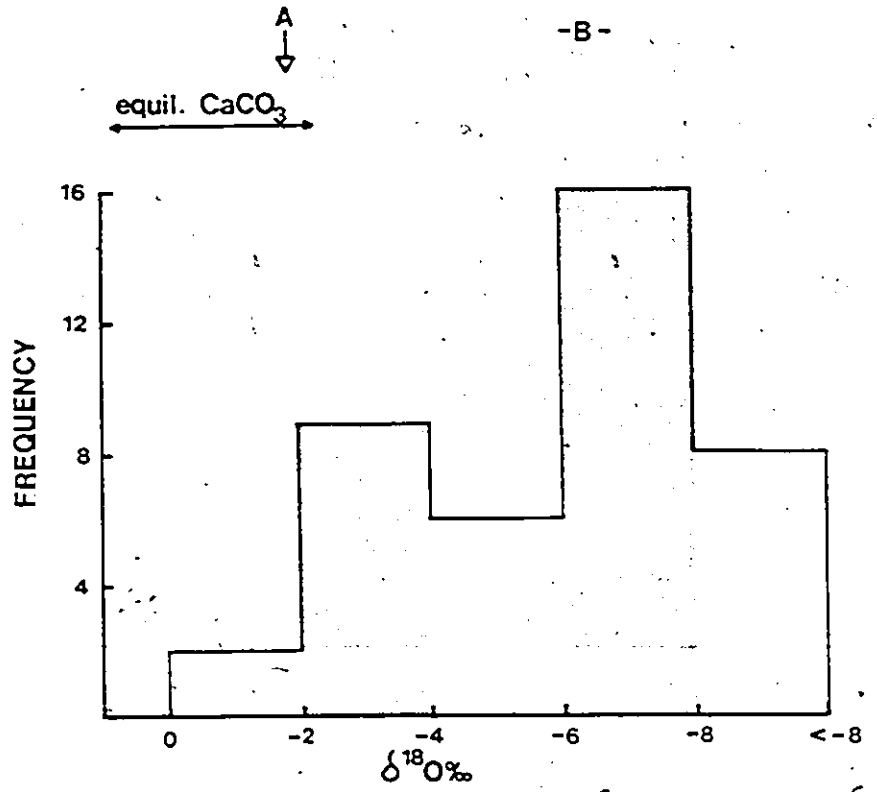

Fig.III-1. Histogram plots of $\delta^{13}C$ (A) and $\delta^{18}O$ (B) for all cement types. A---→ well preserved Cretacecus aragonitic rudists.

trace element evidence for submarine origin (see Chapters I and II). The precursors were A and HMC and their isotopic signatures are only slightly less negative than expected for $CaCO_3$ in equilibrium with present day or Cretaceous seawater; the latter is based on the best preserved aragonitic rudist shells discussed in Section 3.4

Partial factor analysis of all cement samples (Table III-3) shows clearly the advocated two-stage cementation. Factor 2, which controls the distribution of Mg, Sr, Na and $\delta^{18}O$ can be interpreted as diagenetic stabilization of early submarine cements of A (and some HMC) mineralogy. The subsequent occlusion of the residual primary and secondary porosity by ferroan bladed and equant spar of shallow meteoric phreatic origin caused the introduction of the light carbon (Factor 1). Scatter diagrams of Sr and Na vs. $\delta^{18}O$ (Figs. III-2, 3) show a clear negative trend of decreasing Sr and $\delta^{18}O$ with increasing degree of diagenetic reequilibration with meteoric waters, whether for total population or separate cement types. Thus it is not so much the sense as the degree of isotopic shifts which separate the two diagenetic stages. Consequently, the separation in factor analysis is that of a degree. In a slightly modified form this is also the case for Mn, Fe and $\delta^{13}C$ and (Fig. III-4). Overall,

the early fibrous and micritic cements still preserve the vestiges of their originally high contents of Sr and Na, low contents of Mn and Fe, and heavy $\delta^{18}O$ and $\delta^{13}C$. The equant, inclusion-rich, nonferroan and slightly ferroan calcites show more alteration, and the late ferroan bladed and large equant spars showed the largest spread of chemical and isotopic values and the highest degree of equilibration with meteoric waters (Figs. III-2, 3, 4).

TABLE III-3

Partial factor analysis of all cements (N = 37)

	Factor 1	Factor 2
log IR	-0.424	-0.142
log Ca	0.229	0.192
log Mg	0.186	0.708
log Sr	-0.310	0.664
log Mn	0.982	0.101
log Fe	0.532	-0.057
log Na	0.094	0.551
log Zn	-0.009	0.007
log Al	-0.016	-0.081
$\delta^{18}O$	-0.381	0.755
$\delta^{13}C$	-0.694	0.139
Percent of Variation Explained	41.8	33.3
Eigen value	2.483	1.979
Interpretation	Late Cementation	Early Cementation

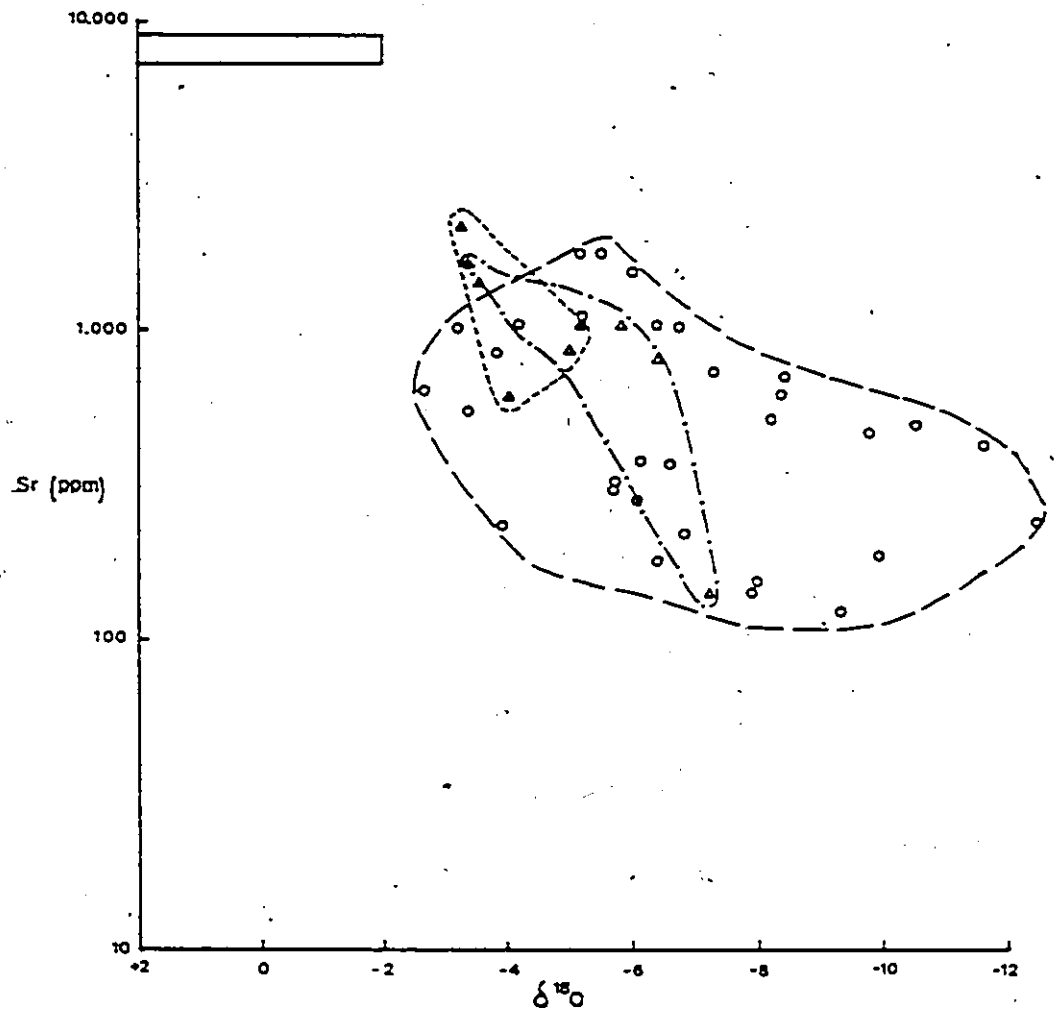

Fig.III-2. Scatter diagram of Sr vs. $\delta 18O$ for all cement types. The closed triangles (▲) represent early radiaxial fibrous and micritic cements. The open triangles (△) stand for inclusion-rich equant spar, while open circles (○) designate combined ferroan bladed and equant spars. The last two types always postdate fibrous and inclusion-rich equant calcite, and they are considered to represent one domain. The box represents the range for inorganic aragonite, and other carbonate minerals, in equilibrium with seawater.

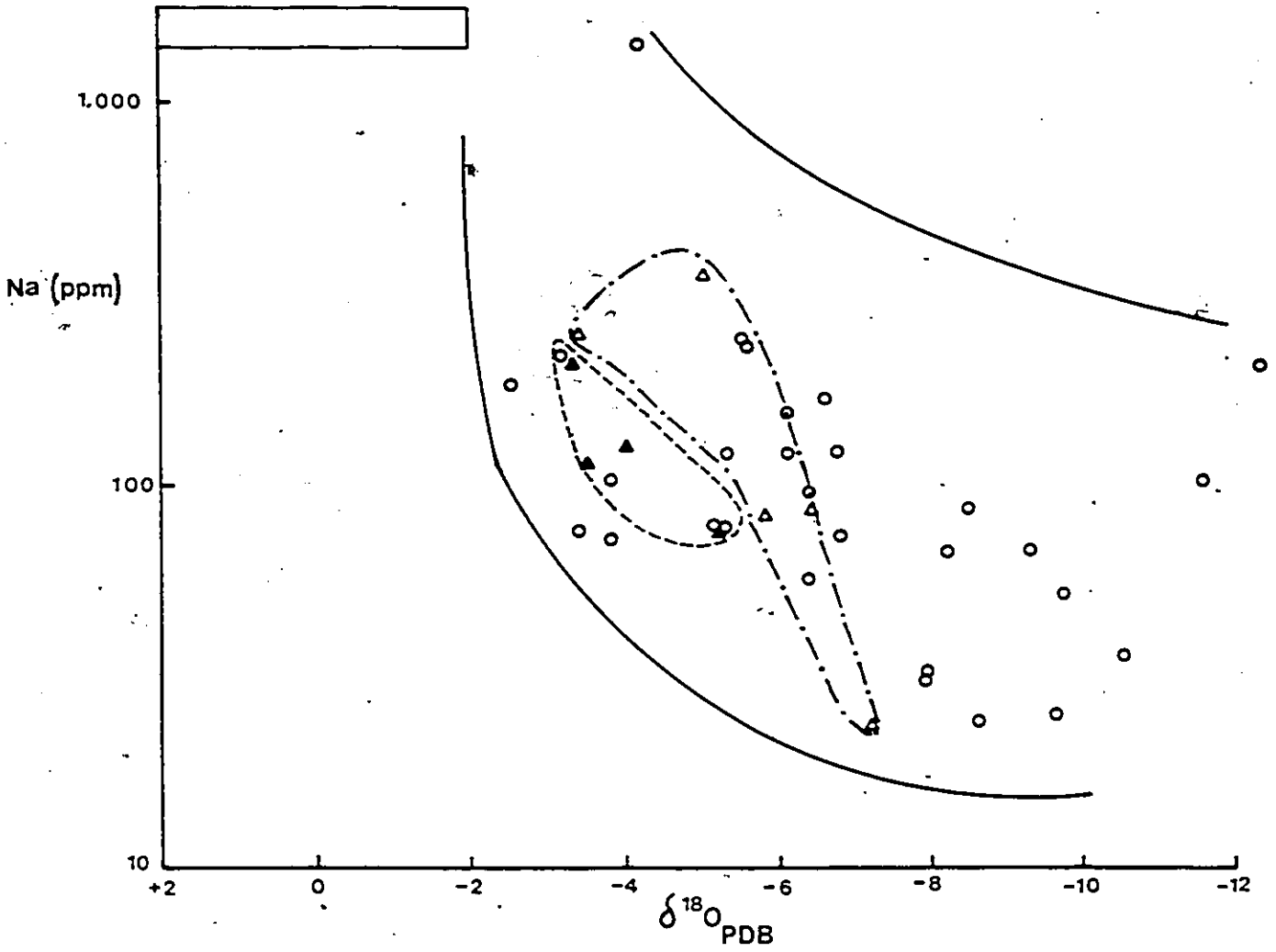

Fig. III-3. Scatter diagram of Na vs. $\delta^{18}O$ for all cement types. Explanations as in Fig. III-2.

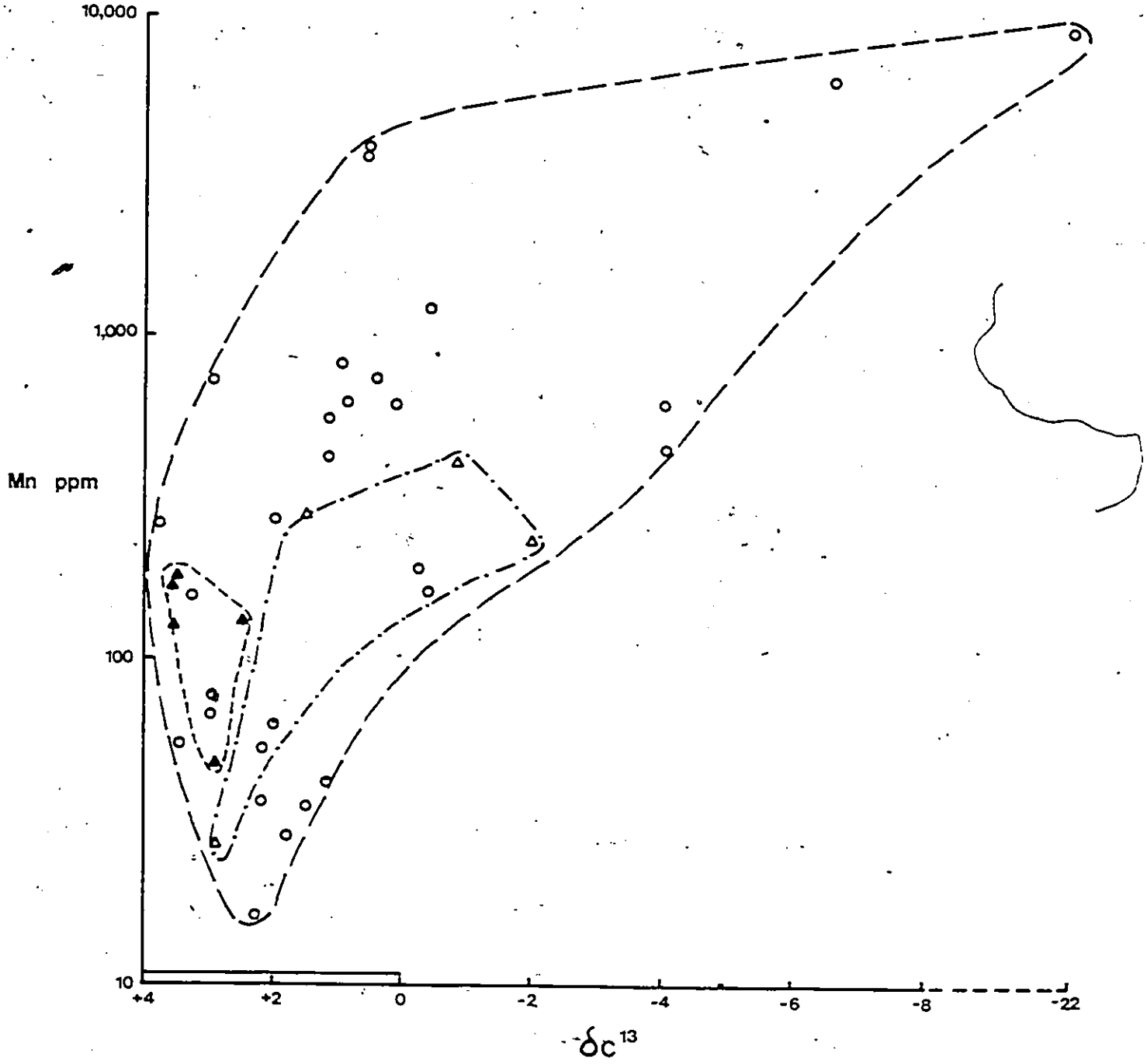

Fig. III-4. Scatter diagram of Mn vs. $\delta^{13}C$ for all cement types. Explanations as in Fig. III-2.

3.4.3 Internal Sediments

Diagenetic stabilization of marine internal sediments, which were originally a mixture of A, LMC and possibly HMC of organic and inorganic origin (see Chapter I), was accomplished through a complex interplay of early and late diagenetic processes. Their textural and elemental evaluations (Chapters I and II, respectively) showed that their diagenetic reequilibration has been achieved through: (1) formation of marine cements in the primary void spaces of rudists and other fossil components; (2) diagenetic mineralogical stabilization of these cements and fossils in meteoric phreatic environment; and (3) late occlusion of the remaining primary and secondary moldic porosity by meteoric phreatic ferroan spar. The overall isotopic variations in oxygen and carbon are from +0.7 to -8.5‰ and from +3.8 to -9.1‰ PDB, respectively (Appendix 3). As in the previous cases of sizeable metastable original mineralogy, oxygen isotopic composition is controlled by steps (1) and (2) above, while carbon mostly reflects step (3) (Table III-4).

TABLE III-4

Partial factor analysis of all internal sediments (N = 30)

	Factor 1	Factor 2
log IR	0.467	-0.068
log Ca	0.516	0.087
log Mg	0.935	0.218
log Sr	0.843	-0.019
log Mn	0.177	0.830
log Fe	0.293	0.669
log Na	0.741	0.080
log Zn	-0.081	0.137
log Al	0.654	0.018
$\delta^{18}O$	0.515	-0.051
$\delta^{13}C$	0.134	-0.833
Percent of Variation Explained	63.7	25.2
Eigen value	4.587	1.811
Interpretation	Diagenetic Stabilization I and Total Carbonate ?	Diagenetic Stabilization II

3.4.4 Aragonitic Skeletal Components

The $\delta^{18}O$ and $\delta^{13}C$ of all originally aragonitic skeletal components (see Chapter II) span the range of +0.7 to -13.4‰ values for the former and +4.0 to -7.0‰ PDB for the latter (Appendix 3). I shall exclude a single value of +0.7‰ $\delta^{18}O$ (sample no. 99b), because of the signs of alteration, and accept -2.1‰ $\delta^{18}O$ and +3.9‰ $\delta^{13}C$ as the starting isotopic composition for the rudist aragonite (see Section 3.4).

Partial factor analysis of all presumably aragonitic components (Table II-5) shows that the previously advocated two-stage diagenetic model is exemplified here. It is evident that the previously deciphered control of $\delta^{18}O$ by early diagenetic calcitization is primarily a consequence of A ⟶ dLMC transition; a feature clearly evident from positive Na (Fig. III-5) and Sr (Fig. III-6) loadings. It should be noted that several skeletal components with partially preserved ultrastructure still have some aragonite preserved (see Figs. III-5, 6, 7). This may indicate that the diagenetic signal observed in $\delta^{18}O$ is partly controlled by a mixture of original oxygen isotopic values for aragonite and of oxygen derived from the neomorphosed calcite. However, exclusion of these mixed samples from factor analysis leads to results analogous to those in Table (III-5). This observation does not,

TABLE III-5

Partial factor analysis of all presumably aragonitic skeletal components (N = 71)

	Factor 1	Factor 2
log IR	0.139	-0.281
log Ca	0.242	-0.085
log Mg	0.228	0.124
log Sr	-0.315	0.586
log Mn	0.741	-0.154
log Fe	0.517	-0.049
log Na	-0.008	0.888
log Zn	0.017	0.155
log Al	0.082	0.049
$\delta^{18}O$	-0.105	0.484
$\delta^{13}C$	-0.796	0.055
Percent of Variation Explained	42.9	23.0
Eigen value	2.419	1.295
Interpretation	Diagenetic Stabilization II	Diagenetic Stabilization I

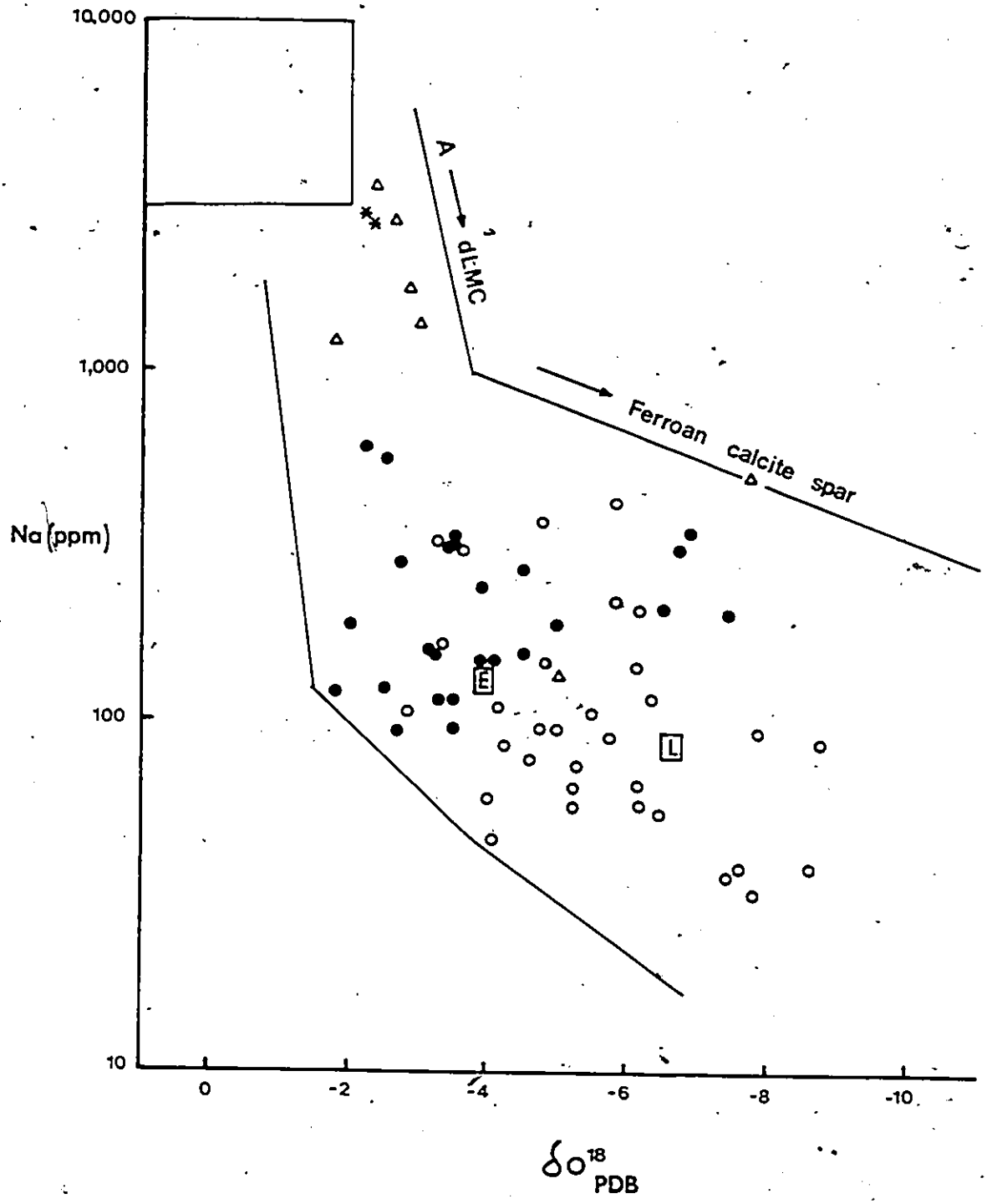

Fig. III-5. Scatter diagram of Na vs. $\delta^{18}O$ for all originally aragonitic components. Explanations as in Fig. II-10.

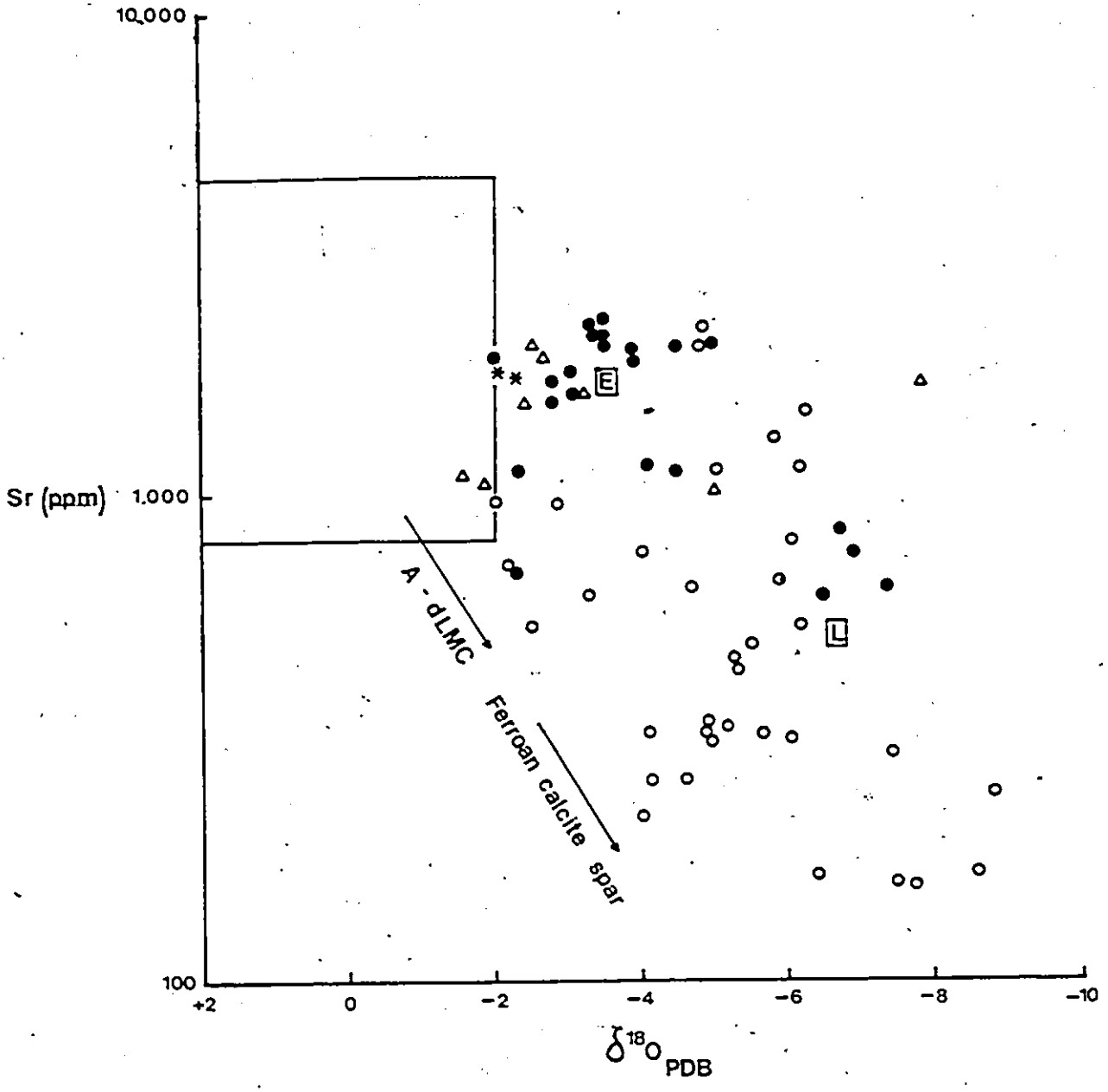

Fig. III-6. Scatter diagram of Sr vs. $\delta^{18}O$ for all originally aragonitic components. Explanations as in Fig.II-10.

therefore, support the "mixing" hypothesis as the cause of isotopic variation in dLMC samples. The figures also demonstrate that samples with well preserved mineralogy and ultrastructures fall within, or close to, the range of $CaCO_3$ in isotopic equilibrium with present day seawater. Samples with moderately preserved ultrastructures suffered some Na loss and their oxygen values have been shifted by ~-1‰, while those without any relic textures have a higher ^{18}O depletion (Fig. III-7).

As already established in the previous section (3.4.1), the $\delta^{13}C$ is controlled by precipitation of the late ferroan calcite cement (Table III-3, Factor 1), as evidenced by the positive loadings of Fe and Mn (Fig. III-4). Again, the well preserved aragonite samples fall within the range of the present day aragonitic marine pelecypods in equilibrium with seawater. The moderately preserved components show partial enrichment of Mn and no, or only a small negative, shift in ^{13}C. Only the samples which suffered more alteration and reequilibration with meteoric waters have gained more Mn and became lighter in $\delta^{13}C$ (Fig. III-8). This clearly indicates that incorporation of soil CO_2 into the aquifer system was confined to late stages of its evolution.

This two-stage development is discernible also in

the $\delta^{18}O$ vs. $\delta^{13}C$ scatter diagram (Fig. III-9). Initially, the loss of ^{18}O is much faster than that of ^{13}C, whereas the subsequent evolution is characterized by considerable gain in ^{12}C and no clear loss of ^{18}O. Considering that A $\longrightarrow$ dLMC transformation is a wet dissolution-reprecipitation process, which is characterized by $\sim 10^4$:1 excess of water derived oxygen over that originating from the precursor aragonite (cf. Veizer, 1983a), it is clear that $\delta^{18}O$ of dLMC reflects that of the waters. Consequently, the lack of pronounced $\delta^{18}O$ difference between still preserved aragonitic specimens, dLMC with preserved ultrastructures, and early cements shows that early diagenetic waters were only $\lesssim 2‰$ depleted if compared to coeval seawater. This is entirely possible for low latitude tropical and subtropical climates. Alternatively, early diagenetic A $\longrightarrow$ dLMC (HMC $\longrightarrow$ dLMC) transformation was achieved in waters similar to seawater in $\delta^{18}O$, but at $\lesssim 8°C$ higher temperature. A combination of these two factors is the most likely possibility. In accord with this reasoning, the diagenetic waters responsible for subsequent precipitation of ferroan calcite spars (cements 3 and 4) were either depleted by $\sim 4 \pm 1‰$ with respect to contemporaneous seawater, or the ambient temperature was $\sim 16 \pm 4°C$ higher than that of coeval seawater. At a

normal geothermal gradient of 35°C/Km, this would require an overburden of ~600+200 metres. The negative shift interpreted as reflecting interaction with meteoric waters of progressively lighter temperatures and/or with progressively lighter meteoric waters (cf. Magaritz, 1983; Campose and Hallam, 1979). In the present context, petrographic data did not show many good evidence for deep burial. Consequently, these shifts are probably due mostly to interactions with isotopically light meteoric waters.

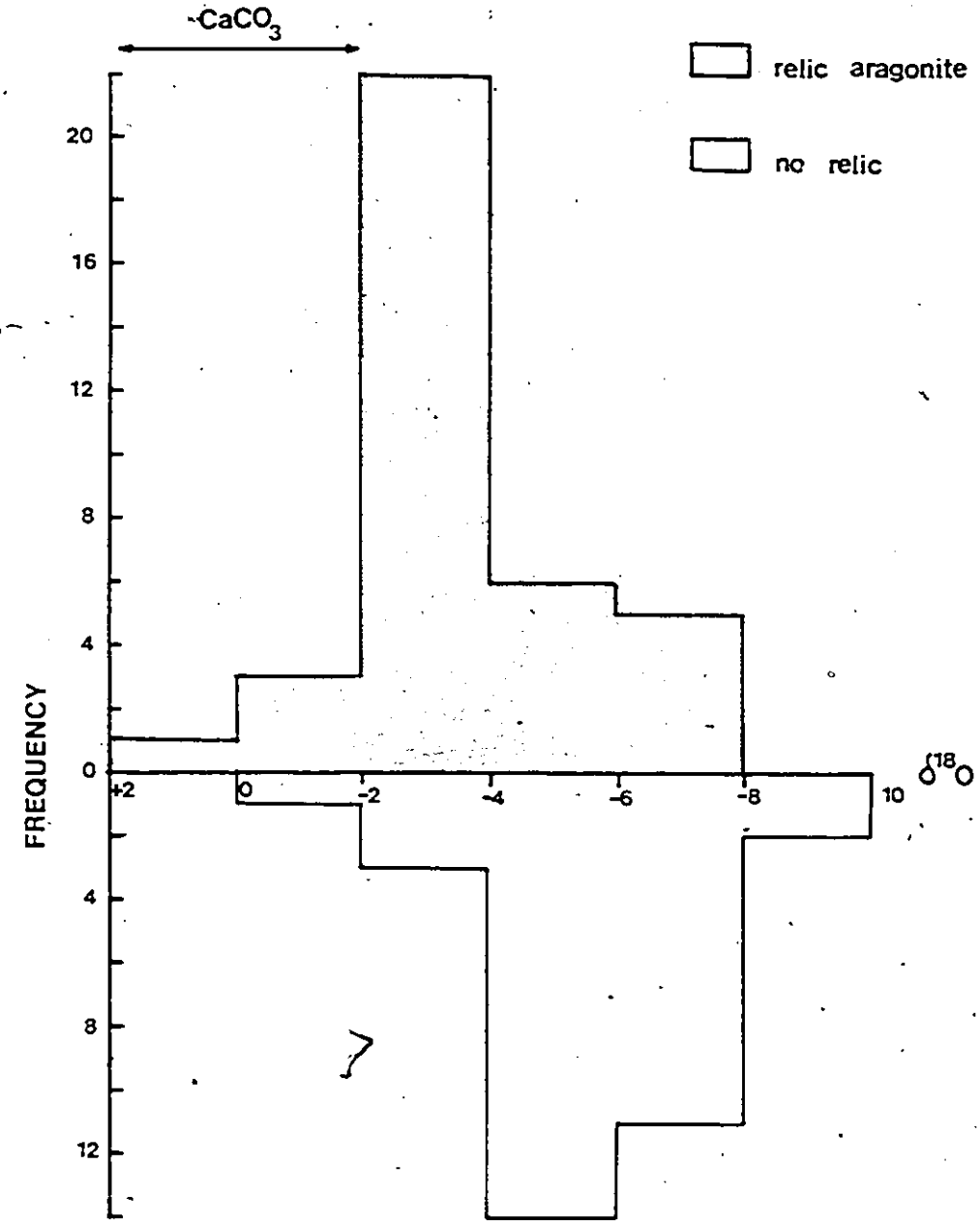

Fig.III-7. Histogram plots of $\delta^{18}O$ for originally aragonitic components with and without partial preservation of relic ultrastructures.

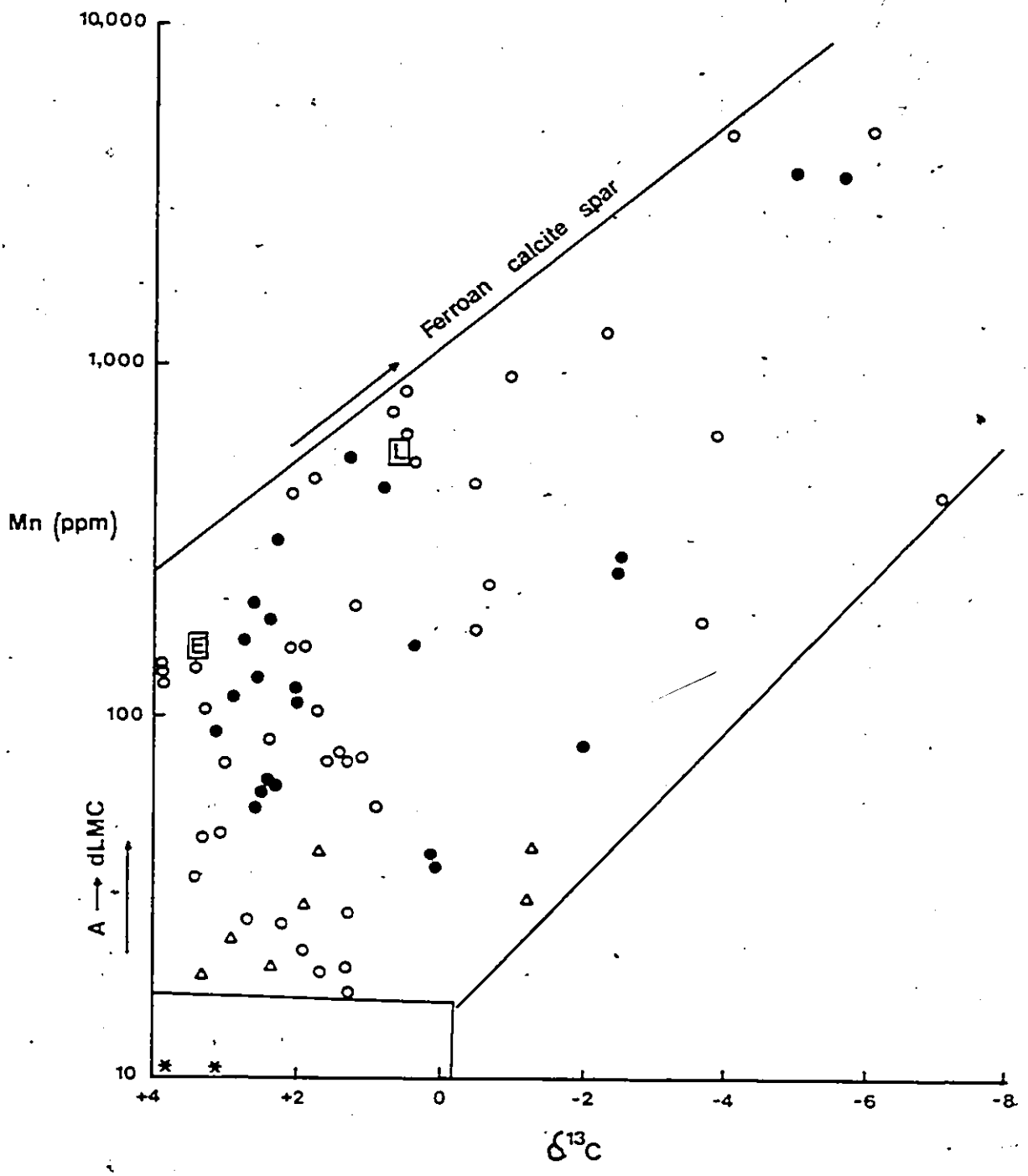

Fig.III-8. Scatter diagram of Mn vs. $\delta^{13}C$ for all originally aragonitic components. Explanations as in Fig.II-10.

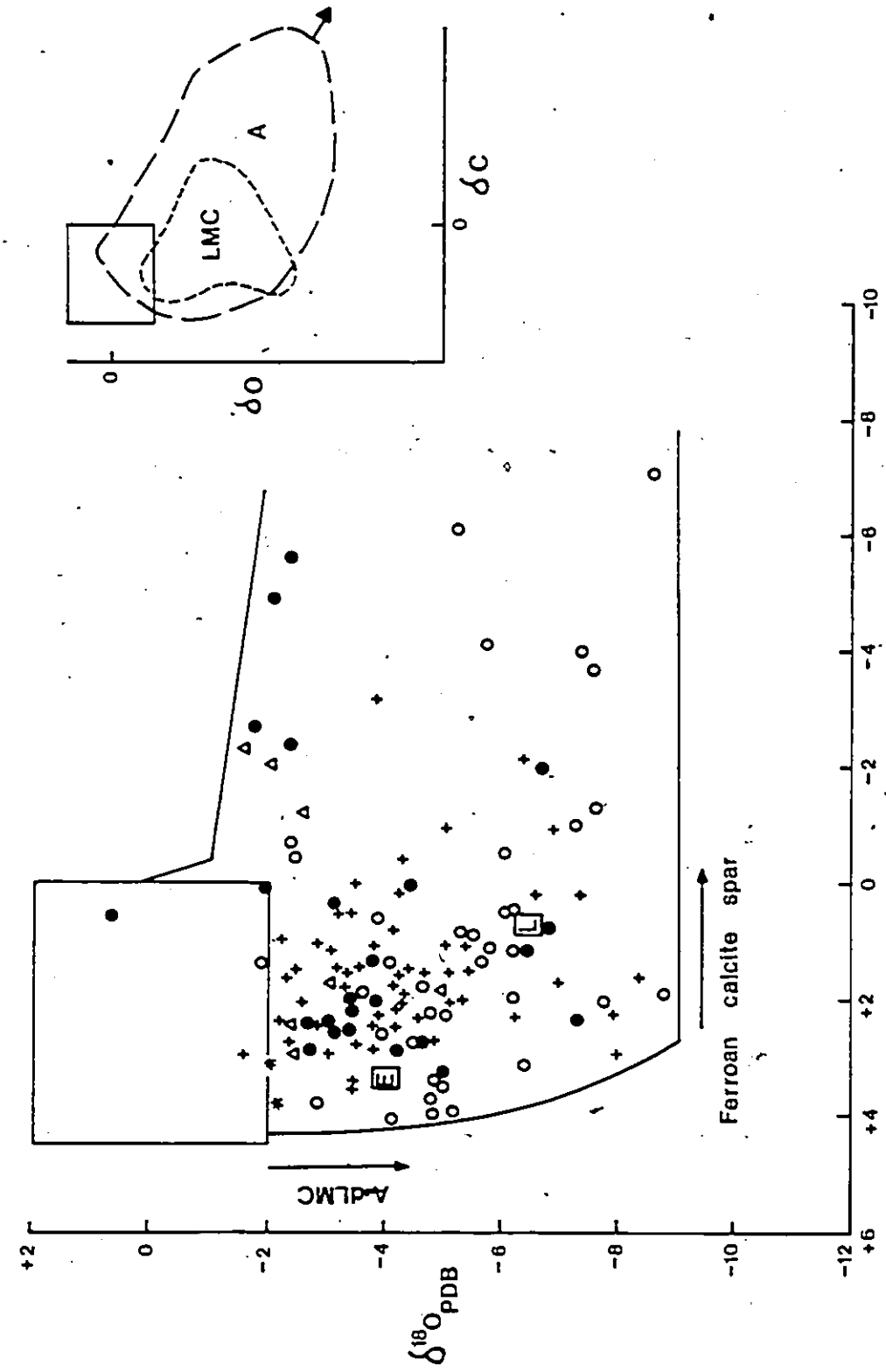

Fig. III-9. Scatter diagram of $\delta 180$ vs. $\delta 13C$ of both originally aragonitic and LMC components. The cross (+) represents LMC components. Other symbols are as in Fig.II-10. The box represents the range for organic and inorganic carbonate in equilibrium with present day seawater.

3.4.5 Low-Mg Calcitic Skeletal Components

These components include hippuritid beads, pillars and outer prismatic layers, cellular-prismatic layers of radiolitids, and simple prismatic layers of requieniids and monopleurids. $\delta^{18}O$ and $\delta^{13}C$ values range from -1.7 to -8.5‰ for the former and from + 3.6 to -3.3‰ PDB for the latter isotope (Appendix 3).

In contrast to originally aragonitic components, the calcitization process (Table III-6, Factor 3) plays only a subordinate role in redistribution of O and C isotopes. This is a consequence of the relatively subordinate importance of this step, because only the volumetrically relatively subordinate early cements (see Section 3.4.2) are involved. The LMC skeletal framework is affected only to a lesser degree. Furthermore, as discussed in the aragonite section, the $\delta^{18}O$ of early diagenetic waters did not differ appreciably from coeval seawater. As a consequence, even extensive recrystallization will show relatively small shifts for O, while other tracer shifts may or may not be considerable. During a subsequent stage of pore occlusion by late ferroan calcite spar, the observed chemical changes include loss of Sr, gain of Mn and Fe, and introduction of light carbon and oxygen (Factors 2 and 1). As was documented in Section 3.4.2, the sense of diagenetic shifts is identical for all cements and

it is only a degree of the shift, which is variable. Thus, in contrast to aragonite, where both aragonite framework and early cements tended to mutually reinforce the role of the calcitization diagenetic factor, the absence of A framework in LMC skeletal parts tends to diminish its importance. By default, the late ferroan calcite spar precipitation, therefore, becomes the controlling factor of isotopic composition.

The above discussed relationships are also discernible in scatter diagrams of Sr, Na, Mn, $\delta^{18}O$ and $\delta^{13}C$ (Figs. III-10, 11, 12). The transformation of early cements within the LMC skeletal framework led to relatively small changes in Sr, $\delta^{18}O$ and $\delta^{13}C$, and to moderate increases in Mn (and Fe). Only the subsequent addition of late ferroan calcite spars caused the marked resetting of chemical and isotopic values. This two-stage development is also discernible in the $\delta^{18}O$ vs. $\delta^{13}C$ scatter diagram (Fig. III-9), where the early diagenetic stage is characterized by some (<2‰) negative shift in $\delta^{18}O$ and no change in $\delta^{13}C$. The late diagenetic introduction of ferroan calcite spars results in further ~3±‰ negative shift in $\delta^{18}O$ and depletion of several per mille in ^{13}C. However, compared to aragonitic skeletal components, the isotopic shifts for LMC are of lesser magnitudes.

TABLE III-6

Partial factor analysis of all LMC skeletal components (N = 60)

	Factor 1	Factor 2	Factor 3
log IR	0.132	0.152	-0.058
log Ca	0.176	0.031	-0.133
log Mg	0.243	0.718	0.048
log Sr	0.022	0.466	0.619
log Mn	0.955	0.113	-0.080
log Fe	0.568	0.174	0.012
log Na	-0.171	-0.198	0.929
log Zn	-0.079	-0.093	-0.093
log Al	-0.044	-0.027	0.049
$\delta^{18}O$	-0.481	0.335	0.112
$\delta^{13}C$	-0.069	-0.620	-0.080
Percent of Variation Explained	31.1	23.5	17.3
Eigen value	1.981	1.499	1.102
Interpretation	Diagenetic Stabilization IIb	Diagenetic Stabilization IIa	Diagenetic Stabilization I

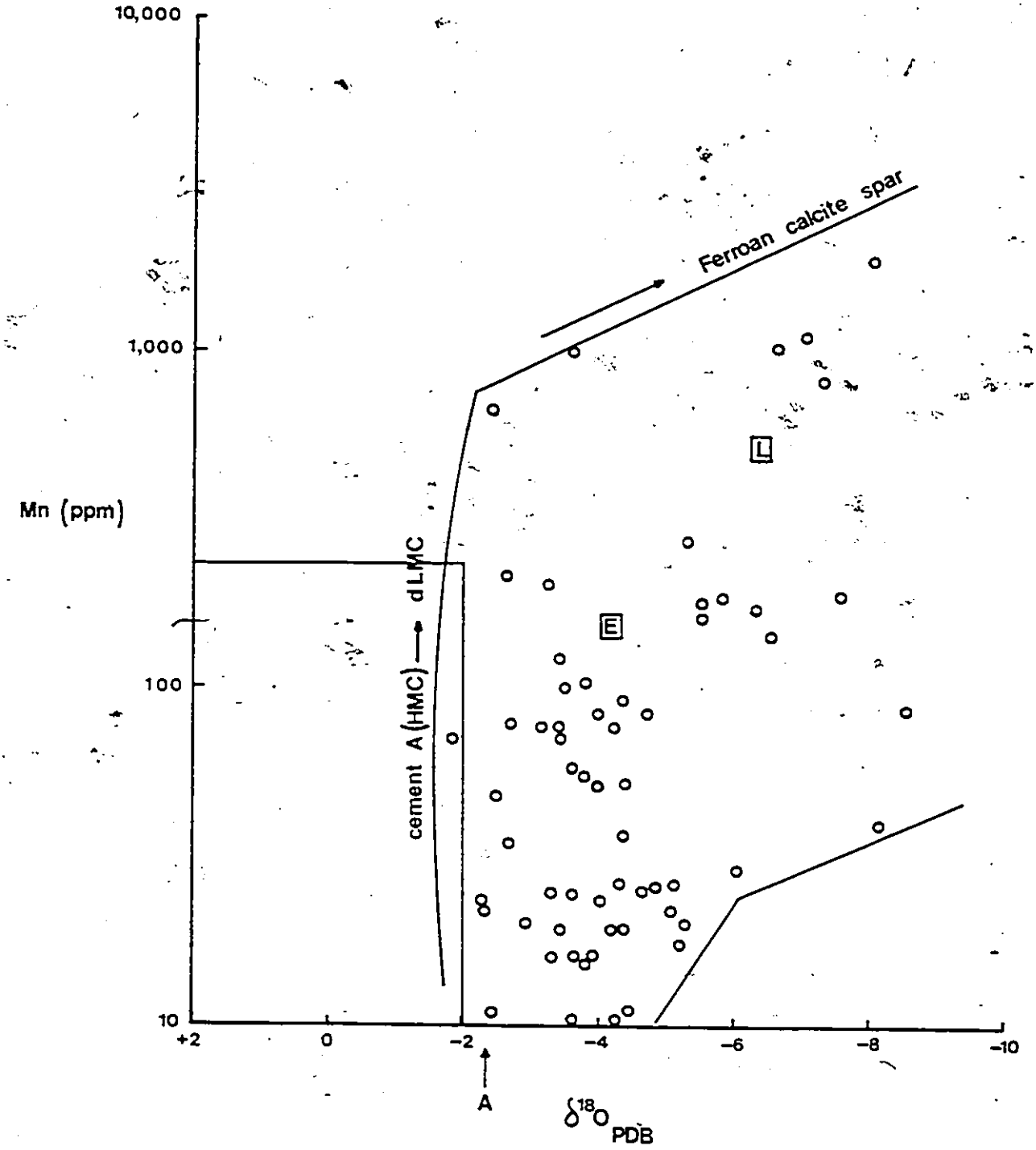

Fig. III-10. Scatter diagram of Mn vs. $\delta^{18}O$ for all originally LMC skeletal components. Explanations as in Fig. III-5.

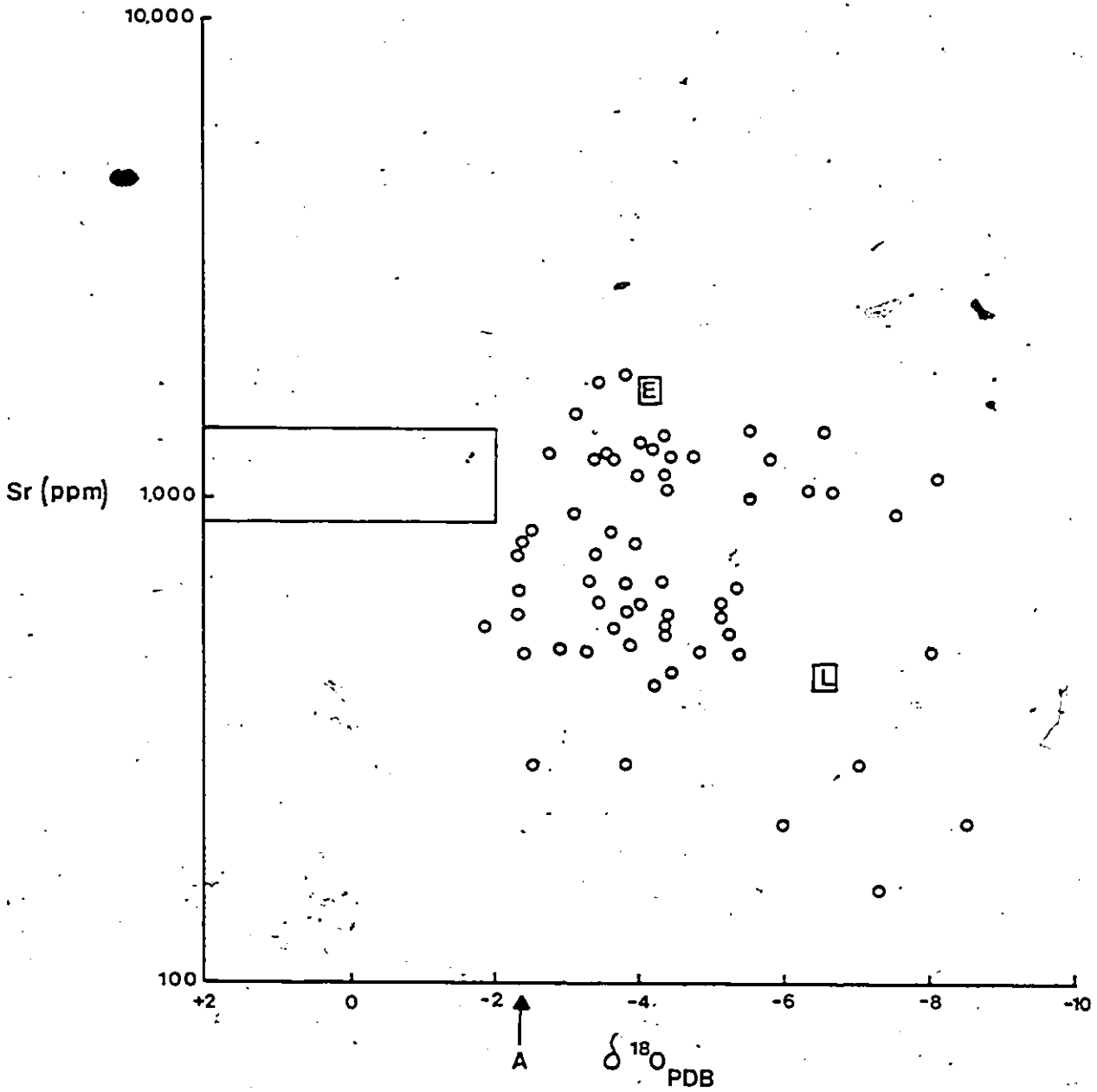

Fig. III-11. Scatter diagram of Sr vs. $\delta^{18}O$ for all originally LMC skeletal components. (A) stands for Cretaceous aragonite. Other explanations as in Fig.III-5.

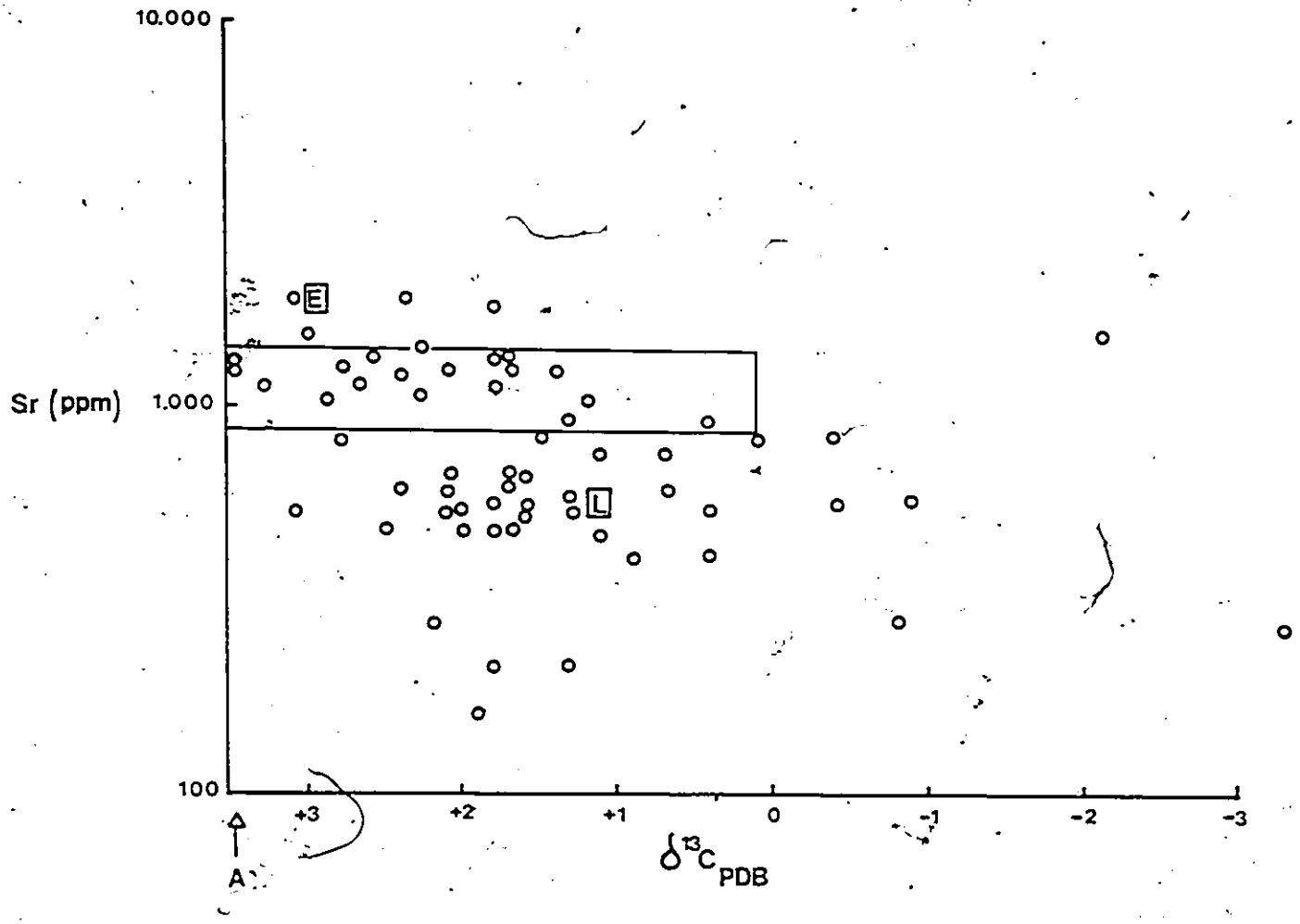

Fig. III-12. Scatter diagram of Sr vs. $\delta^{13}C$ for all originally LMC skeletal components. (A) stands for Cretaceous aragonite. Other explanations as in Fig.III-5.

3.4.6 Family Caprinidae

Isotopic analysis of pallial canal layers and of inner layers, presumably of original aragonitic mineralogy, in variable states of preservation (Appendix 3) gave a range of values -1.7 to -13.4‰ for oxygen and +3.9 to -7.0‰ for carbon. Well preserved, still aragonitic, samples fall within the range of present day marine carbonate deposits (Fig. III-13).

Partial factor analysis of canal layers and inner layers (Table III-7) clearly associate $\delta^{18}O$ variations with early diagenetic calcitization (Factor 2, Tables III-7; Figs. III-13, 14), and $\delta^{13}C$ with late ferroan calcite cements (Factor 1, Table III-7; Fig. III-15). These associations were discussed many times previously and will not be elaborated on here.

TABLE III-7

Partial factor analysis of all caprinids outer and inner layers (N = 41)

	Factor 1	Factor 2
log IR	0.155	-0.119
log Ca	0.055	-0.213
log Mg	0.270	0.036
log Sr	-0.404	0.765
log Mn	0.846	-0.201
log Fe	0.612	-0.126
log Na	-0.068	0.849
log Zn	0.112	0.050
log Al	0.045	-0.006
$\delta^{18}O$	-0.094	0.655
$\delta^{13}C$	-0.840	0.151
Percent of Variation Explained	45.0	23.1
Eigen value	3.168	1.624
Interpretation	Diagenetic Stabilization II	Diagenetic Stabilization I

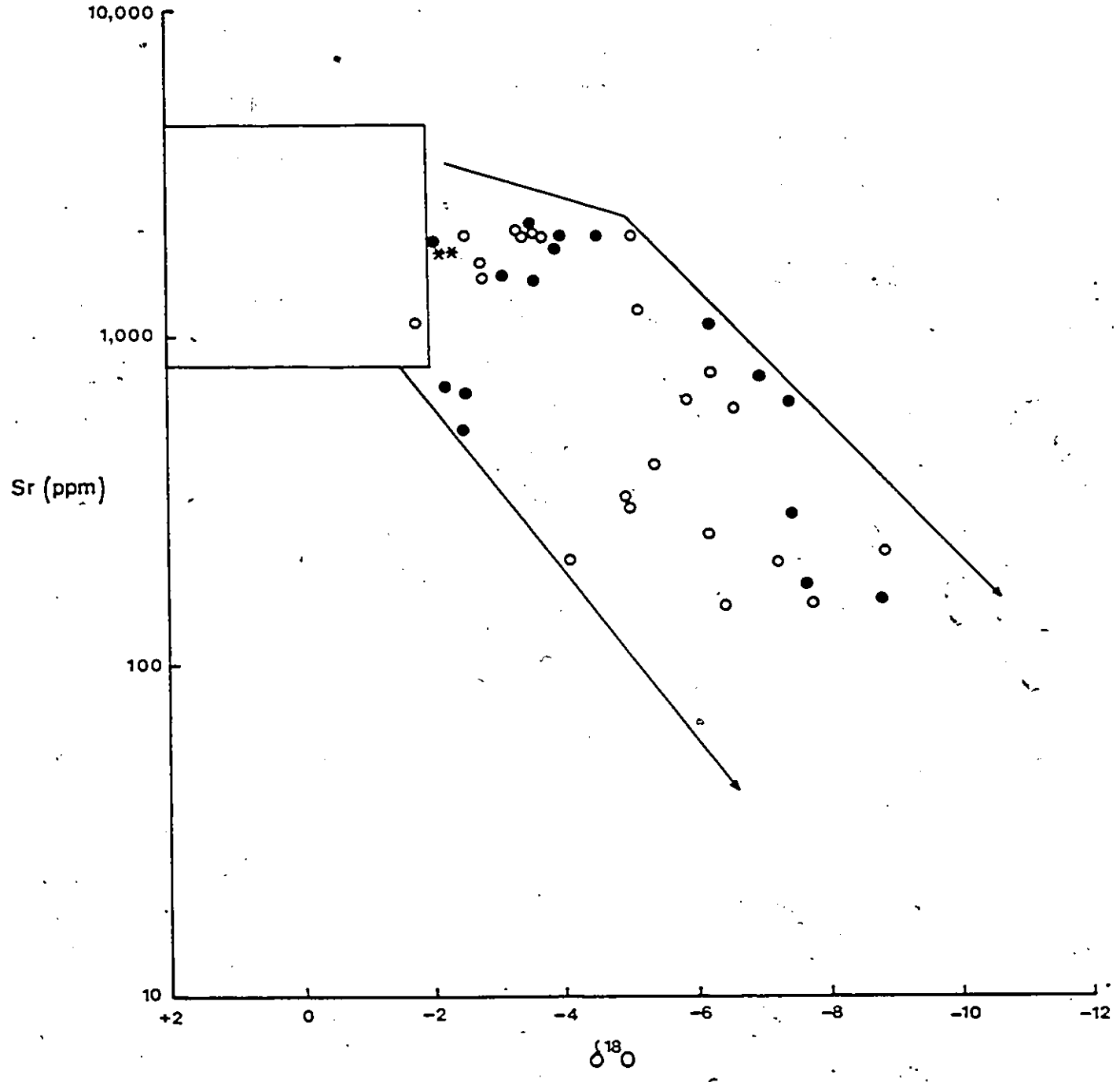

Fig.III-13. Scatter diagram of Sr vs. $\delta^{18}O$ for caprinid outer and inner layers of presumably originally aragonitic composition. The box represents the range of Sr and $\delta^{18}O$ in Recent bivalves and in shallow marine sediments. The star (*) represents well preserved aragonite. Open circles (o) represent outer layers and closed circles (•) inner layers.

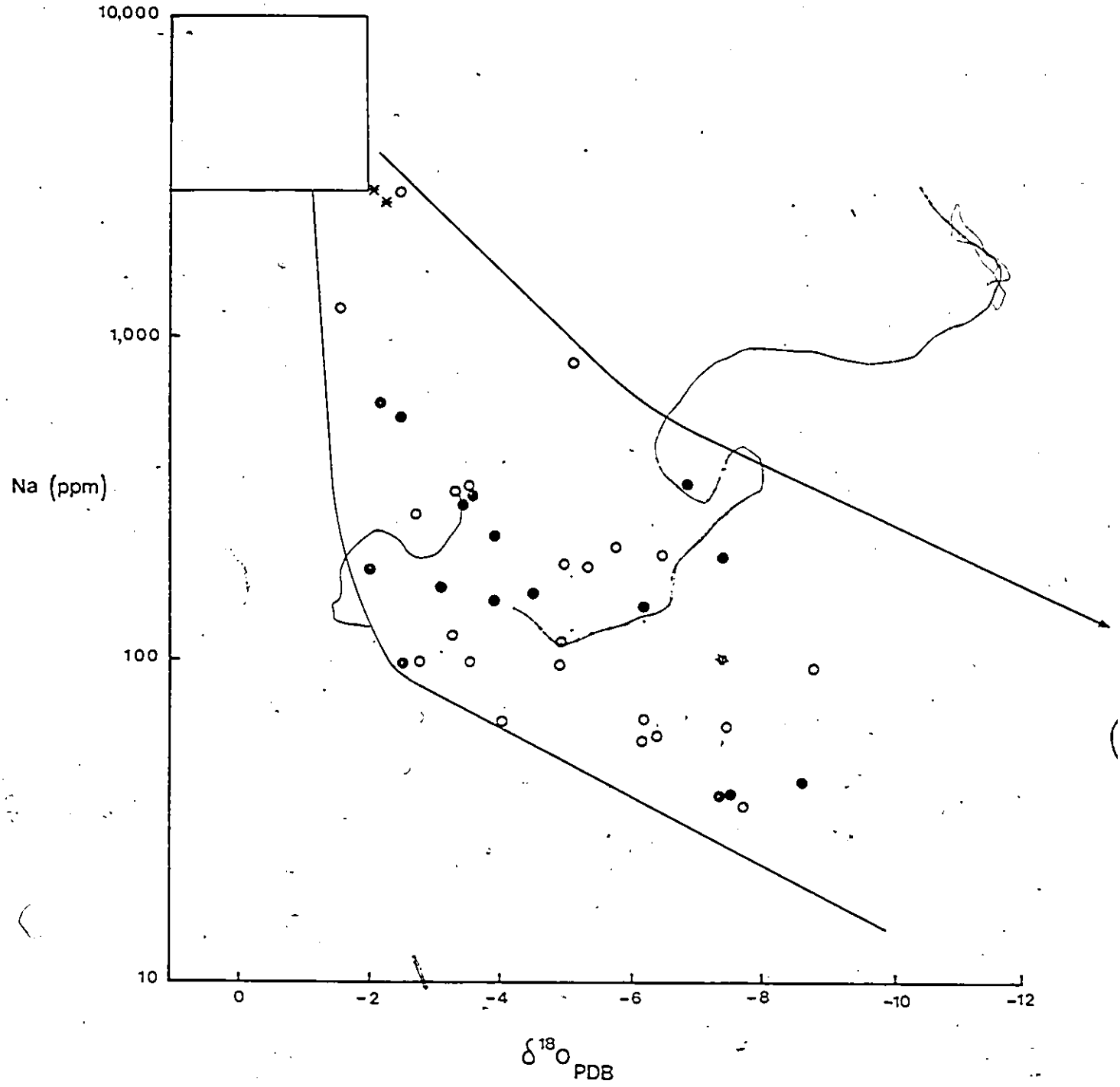

Fig.III-14. Scatter diagram of Na vs. $\delta^{18}O$ for cayinid outer and inner layers of presumably aragonitic composition. Explanations as in Fig.III-13.

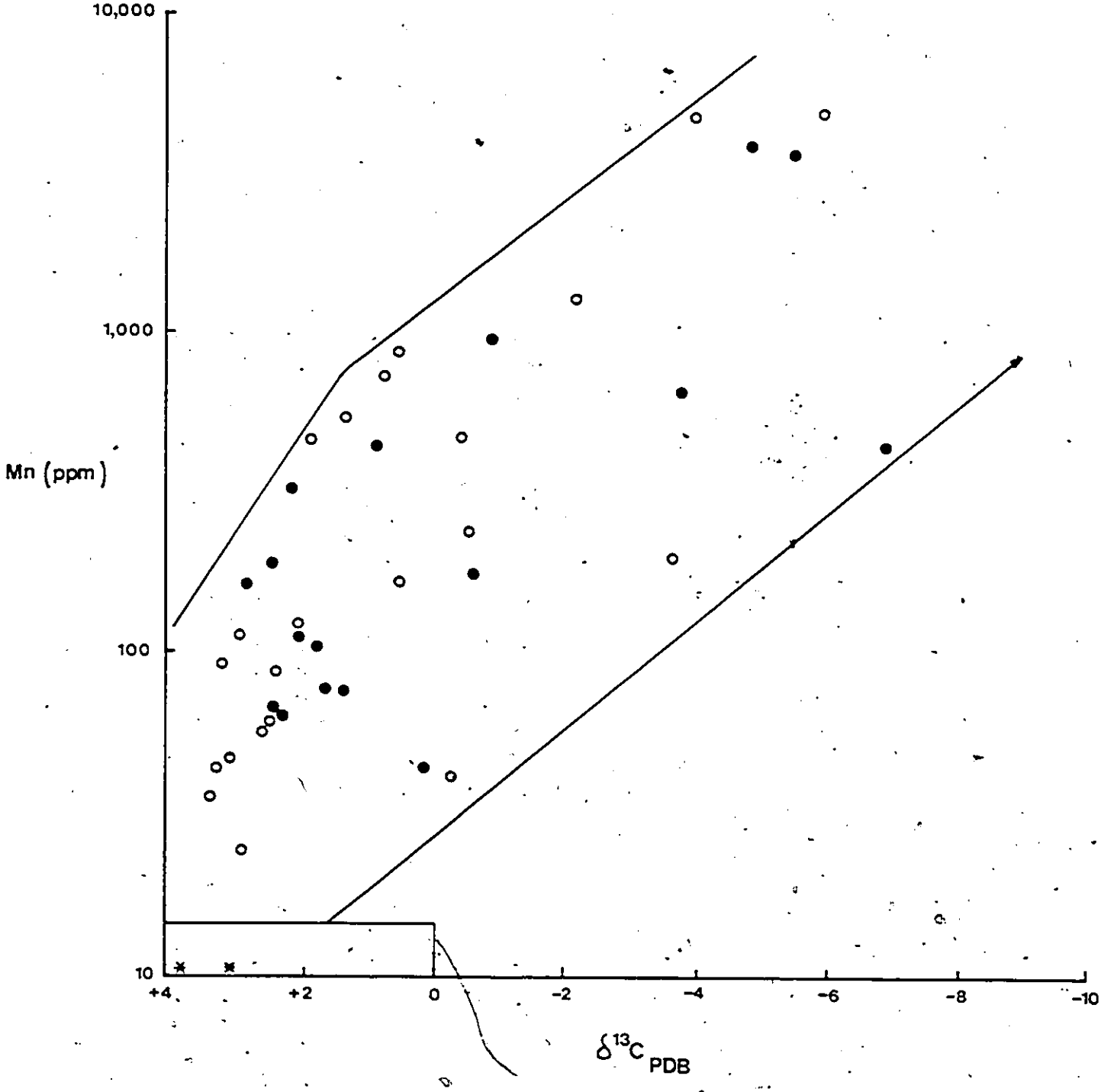

Fig.III-15. Scatter diagram of Mn vs. $\delta^{13}C$ for caprinid outer and inner layers of presumably originally aragonitic composition. Explanations as in Fig.III-13.

3.4.7 Family Hippuritidae

The LMC prismatic layers and the pillars and beads of the hippuritids have $\delta^{18}O$ range from -1.7 to -8.0‰ and $\delta^{13}C$, +3.1 to -0.8‰ PDB. The heaviest values for both isotopes are similar to those for $CaCO_3$ in equilibrium with present day seawater (Figs. III-16, 17).

The major controlling factors of isotopic variations (Table III-7) are the same as previously described for LMC components. Here again early diagenetic calcitization of the metastable minerals contained within the primary pore spaces explains Sr vs. Na relationship (Factor 2). Later stages of diagenetic equilibration with meteoric waters, through the precipitation of ferroan cement, account for $\delta^{13}C$ and $\delta^{18}O$ variations (Factors 1 and 3).

Oxygen and carbon isotopic values for the presumably original aragonitic inner layers of hippuritids range from -2.8 to -6.2‰ for $\delta^{18}O$ and from +4.2 to +0.6‰ PDB for $\delta^{13}C$ (Appendix 3).

Due to the small number of samples (N = 14), the resulting factors do not show any clear diagenetic trends (Table III-8). It seems that the early diagenetic stabilization (Factor 3) exerts control on C, while late ferroan calcite cementation (Factor 1, 2) exert additional control on C and O.

TABLE III-8

Partial factor analysis of
all hippuritid outer layers, pillars and beads (N = 33)

	Factor 1	Factor 2	Factor 3
log IR	0.029	-0.119	0.362
log Ca	0.022	-0.300	0.058
log Mg	-0.005	0.030	0.717
log Sr	-0.089	0.774	0.357
log Mn	0.979	-0.133	0.039
log Fe	0.659	0.043	0.564
log Na	-0.176	0.816	-0.081
log Zn	-0.106	-0.177	0.038
log Al	-0.270	-0.403	0.290
$\delta^{18}O$	-0.533	0.084	0.274
$\delta^{13}C$	-0.091	0.262	0.574
Percent of Variation Explained	36.0	31.1	22.0
Eigen value	2.073	1.793	1.264
Interpretation	Diagenetic Stabilization IIb	Diagenetic Stabilization I	Diagenetic Stabilization IIa

TABLE III-9

Partial factor analysis of
all hippuritid inner layers (N = 14)

	Factor 1	Factor 2	Factor 3
log IR	-0.058	-0.210	0.857
log Ca	0.701	0.070	0.057
log Mg	0.331	0.219	-0.121
log Sr	0.738	0.298	-0.320
log Mn	0.718	-0.419	-0.195
log Fe	0.655	-0.459	0.284
log Na	0.399	0.245	-0.828
log Zn	-0.087	0.903	-0.269
log Al	0.050	-0.045	-0.120
$\delta^{18}O$	0.076	0.829	-0.027
$\delta^{13}C$	0.423	0.474	0.735
Percent of Variation Explained	33.9	29.7	22.2
Eigen value	2.925	2.559	1.911
Interpretation	Total Carbonate ? and Late Diagenetic Stabilization II ?	Diagenetic Stabilization II	Laboratory Leaching and Diagenetic Stabilization I

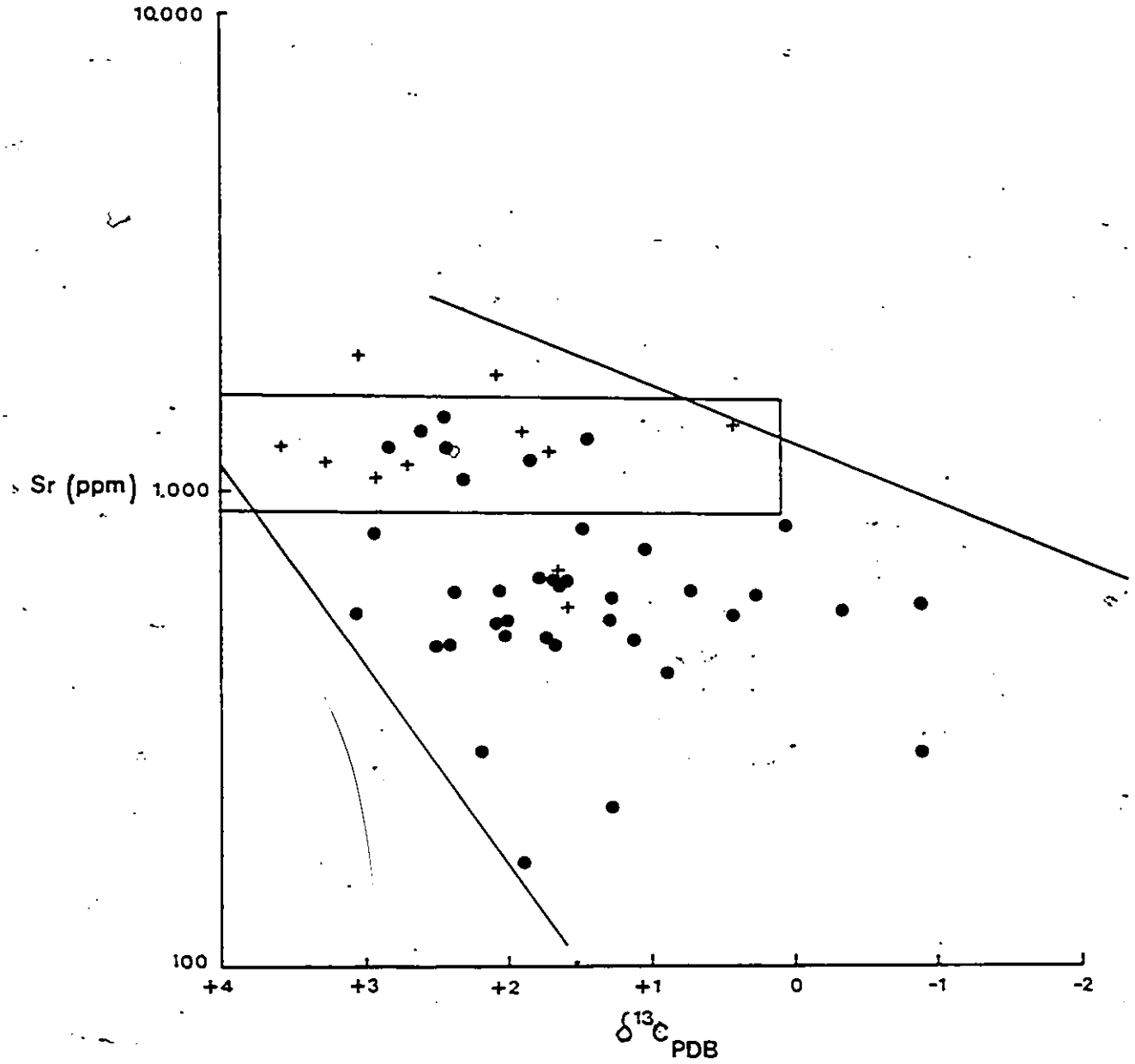

Fig.III-16. Scatter diagram of Sr vs. $\delta^{13}C$ for hippuritid outer layers, pillars and beads of originally LMC composition. Closed circles (•) represent outer layers, and the crosses (+) represent pillars and beads.

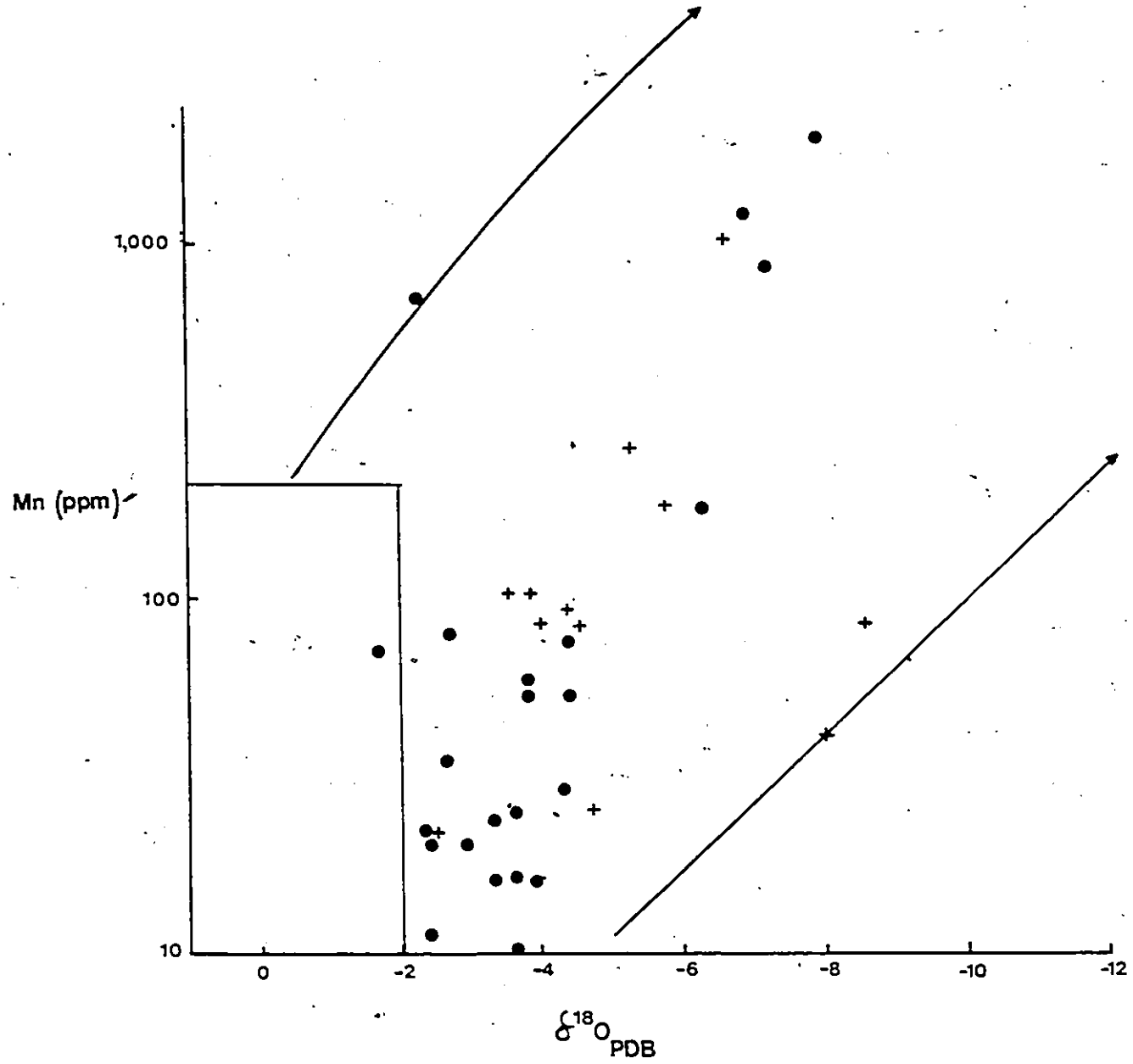

Fig.III-17. Scatter diagram of Mn vs. $\delta^{18}O$ for hippuritid outer layers, pillars and beads of originally LMC composition. Explanations as in Figs.III-5,16.

3.4.8 Family Radiolitidae

The isotopic composition of the originally LMC cellular-prismatic outer layers of radiolitids varies from -2.4 to -6.5‰ for $\delta^{18}O$ and from +3.5 to -3.3‰ PDB for $\delta^{13}C$ (Appendix 3). Their chemical and isotopic variations are controlled by four factors, but only two are shown in Table III-10. Factor 1, which controls Mg, Sr, Mn and possibly $\delta^{18}O$, is not well understood, but may have some bearing on diagenetic repartitioning during late meteoric equilibration stages. Factor 3 which controls the distribution of Na, Al and $\delta^{13}C$ may (in analogy to the general LMC discussion; Section 3.4.5) also represent a late diagenetic signal. However, the matter is complicated by the high proportion of early and late cements in this relatively high porous layer.

The isotopic composition of the presumably originally aragonitic inner layers vary from +0.7 to -7.8‰ for $\delta^{18}O$ and from +3.4 to -2.4‰ PDB for $\delta^{13}C$ (Appendix 3). The controls of isotopic composition, due to the small number of samples (Table III-11), are not well understood. It seems that oxygen isotopic variations are due to late ferroan calcite cements, while the factor controlling C distribution is difficult to interpret.

TABLE III-10

Partial factor analysis of all radiolitids outer layers (N = 20)

	Factor 1	Factor 2
log IR	-0.216	0.157
log Ca	-0.002	-0.091
log Mg	0.886	0.105
log Sr	0.715	0.135
log Mn	0.664	0.269
log Fe	-0.139	0.271
log Na	0.228	0.517
log Zn	-0.085	-0.124
log Al	0.359	0.508
$\delta^{18}O$	0.463	-0.308
$\delta^{13}C$	0.045	-0.887
Percent of Variation Explained	42.5	16.0
Eigen value	3.015	1.136
Interpretation	Diagenetic Stabilization II ?	Diagenetic Stabilization II

TABLE III-11

Partial factor analysis of
all radiolitid inner layers (N = 16)

	Factor 1	Factor 2	Factor 3
log IR	0.167	-0.355	-0.049
log Ca	-0.233	-0.065	-0.706
log Mg	-0.424	0.667	0.139
log Sr	-0.071	-0.279	-0.054
log Mn	-0.843	0.231	-0.264
log Fe	0.103	0.676	-0.076
log Na	0.943	-0.145	0.060
log Zn	0.490	0.011	-0.007
log Al	0.384	0.131	0.517
$\delta^{18}O$	-0.132	0.652	-0.091
$\delta^{13}C$	-0.167	-0.377	0.603
Percent of Variation Explained	28.2	15.0	13.3
Eigen value	2.178	1.154	1.023
Interpretation	Diagenetic Stabilization I	Diagenetic Stabilization II	Total Carbonate ?

3.5 SUMMARY AND IMPLICATIONS OF DIAGENETIC TRENDS

Oxygen and carbon isotopes, in conjunction with trace elements (cf. Chapter II), proved to be sensitive tracers of both, original depositional and later diagenetic processes. The postulated multistage diagenetic transformation of A (HMC) → dLMC and, to a lesser degree, LMC → dLMC, reflected in trace elements (Sr, Na, Mn, Fe and Mg), was corroborated by pronounced trends in $\delta^{18}O$ and $\delta^{13}C$. Diagenetic shifts of $\delta^{18}O$ and $\delta^{13}C$ towards lighter values, observed in skeletal components of rudist shells, were achieved by solution-reprecipitation processes in the presence of meteoric water.

The well preserved aragonitic and low-Mg calcitic skeletal components have oxygen and carbon isotopic compositions similar to Recent marine carbonate sediments. This may argue for comparable O and C isotopic composition of the Cretaceous and Recent seawater, as well as comparable processes of incorporation of these isotopes into skeletal components of rudists and Recent bivalves. The originally aragonitic skeletal components, which have been transformed into dLMC during an early diagenetic stage and show some preservation of their original ultrastructures, have only slightly altered oxygen isotopic composition and unaltered carbon values. This

is due to the presence of meteoric diagenetic waters with $\delta^{18}O$ ~ 2‰ lighter than seawater. The carbon values in these waters were buffered by the dissolving aragonites. Originally aragonitic skeletal components, which were completely dissolved and the voids filled by late meteoric calcitic spar, have considerably altered isotopic composition. This is due either to considerable depletion in ^{18}O and ^{13}C for these diagenetic waters or, for oxygen, to higher temperatures.

Comparison of present results with those obtained by other authors is given in Figures III-18, 19. As a Cretaceous base line, I accept the values obtained for the shells which preserved their original mineralogical mode ($\delta^{18}O$, -2.1‰ and $\delta^{13}C$, +3.9‰, Section 3.4). This summary shows that the field of well preserved aragonite (G) partially overlaps, or falls close, to the fields for present day molluscs, preserved aragonite from Scotland, and whole rudist shells from Texas. Calcitized aragonitic layers with relics (H) show only partial shifts in $\delta^{18}O$ but a considerable one in $\delta^{13}C$. However, the bulk of this negative shift in $\delta^{13}C$ is caused by only three separate layers of the same fossil (samples 97a, 97b, and 97d). Calcitized aragonitic components without preserved ultrastructural relics (I) show a clear depletion in both oxygen and carbon. The

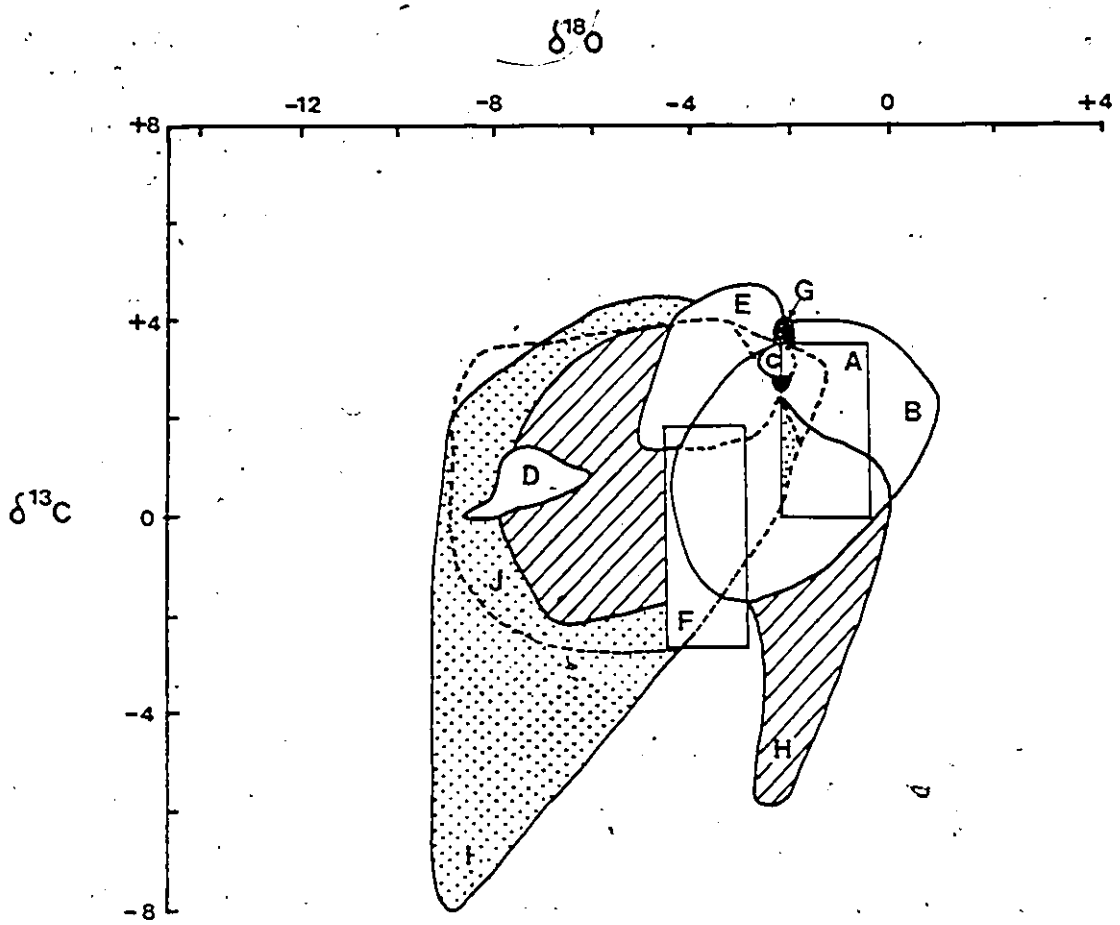

Fig.III-18. Isotopic composition of rudist skeletal components and other carbonate sediments and rocks. A= Recent sediments ; Bermuda, partially cemented (meteoric) (Gross,1964); B= shallow water molluscs and foraminifera (Milliman,1974); C= aragonitic skeleton, Neomiodon, Jurassic, Scotland (Tan and Hudson, 1974); D= calcite-replaced aragonitic shells (Neomiodon), Jurassic, Scotland (Tan and Hudson, 1974); E= whole-fossil rudists, Lower Cretaceous Texas (Moldovanyi and Lohman, 1984); F= Glen Rose Formation, Lower Cretacecus, Texas (Allan and Matthews, 1982); G= preserved aragonite in rudists (present study); H= dLMC replacing originally aragonitic layers with relic ultrastructures (present study); I= dLMC replacing originally aragonitic layers without relic ultrastructures (present study); and J= LMC rudist components (present study).

calcitized aragonitic shells from the Jurassic of Scotland (D) display a similar trend. Similarly, the LMC skeletal components (J) are characterized by similar isotopic displacement. The resulting diagenetic repartitioning trends for O and C indicate three hypothetical trends (Figs. III-18, 20).

The distinguished four cement types, which occluded primary and secondary pore spaces within rudist shell (cf. Section 3.4.2), show similar ranges in oxygen and carbon isotopic values (Fig. III-19). The postulated early, radiaxial fibrous and inclusion-rich micritic cements (E) resemble, isotopically, most Holocene aragonitic and Mg-calcitic cements (fields A and B, respectively), although they are ~2‰ lighter in oxygen. The inclusion-rich equant cement (F), which always predates the bladed and large equant cements (cf. Chapter I), shows a progressive increase in ^{16}O and ^{12}C, and the two types of late ferroan calcites show the maximal depletion.

Theoretically, two factors controlling oxygen and carbon isotopic composition of the final product are of importance in diagenesis. For oxygen, it is increasing temperature and/or the depletion of meteoric waters in ^{18}O. For carbon, the diagenetic water in the aquifer is usually buffered isotopically by the dissolving carbonate precursor and $\delta^{13}C$ does not change. In many

instances, however, the contribution from decomposition of organic matter ($\delta^{13}C \sim -25‰$), whether during early or later, deep burial diagenetic stages, causes depletion in ^{13}C. The consequence may be a diagenetic trend of type 1 (Fig. III-20), or type 2, if the C isotopic composition is buffered by dissolving carbonates. These, and combinations, are the most frequent situations in carbonate rocks. Trend 2 can be either arrested at this stage, or - during deeper burial - incorporate progressively lighter "organic" carbon, thus forming the "inverted J" trends of Lohmann (1983) and Meyers and Lohmann (1984). In some instances, only the C shift is evident, while that for O is only minor (trend 3). Such a trend can evolve only during early shallow burial if the oxygen isotopic composition of diagenetic water and its temperature are not significantly different from that of seawater which deposited the original carbonates. Furthermore, this shallow diagenetic aquifer must be influenced by a carbon source of "organic" derivation. This interpretation differs from that of Lohmann (1983), in that it questions the possibility of buffering of $\delta^{18}O$ of aquifer water by dissolving carbonate as a viable cause of near-constant $\delta^{18}O$ value. Considering the overwhelming dominance of water derived over that of carbonate originating oxygen ($\sim 10^4:1$) in any diagenetic situation (cf. Veizer, 1983a), the explanation of Lohmann is not plausible.

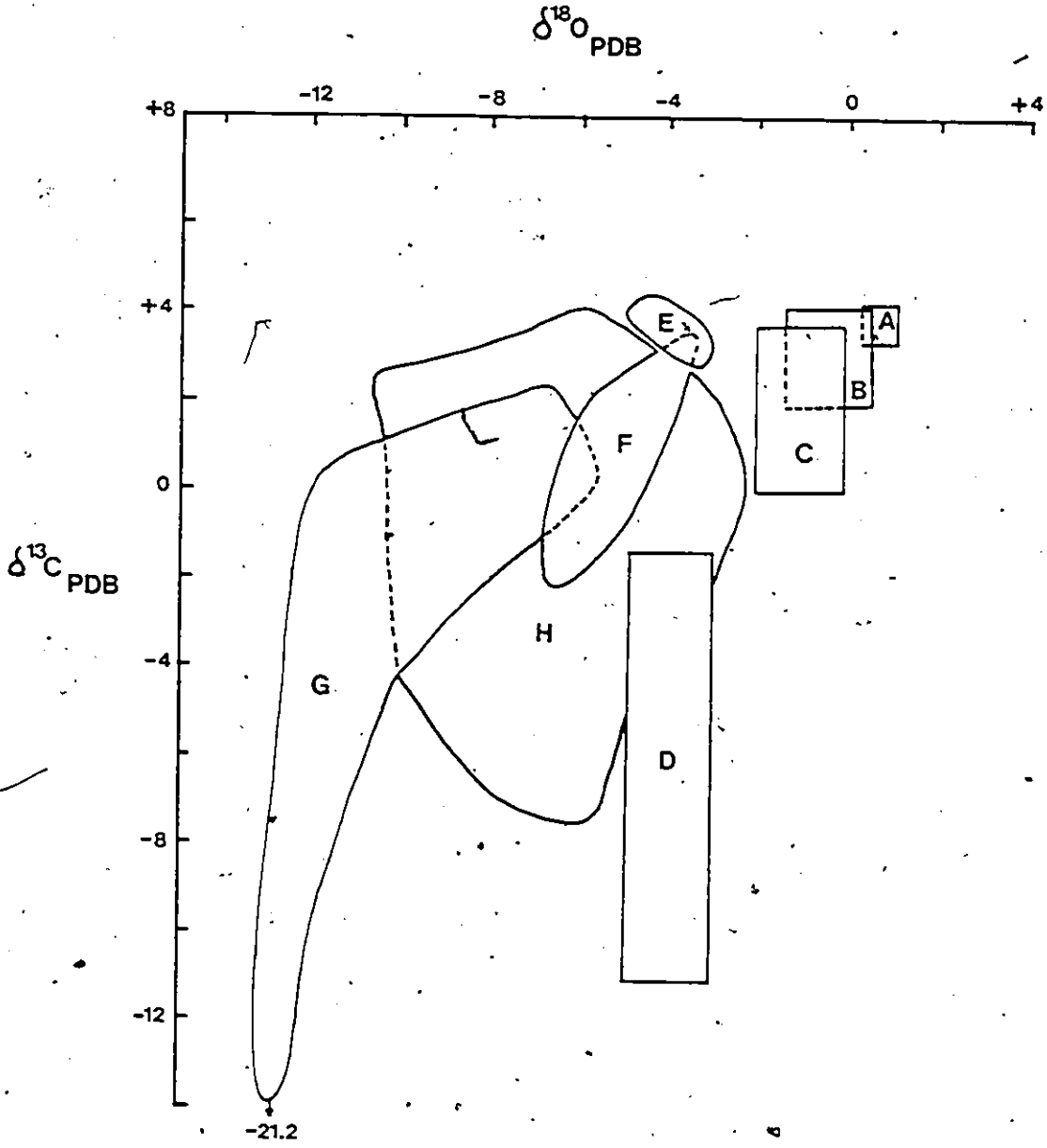

Fig.III-19. Isotopic composition of carbonate cements and associated sediments. A= Submarine aragonite cement, British Honduras (Holocene) (Ginsburg and James, 1976); B= Holocene submarine Mg-calcite cements and sediments, Jamaica (Land and Goreau,1970); C= Recent sediments, Bermuda, partially cemented (meteoric) (Gross,1964); D= Pleistocene limestone from phreatic and vadose realms, Barbcdos (Allan and Matthews, 1977); E= radiaxial fibrous, inclusion-rich cement (this study); F= inclusion-rich equant calcite (this study); H= large ferroan equant calcite (this study); and G= ferroan bladed spar (this study).

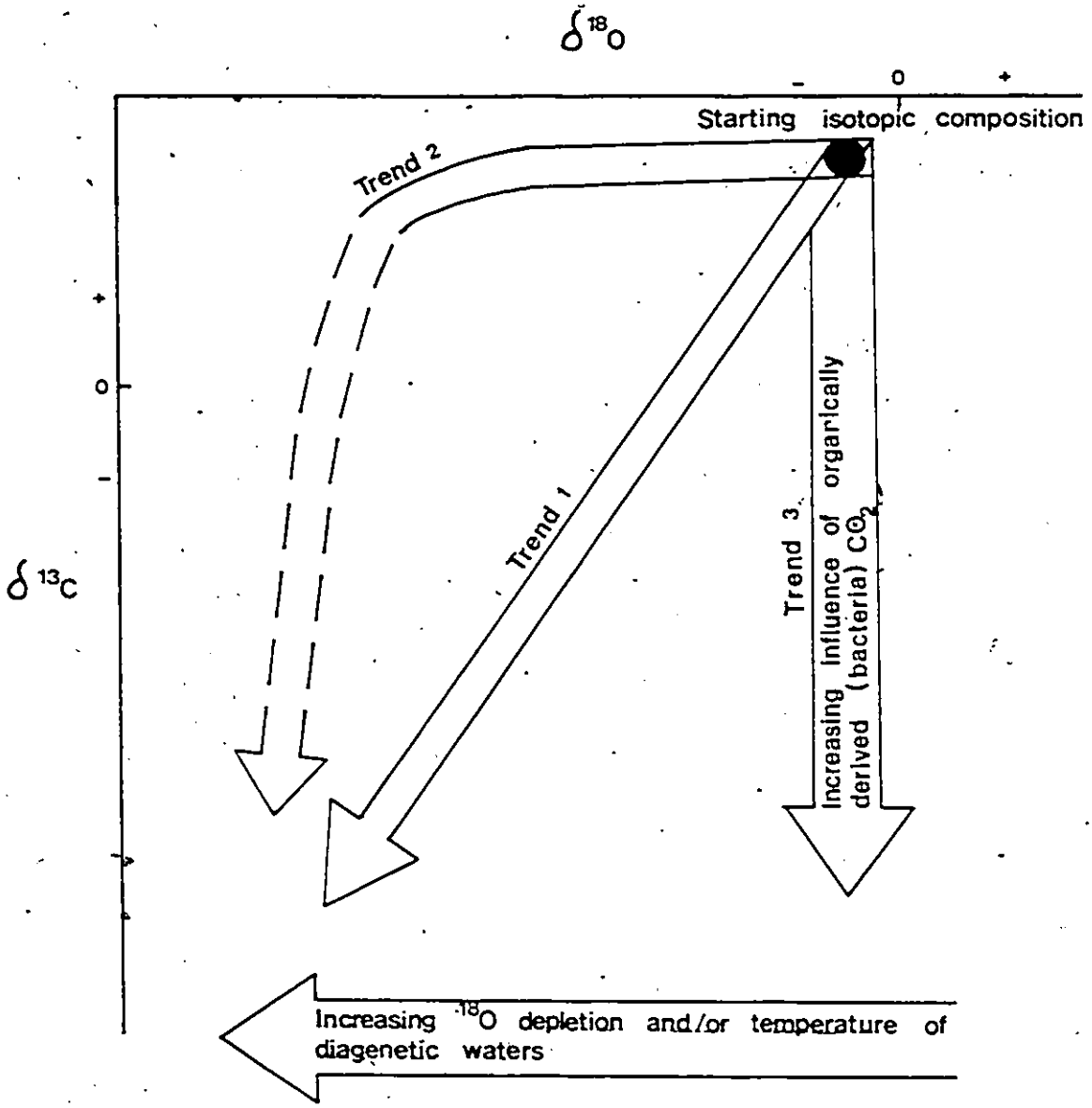

Fig.III-20. Theoretical model for $\delta^{18}O$ and $\delta^{13}C$ repartitioning during carbonate diagenesis (modified after Lohmann 1983).

3.6 CONCLUSIONS

Oxygen and carbon isotopes in skeletal components of rudists and associated rocks, and their comparison with published data, lead to the following conclusions:

(1) Skeletal components with preserved mineralogy of aragonite and low-Mg calcite and with preserved textural and chemical signals, have oxygen and carbon isotopic values similar to those of their Recent marine counterparts. This similarity in isotopic composition between Cretaceous rudists and Recent molluscs and carbonate sediments argues for comparable isotopic composition of the Cretaceous and Recent seawaters, as well as for a similar mode of incorporation of oxygen and carbon isotopes into their shells.

(2) Taking the isotopic composition of skeletal components of rudists with preserved mineralogy as a base line, the calculated palaeotemperatures for Cretaceous Tethyan seawater varied in the range of 22.9 to 29.6°C.

(3) The A → dLMC transformation proceeded in two-stages. During the early wet neomorphic replacement of aragonitic components, the $\delta^{18}O$ and temperature of diagenetic water did not vary much from that of coeval seawater. This resulted in only a slight shift in oxygen isotopic signal. Furthermore, the $\delta^{13}C$ of this diagenetic water has been buffered by the dissolving

aragonite, because the A ⟶ dLMC transformation was achieved in semiclosed micron-sized environments, as attested by partial preservation of the original aragonitic ultrastructures and of Sr and Na concentrations. In contrast, later stages of diagenetic stabilization in meteoric waters led to wholesale leaching of the remaining aragonite and precipitation of dLMC as spar calcites. This stage is characterized by a negative shift in $\delta^{13}C$ and by positive shifts in Mn and Fe as a result of equilibration with shallow meteoric phreatic waters.

(4) The magnitude of diagenetic shifts for stable isotopes during diagenetic stabilization of LMC is smaller than that of aragonites. These diagenetic shifts in $\delta^{18}O$, $\delta^{13}C$, as well as in Sr, Na, Mn, and Fe, have been accomplished through late diagenetic precipitation of ferroan spar cements into primary and secondary pore spaces within little altered LMC rudist components.

(5) Each of the four cement types, occluding primary and secondary pore spaces within rudist shells, has a specific isotopic signature. Early radiaxial fibrous and micritic inclusion-rich cements are characterized by heavy $\delta^{18}O$ and $\delta^{13}C$ indicative of marine A (and HMC) precursors. Inclusion-rich equant spar is characterized by somewhat larger shifts towards

lighter oxygen and carbon isotopic values, and the late ferroan equant and bladed spars contain the most ^{18}O and ^{13}C deficient isotopic composition, with some carbon derived from CO_2 of organic origin within the vadose zone of the meteoric phreatic aquifer.

REFERENCES

REFERENCES

Achauer, C.A., 1977, Contrasts in cementation, dissolution and porosity development between two Lower Cretaceous reefs of Texas: in Bebout, D.G. and Loucks, R.G. (eds.), Cretaceous carbonates of Texas and Mexico, Univ. of Texas, Austin, Bur. Econ. Geol., Rept. of Invest., No. 89, p. 127-137.

Al-Aasm, I.S. and Veizer, J., 1982, Chemical stabilization of low-Mg calcite: an example of brachiopods; Jour. Sed. Petrology, v. 52, p. 1101-1109.

Alexanderson, E.T., 1972, Intergranular growth of marine aragonite and Mg-calcite: evidence of precipitation from supersaturated seawater; Jour. Sed. Petrology, v. 42, p. 441-460.

Allan, J.R. and Matthews, R.K., 1977, Carbon and oxygen isotopes as diagenetic and stratigraphic tools: surface and subsurface data, Barbados, West Indies: Geology, v. 5, p. 16-20.

_____, 1982, Isotope signatures associated with early meteoric diagenesis: Sedimentology, v. 29, p. 797-817.

Anderson, T.F. and Arthur, M.A., 1983, Stable isotopes of oxygen and carbon and their application to sedimentologic and paleoenvironmental problems: SEPM Short Course Notes No. 10, 151 p.

Arthur, M.A. and Schlanger, S.O., 1979, Cretaceous "Oceanic Anoxic Events" as Causal factors in development of reef-reservoired giant oil fields: AAPG, v. 63, p. 870-885.

Badiozamani, K., 1973, The dorag dolomitization model-application to the Middle Ordovician of Wisconsin: Jour. Sed. Petrology, v. 43, p. 965-984.

Barron, Eric J., 1983, A warm, equable Cretaceous: the nature of the problem: Earth-Science Reviews, v. 19, p. 305-338.

Bathurst, R.G.C., 1964, The replacement of aragonite by calcite in the molluscan shell-wall: in Imbrie, J. and Newell, N.D. (eds.), Approaches to Paleoecology, Wiley, New York, p. 357-376.

_____, 1966, Boring algae, micrite envelopes and lithification of molluscan biosparite; Geol. J., v. 5, p. 15-32.

_____, 1975, Carbonate sediments and their diagenesis; Elsevier, Amsterdam, 658 p.

_____, 1980, Lithification of carbonate sediments; Sc.: Prog. Oxford, v. 66, p. 451-471.

_____, 1982, Genesis of stromatactis cavities between submarine crusts in Palaeozoic carbonate mud buildups; J. Geol. Soc. London, v. 139, p. 165-181.

_____, 1983, Early diagenesis of carbonate

sediments; in Parker A. and Sellwood B.W. (eds.); Sediment diagenesis, NATO ASI seris, D. Reidel Publ. Co., p. 349-378.

Bay, A.R. and Bebout, D.G., 1983, Cyclic, shoaling-carbonate banks in the Lower Glen Rose Formation (Cretaceous), south Texas: SEPM Core Workshop, No. 4, p. 429-462.

Bein, Amos, 1976, Rudistid fringing reefs of Cretaceous shallow carbonate platform of Israel: AAPG, v. 60, p. 258-272.

Bermudez, Pedro J., 1959, Cuba: Lexique Stratigraphique Intern., Amérique Latine, Fascicule 11a, p. 1-130.

Berner, R.A., 1980, Early diagenesis: a theoretical approach: Princeton, N.J., Princeton University Press, 241 p.

Bøggild, O.B., 1930, The shell structure of the mollusks: Kgl. Danske Videnskab-Selskab, Mat. Fys. Medd., v. 9, p. 231-325.

Brand, U., 1981a, Mineralogy and chemistry of the Lower Pennsylvanian Kendrick fauna, eastern Kentucky -1: trace elements: Chem. Geol., v. 32, p. 1-16.

_____, 1981b, Mineralogy and chemistry of the Lower Pennsylvanian Kendrick fauna, eastern Kentucky -2: stable isotopes: Chem Geol., v. 32, p. 17-28.

_____, 1982, The oxygen and carbon isotope composition of Carboniferous fossil components: sea water effects: Sedimentology, v. 29, p. 139-147.

_____, 1983, Mineralogy and chemistry of the Lower Pennsylvanian Kendrick fauna, eastern Kentucky, USA -3: diagenetic and paleoenvironmental analysis: Chem. Geol., v. 40, p. 167-181.

_____ and Veizer, J., 1980, Chemical diagenesis of a multicomponent carbonate system -1: trace elements: J. Sed. Petrology, v. 50, p. 1219-1236.

_____, 1981, Chemical diagenesis of a multicomponent carbonate system -2: stable isotopes: J. Sed., Petrology, v. 51, p. 987-997.

_____, 1983, Origin of coated grains: - trace element constraints: in Peryt, T.M., (ed.): coated grains: Springer-Verlag, Berlin, Heidelberg, p. 9-26.

Bricker, O.P. (ed.), 1971, Carbonate cements: Johns Hopkins Press, Baltimore, Md., 316 p.

Buchardt, B. and Weiner, S., 1981, Diagenesis of aragonite from Upper Cretaceous ammonites in geochemical case-study: Sedimentology, v. 28, p. 423-438.

Butterlin, J., 1983, The Caribbean region: in Moullade, M. and Nairn, A.E.M. (eds.): The Phanerozoic geology of the World II, The Mezozoic, B: Elsevier Publ., p. 89-119.

Campose, H.S. and Hallam, A., 1979, Diagenesis of English Lower Jurassic limestones as inferred from oxygen and carbon isotope analysis: Earth Planet. Sci.

Lett., v. 45, p. 23-31.

Carlson, W.D., 1983, The polymorphs of $CaCO_3$ and the aragonite-calcite transformation: Reviews in Mineralogy, v. 11, p. 191-225.

Carter, J.G. and Tevesz, M.J.S., 1978, Shell microstructure of a Middle Devonian (Hamilton Group) bivalve fauna from central New York: Jour. Paleont., v. 52, p. 859-880.

Chave, K.E., 1954, Aspects of the biogeochemistry of magnesium. I. Calcareous marine organisms: Jour. Geol., v. 62, p. 266-283.

_____, 1984, Physics and Chemistry of biomineralization: Annual Review of Earth and Planetary Sci., v. 12, p. 293-307.

Choquette, P.W. and Pray, L.C., 1970, Geologic nomenclature and classification of porosity in sedimentary carbonates: AAPG Bull., v. 54, p. 207-250.

Chubb, L.J., 1955, A revision of Whitfield's type specimens of the rudist mollusks from the Cretaceous of Jamaica, British West Indies: Novitates, no. 1713, p. 1-15.

_____, 1956, Rudist assemblages of the Antillean Upper Cretaceous: Bull. Am. Paleont., v. 37, p. 1-23.

_____, 1961, Rudist assemblages in Cuba: Bull. Am. Paleont., v. 43, p. 413-422.

_____, 1971, Rudists of Jamaica: Paleontogr. Americana, v. 45, p. 162-257.

Coats, A.G., 1973, Cretaceous Tethyan coral-rudist biogeography related to the evolution of the Atlantic Ocean: Special papers in Palaeo., no. 12, p. 169-174.

_____, 1977a, Jamaican Cretaceous coral assemblages and their relationships to rudist frameworks: in Comptes Rendus 2e Symposium International sur les Coraux et Récifs Actuels et Fossiles: Paris, Bur. Recherches Géol. et Miniéres, Mém. 89, p. 336-341.

_____, 1977b, Jamaican coral-rudist frameworks and their geologic setting, AAPG stud. Geology, no. 4, p. 83-91.

Coogan, A.H., 1969, Evolutionary trends in rudist hard parts: in Moore, R.C. (ed.): Treatise on invertebrate paleontology, Part N, v. 2, GSA and Univ. Kansas, p. N766-776.

_____, 1977, Early and Middle Cretaceous Hippuritacea (rudists) of the Gulf coast: Texas Univ., Bur. Econ. Geol., Report Invest., no. 89, p. 32-70.

Coplen, T.B., Kendall, C. and Hopple, J., 1983, Comparison of stable isotope reference samples: Nature, v. 302, p. 236-238.

Craig, H., 1957, Isotopic standards for carbon and oxygen and correction factors for mass spectrometric analysis

of carbon dioxide: Geochim. Cosmochim. Acta, v. 12, p. 133-149.

_____, 1965, The measurement of oxygen isotopic paleotemperatures: in Stable Isotopes in Oceanographi Studies and Paleotemperatures: Consiglio Nazionale delle Ricerche, Laboratorio di Geologica Nucleare, Pisa, p. 1-24.

Crick, R.E. and Ottensman, V.M., 1983, Sr, Mg, Ca, and Mn chemistry of skeletal components of a Pennsylvanian and Recent Nautiloid: Chem. Geol., v. 39, p. 147-163.

Curtis, C.D. and Krinsley, D., 1965, The detection of minor diagenetic alteration in shell material: Geochim. Cosmochim. Acta, v. 29, p. 71-84.

Czerniakowski, L.A., Lohmann, K.C. and Wilson, J.L., (in press), Closed-system marine burial diagenesis: isotopic data from the Austin Chalk and its components: Sedimentology.

Davies, G.R., 1977, Former magnesian calcite and aragonite submarine cements in Upper Paleozoic reefs of the Canadian Arctic: A summary: Geology, v. 5, p. 11-15.

Dechaseaux, C., 1969, Origin and extinction: in Moore. R.C. (ed.): Treatise on invertebrate paleontology, Part N, v. 2, GSA and Univ. Kansas, p. N764-765.

_____ and Sornay, J., 1960, "Récifs" à rudistes:

Soc. Géol., France, Bull., Ser. 7, v. 1, p. 399-402.

Degens, E.T. and Epstein, S., 1962, Relationship between $^{18}O/^{16}O$ ratios in coexisting carbonates, cherts and diatomites: AAPG Bull., v. 46, p. 534-542.

DeRenzi, M. and Marquez-Aliaya, A., 1980, Primary and diagenetic features in the microstructure of some Triassic bivalves: Revista del Instituta de Investigaciones Geologicas Diputacion Provincal, Universidad de Barcelona, v. 34, p. 101-116.

Dickson, J.A.D. and Coleman, M.L., 1980, Changes in carbon and oxygen isotope composition during limestone diagenesis: Sedimentology, v. 27, p. 107-118.

Dodd, J.R., 1965, Environmental control of strontium and magnesium in Mytilus: Geochim. Cosmochim. Acta, v. 29, p. 385-398.

_____, 1966, Processes of conversion of aragonite to calcite with examples from the Cretaceous of Texas: Jour. Sed. Petrology, v. 36, p. 733-741.

_____, 1967, Magnesium and strontium in calcareous skeletons: a review: Jour. Paleont., v. 41, p. 1313-1329.

_____ and Stanton, R.J. Jr., 1981, Paleoecology, Concepts and applications: Wiley-Interscience Publ., 559 p.

Drever, J.I., 1982, The geochemistry of natural waters:

Prentice-Hall, Englewood, Calif., N.J., USA, 338 p.

Dunham, R.J., 1962, Classification of carbonate rocks according to depositional texture: in Ham, W.E. (ed.), Classification of carbonate rocks: AAPG, Tulsa, Okla., p. 108-121.

_____, 1969, Early vadose silt in Townsend mound (reef), New Mexico: in Friedman, G.M. (ed.): Depositional environments in carbonate rocks: a symposium: SEPM, Spec. Publ., no. 14, p. 139-181.

_____, 1971, Meniscus cement in carbonate cements: John Hopkins Univ. Studies in Geology, no. 19; p. 297-300.

Emiliani, C., 1955, Pleistocene temperatures: Jour. Geol., v. 63, p. 538-578.

Epstein, S., Buchsbaum, R., Lowenstam, H.A. and Urey, H.C., 1953, Revised carbonate water isotopic temperature scale: Geol. Soc. Am. Bull., v. 64, p. 1315-1326.

Fisher, W.L. and Rodda, P.V., 1969, Edwards Formation (Lower Cretaceous) Texas: dolomitization in carbonate platform system: AAPG Bull., v. 53, p. 55-72.

Flanagan, F.J., 1973, 1972 values of international geochemical reference samples: Geochim. Cosmochim. Acta, v. 37, p. 1189-1200.

Flügel, E., 1982, Microfacies analysis of limestones: Springer-Verlag, New York, 633 p.

Folk, R.L., 1965, Some aspects of recrystallization in

ancient limestones: in Pray, L.C. and Murray, R.C. (eds.), Dolomitization and limestone diagenesis, SEPM, Spec. Publ., no. 13, p. 14-48.

_____, 1974, The natural history of crystalline calcium carbonate; effect of Mg-content and salinity: Jour. Sed. Petrology, v. 44, p. 40-53.

Friedman, G.M., 1975, The making and unmaking of limestones: or the downs and ups of porosity: Jour. Sed. Petrology, v. 45, p. 379-398.

_____ and Schneidermann, N., 1974, Submarine cementation in reefs: examples from the Red Sea: Jour. Sed. Petrology, v. 44, p. 816-825.

Friedman, I. and O'Neil, J.R., 1977, Compilation of stable isotope fractionation factors of geochemical interest: in Data of geochemistry, 6th ed. (M. Fleischer, ed.), U.S. Geol. Surv. Prof. paper, 440 kk.

Freyetet, P., 1973, Edifices récifaux développés dans un environnement détritique: exemple des biostromes à Hippurites du Senonion inférieur du sillon langnedocien (région de Narbonne, Sud de la France): Paleogeo. Paleoclim., Paleoecol., v. 13, p. 65-76.

Frost, S.H., Bliefnick, D.M. and Harris, P.M., 1983, Deposition and porosity evolution of a Lower Cretaceous rudist buildup, Shuaiba Formation of

eastern Arabian Peninsula: SEPM core workshop, no. 4., p. 381-410.

Fyfe, W.S. and Bischoff, J.L., 1965, The calcite-aragonite problem: in Pray, L.C. and Murray, R.C. (eds.), Dolomitization and limestone diagenesis: a symposium: SEPM, Spec. Publ., no. 13, p. 3-13.

Gavish, E. and Friedman, G.M., 1969, Progressive diagenesis in Quaternary to Late Tertiary carbonate sediments: sequence and time scale: Jour. Sed. Petrology, v. 39, p. 1-32.

Ginsburg, R.N. and James, N.P., 1976, Submarine botryoidal aragonite in Holocene reef limestones, Belize Geology, v. 4, p. 431-436.

_____, Marszalek, D.S. and Schneidermann, N., 1971, Ultrastructure of carbonate cements in a Holocene algal reef of Bermuda: Jour. Sed. Petrology, v. 41, p. 472-482.

Given, K.R. and Wilkinson, B.H., 1984 (in press), Morphology, composition, and mineralogy of abiotic sedimentary carbonates: control by kinetic reaction parameters and physical environment: Jour. Sed. Petrology.

Gladney, E.S. and Burns, C.E., 1983, 1982 compilation of elemental concentrations in eleven United States Geological Survey rock standards: Geostandards Newsletter, v. 7, p. 3-226.

Golubic, S., Perkins, R.D. and Lukas, K.J., 1975, Boring

microorganisms and microborings in carbonate substrates: in Frey, R.W. (ed.): The study of trace fossils: Springer-Verlag, New York, p. 229-259.

Graf, D.L., 1960, Geochemistry of carbonate sediments and sedimentary carbonate rocks: Part I-IV, Illinois State Geol. Surv. Circular, v. 297.

Gross, M.G., 1964, Variations in the $^{18}O/^{16}O$ and $^{13}C/^{12}C$ ratios of diagenetically altered limestones in Bermuda Islands: Geology, v. 72, p. 170-194.

Grossman, E.T. and Ku, T.L., 1981, Aragonite-water isotopic paleotemperature scale based on the benthic foraminifera Hoeglundia elegans: Geol. Soc. Am., Ann. Mtgs., Abstr. with Programs, p. 464.

Hall, A. and Kennedy, W.J., 1967, Aragonite in fossils: Proc. Royal Soc., B168, p. 377-412.

Heckel, P.H., 1974, Carbonate buildups in the geologic record: in Reefs in time and space: SEPM, Spec. Publ., no. 18, p. 90-155.

_____, 1983, Diagenetic model for carbonate rocks in Midcontinent Pennsylvanian Eustatic Cyclothems: Jour. Sed. Petrology, v. 53, p. 733-760.

Hoefs, J., 1980, Stable isotope geochemistry (2nd edition): Springer-Verlag, 1208 p.

_____, 1982, Isotope geochemistry of carbon: in

Schmidt, H.L., Forstel, H. and Keinzinger, K. (eds.): Stable isotopes: Elsevier Scient. Publ. Co., Amsterdam, p. 103-113.

Hudson, J.D., 1962, Pseudo-pleochroic calcite in recrystallized shell-limestone: Geol. Mag., v. 99, p. 492-500.

_____, 1977, Stable isotopes and limestone lithification: Jour. Geol. Soc. London, v. 133, p. 637-660.

_____ and Coleman, H.L., 1978, Submarine cementation of the Scheck Limestone Conglomerate (Jurassic, Austria): isotopic evidence: N. Jb. Geol. Paläont. Mn., v. 9, p. 534-544.

Ishikawa, M. and Ichikuni, M., 1984, Uptake of sodium and potassium by calcite: Chem. Geology, v. 42, p. 137-147.

Jacka, A.D. and Brand, J.P. 1977, Biofacies development and differential occlusion of porosity in a Lower Cretaceous (Edwards) reef: Jour. Sed. Petrology, v. 47, p. 366-381.

James, N.P., 1983, Depositional models for carbonate rocks: in Parker, A. and Sellwood, B.W. (eds.): Sediment diagenesis, NATO ASI Series, D. Reidel Publ., p. 289-348.

_____ and Choquette, D.W., 1984, Diagenesis-6 Limestones - the sea floor diagenetic environment:

Geoscience Canada, v. 10, p. 162-179.

_____ and Klappa, C.F., 1983, Petrogenesis of Early Cambrian reef Limestones, Labrador, Canada: Jour. Sed. Petrology, v. 53, p. 1051-1096.

_____, Ginsburg, R.N., Marszalek, D.S. and Choquette, P.W., 1976, Facies and fabric specificity of early subsea cementation in shallow Belize (British Honduras) reefs: Jour. Sed. Petrology, v. 46, p. 523-544.

Kauffman, E.G., 1973, Cretaceous Bivalvia: in Hallam, A. (ed.): Atlas of Cretaceous Paleogeography: Elsevier Publ., p. 353-383.

_____, 1974, Cretaceous assemblages, communities, and associations: Western interior United States and Caribbean Islands: in Ziegler, A.M., Walker, K.R., Anderson, E.J., Kauffman, E.G., Ginsburg, R.N. and James, N.P. (eds.): Principles of benthic community analysis: Short course, Univ. of Miami, p. 12.1-12.27.

_____ and Sohl, N.F., 1974, Structure and evolution of Antillean Cretaceous rudist frameworks: Verhandl. Naturf. Ges. Basel., v. 84, p. 399-467.

_____, 1976, Middle Cretaceous events in the Caribbean province: Annales Du Muséum d'Histoire Naturelle de Nice, Tome IV, p.

XXIX.1-XXIX.5.

Keith, M.L., Anderson, G.M. and Eichler, R., 1964, Carbon and oxygen isotopic composition of mollusk shells from marine and fresh-water environments: Geochim. Cosmochim. Acta, v. 28, p. 1757-1786.

_____ and Weber, J.N., 1965, Systematic relationships between carbon and oxygen isotopes in carbonates deposited by modern corals and algae: Science, v. 150, p. 498-501.

Kendall, A.C., 1975, Post-compactional calcitization of molluscan aragonite in a Jurassic Limestone from Saskatchewan, Canada: Jour. Sed. Petrology, v. 45, p. 399-404.

Kennedy, W.J. and Hall, A., 1967, The influence of organic matter on the preservation of aragonite in fossils: Proc. Geol. Soc., London, v. 1643, p. 253-255.

_____ and Taylor, J.D., 1968, Aragonite in rudists: Proc. Geol. Soc., London, v. 645, p. 323-331.

_____ and Hall, A., 1969, Environmental and biological controls on bivalve shell mineralogy: Biol. Rev. Cambridge Phil. Soc., v. 44, p. 499-530.

Kerr, R.S., 1977, Facies, diagenesis, and porosity development in a Lower Cretaceous bank complex, Edwards Limestone, north-central Texas: in Bebout, D.G. and Loucks, R.G. (eds.): Cretaceous carbonates of

Texas and Mexico: application to subsurface exploration: Bur. of Eco. Geol., The University of Texas, p. 216-233.

Khudoley, K.H. and Meyerhoff, A.D., 1971, Paleogeography and geological history of Greater Antilles: Geol. Soc. Am. Mem., no. 129, 199 p.

Kinsman, D.J.J., 1969, Interpretation of Sr^{2+} concentrations in carbonate minerals and rocks: Jour. Sed. Petrology, v. 39, p. 486-508.

Knauth, L.P. and Epstein, S., 1976, Hydrogen and oxygen isotope ratios in nodular and bedded cherts: Geochim. Cosmochim. Acta, v. 40, p. 1095-1108.

Kobluk, D.R. and Risk, M.J., 1977, Micritization and carbonate-grain binding by endolithic algae: AAPG Bull., v. 61, p. 1069-1082.

Land, L.S. and Goreau, T.F., 1970, Submarine lithification of Jamaican reefs: Jour. Sed. Petrology, v. 40, p. 457-462.

_____ and Hoops, G.K., 1973, Sodium in carbonate sediments and rocks: a possible index to the salinity of diagenetic solution: Jour. Sed. Petrology, v. 43, p. 614-617.

Lindholm, R.C. and Finkelman, R.B., 1972, Calcite staining: semiquantitative determination of ferrous iron: Jour. Sed. Petrology, v. 4, p. 239-242.

Lohmann, K.C., 1983, Unravelling the diagenetic history of

carbonate reservoirs: integration of petrographic and geochemical techniques: AAPG short course, Section V, p. 1-41.

Longman, M.W., 1980, Carbonate diagenetic textures from near-surface diagenetic environments: AAPG Bull., v. 64, p. 461-487.

_____, 1981, A process approach to recognizing facies of reef complexes: SEPM, Spec. Publ., no. 30, p. 9-40.

_____ and Mench, P.A., 1978, Diagenesis of Cretaceous limestones in the Edwards aquifer system of south-central Texas: a scanning electron microscope study: Sedim. Geol., v. 21, p. 241-276.

Lorens, R.B., 1981, Sr, Cd, Mn and Co distribution coefficients in calcite as a function of calcite precipitation role: Geochim. Cosmochim. Acta, v. 45, p. 553-561.

_____ and Bender, M.L., 1977, Physiological exclusion of magnesium from Mytilus edulis calcite: Nature, v. 269, p. 793-794.

Lowenstam, H.A., 1954b, Factors affecting the aragonite: calcite ratios in carbonate-secreting marine organism: Jour. Geol., v. 62, p. 284-322.

_____, 1961, Mineralogy, $^{18}O/^{16}O$ ratios, and strontium and magnesium contents of recent and fossil brachiopods and their bearing on history of

the oceans: Jour. Geol., v. 69, p. 241-260.

_____, 1963, Biologic problems relating to the composition and diagenesis of sediments: in Donnelly, T.W. (ed.): The earth sciences - problems and progress in current research: Univ. Chicago Press, Chicago, Ill., p. 137-195.

_____, 1964, Coexisting calcites and aragonites from skeletal carbonates of marine organisms and their strontium and magnesium contents: in Miyake, Y. and Koyama, T. (eds.): Recent researches in the fields of hydrosphere, atmosphere and nuclear geochemistry: Maruzen, Tokyo, p. 373-404.

_____ and Epstein, S., 1954, Paleotemperatures of the post-Aptian Cretaceous as determined by the oxygen isotope method: Jour. Geol., v. 62, p. 207-248.

_____, 1959, Cretaceous paleo-temperatures as determined by the oxygen isotope method, their relations to and the nature of rudist reef: Rep. Int. Geol. Congr., 20th, Mexico 1956: El Sistemo Cretacico, 1, p. 65-76.

Lozo, F.E. and Smith, I., 1964, Revision of Comanche Cretaceous stratigraphic nomenclature, southern Edwards Plateau, southwest Texas: Gulf Coast Assoc. Geol. Soc. Trans., v. 14, p. 285-306.

MacIntyre, I.G., 1977, Distribution of submarine cements in a

modern Caribbean fringing reef, Galeta Point, Panama: Jour. Sed. Petrology, v. 47, p. 503-516.

MacKenzie, F.T., Bischoff, W.D., Bishop, F.C., Loijens, M., Schoonmaker, J. and Wollast, R., 1983, Magnesian calcites: low-temperature occurrence, solubility and solid solution behaviour: in Reeder, R.J. (ed.): Carbonates: mineralogy and chemistry: Reviews in mineralogy, v. 11, p. 97-144.

Magaritz, M., 1983, Carbon and oxygen isotope composition of recent and ancient coated grains: in Peryt, T.M. (ed.): Coated grains, Springer-Verlag, Berlin Heidelberg, p. 27-37.

Majid, A.H., 1983, Lithofacies, chemical diagenesis and dolomitization of the Tertiary carbonates of the Kirkuk oil field, Iraq: Ph.D. Thesis, Univ. of Ottawa, 270 p.

Marshall, J.D., 1981, Zoned calcites in Jurassic ammonite chambers: trace elements, isotopes and neomorphic origin: Sedimentology, v. 28, p. 867-887.

_____ and Ashton, M., 1980, Isotope and trace element evidence for submarine lithification of hardgrounds in the Jurassic of eastern England: Sedimentology, v. 27, p. 271-289.

Marshall, J.F., 1983, Submarine cementation in a high-energy platform reef: One Tree reef, Southern Great

Barrier reef: Jour. Sed. Petrology, v. 53, p. 1133-1149.

Masse, J.P. and Philip J., 1981, Cretaceous coral-rudist buildups of France: SEPM Spec. Publ., no. 30, p. 399-426.

Mattson, P.H., 1967, Cretaceous and Lower Tertiary Stratigraphy in West-Central Puerto Rico: U.S. Geol. Surv. Bull., v. 1254-B, 35 p.

Maurin, A.F., Philip, J. and Brunel, P., 1981, Possible microbial accretions in Cenomanian mounds, S.E. France: in Monty, C. (ed.): Phanerozoic Stromatolites: Springer-Verlag, Berlin, p. 121-133.

McIntire, W.L., 1963, Trace element partition coefficients - a review of theory and application to geology: Geochim. Cosmochim. Acta, v. 27, p. 1209-1264.

Meyers, W.J. and Lohman, K.C., 1984, (in press), Isotope geochemistry of regionally extensive calcite cement zones and marine components in Mississippian Limestones, New Mexico: SEPM Spec. Publ.

Milliman, J.D., 1974, Marine carbonates: Springer-Verlag, Berlin, 375 p.

Moldovanyi, E.P. and Lohman, K.C., 1984, Isotopic and petrographic record of phreatic diagenesis within the Lower Cretaceous Sligo and Cupido Formation: Jour. Sed. Petrology, v. 54, p. 972-985.

Moore, C., 1979, Porosity in carbonate rock sequences: AAPG

Continuing Education course note series, no. 11, p. A1-124.

Morse, J.W., 1983, The kinetics of calcium carbonate dissolution and precipitation: in Reeder, K.J. (ed.): Carbonates: mineralogy and chemistry: Reviews in mineralogy, v. 11, p. 227-264.

Muller, G., 1971, "Gravitational" cements: an indicator for the vadose of the subaerial diagenetic environment: in Bricker, O.P. (ed.): Carbonate cements: Johns Hopkins Univ. Press, Baltimore, p. 301-302.

Nelson, H.F., 1973, The Edwards reef complex and associated sedimentation in central Texas: Bur. Econ. Geol., Univ. of Texas, Guidebook 15, 19 p.

Nie, N.H., Hull, C.H., Jenkins, J.G., Steinbrenner, K. and Bent, D.H., 1975, Statistical package for the social sciences: McGraw-Hill (2nd edition), New York, 675 p.

Pease M.H. Jr., 1968, Cretaceous and Lower Tertiary Stratigraphy of the Naranjito and Aguas Buenas quadrangles and adjacent areas, Puerto Rico: U.S. Geol. Surv. Bull., no. 1254, 57 p.

Perkins, B.F., 1961, Biostratigraphic studies in the Comanche (Cretaceous) series of Northern Mexico and Texas: G.S.A., Mem. no. 83.

_____, 1969, Cretaceous reefs of the Gulf of Mexico region (abs.): Jour. Paleon., v. 43, p. 894-895.

_____, 1970, Genetic implications of rudist reef architectures (abs.): AAPG Bull., v. 54, p. 863-864.

_____, 1971, Traces of rock-boring organisms in the Comanche Cretaceous of Texas: in Trace fossils: a field guide, School of Geoscience Misc. Publ., 71-1, Louisiana State Univ., p. 137-147.

Perry, E.C. Jr., 1967, The oxygen isotope chemistry of ancient cherts: Earth Planet, Sci. Letters, v. 3, p. 62-66.

Petta, T.J., 1977, Diagenesis and geochemistry of a Glen Rose patch reef complex, Bandera County, Texas: in Bebout, D.G. and Loucks, R.G. (eds.): Cretaceous carbonates of Texas and Mexico: Application to subsurface exploration: Bur. Econ. Geol., Univ. Texas at Austin, Texas, p. 138-167.

Philip, J., 1972, Paléoécologie des formation à rudistes du Crétacé supérieur: L'exemple du S.E. de la France: Palaeoecol., Palaeogeog., Palaeoclimat., v. 12, p. 205-222.

_____, 1974, Les formations calcaires à Rudistes du Crétacé supérieur provencal et rhodanien: stratigraphie et paléogéographie: Bull. Bur. Rech. Géol. Min., 2e sér., no. 3, p. 107-151.

_____, 1978, Stratigraphie et paléoécologie des formations à Rudistes du Cénomanien: l'exemple de la

Provence: Géol. Méditerranéenne, t. 5, no. 1, p. 155-168.

_____, 1980, Crétacé supérieur de Provence: Géobios, Mém. spécial, no. 4, p. 99-109.

_____, 1981, Les rudistes du Crétacé Moyen de la Province Méditerranéenne Occidentale: évolution, paléoécologie, paléobiogéographie: Cretaceous research, v. 2, p. 395-403.

Pilkey, O.H. and Harris, R.C., 1966, The effect of intertidal environment on the composition of calcareous skeletal material: Limnol Ocean, v. 11, p. 381-385.

Pingitore, N.E., 1976, Vadose and phreatic diagenesis: Processes, products and their recognition in corals: Jour. Sed. Petrology, v. 46, p. 985-1006.

_____, 1978, The behaviour of Zn^{+2} and Mn^{+2} during carbonate diagenesis: Theory and applications: Jour. Sed. Petrology, v. 48, p. 799-814.

_____, 1982, The role of diffusion during carbonate diagenesis: Jour. Sed. Petrology, v. 52, p. 27-39.

Polifka, J.R., Atwood, D.K., Pilkey, O.H. and Kier, J.S., 1972, Compositonal changes of Recent mollusc shells on the sea floor: Nature Physical Science, v. 240, p. 89-90.

Prezbindowski, D.R., 1977, Carbon and oxygen isotopic evolution of whole rock and cements from the Stuart City Trend (Lower Cretaceous, south-central Texas): in Bebout, D.G. and Loucks, R.G. (eds.): Cretaceous Carbonates of Texas and Mexico: application to subsurface exploration: Bur. Econ. Geol., The Univ. of Texas at Austin, Texas, p. 201.

Ragland, P.C., Pilkey, O.H. and Blackwelder, B.W., 1979, Diagenetic changes in the elemental composition of unrecrystallized mollusk shells: Chem. Geol., v. 25, p. 123-134.

Randazzo, A.F., Sarver, T.J. and Metrin, D.B., 1983, Selected geochemical factors influencing diagenesis of Eocece Carbonate rocks, Peninsular Florida, USA, Sed. Geol., v. 36, p. 1-14.

Rhoads, D.C. and Lutz, R.E. (eds.), 1980, Skeletal growth of aquatic organisms: biological records of environmental change: Plenum Press, 750 p.

Rose, P.R., 1970, Stratigraphic interpretation of submarine vs. subaerial discontinuity surfaces: an example from the Cretaceous of Texas: G.S.A. Bull., v. 81, p. 2787-2797.

_____, 1972, Edwards Group, surface and subsurface, Central Texas: Bur. Econ. Geol., The Univ. of Texas at Austin, Rept. Invest., no. 74.

Rubinson, M. and Clayton, R.N., 1969, Carbon-13 fractionation

between aragonite and calcite: Geochim. Cosmochim. Acta, v. 33, p. 997-1002.

Saltzman, E.S. and Barron, E.J., 1982, Deep circulation in the late Cretaceous: oxygen isotope paleotemperatures from Inoceramus remains in DSDP cores: Paleogeography, Paleoclimat., Paleoecol., v. 40, p. 167-181.

Sandberg, P.A. and Hudson, J.D., 1983, Aragonite relic preservation in Jurassic calcite-replaced bivalve: Sedimentology, v. 30, p. 879-892.

_____, Schneidermann, N., and Wunder, S.J., 1973, Aragonite ultrastructural relics in calcite-replaced Pleistocene skeletons: Nature, Phys. Sci., v. 245, p. 133-134.

Scherer, M., 1977, Preservation, alteration and multiple cementation of aragonitic skeletons from the Cassian Beds (U. Triassic, Southern Alps): petrographic and geochemical evidence: N. Jb. Geol. Palaont., Abh., v. 154, p. 213-262.

Shackleton, N.J. and Kennett, J.P., 1975, Paleotemperature history of the Cenozoic and the initiation of Antarctic glaciation: oxygen and carbon isotope analyses in DSDP Sites 277, 279 and 281: in Kennett, J.P., Houtz, R.E., et al. (eds.): Initial Reports of the Deep Sea Drilling Project, v. 29, p. 743-755.

Shinn, E.A., 1969, Submarine lithification of Holocene carbonate sediments in the Persian Gulf: Sedimentology, v. 12, p. 109-144.

_____, 1971, Aspects of diagenesis of algal cup reefs in Bermuda: G.C.A.G.S. Trans., v. 21, p. 387-394.

Skelton, P.W., 1974, Aragonitic shell structure in the rudist Biradiolites, and some paleobiological inferences: Provence Univ. Annu., Geol. Mediterr. 1:2, p. 63-74.

_____, 1976, Functional morphology of the Hippuritidae: Lethaia, v. 9, p. 83-100.

_____, 1979, Preserved ligament in a radiolitid rudist bivalve and its implication of mantle marginal feeding in the group: Paleobiology, v. 5, p. 90-106.

Sohl, N.F., 1960a, Archeogastropoda, Mesogastropoda and stratigraphy of the Ripley Owl Creek and Prairie Bluff Formations: U.S. Geol. Surv. Prof. Paper, no. 331-A, 141 p.

_____, 1960b, Neogastropoda, Opisthobranchia and Basommatophora from the Ripley Owl Creek and Prairie Bluff Formations: U.S. Geol. Surv. Prof. Paper, no. 331-B, 335 p.

_____, 1976, Notes on Middle Cretaceous macrofossils from the Greater Antilles: Annales Du Muséum D'Histoire Naturelle De Nice, Tome IV,

p. XXXI.1-XXXI-6.

Tan, F.C. and Hudson, J.D., 1974, Isotopic studies of the paleoecology and diagenesis of the Great Estuarine Series (Jurassic) of Scotland: Scott. Jour. Geol., v. 10, p. 91-128.

Tarutani, T., Clayton, R.N. and Mayeda, T.K., 1969, The effect of polymorphism and magnesium substitution on oxygen isotope formation between calcium carbonate and water: Geochim. Cosmochim. Acta, v. 33, p. 987-997.

Thompson, G., Bankston, D.C. and Pasley, S.M., 1970, Trace element data for reference carbonate rocks: Chem. Geol., v. 6, p. 165-170.

Turner, J.V., 1982, Kinetic fractionation of C-13 during calcium carbonate precipitation: Geochim. Cosmochim. Acta, v. 46, p. 1183-1192.

Veizer, J., 1974, Chemical diagenesis of Belemnite shells and possible consequences for paleotemperature determination: N. Jb. Geol. Paläont. Abh., v. 147, p. 91-111.

_____, 1977, Diagenesis of Pre-Quaternary carbonates as indicated by tracer studies: Jour. Sed. Petrology, v. 47, p. 565-581.

_____, 1978a, Simulation of limestone diagenesis - a model based on strontium depletion: Discussion: Can. Jour. Earth Sci., v. 15, p. 1683-1685.

_____, 1978b, Strontium, abundance in common sediments and sedimentary rock types: in Wedepohl, K.H. (ed.), Handbook of geochemistry 11-5, Springer, Heidelberg, K1-13.

_____, 1983a, Chemical diagenesis of carbonates: Theory and application of trace element techniques: AAPG Continuing Education course note series, no. 10, p. 3.1-3.100.

_____, 1983b, Trace elements and isotopes in sedimentary carbonates: Min. Soc. Am.: Reviews in Mineralogy, v. 11, p. 265-299.

_____ and Fritz, P., 1976, Possible control of post-depositional alteration in oxygen paleotemperature determinations: Earth Planet. Sci. Letters, v. 33, p. 255-260.

_____ and Hoefs, J., 1976, The nature of $^{18}O/^{16}O$ and $^{13}C/^{12}C$ secular trends in sedimentary carbonate rocks: Geochim. Cosmochim. Acta, v. 40, p. 1387-1395.

_____, Holser, W.G. and Wilgus, C.K., 1980, Correlation of $^{13}C/^{12}C$ and $^{34}S/^{32}S$ secular variations: Geochim. Cosmochim. Acta, v. 44, p. 579-587.

_____, Lemieux, J., Jones, B., Gibling, M.R. and Savelle, J., 1978, Paleosalinity and dolomitization of a Lower Paleozoic carbonate sequence, Somerset

and Prince of Wales Islands, Arctic Canada: Can. Jour. Earth Sci., v. 15, p. 1448-1461.

Vogal, K., 1978, Function of pallial canals of Caprinidae: Neues. Jahrb. Geol. Paläontol., Abh., v. 157, p. 159-163.

Wagner, P.D. and Matthews, R.K., 1982, Porosity preservation in the Upper Smackover (Jurassic) carbonate grainstone, Walker Creek Field, Arkansas: response of paleophreatic lens to burial processes: Jour. Sed. Petrology, v. 52, p. 3-18.

Walls, R.A., Mountjoy, E.W. and Fritz, P., 1979, Isotopic composition and diagenetic history of carbonate cement in Devonian Golden Spike reef, Alberta, Canada: GSA Bull., v. 90, p. 963-982.

_____, Ragland, P.C. and Crisp, E.L., 1977, Experimental and natural early diagenetic mobility of Sr and Mg in biogenic carbonates: Geochim. Cosmochim. Acta, v. 12, p. 1731-1737.

Wanless, H.R., 1983, Burial diagenesis in limestones; in Parker A. and Sellwood B.W. (eds); Sediment diagenesis, NATO ASI series, D. Reidel Publ. Co., p. 379-417.

Wardlow, N., Oldershaw, A. and Stout, M., 1978, Transformation of aragonite to calcite in a marine gastropod: Can. Jour. Earth Sci., v. 15, p. 1861-1866.

Warme, J.E., 1975, Borings as trace fossils, and the

processes of marine bioerosion: in Frey, R.W. (ed.): The study of trace fossils, Springer-Verlag, p. 181-227.

Weaver, J.D. and Mitchell, R.C. 1959, Puerto Rico: Lexique Stratigraphique International, Amérique Latine, Fascicule 11a, p. 315-350.

Weber, J.N. and Raup, D.M., 1966, Fractionation of the stable isotopes of carbon and oxygen in marine calcareous organisms - the Echinoidea. Part I. variation of ^{13}C and ^{18}O content within individuals: Geochim. Cosmochim. Acta, v. 30, p. 681-703.

_____, 1968, Comparison of $^{13}C/^{12}C$ and $^{18}O/^{16}O$ in the skeletal calcite of recent and fossil echinoids: Jour. Paleont., v. 42, p. 37-50.

_____ and Woodhead, P.M.J., 1970, Carbon and oxygen isotope fractionation in the skeletal carbonate of reef-building corals: Chem. Geol., v. 6, p. 93-117.

Weiner, S. and Lowenstam, H.A., 1980, Well-preserved mollusk shells: Characterization of mild diagenetic processes: in Hare, P.E. (ed.): Biogeochemistry of amino acids, John Wiley Inc., p. 95-114.

Weyl, P.K., 1964, The solution alteration of carbonate sediments and skeletons: in Imbrie, J. and Newell, N. (eds.): Approaches to paleoecology,

Wiley, New York, p. 345-356.

White, A.F. 1977, Sodium and potassium co-precipitation in aragonite: Geochim. Cosmochim. Acta, v. 41, p. 613-625.

Wilkinson,B.H., 1983, Carbonate petrography: AAPG short course, part III, p. 1-35.

Wilson, J.L., 1975, Carbonate facies in geologic history: Springer-Verlag, New York, 471 p.

Winland, H.D., 1969, Stability of calcium carbonate polymorphs in warm, shallow seawater: Jour. Sed. Petrology, v. 39, p. 1579-1587.

Zeman, J., 1969, Crystal Chemistry: in Wedepohl, K.H. (ed.): Handbook of geochemistry, Springer-Verlag, Berlin, v.1, p. 12-36.

Zolotarev, V.N., 1976, Early diagenetic alterations in the chemical composition of marine mollusk shells: Lithol. Miner. Resource, v. 3, p. 287-295.

APPENDICES

APPENDIX I

GEOGRAPHIC LOCATIONS, GENERA, AGES AND FORMATIONS OF THE STUDIED SAMPLES.

Note: Not all samples listed below were studied for geochemical and isotopic purposes.

Sample No.	Genus and Localities	Age and /or Formation
FRENCH LOCALITIES: (Mixture of hippuritids, radiolitids and requieniids)		
1, 2, 3, 4, 5, 6, 7, 8, 9, 10, 11, 12, 13, 14, 15, 16, 17, 18, 19, 20, 21, 22, 23, 24, 25, 26, 27, 28, 29, 91, 92, 93, 94, 95, 210, 211, 212, 213, 214, 215, 216, 217, 221	NW City of Marseille - Chainon de la Fare, near St. Chamas	Santonian
30, 31, 32, 33, 34, 35, 36, 37, 38, 39, 40, 41, 42, 43, 44, 45, 46, 47, 48, 49, 50, 51, 52	3 km. east of City of Martiques	Santonian

Sample No.	Genus and Localities	Age and /or Formation
58	Gattigues, Gard France	
59	Cossis	U. Turonian
60	La Cadieré	Santonian
61, 62	St. Baumes Mountaines	Coniacian
53, 54, 66, 67, 68, 69, 70, 71, 72, 73, 74, 75, 76, 77, 78, 79, 80, 81	West of City of Marseille - Massif de la Sainte Baume	Coniacian
55, 56, 223, 224	West of City of Marseille	Exact age unknown
63, 64, 65, 218, 219	2 km. East of City of Martique	Cenomanian
82, 83, 84, 85, 86, 87, 88, 89, 220	3 km. South of City of Martique	Barremian (Urgonian Facies)
57, 90	12 km. West of City of Marseille, near town of Mejean (Bassin d'Ensués la Redonne	Turonian
JAMAICA:		
107	Chiapasella; Central inlier, Middlesex County, Claredon Parish	U. Cretaceous
108	Thyrastylou; Central inlier, Middlesex County, Clarendon Parish	U. Cretaceous

Sample No.	Genus and Localities	Age and /or Formation
109	Antillocaprina; Central inlier, Middlesex County, Clarendon Parish	U. Cretaceous
111	Chiapasella; Central inlier, Middlesex County, Clarendon Parish	U. Cretaceous
113	Thyrastylon; Central inlier, Clarendon Parish	U. Cretaceous, Guinea Corn Formation
114	Sauvagesia; Central inlier, Middlesex County, Clarendon Parish	U. Cretaceous
119	Barrettia; Central inlier, Middlesex County, Clarendon Parish	U. Cretaceous
123	Antillocaprina; Central inlier, Trout Hill, Middlesex County	U. Cretaceous
126	Chiapasella; Central inlier, Middlesex County	U. Cretaceous
131	Bournonia; Central inlier Middlesex County	U. Cretaceous
139	Chiapasella; Central inlier, Rio Minho section	U. Cretaceous, Guinea Corn Formation
143	Antillocaprina; Central inlier	U. Cretaceous Guinea Corn Formation
144	Chiapasella; Central inlier, Rio Minho section	U. Cretaceous Guinea Corn Formation
148	Bournonia; Central inlier Rio Minho section	U. Cretaceous, Guinea Corn Formation
149	Enclosing rock of 148	
152	Biradiolites; Central inlier Rio Minho section, Claredon Parish	U. Cretaceous Guinea Corn Formation
202	Antillocaprina; Central inlier Clarendon Parish	U. Cretaceous
110	Titanosarcolite, Locality unknown	
168	Barrettia, Locality unknown	

Sample No.	Genus and Localities	Age and /or Formation
200	Barrettia, Locality unknown	
120	Prabarrettia; Benbow inlier	L. Cretaceous, Seafield Lst.
112	_____; Maldon inlier	U. Cretaceous Maldon Lst.
115	Antillocaprina; Maldon inlier, St. James Parish	U. Cretaceous, Vaughansfield Fm.
130	Titanosarcolites; Maldon inlier	U. Cretaceous
141	Titanosarcolites; Maldon inlier, Westmoreland Parish	U. Cretaceous
145	Titanosarcolites; Maldon inlier	U. Cretaceous
154	Thyrastylon; Maldon inlier, St. James Parish	U. Cretaceous
203	Antillocaprina; Maldon inlier, St. James Parish	U. Cretaceous, Vaughansfield Fm.
209	_____; Maldon inlier	U. Cretaceous
116	Antillocaprina; Marchmont inlier, Westmoreland Parish	U. Cretaceous
117	Enclosing rock of 116	
118	Parastoma; Marchmont inlier, Westmoreland Parish	U. Cretaceous
121	Bournonia; Marchmont inlier, Westmoreland Parish	U. Cretaceous
122	Antillocaprina; Marchmont inlier, Westmoreland Parish	U. Cretaceous
133	Antillocaprina; Marchmont inlier Westmoreland Parish	U. Cretaceous
134	Enclosing rock of 133	
135	Biradiolites; Marchmont inlier Westmoreland Parish	
136	Enclosing rock of 135	

Sample No.	Genus and Localities	Age and /or Formation
137	Antillocaprina; Marchmont inlier	U. Cretaceous
138	Enclosing rock of 137	
146	Antillocaprina; Marchmont inlier	U. Cretaceous
147	Antillocaprina; Marchmont inlier	U. Cretaceous
150	Titanosarcolites; Marchmont inlier	U. Cretaceous
151	Thyrastylon; Marchmont inlier	U. Cretaceous
155	Thyrastylon; Marchmont inlier	U. Cretaceous
125	Thyrastylon; Marchmont inlier	U. Cretaceous
129	Antillocaprina; Marchmont inlier	U. Cretaceous
142	Sauvagesia; Marchmont inlier	U. Cretaceous
153	Plagioptychus; Marchmont inlier	U. Cretaceous
204	Antillocaprina; Marchmont inlier	U. Cretaceous
127	Monopleura; Sunderland inlier	U. Cretaceous
128	Antillocaprina; Sunderland inlier	U. Cretaceous
132	Antillocaprina; Green Island inlier	
140	Antillosarcolites; Green Island inlier	U. Cretaceous
	PUERTO RICO:	
175	Titanosarcolites; Municipio de Cabo Rojo, Grid 74, 750 x 18525	U. Cretaceous
179	Mitrocaprina; Municipio de Cabo Rojo	U. Cretaceous
190	Durania; Municipio de Cabo Rojo	U. Cretaceous
192	Durania; Municipio de Cabo Rojo	U. Cretaceous
182	Plagioptychus; Municipio de Cioles	U. Cretaceous
183	Enclosing rock of 182	

Sample No.	Genus and Localities	Age and /or Formation
176	Antillocaprina; San German	U. Cretaceous, San German Fm.
181	Mitrocaprina; Municipio de Salinas	U. Cretaceous
177	Antillocaprina; Municipio de Barranquites	U. Cretaceous, Botijas Lst.
178	Enclosing rock of 177	
191	Durania; Municipio de Barranquito	U. Cretaceous
188	Radiolites, Locality unknown	
189	Radiolities, Locality unknown	
186	Monopleura; Municipio de Pennelas	U. Cretaceous
187	Enclosing rock of 186	
180	Caprinidae; Municipio de Coamo	U. Cretaceous
184	Caprinidae-Toucasia; Municipio de Cayey	U. Cretaceous, Rio Maton Lst.
185	Enclosing rock of 184.	

CUBA:

98	Parastroma; Havana Province	
103	Antillocaprina; Havana Province	
104	Antillocaprina; Havana Province	
162	Sauvagesia; Havana Province 1.5 km. West of of San Antonio	

Sample No.	Genus and Localities	Age and /or Formation
99	Biradiolites; Santa Clara Province	M. Cretaceous
105	Plagioptychus; Santa Clara Province	M. Cretaceous
106	Praebarrettia; Santa Clara Province	M. Cretaceous
159	Barrettia; Santa Clara Province	M. Cretaceous
160	Bournonia; Santa Clara Province	M. Cretaceous
161	Parastroma; Santa Clara Province	M. Cretaceous
163	Titanosarcolite; Santa Clara Province	M. Cretaceous
165	Barrettia, Santa Clara Province	M. Cretaceous
201	Plagioptychus; Santa Clara Province	M. Cretaceous
205	Bournonia; Santa Clara Province	M. Cretaceous
207	Chiapasella; Santa Clara Province	M. Cretaceous
208	Barrettia; Santa Rosa Province	Cretaceous
166	Pseudovaccinites; Locality unknown	Cretaceous
206	Sauvagesia; Locality unknown	Cretaceous
100	Durina; Matazas Province	U. Cretaceous
156	Praebarrettia; Matazas Province	U. Cretaceous
157	Antillocaprina; Matazas Province	U. Cretaceous
158	Antillocaprina; Matazas Province	U. Cretaceous
101	Titanosarcolite; Camaguey Province	Cretaceous
102	Enclosing rock of 101	
164	Chiapasella; Pinar del Rio Province	U. Cretaceous

Sample No.	Genus and Localities	Age and /or Formation
	TEXAS AND GULF COAST AREAS:	
193, 194, 195	Caprinids; Lake Whitney Dam, Texas	L. Cretaceous, Edwards Fm.
195, 196	Enclosing rocks	
197, 198, 199	Caprinids; Lake Whiteny Dam, Texas	L. Cretaceous Edwards Fm.
169, 170, 171, 173, 174, 175	Radiolitids; Gulf Coast area	U. Cretaceous, Prairie Bluff Fm.
97, 172	Caprinids; Gulf Coast area	U. Cretaceous, Prairie Bluff Fm.
96	Antillocaprina; Bluff along Coon Creek, Tennessee	U. Cretaceous, Ripley Fm.
167	Plagioptychus; Coon Creek, Tennessee	U. Cretaceous, Ripley Fm.

APPENDIX II

SUMMARY OF PETROGRAPHY OF THE STUDIED SAMPLES

Summary of sample description and brief petrography of the separated skeletal and nonskeletal components of rudist shells.

Sample:

Family Hippuritidae - French Localitites

1a: outer shell layer, thin, fine compact, prismatic ultrastructure; rarely bored by sponges and algae.
1b: internal body cavity infilled by micritic internal sediments.
7a: outer shell layers: relatively thick, fine compact, prismatic ultrastructure, partly bored by algae.
7b: pillar, composed of fine compact prismatic ultrastructure.
7c: inner shell layer, thin cemented by equant spar.
7d: mantle cavity infilled by large equant ferroan spar.
8a: outer shell layer, compact fine prismatic, bored and the bores infilled by micritic-silty internal sediments.
8b: pillar, fine prismatic ultrastructure.
8c: space fill cement, late ferroan large equant spar.
8d: pelletal micritic internal sediments infilling body cavity, with some carbonate clasts and shell fragments.
10a: outer fine compact prismatic layer, abundantly bored (removed during separation for chemical analysis) by clionid sponges infilled by micritic material.
10b: pillar, similar ultrastructure as outer layer.
10c: inner shell cavity, infilled by micritic pelletal sediments, rudist shell fragments, partly cemented.
13a: outer thin layer of simple prismatic ultrastructure, partly recrystallized.
13b: silty-micritic internal sediments infilling the body cavity, with some shell fragments.
13c: part of the outer layer, recrystallized and/or cemented.
14a: outer layer, compact fine prismatic ultrastructure, bored.
14b: inner layer, occupied by nonferroan fine equant spar.

Sample:

14c: body cavity infilled by late ferroan, clear large equant spar.
14d: part of the outer layer almost completely replaced by micritic sediments.
14e: well preserved pillar.
15a: outer shell layer, fine compact prismatic, well preserved, partly bored.
15b: thin inner layers, preserved by micrite envelopes, cemented by equant spar.
20a: outer preserved prismatic layer.
20b: inner cavity infilled by micritic material with rudist fragments.
23a: outer layer, fine prismatic ultrastructure, bored heavily by sponges.
23b: pillar, has the same ultrastructure as the outer layer.
23c: thin inner layer replaced by small equant spar, no relic ultrastructure.
27a: outer thick prismatic layer, bored and occupied by micritic sediments.
27c: inner layer replaced by fine equant spar.
27d: mantle cavity, infilled by micritic, pelletal internal sediments with some fragments of broken rudist shell fragments.
43a: well preserved prismatic layer.
43b: inner layer with clear relics of crossed-lamellar ultrastructure, XRD analysis showed traces of aragonite still exist.
43c: cloudy crystallites, could represent an early generation of cement.
48a: outer shell layer, simple fine prismatic compact ultrastructure, rarely bored.
56a: outer shell layer, simple fine prismatic compact ultrastructure, rarely bored.
56b: pillar, prismatic ultrastructure, partly bored.
56c: inner shell layer leached and infilled by equant-bladed crystals with no visible relic ultrastructure.
56d: body cavity infilled by late equant ferroan spar.
58a: thick outer layer, fine prismatic compact ultrastructure, invariably bored and the bores infilled by micritic internal sediments.
58b: middle thin shell layer (750 μ) retains faint relics of original crossed-lamellar ultrastructure.
58c: pillar, composed of simple fine prisms.
58d: mantle body cavity occupied by ferroan equant spar.
59a: outer layer, fine compacted prismatic ultrastructure, heavily bored by various borers and they are infilled by micritic pelletal sediments.

Sample:

59b: pillar, prismatic ultrastructure.
59c: inner shell layer protected by micritic envelopes, but infilled by ferroan equant calcite.
59d: accessory body cavity infilled by micritic internal sediments.
59e: ferroan equant calcite enclosed inside micrite envelopes.
61a: outer prismatic layer.
61b: inner shell layer presently cemented with no relic ultrastructure.
61c: body cavity infilled by large ferroan equant calcite.
61d: pillar of prismatic ultrastructure.
61e: another pillar.
62a: outer layer, well preserved compact fine prismatic ultrastructure, partly bored by sponges and algae and the bores infilled by micritic sediments.
62b: inner part of the outer shell layer.
62c: pillar with similar ultrastructure as the outer layer.
62d: another pillar.
62e: inner shell layer composed of nonferroan pseudospars.
62f: major body cavity infilled by two generations of ferroan spar.
90a: outer prismatic shell layer, partly bored.
90b: pillar.
90c: inner shell layer with neomorphosed calcite.
91a: cellular-prismatic outer layer.
91b: inner part of the outer layer.
91c: pillar.
91d: traces of inner shell layer replaced by equant calcite.
91e: mantle body cavity occupied by large equant ferroan cement.
92a: fossil completely replaced by enclosing rocks (wackestone) with rudist fragments (this sample was not included in the statistical evaluations).
95a: outer shell layer, fine compact prismatic ultrastructure, partly bored by sponges and the bores infilled by micritic pelletal internal sediments.
95b: middle shell layer, retains no visible relic ultrastructure, bounded by micritic envelopes, now composed of ferroan equant calcite.
95c: inner body cavity infilled by micritic pelletal sediments with some fossil debris.
223a: outer shell layer, well preserved prismatic ultrastructure.

Sample:

223b: pillar of same ultrastructure as the outer layer.
223c: middle and inner shell layers with no relic ultrastructure.
223d: central body cavity occupied by fibrous inclusion-rich nonferroan cement.
224a: outer shell prismatic layer.
224b: pillar.
224c: middle and inner shell layer replaced by equant calcite.
224d: early fibrous, inclusion-rich, nonferroan cement.

Family Radiolitidae - French Localities

18a: outer shell layer, well developed cellular-prismatic ultrastructure. The cells infilled by large equant cement. Well developed growth lines.
18b: inner body cavity infilled by micritic sediments with rudist shell fragments.
30a: outer thick cellular-prismatic layer, cells oval or polygonal in cross section, partly bored by algae.
30b: part of the inner most outer layer, bored.
30c: inner big body cavity infilled by silty micritic pelletal sediments, rudist fragments and miliolid foraminifera.
33a: outer thick cellular-prismatic layer.
33b: middle layer, cement replacing original aragonite, no visible relic ultrastructure.
33c: body cavity; micritic with many small fossil fragments.
35a: outer thick cellular layer, well developed growth lines, rarely bored.
35b: small lenticular body, could be a tooth, contains nonferroan pseudospar with brown relics.
35c: mantle cavity infilled by late ferroan equant spar.
35d: secondary cavity infilled by micritic internal sediments.
37a: outer thick cellular layer, cell walls are preserved, cell interiors are infilled partly by internal sediments and cements.
37b: inner body cavity, pelletal, micritic, rich in fossil debris such as rudist fragments, miliolids...
38a: outer thick cellular layer, polygonal cells infilled by nonferroan fine equant cement and internal micritic sediments.
38b: internal cavity infilled by silty-micritic sediments with rudist and foraminifera fragments.

Sample:

39a: part of the outer thick cellular-prismatic layer.
41a: outer layer with cellular-prismatic ultrastructure, cells rectangular in cross-section, partly compressed.
41b: middle layer, very thin, retains some vestige of its original crossed-lamellar ultrastructure.
41c: large equant spar infilling part of the body cavity.
41d: another part of the outer layer.
42a: outer shell layer.
42b: inner layer, infilled by equant ferroan spar cement.
42c: body cavity infilled by marine internal sediments.
47a: well developed cellular-prismatic outer layer with well-defined growth lines.
47b: thin middle layer, micritic enveloped, faint relics of pseudospar.
47c: inner cavity infilled by micritic pelletal sediments with some broken rudist fragments.
60a: outer cellular-prismatic layer with well preserved growth lines, cells infilled by fine equant calcite.
60b: large ferroan equant spar occupying body cavity.
63a: outer cellular layer, thick cell walls, two generations of cement occupying cell chambers (isopachous and equant).
63b: internal cavity, micritic with large rudist fragments, few quartz grains and some spar.
64a: thick cellular-prismatic layer.
64b: inner cavity infilled by marine micritic, pelletal internal sediments, with some sparry calcite pockets.
65a: outer thick cellular layer, cells polygonal with well preserved cell wall. Cell interior occupied by two-stage of cementation (early rim (<5 μ), and late ferroan equant).
65b: internal cavity infilled by micritic internal sediments, rich in rudist fragments and other fossils.
66a: outer thick cellular-prismatic layer, partly compacted, cells occupied by fine equant calcite.
66c: body cavity infilled by micritic sediments with small fragments of rudists.
70a: outer thick cellular-prismatic layer, cell walls well developed, cell chambers infilled by ferroan equant spar.
70b: internal body cavity infilled by micritic internal sediments with some large rudist fragments.
71a: outer thick cellular-prismatic layer. Some cells are infilled by internal sediments, where the others are by equant cement.

Sample:

71b: internal cavity occupied by two or more generations of cement, some patches of micrite also exist.
76a: outer thick layer, partly bored.
76b: internal body cavity infilled by pelletal, micritic sediments with miliolid foraminifera and some cement.
77a: outer thick cellular-prismatic layer. In some cells silty-micritic sediments present, partly cemented.
77b: large ferroan equant spar infilling internal parts.
78a: outer cellular layer.
78b: inner cavity, micritic with some cement.
218a: outer cellular-prismatic layer.
218b: inner part mostly occupied by silty-micritic sediments with rudist fragments.

Family Requieniidae - French Localities

82a: outer thin layer (~ 1mm.) made up of nonferroan simple prisms, partially recrystallized.
82b: internal cavity infilled by pelletal, micritic, partly cemented sediments, with fossil fragments; some of them have moldic porosity.
84a: outer thin prismatic layer.
84b: internal cavity, micritic chalky sediments.
85a: outer thin prismatic layer, partly recrystallized.
85b: internal cavity infilled by micritic sediments.
86a: outer thin layer, composed of simple recrystallized prisms.
86b: internal body cavity infilled by micritic, pelletal sediments with some fossil fragments, such as bryozoans and coral.
87a: outer thin layer, recrystallized or cemented.
87b: inner micritic chalky material, similar in composition to its enclosing rock.
89a: outer thin prismatic layer, recrystallized.
89b: internal cavity occupied by micritic sediments with some foraminiferal and rudist shell fragments.

Family Caprinidae - American Localities

96a: aragonitic canals, soft composed of 100% aragonite.
97a: outer thick canal layer, partly preserved (19% A, 81% LMC). Canal walls have lamellar ultrastructure. Canals infilled partly by ferroan spar and/or micritic sediments.
97b: middle layer, with relic lamellar ultrastructure (99% LMC).

Sample:

97c: ferroan bladed cement infilling a cavity.
97d: inner layer, similar in texture to 97b, with 99% LMC.
101a: canal layer; canals polygonal in shape. They are infilled by fine equant spar increasing in size towards the center of the canal. Some canals are infilled by internal sediments.
101b: inner layer, with micritic envelope, no relic ultrastructure.
104a: aragonitic canals (90% A, ~95% LMC).
105a: outer layer of bifurcating canals; canal walls have pelletal internal sediments with some fossil fragments.
105b: inner layer, thin and has relic ultrastructure.
109a: outer plated canals infilled by marine internal sediments, canal walls are recrystallized to microspar.
109b: inclusion-rich equant ferroan spar.
109c: large equant highly ferroan spar cement.
110a: outer canal layer; canals infilled partly by micritic, pelletal internal sediment; no relic ultrastructure in canal walls.
110b: inner layer with no relic ultrastructure.
110c: internal cavity infilled by micritic, pelletal sediments.
115a: outer canal layer, canal wall preserved some relics of their original ultrastructure.
115b: inner layer with relic lamellar ultrastructure.
116a: part of the canal layer, canals polygonal in cross-section with some preserved ultrastructure. Two stages of cementation are noticed inside the canals, early isopachous and late equant.
116b: cavity fill, sand size sediments with some fossil fragments and calcareous cement.
122a: outer canal layer, some canals are infilled by micritic internal sediments. Canal walls have relic ultrastructure.
122b: lath-shaped component in the inner part of the shell made up of lamellar ultrastructure.
123a: outer canal layer, canals elliptical in shape and infilled by micritic sediments; canal walls are poorly preserved.
123b: pseudospar patches with some micrite.
123c: ferroan equant spar.
123d: inner cavity with micritic sediments; rudist fossil fragments also exist.
128a: outer thin compacted layer, homogeneous or fine prismatic ultrastructure, partly preserved.
128b: inner layer with brown relics.

Sample:

128c: inner cavity, pelletal micrite rich in fossil fragments, such as Nummulites sp., rudist fragments, green algae, miliolids, crinoidal stems.
130a: outer layer, canals infilled by internal peloidal sediment. Canal walls are partly preserved.
130b: equant calcites between the canals.
130c: internal body cavity, infilled by micritic pelletal sediments.
132a: poorly preserved canal layer. Some canals infilled by pelletal material partly recrystallized and/or cemented.
132b: large equant ferroan calcite in the body cavity.
133a: outer canal layer, polygonal or oval canals. Some canals are infilled by micritic internal sediments and cement.
133b: inner bigger canals.
133c: ferroan equant spar.
133d: inner body cavity infilled by micritic sediments, pelleted.
137a: outer layer, polygonal cells occupied by equant calcite.
137b: middle and inner layers, have preserved brown relic ultrastructures.
140a: outer canal layer; canals poorly developed, but some of them have preserved canal walls; partly bored by algae.
140b: inner body cavity, micritic and cemented.
141a: large and small canals in the outer layer infilled by micritic sediments. Canal walls have inclusions and are partly preserved.
141b: ferroan equant spar calcite.
141c: internal cavity, micritic with foraminifera and rudist fragments.
143a: poorly preserved canal layer. Canals infilled by internal sediments similar in composition to that in the body cavity.
143b: inner layer cemented with no visible relic ultrastructure.
143c: internal body cavity, micritic with some microfossils.
145a: outer canal layer with small rounded or oval canals; poorly preserved canal walls, partly cemented.
145b: inclusion-rich equant calcite.
145c: inclusion-rich fibrous spar.
145d: inner component with preserved relics of crossed-lamellar ultrastructure.

Sample:

146a:	outer canal layer, canal walls neomorphosed to pseudospar. Canals infilled by micritic internal sediments; partly recrystallized.
146b:	neomorphic spar beneath the canals.
146c:	inner body cavity, pelletal, micritic rich in rudist fragments and possibly corals.
147a:	outer canal layer with preserved relics of canal walls. Canals infilled by internal sediments and/or cements.
147b:	body cavity infilled by large ferroan equant spar calcite.
150a:	outer canal layer, canals are small and in most of the times infilled by peloidal internal sediments. Canal walls are preserved as relics.
150b:	inner body cavity micritic with fragments of rudists, echinoderms and foraminifera.
150c:	neomorphic spar between the canals.
153a:	outer thin, brown, well preserved calcitic (100% LMC) simple prismatic layer, partly recrystallized.
153b:	middle and inner layers, well preserved relic lamellar ultrastructure.
153c:	internal cavity infilled by brown peloidal internal sediments partly recrystallized.
157a:	outer canal layer, canal walls are invariably preserved.
157b:	inner layer, with relic ultrastructure.
157c:	internal cavity infilled by inclusion-rich equant nonferroan spar cement.
158a:	outer canal layer; canals infilled by internal sediment and/or equant calcite.
158b:	internal body cavity infilled by silty-micritic sediments with fossil fragments (e.g. rudists, Nummulites, Discocyclina sp).
163a:	outer canal layer; canals are partly occupied by micritic material and microspar.
163c:	internal cavity fill; made up of ferroan bladed spar calcite.
167a:	aragonitic soft canal layer (A ~ 98%).
172a:	outer canal layer, poorly preserved. Some canals infilled by micritic sediments.
172b:	inner layer, shows no relic ultrastructure.
172c:	cavity fill of silty-micritic sediments with intraclasts and rudist shell fragments
175a:	outer canal layer, poorly preserved and bored.
175b:	inner layer, cemented and shows no relic ultrastructure.
175c:	large equant ferroan spar cement.
176a:	ferroan bladed spar cement.

Sample:

176b: inner lath-shaped crystalline body, may represent, remnant of crossed-lamellar ultrastructure.
177a: poorly preserved outer canal layer, cemented.
177b: inner body cavity occupied by inclusion-rich equant calcite.
179a: outer canal layer. Canals partially infilled by internal sediment and/or cement.
179b: middle layer cemented by fine ferroan equant calcite.
179c: inner body cavity infilled by large ferroan equant spar cement.
180a: outer part, poorly preserved and cemented.
180b: middle layer has some relic ultrastructures.
180c: internal cavity infilled by late ferroan equant spar cement.
181a: highly altered canals. They are infilled by equant calcite. This part is partly bored.
181b: middle layer, now cemented by nonferroan fibrous calcite.
181c: internal cavity, micritic sediments with fragments of crinoids, rudists and some selective dolomite and silica.
184a: poorly preserved canal layer.
193a: outer canal layer. The canals are partly infilled by micritic internal sediments.
193b: inner layer, cemented and no relic ultrastructure preserved.
193c: inner cavity infilled by silty-micritic sediments with some fossil fragments.
194a: outer canal layers, canal walls remain as dusty micritic outlines. Some canals occupied by peloidal sediments (geopetal fabrics) and some by cement.
194b: large equant cement filling a cavity.
194c: silty-micritic sediments with some pellets and rudist fragments, filling another cavity.
195a: part of the outer canal layer.
195b: coarse ferroan equant spar calcite.
197a: outer canal layer; large and small size canals. Canal walls neomorphosed. Canals infilled partly by peloidal sediments and partly by ferroan equant cement.
197b: coarse equant ferroan calcites occupying a cavity.
199a: outer canal layers. Canals of bifurcating arrangement. Canal walls remain as micritic envelopes. Some of the canals are occupied partly by pelletal sediments, others by cement.
199b: inner cemented layer.

Sample:

199c: coarse equant spar cement increasing in size towards the center of the cavity.
201a: outer canal layer. Canals infilled by internal sediments and their intraclasts.
201b: internal cavity infilled by micritic-silty sediments with fossil fragments.
202a: outer canal layers; canal infilled by ferruginous sediments. Some of the canals are leached away and remain as empty pores.
202b: middle layer, cemented; no relic ultrastructures.
202c: internal cavity infilled by coarse ferroan equant spar.
203a: outer canal layer, preserved canal walls; partly bored.
203b: inner cavity infilled by micritic sediments with rudist and other fossil fragments.

Family Hippuritidae - American Localities

98a: part of the outer prismatic layer; recrystallization has affected these prisms.
106a: thick outer layer of prismatic ultrastructure. Partial cementation exists between planes of prisms.
106b: internal cavity occupied by ferroan equant spar cement.
106c: inner layer with preserved relics of crossed-lamellar ultrastructure.
118a: thick cellular-prismatic outer layer. Cells are occupied by ferroan equant calcite.
118b: internal body cavity infilled by marine internal sediments with rudist fragments, crinoids and bryozoans.
120a: poorly preserved outer layer, highly cemented and recrystallized.
120b: inner cavity fill of pelletal, micritic sediments.
156a: thick cellular-prismatic layer. Cells infilled by micrite and some cement.
156b: inner cavity infilled by coarse ferroan equant calcite.
156c: pillar.
159a: thick beaded prismatic, partly bored, outer layer. Equant cement may exist between the beads.
159b: ferroan equant spar calcite.
159c: the beads.
161a: well preserved aragonitic (~83% A, ~17% LMC) composite prismatic outer layer.

Sample:

161b: inner layer with preserved lamellar ultrastructure (A < 3%, LMC ~ 97%).
165a: thick beaded prismatic outer layer. Long prisms forming a non-denticular composite prismatic ultrastructure.
165b: the bead, made up of fine prisms of LMC.
166a: thick compact fine prismatic layer, well preserved.
166b: pillar, well preserved as fine prismatic ultrastructure.
166c: middle and inner layers, now cemented and with no clear relic ultrastructures.
168a: outer layer with large prism. Cells infilled by equant calcite, partly bored.
168b: pillar of prismatic habit.
168c: ferroan equant calcite spar filling a large void.
200a: part of the highly recrystallized and cemented outer prismatic layer.
200b: pillar; cemented.
200c: inner thin layer replaced by cement.
200d: internal cavityinfilled by coarse ferroan equant spar calcite.
208a: thick beaded prismatic layer.
208b: beads, composed of very fine prisms.
208c: internal body cavity infilled by micritic, pelletal sediment with rudist and coral fragments.

Family Monopleuridae - American Localities

127a: outer prismatic, partly preserved layer, bored by sponge borings. The bores are infilled by micritic sediments.
127b: middle layer present as brown, nonferroan pseudospar.
127c: pillar-like body.
127d: inclusion-rich nonferroan equant calcite.
186a: outer thin layer with prismatic ultrastructure; partly recrystallized.
186b: radiaxial fibrous nonferroan cement; inclusion-rich.
186c: internal cavity infilled by micritic sediments with some fossil fragments.

Family Radiolitidae - American Localities

99a: outer cellular-prismatic layer; cell walls are partly recrystallized; some borings exist.
99b: middle and inner layers with relic ultrastructures.
99c: internal cavity infilled by micritic, pelletal sediments with rare fossil fragments.

Sample:

100a: thick, compacted cellular-prismatic layer. Prisms are partly recrystallized and bored.
100b: middle and inner layers, having neomorphic calcite.
100c: internal cavity infilled by micritic, pelletal internal sediments with some rudist fragments.
107a: outer thick cellular-prismatic layer, well preserved and rarely bored.
107b: inner layer preserved nonferroan equant calcite bounded by micritic envelopes.
107c: coarse ferroan equant calcite spar filling internal body cavity.
108a: outer thick cellular layer. Cells are infilled by micritic to microsparitic and equant calcite.
108b: middle thin layer present as brown nonferroan pseudospar with ghosts of lamellar ultrastructure.
111a: outer cellular layer, poorly preserved. The cells chambers are infilled by two generations of cement.
111b: internal cavity infilled by micritic sediments with some rudist fragments.
113a: thick cellular layer; cells are occupied by fine equant calcite cement and/or micritic sediments.
113b: internal body cavity infilled by coarse equant inclusion-rich ferroan calcite.
114a: outer cellular-prismatic layer, cell walls are well developed and composed of fine prisms.
114b: ferroan bladed cement in the body cavity.
121a: outer thick cellular-prismatic layer. Cells infilled by internal micritic sediments; partly recrystallized to microspar.
121b: coarse ferroan equant spar calcite.
121c: silty material in body cavity.
125a: outer thick cellular-prismatic layer; cell walls are fairly well preserved. Cell chambers are partly occupied by internal sediments and equant spar.
125b: internal body cavity; micritic, cemented with fossil fragments (e.g. rudists).
126a: heavily bored and micritized cellular layer.
126b: coarse ferroan equant spar calcite.
126c: central body cavity infilled by micritic, pelletal sediments with a lot of rudist shell fragments.
131a: outer cellular-prismatic layer; cell walls are well developed. This layer is partly bored by algae.
131b: well preserved aragonitic middle layer with crossed-lamellar ultrastructure (A ~ 94%).
131c: well preserved aragonitic inner layer (A ~ 94%).
135a: outer thick cellular-prismatic layer, partly compacted. Prisms are well developed. Part of the cells are infilled by micritic sediments and/or fine equant calcite.

Sample:

135b: internal cavity infilled by micritic sediments with some rudist fragments.

139a: cellular layer; cells are poorly developed.

139b: neomorphic spar of the middle layer.

139c: internal cavity infilled by micritic sediments with some rudist fragments.

142a: thick cellular-prismatic layer; cells are polygonal with preserved cell walls. Growth lines are well represented as micritic diffused (organic?) lines. The cells are partly infilled by fine ferroan equant calcite.

142b: coarse ferroan equant spar calcite occupying inner cavity.

144a: outer cellular-prismatic layer; cell walls are well developed. Cells are partly infilled by equant calcite and micritic internal sediments.

144b: internal cavity infilled by micritic sediments and ferroan equant spar.

148a: outer cellular-prismatic layer. Cells are partly compressed, bored by algae and sponges and encrusted by micritic sediments.

148b: middle and inner layers with preserved relics of crossed-lamellar ultrastructure.

148c: internal cavity occupied by micritic sediments and two generations of cements, bladed and equant.

151a: outer cellular-prismatic layer, rarely bored.

151b: inner layer, cemented and has no relic ultrastructure.

151c: internal body cavity infilled by micritic internal sediments with some fossil fragments.

154a: outer cellular-prismatic layer, algal boring and encrustation of internal sediments with some fossil fragments is present.

154b: middle and inner layers: calcitic with well preserved original relics of aragonitic structures.

154c: inclusion-rich radiaxial fibrous cement occupies a primary body cavity.

155a: well preserved outer cellular-prismatic layer. Cells are occupied by fine equant calcite.

155b: middle layer with neomorphosed calcite.

155c: internal cavity infilled by pelletal, micritic sediments.

160a: outer cellular-prismatic layer; folded and compressed. This part is bored and the bores are infilled by micritic fossiliferous (foraminifera) sediments.

Sample:

160b: middle part of the shell. The original material has been leached away and then infilled by micritic marine internal sediments.
160c: internal cavity infilled by micritic fossil-rich sediments (e.g. foraminifera, rudists).
162a: outer cellular-prismatic layer. Cells are infilled with two generations of cement.
162b: the body cavity is occupied by marine internal sediments micritic with rudist shell fragments.
164a: outer cellular layer. Cells are polygonal and their inner chambers are occupied by fine equant calcite.
164b: thin middle layer with preserved relics of original aragonitic ultrastructure.
164c: coarse ferroan equant spar calcite.
169a: part of outer thick cellular layer; partly bored.
170a: outer cellular-prismatic layer.
171a: outer cellular-prismatic layer. Cells are well developed; partly bored.
173a: part of the outer cellular-prismatic layer.
174a: cellular-prismatic layer. Cells and growth lines are well developed.
190a: cellular-prismatic layer. Cells are well developed. Cells infilled by equant calcite.
191a: cellular-prismatic layer.
192a: outer cellular layer, poorly preserved. Cell chambers are occupied by ferroan equant calcite.
192b: thin middle layer.
192c: coarse ferroan equant spar calcite.
205a: outer thick cellular-prismatic layer. Cells are partly compacted and infilled by equant calcite.
205b: middle layer with relic original ultrastructure.
205c: inner layer with no relic ultrastructure.
205d: internal cavity, silty-micritic, pelletal with some rudist fragments.
206a: outer thick cellular layer; partly bored.
206b: inner layer with neomorphic spar.
206c: inner cavity infilled by late equant cement.
207a: outer layer with cellular-prismatic ultrastructure.
207b: inner layer with relic ultrastructure.
207c: two original bodies inside the shell; could be teeth or myophores with relic ultrastructure.

APPENDIX III

CHEMICAL AND ISOTOPIC RESULTS

Chemical data are concentrations recalculated on the total carbonate (I.R.-free) basis.
I.R. and Ca are in %; Mg, Sr, Mn, Fe, Na, Zn and Al are in ppm;
$\delta^{18}O$ and $\delta^{13}C$ are 0/00 relative to PDB.
For sample location and description, see Appendices I and II.

Sample	I.R.	Ca	Mg	Sr	Mn	Fe	Na	Zn	Al	$\delta^{18}O$	$\delta^{13}C$
	Hippuritids - French Localities										
1a	2.62	32.08	3043	588	15	294	170	8.2	124		
1b	7.33	32.46	2133	364	24	467	171	10.8	216	-4.9	+2.6
7a	5.53	37.38	3830	670	5	106	298	8.5	128	-3.7	+1.6
7b	1.80	32.14	2480	495	15	281	122	9.1	122		
7c	1.37	28.42	2092	313	22	255	43	10.2	61	-6.0	+2.0
7d	1.46	30.73	918	500	37	1026	36	13.7	41	-10.5	+2.2
8a	1.10	30.73	3903	653	22	153	163	13.2	41	-2.3	+1.7
8b	1.34	21.77	3490	587	23	163	130	13.7	41	-2.3	+1.6
8c	4.65	28.72	2112	368	20	790	57	11.1	54		
8d	6.41	33.46	3145	339	24	414	145	7.5	194	-5.2	+3.2
8e	4.40	33.29	2653	334	26	337	168	11.5	158		
10a	1.03	32.27	2553	663	16	158	250	12.2	77		
10b	6.05	31.54	1655	664	24	302	280	17.5	88	-3.3	+1.7
10c	5.59	24.03	1436	501	38	1229	59	10.6	212		
13a	1.60	24.33	663	857	16	102	816	12.1	20	-3.6	+0.1
13b	1.70	29.45	691	311	26	143	219	13.4	41		
13c	1.90	28.17	931	122	16	128	36	14.2	66		
14a	2.6	24.58	3257	541	24	284	227	14.4	186	-3.6	+2.1

Sample	I.R.	Ca	Mg	Sr	Mn	Fe	Na	Zn	Al	$\delta^{18}O$	$\delta^{13}C$
14b	2.03	24.58	3572	268	31	309	62	10.3	124		
14c	0.80	31.81	1263	485	35	848	25	12.1	101	-9.6	+1.5
14d	2.84	30.79	2765	428	31	351	156	12.3	124		
14e	0.57	27.88	2718	495	25	303	174	13.1	40	-4.7	+1.7
15a	1.56	24.07	4362	582	15	291	204	14.2	102		
15b	0.79	23.95	2121	449	36	990	38	10.0	76		
20a	1.10	30.60	3003	520	28	291	122	13.2	102		
20b	4.36	30.43	2132	426	44	510	185	16.8	189	-7.1	+1.6
23a	2.05	31.05	3433	596	15	206	237	13.4	62		
23b	4.44	32.62	3538	673	16	288	210	14.1	42		
23c	2.32	30.43	2913	387	31	567	57	17.5	41		
27a	2.57	32.37	3247	596	15	412	268	9.2	62		
27c	3.50	22.35	2396	333	26	333	65	7.2	104	-5.2	+2.3
27d	4.43	31.44	4993	268	39	168	116	9.4	158		
43a	2.15	35.19	3990	495	20	77	232	12.3	41	-2.9	+1.2
43b	1.22	24.07	1684	1036	29	184	133	10.2	41	-5.0	+2.0
43c	2.89	23.80	1495	655	37	314	88	9.2	61		
48a	1.40	31.75	2066	816	16	153	508	10.1	41	-3.9	+1.5
56a	5.16	36.04	4127	1271	59	564	229	7.4	43	-3.6	+2.8
56b	4.41	33.05	2937	1074	93	1021	253	10.5	63	-4.3	+2.9
56c	2.13	30.40	2895	1134	136	1201	57	8.2	41	-5.2	+4.0
56d	2.78	30.53	3359	1072	176	1005	79	10.2	61	-5.2	+3.6
58a	1.43	30.73	2434	490	16	153	173	10.0	41	-3.3	+1.7
58b	1.68	32.01	2865	254	19	327	87	10.2	20	-4.2	+1.5
58c	1.71	27.45	3306	403	22	184	133	10.2	41		
58d	0.97	28.14	3000	242	28	364	101	11.1	61	-3.8	+1.8
59a	2.77	31.05	4778	474	11	186	225	13.9	124	-2.4	+2.5
59b	2.45	26.0	3433	531	6	184	232	12.2	77		
59c	2.59	24.40	2969	325	18	160	46	11.3	62	-4.1	+3.5
59d	1.90	23.95	2571	240	22	413	92	13.7	102		
59e	4.99	22.45	4168	326	26	316	89	12.5	126		
61a	2.31	24.58	4546	699	63	732	181	13.9	10		

Sample	I.R.	Ca	Mg	Sr	Mn	Fe	Na	Zn	Al	$\delta^{18}O$	$\delta^{13}C$
61b	3.30	29.02	4172	495	77	990	109	10.4	10	-5.5	+1.2
61c	1.21	34.57	1658	1673	52	765	122	11.2	10	-6.1	+2.2
61d	7.41	40.11	4795	1295	73	514	320	25.1	10		
61e	1.66	31.98	3839	735	52	291	204	13.7	21		
62a	5.49	23.63	6041	596	54	590	245	14.3	106	-3.8	+1.3
62b	1.58	32.27	4546	668	17	327	181	12.2	41		
62c	1.37	28.17	5189	495	26	301	143	13.7	41		
62d	0.68	23.95	4182	606	28	303	167	14.1	41	-3.3	+1.4
62e	1.10	30.73	3683	531	49	939	56	11.2	41		
62f	0.78	22.43	4318	636	51	848	58	13.1	41		
90a	1.90	30.60	4959	1332	78	510	612	14.2	61	-4.2	+2.6
90b	7.96	25.78	4109	1196	88	853	359	10.8	43	-4.0	+2.7
90c	13.68	31.40	2703	2366	124	1512	93	11.5	45	-4.8	+4.0
91a	3.09	31.37	3938	273	35	333	115	10.4	42	-2.6	+2.2
91b	4.70	36.85	3789	505	26	105	189	8.6	63		
91c	2.63	28.98	2691	448	16	155	170	10.3	41		
91d	1.75	35.85	2893	337	32	301	69	11.2	61		
91e	2.58	30.40	985	515	33	778	26	10.3	41		
92a	5.91	25.23	2394	378	33	489	155	10.6	340		
95a	2.60	19.40	4175	513	26	155	191	10.3	41		
95b	1.73	28.68	1898	423	29	612	56	8.1	21		
95c	3.19	32.70	1438	448	26	714	42	10.3	10		
223a	3.10	32.68	5016	1286	80	479	224	13.5	42	-2.7	+2.4
223b	2.47	28.72	3247	1974	104	644	119	8.2	41	-3.8	+3.1
223c	1.30	33.29	3628	990	147	633	102	10.2	41	-2.8	+3.7
223d	3.80	32.70	2813	1068	134	1010	57	11.4	62		
224a	2.20	32.34	4658	1459	53	464	435	11.3	41	-4.4	+2.3
224b	7.40	30.55	4304	1239	104	500	217	12.9	22	-3.5	+3.6
224c	3.11	33.98	3469	1177	142	641	115	12.5	21	-4.1	+4.2
224d	1.70	33.29	2985	2454	132	643	61	12.2	21		

Sample	I.R.	Ca	Mg	Sr	Mn	Fe	Na	Zn	Al	$\delta^{18}O$	$\delta^{13}C$
	Radiolitids - French Localities										
18a	2.10	32.47	1959	603	26	351	304	13.9	77	-5.1	+2.1
18b	3.70	27.45	1625	453	32	474	177	16.6	156		
30a	2.40	35.06	2505	443	15	247	237	11.3	62		
30b	4.30	30.38	2474	351	18	495	158	10.5	211		
30c	4.00	26.27	2250	339	17	354	135	10.4	104		
33a	2.20	30.79	1340	495	20	206	258	15.4	62	-5.3	+1.7
33b	2.68	31.05	1129	263	26	309	77	10.3	62	-4.7	+2.8
33c	2.70	28.46	1478	309	23	258	108	10.3	62	-4.7	+1.4
35a	2.00	22.66	2372	653	6	158	296	10.2	41	-4.3	+1.8
35b	2.30	27.17	1778	675	11	258	77	12.3	62		
35c	2.04	27.68	1907	825	15	208	72	10.3	62	-3.8	+2.3
35d	2.19	24.58	2570	531	18	284	119	12.3	77		
37a	1.90	32.27	2653	408	19	153	194	10.1	20	-4.2	+0.9
37b	4.30	24.83	1832	358	26	316	147	14.7	126		
38a	2.60	27.17	2758	356	11	232	103	7.2	41		
38b	4.20	19.94	2500	411	33	337	185	12.5	105		
39a	2.79	29.75	3247	401	16	232	185	6.7	62		
41a	2.78	29.75	2830	541	26	232	180	12.2	41	-4.4	+2.0
41b	2.38	29.80	2191	351	29	330	181	8.2	41		
41c	4.32	19.69	758	144	41	957	31	3.1	21	-7.9	+1.2
41d	2.61	19.66	2680	665	18	232	381	5.1	41	-4.7	+1.8
42a	0.83	30.42	1818	530	19	293	273	4.5	61	-4.3	+1.6
42b	2.00	21.77	2245	531	22	357	219	7.1	61		
42c	2.39	26.00	2886	337	26	397	93	8.4	103	-4.4	+2.2
47a	2.44	24.06	3080	500	15	258	278	6.7	41	-3.8	+2.0
47b	2.00	30.47	1990	327	16	327	92	6.1	41	-5.7	+1.5
47c	1.57	28.17	3122	529	18	281	128	3.0	61	-4.7	+2.1
60a	1.45	32.14	3673	806	49	301	155	12.1	61	-2.4	+2.8
60b	4.06	24.96	3837	1016	54	300	211	13.6	126	-3.2	+3.5
63a	1.73	29.45	1888	214	29	918	163	10.2	61	-6.0	+1.3

Sample	I.R.	Ca	Mg	Sr	Mn	Fe	Na	Zn	Al	$\delta^{18}O$	$\delta^{13}C$
63b	5.95	31.50	1702	191	36	239	117	12.7	213		
64a	1.30	30.70	2556	311	22	1510	245	12.2	77		
64b	4.30	25.10	2632	274	26	400	184	11.5	158		
65a	1.59	27.55	1179	206	26	811	117	12.1	41		
65b	6.20	32.25	2285	215	34	489	161	16.1	194		
66a	2.04	30.79	4407	588	20	619	366	12.3	62		
66c	10.26	26.33	5002	502	31	1228	246	15.0	424	-4.0	+2.8
70a	3.30	31.37	3516	542	26	698	186	14.0	42		
70b	6.65	27.12	4132	559	33	806	253	11.8	214		
71a	1.70	26.89	2755	561	38	1184	306	10.1	10		
71b	3.20	35.29	4219	510	50	1521	198	12.3	21	-5.4	+2.9
76a	2.20	28.46	4899	608	51	809	320	10.2	41	-4.0	+2.4
76b	12.90	26.25	3631	515	59	1132	328	12.6	345		
77a	1.50	29.50	3536	638	32	903	334	10.2	61		
77b	1.93	35.85	2679	724	44	1490	24	11.2	41	-8.6	+2.6
78a	2.06	24.58	4820	784	38	814	557	10.2	41		
78b	2.91	27.17	3742	418	57	2026	93	11.2	103		
218a	3.00	35.06	2268	320	35	330	206	11.3	61		
218b	4.50	29.32	3505	258	39	368	134	12.5	189		
Requieniids - French Localities											
82a	1.67	30.22	490	607	19	102	638	11.2	41	-3.4	+0.7
82b	1.15	30.73	704	107	38	153	53	13.2	41	-5.3	+0.4
84a	0.93	30.29	540	576	11	141	594	12.0	41	-4.4	-0.4
84b	0.95	29.15	662	96	17	182	40	11.2	41	-6.1	+0.4
85a	1.99	19.46	444	541	17	173	429	10.1	41		
85b	2.0	17.92	648	99	17	230	51	8.3	61	-5.6	+0.8
86a	0.92	21.49	427	545	19	202	515	9.0	61	-4.3	+0.4
86b	1.08	21.77	612	92	32	321	46	9.1	61	-5.8	+0.2
87a	1.50	28.68	508	582	22	230	648	10.0	61	-5.1	-0.9

Sample	I.R.	Ca	Mg	Sr	Mn	Fe	Na	Zn	Al	$\delta^{18}O$	$\delta^{13}C$
87b	0.74	16.47	689	131	33	291	87	12.0	76	-5.8	+0.6
89a	0.73	31.69	404	533	17	204	571	11.0	41	-5.2	+1.3
89b	0.95	27.17	667	108	22	303	66	10.0	76	-6.4	+0.1
	Caprinids - American Localities										
96a	8.33	34.47	64	1805	7	1780	2830	10.9	82	-2.1	+3.2
97a	0.78	25.30	10645	1111	1273	1056	1220	10.1	40	-1.7	-2.2
97b	0.56	38.28	15422	717	3636	1818	611	8.0	61	-2.2	-4.9
97c	0.27	33.48	5903	263	8838	4646	207	11.6	40	-13.2	-21.2
97d	1.05	34.64	19325	695	3528	1881	563	8.6	61	-2.5	-5.5
101a	0.92	29.15	1833	154	40	93	66	11.1	60		
101b	1.09	28.93	2858	137	33	93	51	10.1	81		
104a	1.09	29.69	379	2020	24	93	2882	10.0	40	-2.5	+3.0
105a	1.28	34.83	9919	2138	61	93	341	11.1	101	-3.5	+2.6
105b	1.50	29.81	10655	2315	63	141	335	8.1	102	-3.5	+2.4
109a	2.47	38.61	3554	1138	267	662	77	11.2	103		
109b	1.16	27.94	3251	1098	294	1225	83	8.0	81	-5.8	+1.7
109c	1.05	34.26	3225	536	637	1668	68	10.2	61	-8.2	+0.1
110a	3.28	37.11	7394	1003	79	144	130	9.3	165		
110b	0.94	33.21	5444	1141	76	76	146	8.0	60	-6.2	+1.7
110c	3.30	36.59	6848	978	81	144	109	11.3	103		
115a	1.38	32.66	9817	2201	58	157	334	9.1	132	-3.3	+2.7
115b	0.78	23.27	11666	1515	66	93	308	8.5	40	-3.5	+2.5
116a	31.31	31.46	5452	434	4737	4082	197	14.5	1224	-5.3	-6.0
116b	1.09	29.94	6862	430	8163	4272	182	11.2	61	-5.1	-9.1
122a	0.84	33.97	7381	1768	197	197	185	10.0	111		
122b	1.58	31.63	4360	2083	168	447	158	11.1	82	-4.5	+2.9
123a	1.54	29.33	8161	645	179	234	123	7.6	41		
123b	1.39	26.98	4741	674	183	472	112	11.7	41	-3.4	+1.5
123c	1.45	35.54	5025	1056	191	457	96	7.1	81	-6.4	-0.3

Sample	I.R.	Ca	Mg	Sr	Mn	Fe	Na	Zn	Al	$\delta^{18}O$	$\delta^{13}C$
123d	5.99	33.91	3862	691	160	415	271	10.6	277		
128a	5.76	36.23	5605	624	552	679	218	13.2	425	-6.5	+1.4
128b	1.11	37.34	4064	779	450	329	350	8.0	61	-6.9	+0.9
128c	11.02	36.70	3737	336	1907	2261	101	12.9	887	-5.9	-1.7
130a	3.90	33.43	8184	2092	124	385	94	11.4	229	-3.5	+2.1
130b	1.10	31.97	6896	1871	106	228	96	10.1	111		
130c	4.80	30.84	9821	1259	133	263	122	12.3	210	-2.5	+2.7
132a	3.20	39.41	3386	311	2066	1860	150	9.2	207		
132b	1.51	31.88	2571	320	3877	2846	246	11.1	112	-5.5	+0.6
133a	2.50	33.20	5190	672	4639	3179	226	11.2	113	-5.8	-4.0
133b	2.33	34.71	6774	747	7835	5464	197	10.2	184		
133c	0.50	34.43	4201	394	6565	2915	161	8.5	16	-6.1	-6.6
133d	5.57	34.56	4719	328	5063	3284	148	11.6	211	-6.0	-5.3
137a	0.79	36.50	6653	1040	101	254	303	8.0	101		
137b	1.05	34.00	7786	1153	158	1062	76	9.1	61		
140a	1.48	28.28	1452	964	1122	964	376	9.1	41		
140b	9.05	29.54	2399	456	1518	2310	231	23.6	671	-5.3	+1.6
141a	7.78	36.20	6025	2256	150	694	148	10.8	607		
141b	2.59	32.47	6268	2177	93	457	149	8.2	164		
141c	9.11	34.83	5876	2279	151	765	138	12.9	925		
143a	3.90	32.64	9099	900	593	1582	88	10.4	250		
143b	2.00	32.52	10214	867	590	1276	77	11.2	133		
143c	1.13	30.73	10243	881	555	1356	108	8.6	830	-2.6	+0.5
145a	1.13	36.07	6847	658	44	121	160	8.0	16		
145b	1.98	35.08	5893	1735	26	142	250	10.1	60	-3.4	+2.9
145c	1.77	31.18	7281	2378	49	87	214	9.1	61	-3.3	+2.9
145d	1.36	33.34	6694	1927	41	127	188	10.1	61	-2.0	+0.2
146a	3.13	36.30	7045	2128	162	460	119	8.7	207	-3.3	+0.5
146b	1.40	30.54	4239	1990	112	304	150	11.2	112	-3.9	+2.1
146c	5.28	26.50	1278	1890	119	507	121	12.4	296	-3.5	-3.7
147a	0.80	38.53	4713	2101	93	293	190	7.5	101	-5.0	+3.3
147b	0.73	35.74	5045	1884	158	909	121	7.0	40	-5.3	+3.5

Sample	I.R.	Ca	Mg	Sr	Mn	Fe	Na	Zn	Al	$\delta^{18}O$	$\delta^{13}C$
150a	9.80	26.15	9939	1912	186	1053	133	13.8	931		
150b	10.40	39.76	8404	1871	211	1174	157	13.2	1022	-3.2	+2.8
150c	1.47	32.61	5863	1695	125	396	168	10.0	41		
153a	0.90	33.46	3219	1288	40	227	864	10.1	111	-5.1	-0.2
153b	1.00	39.04	9667	2000	76	581	242	9.0	40	-3.9	+1.4
153c	11.40	27.76	7946	2076	135	1354	124	13.3	429		
157a	0.74	15.46	3216	1778	116	86	282	7.5	81	-2.7	+3.0
157b	1.45	29.30	3685	1622	191	122	162	7.1	61	-3.1	+2.5
157c	0.97	26.87	6322	1252	172	86	304	8.0	40		
158a	1.15	36.32	7237	916	243	93	154	7.0	81		
158b	3.75	31.04	2870	407	833	468	99	7.6	187		
163a	6.02	30.87	4334	506	112	346	43	6.3	277		
163b	1.01	36.99	6340	738	652	2659	56	8.5	16		
163c	8.77	33.85	12302	910	246	1643	90	10.9	439		
167a	1.14	35.31	76	1782	4	76	2632	11.1	16	-2.3	+3.9
172a	0.70	36.76	5333	374	1349	9595	61	9.7	61		
172b	0.90	32.45	9084	514	172	10808	92	11.9	131	-2.5	-0.6
172c	28.30	25.55	8069	600	237	13947	317	20.9	2148		
175a	2.90	36.18	2152	156	278	144	38	10.1	103		
175b	8.03	35.50	2693	174	675	642	38	9.7	109	-7.5	-3.8
175c	1.40	36.40	1116	157	624	472	32	10.0	132	-7.9	-4.0
176a	1.74	32.71	3024	474	743	8401	102	11.2	81	-11.6	+0.5
176b	0.81	28.39	4018	1293	106	2273	120	8.6	60	-13.4	+1.8
177a	4.20	35.10	5466	219	242	1356	61	8.3	230	-7.2	-0.5
177b	1.56	31.88	1286	143	488	1880	24	6.0	81		
179a	4.25	34.09	1954	157	188	240	34	10.4	104	-7.7	-3.6
179b	1.09	32.99	1891	167	403	329	40	11.1	16	-8.6	-7.0
179c	5.27	36.84	2381	195	449	422	53	8.9	63	-9.7	-4.0
180a	1.68	35.23	2070	234	488	158	90	9.1	134	-8.8	+1.9
180b	1.13	35.31	1581	638	330	172	207	10.1	81	-7.4	+2.4
180c	5.13	32.83	1126	127	591	164	69	10.5	359	-9.3	+1.2
181a	2.07	23.33	2000	260	894	1588	56	8.1	16	-6.2	+0.6

Sample	I.R.	Ca	Mg	Sr	Mn	Fe	Na	Zn	Al	$\delta^{18}O$	$\delta^{13}C$
181b	1.25	37.12	1727	291	957	1418	37	8.1	61	-7.4	-0.9
181c	12.69	29.32	2772	379	1237	1386	107	11.3	69	-6.8	-1.4
184a	1.17	37.34	3730	213	739	2379	61	8.0	111	-4.0	+0.8
193a	0.57	29.29	6308	434	28	171	127	8.5	81		
193b	1.65	33.19	1679	153	184	2238	26	8.6	41		
193c	0.86	31.40	3163	313	35	266	88	11.6	16		
194a	1.04	32.73	3871	313	51	263	86	10.0	61		
194b	1.62	31.43	2961	313	78	461	57	10.2	61		
194c	1.29	29.24	3399	305	50	254	91	9.1	41		
195a	0.77	39.55	1796	161	47	157	55	9.0	40	-6.4	+3.2
195b	1.21	30.00	1170	162	89	228	38	7.1	16		
197a	0.99	39.04	2944	343	35	223	96	11.6	60	-4.9	+3.5
197b	1.30	35.85	3232	233	77	456	75	10.0	61	-6.8	+3.0
199a	1.30	34.58	4347	302	46	233	111	10.0	61	-4.9	+3.4
199b	1.16	15.24	2728	177	51	224	61	7.6	16		
199c	1.52	32.39	2403	188	68	333	56	11.1	61	-6.4	+3.0
201a	2.93	34.15	3515	577	206	1340	67	10.3	136		
201b	3.86	33.43	3800	733	157	937	68	11.4	209		
202a	1.20	34.55	5344	800	455	1508	66	11.1	111	-6.2	-0.4
202b	0.91	19.26	6944	980	343	1869	81	8.0	101		
202c	1.47	34.65	3239	645	421	1218	88	9.1	61	-8.5	+1.2
203a	5.01	31.75	6847	1579	87	268	91	10.0	344	-2.7	+2.5
203b	9.44	40.90	6685	1381	91	492	116	9.3	674		
Hippuritids - American Localities											
98a	0.79	24.84	5267	535	74	263	447	6.0	40	-1.7	+3.1
106a	0.89	32.45	6122	778	706	3687	162	11.1	81	-2.3	+1.1
106b	0.48	35.49	4975	672	1286	5707	178	10.1	81	-2.5	-0.4
106c	0.95	35.24	4778	1343	207	2374	457	8.0	40	-5.8	+1.3
118a	2.11	26.69	6389	720	228	665	77	6.1	82		

Sample	I.R.	Ca	Mg	Sr	Mn	Fe	Na	Zn	Al	$\delta^{18}O$	$\delta^{13}C$
118b	10.41	42.62	6636	787	245	1028	123	12.8	737	-4.9	+1.7
120a	9.50	33.42	7354	493	1939	2652	88	10.8	66	-8.0	+2.4
120b	3.0	32.60	1361	165	1959	1010	41	8.7	103	-13.6	+1.6
156a	5.32	32.36	6105	687	552	2748	74	11.6	86		
156b	0.70	37.26	5151	561	621	1818	76	5.0	40	-3.4	+0.9
156c	1.43	30.06	6533	695	406	2853	83	11.1	81		
159a	1.70	31.15	2909	154	883	398	83	9.1	40	-7.3	+1.9
159b	0.84	23.07	6105	333	176	140	192	8.5	60		
159c	0.61	30.83	4453	1273	86	93	832	10.1	81	-4.7	+1.7
161a	1.14	26.42	445	1549	20	76	3543	11.1	223	-2.3	+2.5
161b	0.36	29.09	3282	1613	42	77	1341	22.1	60	-3.1	+1.8
165a	1.89	29.16	2243	1081	173	341	698	10.0	41	-6.3	+2.3
165b	1.04	23.61	3037	1242	192	695	715	12.0	16	-5.8	+1.4
166a	0.34	31.24	3269	414	75	126	61	10.0	81		
166b	0.80	38.53	1386	212	87	121	37	11.1	81	-8.5	+1.8
166c	1.06	17.76	3314	452	56	197	73	9.1	16	-5.3	+1.0
168a	0.52	30.55	2158	283	1197	449	116	11.6	60	-7.0	-0.8
168b	5.58	32.70	1748	657	287	234	593	7.4	42	-5.3	+2.1
168c	0.89	39.04	1310	1010	128	157	1470	6.0	16	-4.2	-0.4
200a	1.13	36.20	1837	304	1043	860	77	6.0	40		
200b	4.27	33.69	1494	402	1076	470	143	10.3	17	-6.6	+0.4
200c	0.76	28.39	2111	547	662	331	222	6.0	101	-6.2	+0.6
200d	1.22	33.05	2006	388	806	456	177	9.1	61	-6.6	+1.0
108a	0.52	34.59	3763	1192	27	571	869	6.0	61	-4.3	+1.8
208b	0.63	28.12	4462	1166	39	335	1220	11.9	17	-8.1	+3.3
208c	0.70	23.57	1219	253	636	146	88	10.1	81	-4.2	-1.1
	Monopleurids - American Localities										
127a	1.56	34.74	10966	950	195	480	310	7.7	134	-7.5	+0.4
127b	1.11	29.46	8128	886	81	397	304	10.1	81	-6.7	-1.9

Sample	I.R.	Ca	Mg	Sr	Mn	Fe	Na	Zn	Al	$\delta^{18}O$	$\delta^{13}C$
127c	1.16	36.83	8462	711	253	658	249	8.6	101		
127d	1.43	25.48	7371	893	406	335	351	10.1	61	-5.0	-0.8
186a	1.47	39.84	4649	1020	167	143	397	10.1	81	-5.5	+1.2
186b	0.64	34.62	8534	610	178	122	126	11.9	61	-4.0	+3.6
186c	2.72	37.18	4697	639	155	129	108	10.1	113	-7.1	+2.3
	Radiolitids - American Localities										
99a	2.65	29.66	3799	887	226	966	617	11.3	205	-2.5	-0.4
99b	1.82	34.79	6335	459	530	2243	122	10.1	102	+0.7	+0.7
99c	7.97	35.46	7915	408	587	2511	130	7.6	457	+0.7	+0.5
100a	0.82	36.72	4218	859	257	254	351	9.0	40		
100b	0.71	32.13	11199	975	78	808	192	8.5	60	-2.0	+1.5
100c	2.89	30.24	6231	953	320	338	221	9.2	185	-2.4	+0.8
107a	1.49	36.31	4355	1411	181	289	142	9.2	61	-5.5	+1.7
107b	0.95	30.67	6389	1500	157	263	116	11.1	60	-6.3	+2.2
107c	1.70	32.42	4196	778	275	1221	41	8.2	81	-7.3	+2.0
108a	0.41	31.43	6302	1848	70	182	337	5.0	40	-3.4	+1.8
108b	0.84	15.21	8547	1838	76	266	143	5.0	101	-4.1	+3.1
111a	1.02	27.91	3503	940	228	121	61	8.5	61		
111b	4.28	37.24	7126	1494	157	434	248	5.7	355	-4.9	+1.8
113a	1.22	18.81	12593	973	208	93	334	8.1	40	-3.2	+1.3
113b	1.33	35.38	5745	816	247	597	88	10.0	16	-6.4	-2.0
114a	1.10	35.02	5450	1234	37	126	600	8.0	101	-4.4	+2.1
114b	0.99	38.53	4333	1015	61	126	124	10.0	111	-6.7	+2.0
121a	0.91	34.48	5567	1374	91	374	91	10.0	80		
121b	0.46	31.53	2598	293	258	1061	37	8.5	40	-6.1	+3.8
121c	0.29	35.49	5572	1353	103	444	126	10.1	303		
125a	1.10	33.24	8384	1507	76	202	303	10.1	133	-3.1	+3.0
125b	10.86	36.66	4136	965	168	2076	185	12.3	831		
126a	1.00	33.72	6333	1020	70	141	305	8.0	81		

Sample	I.R.	Ca	Mg	Sr	Mn	Fe	Na	Zn	Al	$\delta^{18}O$	$\delta^{13}C$
126b	1.0	31.18	5389	806	56	76	96	11.6	111		
126c	3.30	36.07	3242	1264	91	362	103	10.2	165	-8.5	+1.0
131a	2.44	32.69	4626	1400	149	477	554	8.1	185	-6.5	-2.1
131b	1.12	37.85	3229	2045	43	93	558	8.5	16	-7.7	-1.1
131c	1.34	28.51	535	1048	30	76	1815	12.0	41	-2.7	-1.2
135a	1.10	33.0	5046	775	127	183	209	7.6	61	-3.4	+0.7
135b	3.72	28.83	7318	832	131	642	184	8.8	291		
139a	2.10	31.92	10739	1854	124	288	106	9.2	185		
139b	0.50	34.22	2764	2076	106	374	201	9.9	16	-4.8	+3.4
139c	9.20	30.40	7172	2384	137	716	150	14.3	881		
142a	1.04	35.78	3504	1213	77	197	119	8.0	61	-3.4	+3.5
142b	1.90	37.09	3700	739	253	1529	58	11.1	82		
144a	1.07	41.36	8231	1193	91	223	480	11.6	81		
144b	1.82	38.37	4597	1193	133	341	107	2.8	111		
148a	1.69	35.49	5707	1092	46	229	539	5.5	132		
148b	0.95	33.97	9222	1414	30	182	208	9.1	60		
148c	1.12	37.11	5389	913	114	1066	111	8.6	81		
151a	1.72	38.67	5321	1663	33	76	580	6.0	81		
151b	0.87	36.25	3219	712	52	606	111	7.5	16		
151c	6.49	35.97	5882	1711	47	321	173	10.5	353	-4.7	+3.8
154a	0.59	31.05	6806	1358	23	140	859	8.5	60	-4.0	+1.8
154b	0.71	32.70	8555	1172	38	806	278	11.8	81	-4.5	+0.2
154c	8.62	29.14	5000	1457	137	1698	115	8.7	327	-3.5	+2.5
155a	0.99	33.97	4611	1815	83	91	165	9.0	40		
155b	0.93	21.29	4956	2131	136	449	124	8.0	16		
155c	1.62	19.91	5293	2035	142	560	83	8.1	163		
160a	0.76	33.39	4047	687	242	444	462	10.0	40		
160b	3.20	32.41	5886	318	474	857	147	10.2	113	-4.7	+2.3
160c	0.67	31.34	6480	278	504	957	106	11.1	40		
162a	0.89	35.49	4518	1158	91	960	133	9.0	101		
162b	2.19	30.79	4072	1053	180	1022	268	6.1	133		
164a	1.04	35.27	4418	1294	399	1820	101	10.1	61		

Sample	I.R.	Ca	Mg	Sr	Mn	Fe	Na	Zn	Al	$\delta^{18}O$	$\delta^{13}C$
164b	1.29	19.83	3154	1581	420	1662	78	8.6	41		
164c	1.30	33.82	5350	1827	729	2533	76	11.9	41	-5.2	+2.9
169a	1.40	35.38	5243	649	193	4969	122	11.1	81		
170a	0.75	30.61	4158	1227	490	1813	202	10.1	16		
171a	1.40	33.60	3347	259	1357	3600	139	10.0	16		
173a	6.54	34.12	2921	623	94	600	132	12.6	107		
174a	8.0	31.37	4998	255	375	245	92	8.6	65		
190a	5.15	29.12	47573	274	1071	2637	69	12.1	63	-3.7	-3.3
191a	0.85	35.74	3940	151	631	2273	33	8.5	81		
192a	3.66	33.36	1074	1890	202	234	157	6.2	41		
192b	3.24	33.48	853	1882	160	207	98	10.2	41	-7.8	+2.0
192c	7.86	41.15	1493	653	505	426	53	10.8	63		
205a	1.18	40.39	2505	769	283	228	466	11.9	16		
205b	1.04	30.45	3882	758	130	126	189	6.0	61	-4.0	+2.7
205c	0.68	31.34	7699	803	70	86	283	8.0	16		
205d	1.54	34.94	2582	229	612	330	165	8.1	41		
206a	0.86	40.43	9823	1160	167	86	139	8.0	16		
206b	0.75	36.25	9137	1343	146	93	119	6.0	60		
207a	2.61	32.24	2374	526	391	1809	92	10.2	185		
207b	0.76	29.15	9824	1015	253	4293	120	7.0	60	-1.8	-2.4
207c	0.90	36.88	9113	1177	271	4747	121	9.0	16	-2.3	-2.4
	Enclosing Rocks - French Localities										
3	5.82	31.90	2340	340	27	596	99	13.8	106		
5	16.28	33.86	3524	477	31	355	307	14.3	265	-3.6	+2.1
6	7.89	31.42	3815	473	51	435	217	12.9	163		
11	8.68	24.41	3066	374	21	246	159	10.8	165		
12	5.84	29.90	2191	404	39	452	160	14.3	160	-6.6	+2.0
16	11.72	27.15	3559	369	30	375	201	13.5	227		
17	8.78	32.40	2593	352	42	516	110	13.1	132		

Sample	I.R.	Ca	Mg	Sr	Mn	Fe	Na	Zn	Al	$\delta^{18}O$	$\delta^{13}C$
22	5.61	28.03	2447	489	38	534	266	11.7	160		
24	4.13	31.70	3884	337	53	416	179	11.5	126		
25	5.25	30.76	3830	319	18	239	149	12.0	160		
28	8.94	28.96	1780	379	19	407	236	10.9	219	-4.6	+2.3
31	3.40	29.02	3375	401	17	385	234	12.3	125		
34	4.07	26.55	3268	374	29	332	263	15.7	126		
36	3.91	24.05	3188	349	40	427	266	16.6	125		
40	4.51	32.76	3032	418	26	347	295	10.5	158		
46	3.89	27.45	2550	354	45	490	245	15.6	125		
54	9.32	33.46	4210	978	223	911	467	15.0	222	-2.8	+2.3
55	26.90	25.78	5671	137	193	1712	1123	24.6	493		
67	6.37	29.04	3290	548	41	430	409	12.7	161		
81	7.70	30.01	4304	603	40	674	359	11.9	217		
83	0.76	30.42	646	141	31	182	15	16.1	40		
94	5.59	29.90	2367	383	23	457	179	12.6	128		
210	6.70	20.51	2161	505	40	398	317	14.5	194		
211	2.92	32.60	1412	170	23	186	57	13.9	61		
212	5.10	20.34	1500	181	28	172	80	12.6	64		
213	3.17	28.02	1641	234	38	234	146	12.3	104		
214	1.72	17.92	1240	173	37	199	51	13.7	61		
215	5.02	31.77	2048	394	38	489	128	14.3	106		
216	4.52	23.77	1568	342	18	221	158	9.4	79		
217	2.83	32.08	902	129	31	167	41	12.3	41		
219	3.43	26.40	2953	323	48	432	235	12.5	167		
220	0.65	31.43	682	126	30	101	55	15.1	20		
221	6.55	25.36	2516	378	24	339	177	14.5	161		
222	12.51	39.23	4366	736	37	759	586	18.3	356		
225	0.77	31.69	702	106	38	101	47	11.1	61		

Sample	I.R.	Ca	Mg	Sr	Mn	Fe	Na	Zn	Al	$\delta^{18}O$	$\delta^{13}C$
	Enclosing Rocks - American Localities										
102	0.99	32.95	1889	126	51	76	37	10.0	81		
117	61.30	16.21	8242	426	3875	8139	299	43.9	5323		
134	45.50	29.01	6539	596	4036	5872	275	21.6	4220		
136	16.21	34.63	5520	1147	203	956	301	13.7	1362		
138	6.29	19.82	8159	848	101	550	283	9.6	263	-3.8	+1.6
149	8.07	36.05	6871	1256	98	923	252	10.8	653	-5.4	+1.5
178	7.63	38.07	5244	228	309	840	74	8.6	412	-5.4	+0.6
183	5.55	36.95	8040	1165	307	869	159	10.4	403		
185	14.54	24.98	7471	281	691	1705	76	11.7	937		
196	1.04	19.03	3337	319	51	324	288	15.1	61	-4.7	+3.3
198	0.74	16.19	2772	381	93	595	94	8.0	60		
206	1.25	35.47	6419	1204	153	456	66	8.6	101		